UNIVERSITÉ DE LILLE

École Doctorale Biologie-Santé

THÈSE

Pour l'obtention du grade de

DOCTEUR DE L'UNIVERSITÉ DE LILLE

Spécialité: Neurosciences

Elevated prenatal anti-Müllerian hormone reprograms the fetus and induces polycystic ovary syndrome (PCOS) in adulthood

---

Nour El Houda MIMOUNI

Thèse présentée et soutenue à Lille, le 25 octobre 2019

Composition du Jury:

Pr. Joëlle COHEN-TANNOUDJI	Professeur, CNRS UMR 8251, Paris	Présidente
Dr. Philippe CIOFI	Chargé de Recherche, INSERM U862, Bordeaux	Rapporteur
Pr. Terhi PILTONEN	Clinical Researcher for the Academy of Finland	Rapportrice
Pr. Sophie CATTEAU-JONARD	PU-PH, Hôpital Jeanne de Flandre, Lille	Examinatrice
Dr. Vincent PREVOT	Directeur de Recherche, INSERM U1172, Lille	Examinateur
Dr. Paolo GIACOBINI	Directeur de Recherche, INSERM U1172, Lille	Directeur de thèse

À mes chers parents,

À mon rayon de soleil, ma mamie,

Claudine Besson

Acknowledgements

As PhD stands for Dr of Philosophy, it seems like quite a proper time for me to "philosophically" reflect on this PhD journey, which has challenged me both scientifically and personally during these years.

I am convinced that this work would have never been achieved without the support of many people whose generosity, kindness and interest regarding the project, greatly contributed to the realization of this modest work.

I will naturally start with my thesis director: Dear Paolo, I could never find the words to express my gratitude towards you, you have been an amazing mentor to me during these years, where you guided me and supported me, I have never met a researcher more hardworking and passionate than you. I truly admire your enthusiasm for research and science. Oh mon Dieu! Time flies! I remember coming for the PhD concours scared and you were so kind, helpful and positive. So thank you for believing in me since that day and for the trust that you have put in me for this ambitious project

Thank you for listening to my ideas, and always keeping your door open even for my meaningless reactions (when I come back disappointed from the animal facility after we lost litters from our subfertile mice, or excited when the treatment worked and they are cycling again :') I can go on for many lines about your qualities as a mentor but most of all you know how to bring out the best from each student with your high degree of rigor. I am excited for the next chapter of the AMH- PCOS story.

Dear Vincent, thank you for welcoming me in your lab few years ago, which I am honored to be a part of, I would like to express my gratitude for your constant words of encouragements, never-ending exciting ideas and helpful advice. I think that I speak on behalf of all the PhDs and Post-Docs by saying that with your high expectations and work ethics you push us to become better scientists and finally, thank you for accepting to examine my work.

Professeur Cohen-Tannoudji, vous me faites l'honneur aujourd'hui de présider mon jury de thèse et de juger mon travail. Dès les premiers cours que j'ai suivis avec vous en neuroendocrinologie dans le cadre du Master « Reproduction et Développement » vous avez suscité en moi une grande admiration envers votre maitrise de la neuroendocrinologie et votre pédagogie et a renforcé ma curiosité scientifique ainsi que mon désir de poursuivre une thèse en neuroendocrinologie. Je vous adresse donc, ma sincère reconnaissance et de mon plus profond respect.

Dr. Philippe Ciofi, je vous remercie pour l'honneur que vous me faites en acceptant d'examiner ce travail de thèse. Depuis le début de cette thèse, vous m'avez apporté de nombreux conseils et avez fait progresser ma réflexion avec nos échanges scientifiques que je qualifierai de

scientifiquement exotiques (Je fais allusion, entre autres, à nos discussions sur la différenciation sexuelle chez hyènes !). Je vous adresse mes sincères remerciements ainsi que ma profonde gratitude.

Pr. Terhi Piltonen, I would like to express my deep gratitude to you, for accepting to be a part of my thesis committee, thank you for taking the time to evaluate my work and I'm looking forward for your feedback and precious advice.

Pr. Sophie Catteau-Jonard, je vous remercie pour l'honneur que vous me faites en acceptant d'examiner ce travail de thèse. Ainsi que d'avoir changé votre planning de consultations pour pouvoir siéger parmi les membres de ce jury. Je vous remercie pour l'intérêt et la considération que vous avez portés à ce travail.

Ariane, Bénédicte et Virginie, je tiens à vous remercier pour votre bienveillance envers moi ainsi que pour vos précieux conseils tout au long de ces années. Merci d'avoir répondu à toutes mes questions et de m'avoir apporté votre soutien. Nos échanges scientifiques furent très bénéfiques et constructifs.

I gratefully acknowledge the hospital university center (CHU Lille) for providing me with a generous PhD fellowship after the doctoral school concours admission.

Pr. Sablonnière and François Delcroix je vous remercie pour toute votre aide et vous exprime ma profonde reconnaissance.

Moreover, I would like to thank all the people who contributed to the data presented in this work: Especially the animal Core Facility and Meryem Tardivel and Antonino of the Imaging Core Facility of the University of Lille for their help and technical assistance.

Céline, Sophie, Michèle et Nathalie, Thank you for your maternal behaviour twoards us in the research center, you have provided us with a genenours help not only at an adminstrative level. It was great to have you by our side daily.

A special thanks goes to you Céline, always worrying about when I leave the lab and asking me to not to stay too late ! Your support meant alot to me.

Dr. Ahmed Ziyaat, mon cher Ahmed, tu as remporté le trophé du meilleur directeur/chef pour les bonnes raisons, j'éprouve beaucoup d'admiration pour toi sur le plan scientifique et personnel, tes qualités humaines sont toutes à ton honneur. Ce fut un réel plaisir d'effectuer mon projet de recherche M2 sous ta direction à l'institut Cochin. Je te remercie infiniment, et remercie l'excellente équipe de Cochin dirigée par le Dr. Daniel Vaiman et le Pr. Jean Philippe Wolf pour leur acceuil chaleureux et leurs précieux conseils qui m'ont fait avancer dans ma reflexion scientifique. Tu m'as tant appris Ahmed, et je te suis reconnaissante pour toutes les connaissances scientifiques et techniques que tu m'as transmises pendant mon master et ma thèse aussi. Tu as été et tu resteras encore l'une des figures scientifiques qui m'a le plus inspirée et soutenue durant mon parcours.

Pr. Nicolas De roux, et Dr. Fabien Guimiot, vous avez été les premiers a réelement me faire découvrir le monde recherche, et les neurones GnRH qui me fascinent encore au jour d'aujourd'hui. Je vous remercie de m'avoir fait confiance et de m'avoir acceuillie et initiée à l'expermimentation animale et l'embryologie et surtout de m'avoir apporté votre aide et soutien pendant la réalisation de mon projet de M2 à l'hôpital Robert Debré. Veuillez trouvez dans ces remerciements l'expression de mon profond respect.

Because Family rhymes with priority in life <3

I would like to dedicate a very special gratitude to my loved ones who have shaped who I have become today:

Les larmes aux yeux et un coeur rempli d'émotions je commence par mes chers parents, qui comme une graine, m'ont arosé d'amour et de soutien, jusqu'à ce que je m'épanouisse et je fleurisse. Vous avez été les premiers à croire en moi, depuis mes premiers pas à l'école jusqu'à l'université. Je n'arrive pas à trouver les mots adéquats pour exprimer ma reconnaissance et mon amour envers vous, sans vous je ne serai pas là aujourd'hui, même noyés dans vos livres vous avez toujours prioritisé la vie de famille et trouvé du temps pour m'encourager.

Maman chérie, j'espère qu'un jour je serai aussi courageuse et forte que toi, te voir combattre ce cancer devatstateur avec le sourire et l'optimisme fut un grand tournant de ma vie et a vraiment redéfini ma façon de voir les choses, tu es la femme la plus intelligente, douce et forte que je connaisse, et ta bonté et gentillesse n'ont pas de limites.

Papounet adoré, je sais que la majorité des filles admirent leurs papas, je fais partie de cette catégorie mais pas pour les mêmes raisons, tes qualités humaines et intellectuelles ne cessent de m'impressionner, tu es une encyclopédie vivante, et un papa formidable, tu m'inspire de jour en jour.

Mes petits frères adorés, Minou et Minouche, j'ai de la chance d'être la grande sœur de deux frères uniques de part leur énergie et leurs personnalités différentes mais complémentaires. Vous avez toujours été là pour moi dans les moments difficiles comme dans les moments de joie. Sachez que je suis déjà très fière de vous et crois très fort en vous et en ce que vous allez accomplir bientôt ☺ Je vous aime <3 <3 Votre petite Minouchette.

Habibi, I have known you since the age of 16, and ever since you became my special person, my best friend and my partner in crime, even if our lives took a different path we found each other again and start this new exciting adventure. Words cannot express my gratitude for your unconditional love and patience. This year has been by far one of the most stressful years in my life, organizing two weddings in two countries, working late every day and every week-end and then came the manuscript preparation. Thank youuuuuu for putting up with all of this exhausting yet passionate life-style of a researcher, I love you to the moon and back, and I will forever be grateful for your support. Your butterfly girl forever.. Ich Ich PS: Now we can finally take the time to go on our "postponed" Honeymoon :p !!

Mamie Claudine, tu trouves toujours les bons mots ou les bons plats réconfortants pour me réchauffer le coeur, tu mon rayon de soleil, et je t'aime de tout mon cœur, sans toi je n'en serai pas là aujourd'hui, je te promets que je ne te ferai plus répéter ta phrase : Tu habites à 1 heure de Paris en train et tu rends pas assez souvent visite à ta grand-mère, tu es l'une des personnes les plus chères à mes yeux et je te suis très reconnaissante pour ta douceur et gentiellesse mon petit bijou.

Mamie Lala, mon ange guardien, il y'a déjà plusieurs années que tu nous as quitté, mais je sais que tu veilles sur nous de là haut. Tu m'as toujours appelée docteur alors que je commençais tout juste mon parcours universitaire, je te remercie d'avoir cru en moi et de m'avoir tant appris, surtout d'essayer d'apprécier les choses importantes de la vie et d'être toujours reconnaissante, je finis ce paragraphe avec une phrase que tu disais souvent : Wa hada min fadli Rabbi <3

A ma chère tante Jamie, qui depuis mon jeune âge a développé en moi une curiosité scientifique immense grâce à son instinct de journaliste. Je me souviens, de toutes les fois où tu m'emenais à la cité des sciences à Paris, et tu m'attendais des heures et heures avec beaucoup de patience, pendant que je passais mon temps à regarder le parcours de petites fourmies ou à découvrir les mystères du corps humain ! Merci pour ton soutien et ta générosité envers moi, tu as été la première personne à m'offrir un microscope et je n'en m'en suis jamais séparée.

A tous les membres de ma famille, grands et petits que je ne cite pas ici mais à qui je pense très fort.

Mina ma Brooke <3 Ma vie ne serait juste pas pareille sans toi, tu es une personne tellement sensible et adorable, je te remercie pour tout ce que tu as fait pour moi, et je chéri chaque moment passé ensemble, tu es ma sœur de cœur et je vous aime toi et Lydia ma petite princssse plus que tout !

Mon adorable Mimi, inséparables depuis nos 5 ans, nous avons tellement passé de moments forts en émotions ensemble, je suis fière de toi, tu as poursuivi tes rêves jusqu'à ce qu'ils se réalisent. Merci d'avoir toujours été là pour moi, Ich liebe dich.

Saly, Narimène, mes copines chéries et mes binômes qui n'ont jamais cessé de me surprendre depuis notre première dissection de lapin ensemble, je vous aime fort.

F·R·I·E·N·D·S

It would not have been possible to accomplish this work without the support, guidance and kindness that I've received from many special people. Indeed, when I moved from Paris to Lille, I did not just meet new colleagues but also amazing friends:

Monica, I'll start with you, my "lab wife", thank you for being an extraordinary friend, a shoulder to cry on and a positive soul pushing me forward. Your kindness has no limit, so just thank you for everything you taught me, for our endless passionate discussions and laughter moments while mounting brains and listening to Rosalia. I cannot imagine how I would have survived without you around amor mio, meeting you was a blessing.

Samuel, the "golden boy", you are one of the smartest and funniest guys that I have ever met, you continue to amaze me every day. You have been a big brother and an adorable friend to me all those years, I will never forget your love and support since I arrived.. I don't want this paragraph to end because I have so much to say but I'm already crying, so just know that I hope that you are happy in Oxford,but the lab is not the same without you and that even if you left an empty desk few months ago your place in my heart is only getting bigggeeeeer (I bet that Moni is laughing reading this: jajaja) Thank you always having my back and for all the souvenirs that we created together my dear.

Mary, Meri Jaan, my twinsie, I feel so lucky to have you in my life, you are the Christina to my Meredith or vis versa, you have lightened up my life with your tenderness and support, this work would have not been accomplished without you. Thank you for everything, from our sleepless nights discussing "life" with a hot chocolate and a blanket, our midnight walks in Paris, our 10pm western blots revelation to our crepes on that bench in Luxembourg. This year have been the toughest year for both of us which means that after the rain there is always sunshine. You're an extraordinary bestie and I love you dearly. Bisous to my dear friend Morgan who have always been there.

Valerie or should I say future Dr. Leysen? 😀 we have started this PhD journey together, you are one of the sweetest people I know, your heart is pure gold. You are always there to help whom ever needs help. I know that you will have a bright future ahead of you and I believe in you. I will never forget the moments that we have spent together laughing, crying or both at the same time. I couldn't end this paragraph without sending some bisous to Bompa and Bomma wishing them a long healthy life <3

Giuli, my dear Giuili, you were one of the first people I have met in Lille and were so welcoming and kind (you even introduce me to the famous Quai du Wault) and you have been a great friend ever since, thank you for all our moments in and outside the lab, our shared passion for art had brought us even closer and I will treasure all those memories forever, " This is not a spoon sweetie!" "Not the eye"! I miss you so much already, I miss your singing in the lab and our incredible evenings.

Dani, my sweet Dani, I want to thank you for the bottom of my heart for your love, support and one of a kind hugs! You are a brilliant scientist and an amazing friend. Your positive energy is always

there, even when we leave the lab at crazy hours and on weekends, completely destroyed. Thank you to Chechito as well, I am happy to count you both among my dearest friends and I love you both so much.

Anne-laure, mon « Jean-Mi », je n'arrive même pas à imaginer comment j'aurais survécu toutes ces années de thèse sans ta présence. Rien que d'avoir nos bureaux côte à côte me remontait le moral en arrivant le matin, car je savais que nous allions travailler et rire ensemble. Tu es une personne formidable et tu comptes beaucoup pour moi. J'ai hâte de continuer à travailler avec toi et d'enchainer nos débats scientifiques.

Oh Maria, thank you, for your constant support since the very beginning and your kindness towards me, you are a very sensitive girl with a big heart, and I'm so happy that we have shared so many memories together from sharing the bench to your beautiful wedding in Spain. Much love and Besitos to Carlos as well.

Nadia, my adorable greek friend, Dr.No, Thank you for your constant support. I'm soooo thrilled that you are coming back to the lab soon, you brought so much love and laughter to my days and among all memories our crazy Eurovision nights are priceless and I'm looking forward to our new adventures, let's see how many stroke faces you are going to pull out this year Hahaha..

Mégane, My friend, qui a toujours été présente pour moi, je te remercie du fond du cœur pour ton soutien continu, tous nos moments de folie et nos karaokés en voiture Hahahaha ! Tu ne cesses de me faire rire et de m'étonner. Je te souhaite beaucoup de succès.

Mauro, I'm happy that you have joined the lab and to be working with you. The more I get to know you the more I feel close to you. You became one of my closest friends here in Lille and I cannot wait for our trip to Brazil together. PS: Maybe we can make our own version of the horror movie "ça" and call it the "unborn fetus", what do you think?! Allez, I laaave you puppy! Bisous Bisous

Maëliss, je te remercie pour tes précieux conseils et pour tous les moments passés ensemble, je suis si heureuse que tu fasses partie de l'équipe et j'ai l'impression de te connaitre depuis longtemps. Même si je ne sais pas comment tu peux rester Zen malgré ton emploi du temps de folie, mais je sais que tu es une amie formidable avec qui je peux discuter de sciences comme de philosophie de la vie et j'ai hâte de continuer à travailler ensemble en restant motivées grâce à nos Ted talk. Team Placenta !! Gros bisous à Tristan et notre petit Gaspard, la vedette du labo !

Mon Gaëtano, saches que je t'ai toujours considéré comme mon petit frère et je serai toujours là pour toi. Merci pour ton soutien, c'est toujours vers toi que je me tourne quand j'ai besoin d'aide, et tu trouves toujours le temps pour m'apporter ton aide (même si la solution est parfois simple, comme fermer toutes les fenêtres de Firefox..).

Manon, future Dr. Duquenne, Je te remercie pour ton soutien et nos moments nostalgiques à chanter du Cabrel ou de l'Aznavour, alors je termine ce paragraphe en chantant : ♫ ♫ La thèse c'est fini, et

dire que c'était la ville de mon premier amour ♫ ♫ ♫ Allez, plus que quelques semaines et nous chanterons ce remix ensemble, lol ! je te souhaite énormément de succès et de réussite.

Sara, Che carina ! I will never forget all the tears and laughter we have shared, nor our "creative" time in behavior testing trying to figure out how to place the cameras and synchronize the tasks. Grazie Mille for always believing in me and supporting me and most importantly thank you for always having chocolate to share. You are a very sweet person and I hope that you are enjoying Japan and I wish you all the best.

Brooke, I hope that you are happy no matter where you are, and that you are following your dreams. You were the one starting this ambitious project with Paolo, and I'm grateful for everything you taught me.

Sarah et Emilie, je vous remercie sincèrement pour votre précieuse aide et vos conseils bienveillants, vous êtes un exemple d'équilibre de vie professionnelle et personnelle, je vous adore!

Marion, tu es une fille géniale, et je te souhaite beaucoup de réussite, je te remercie pour tous tes gestes attentionnés et ta gentillesse. Et surtout pour la merveilleuse collection de sucre que tu m'apportes à chaque fois, tu sais à quel point ça me rend heureuse 😁

Vicky, C'est fantastiiiiiiique ! you are a sweetheart and I love you.

Elenoraaaaaa, my twin, I'm thrilled that your are staying for your PhD, I cannot wait for our adventures to come. Never change you are special !

Anne Loyens et Daniele Mazur (Mère Noël et Dani-Chou) merci mille fois pour vos conseils, vos encouragements et votre soutien pendants ces années.

Kévin et Mégane, la thèse ça crée des liens.. Et oui ! nos chemins se sont croisés il y'a trois ans maintenant, et je tenais à vous remercier pour votre immense soutien, j'espère que les moments de stress vont bientôt passer et que nous allons finalement goûter à un peu de tranquillité, du moins pour quelques semaines.. Je vous souhaite à tous les deux beaucoup de succès.

Cécile, Pallavi, Sreekala, Romain, Ines, Virginia, Florent, Tori thank you for your indescribable kindness and companionship.

Dr. Sébastien Annicotte, Cyril, Chacha et Fred, je suis si heureuse de collaborer avec une équipe aussi dynamique et agréable que la votre et j'ai vraiment hâte de continuer avec vous.

Ahmed et Daniel, je te remerce chaleureusement pour les moments agréables que j'ai passé au sein de votre équipe à l'institut Cochin où j'ai beaucoup appris. Je vous suis reconnaissante pour tout !

Isabel, my sweet Isabel, thank you for your precious help and kindness, you are adorable <3

I. Publications

- *"Prenatal exposure to anti-müllerian hormone reprograms the fetus and induces polycystic ovary syndrome (PCOS) in adulthood"*

Brooke Tata*, **Nour El Houda Mimouni** *, Anne-Laure Barbotin, Samuel A. Malone, Anne Loyens, Pascal Pigny, Didier Dewailly, Sophie Catteau-Jonard, Inger Sundström-Poromaa, Terhi T. Piltonen, Federica Dal Bello, Claudio Medana, Vincent Prevot, Jerome Clasadonte and Paolo Giacobini. (*Nature Medicine 2018).*

- *"Defective Anti-Müllerian Hormone Signalling Disrupts GnRH Neuron Development and Underlies Congenital Hypogonadotropic Hypogonadism"*

Samuel A. Malone, Georgios E. Papadakis, Andrea Messina**, Nour El Houda Mimouni**, Sara Trova, Monica Imbernon Cécile Allet, Irene Cimino, James S. Acierno, Daniele Cassatella, Cheng Xu, Richard Quinton, Gabor Szinnai, Pascal Pigny, Lur Alonso-Cotchico, Laura Masgrau, Jean-Didier Maréchal, Vincent Prevot, Nelly Pitteloud and Paolo Giacobini (*eLife 2019).*

- *"Development of Metabolic Disturbances in a Mouse Model of Polycystic Ovary Syndrome"*

Nour El Houda Mimouni, Emilie Caron, Monica Imbernon ,Cyril Bourouh, Mauro Silva, Gaëtan Ternier, Jean Sébastien Annicotte, Vincent Prévot and Paolo Giacobini *(In preparation).*

- *"Prenatal AMH exposure induces a transgenerational transmission of the PCOS-like phenotype across multiple generations in rodents"*

Nour El Houda Mimouni, Anne-Laure Barbotin, Isabel Paiva, Anne-Laurence Boutiller, Vincent Prévot and Paolo Giacobini *(In preparation).*

- *"Plasticity of the hypothalamus in PCOS"*

AL. Barbotin, G. Kuchinski, **NEH Mimouni**, S. Jonard, D. Mazur, PV. Simon Jissendi , V. Prevot, V. Mitchell, D. Dewailly, P. Giacobini *(In preparation).*

- *"Developmental programing with Anti-Müllerian Hormone (AMH) promotes sexual dysfunction in a preclinical mouse model of PCOS"*

Silva. MSB, Trova. S, **Mimouni. NEH**, Boehm. U, Prevot. V. & Giacobini. P. *(In preparation).*

II. Meetings:

- **NeuroFrance colloque, May 2019, Marseille.** *" Prenatal exposure to Anti-Mullerian Hormone reprograms the fetal brain and induces a complex neuroendocrine and metabolic PCOS-like phenotype in rodents"*

- **Journée thématique Society of Neuroendocrinolgy (SNE) « Intercellular Communication via Extracellular Vesicle » September 2018- Paris** *"Prenatal exposure to anti-müllerian hormone reprograms the fetus and induces polycystic ovary syndrome (PCOS) in adulthood"*
- **Journée André Verbert, September 2018- Lille** *"Postnatal treatment with GnRH antagonist in a new PCOS mouse model rescues the neuroendocrine phenotype"*
- **1st EUCRE conference, March 2018- Prato, Italy** *"Polycystic ovary syndrome neuroendocrine defects are transferred forward to multiple generations"*
- **JPARC PhD Day 2018, Jean Pierre Aubert Research Center, March 2018-Lille** "*Exploring the role of the anti-Müllerian hormone in the development and function of GnRH neurons: Implication in the Polycystic ovary syndrom (PCOS) ?"*
- **Colloque Société de Neuroendocrinologie (SNE) Septembre 2017- Dijon.** *" Prenatal exposure to Anti-Mullerian Hormone reprograms the fetal brain and induces PCOS-like traits in adulthood"*
- **21st Annuel LARC- Neuroscience Meeting, Octobre 2017- Lille.** "*Exploring the role of the anti-Müllerian hormone in the development and function of GnRH neurons: Implication in the Polycystic ovary syndrome (PCOS)?"*
- **Hellenic Society for Neuroscience (HSfN) Meeting, December 2017, Athens-Greece.** "*Postnatal treatment with GnRH antagonist in a new PCOS mouse model rescues the neuroendocrine phenotype"*
- **NeuroFrance colloque, May 2017, Bordeaux.** *" Prenatal exposure to Anti-Mullerian Hormone reprograms the fetal brain and induces PCOS-like traits in adulthood"*
- **JPARC PhD Day 2017, Jean Pierre Aubert Research Center, March 2017- "***Cartography of Anti-Müllerian Hormone expression in mice* **"**

III. Trainings

- Training in animal experimentation.
- Specific training for surgical experimental procedures.
- Lifeguard rescuer at workplace.

Table of contents

Figures & Tables

Supplementary data

Chapter 6

Abstract

Polycystic ovary syndrome (PCOS) is the main cause of female infertility worldwide with high comorbidity and economic burden. It is mainly characterized by hyperandrogenism, oligo/anovulation and polycystic appearing ovaries. Moreover, most women with PCOS exhibit higher levels of circulating luteinizing hormone (LH), suggestive of heightened gonadotropin-releasing hormone (GnRH) release. Additionally, PCOS patients also exhibit 2-3x higher levels of Anti-Müllerian Hormone (AMH) as compared to healthy controls.
While the exact origin of PCOS is unknown, familiar clustering and twin studies of PCOS patients and their relatives suggest a strong heritable component in PCOS. However, the candidate genes identified account for only <10% of the estimated 70% heritability of PCOS, implying that it may originate during intrauterine development and that environmental factors, such as hormonal imbalances during fetal life, could be involved in the onset of PCOS.

In this study, we first measured AMH levels in a cohort of pregnant women with PCOS and control women which revealed that AMH is significantly more elevated in the former group versus the latter, we then modelized our clinical findings by exposing pregnant mice to high concentration of AMH during a specific temporal window and showed that this fetal exposure leads to a cascade of alterations impacting the maternal brain, the ovaries, and the placenta, which consequently reprogram the fetal brain and induce the acquisition of the major PCOS cardinal neuroendocrine reproductive features, namely hyperandrogenism, elevation in LH pulse frequency and oligo-anovulation, and a persistent rise in the GnRH neuronal firing activity in adulthood. Moreover, our results show that the long-term consequences of a short exposure to elevated AMH levels during gestation expand beyond the first generation exposed and that PCOS-like manifestations seem to be transmitted across subsequent generations of females.
Intrestingly, using a pharmacological approach, we demonstrate that tempering GnRH signaling pathway rescues the neuroendocrine phenotype of PCOS-like animals, restoring their normal hormonal levels, estrus cyclicity and ovarian morphology.

Lastly, we sought to understand how early exposure to AMH excess would affect the neuroendocrine and reproductive features of the male offspring. Here, we demonstrate that prenatal AMH treatment profoundly impacts the Hypothalamic-Pituitary-Gonadal (HPG) axis function in males, which fail to engage the testosterone surge at birth observed in control newborns, leading to a feminization of sexually dimorphic circuitries of their brains, an increase in LH, a drastic decrease in testosterone levels, severe alterations in the testicular steroidogenesis and morphology as well as a higher risk of developing cryptorchidism in adulthood. Thus, it could be of clinical interest to relate findings from this study to the reproductive phenotype of sons of PCOS women, who are exposed during gestation but not systematically investigated in adulthood.

Collectively, our results challenge the concept of PCOS originating *in utero* and appear to consolidate the role of AMH as a trigger of the pathogenesis, suggesting that an altered hormonal milieu during early life associated with PCOS may not only affect the female fetus but also the male fetus exposed and that these alterations could be transmitted across multiple generations.
These findings point to PAMH mouse model as an excellent preclinical tool to investigate both neuroendocrine disturbances of PCOS and how developmental programming effects are transmitted, while offering a therapeutic avenue for the treatment of the disease.

Key words: PCOS, Fetal programming, AMH, GnRH, transgenerational transmission.

Résumé

Le syndrome des ovaires polykystiques (SOPK) est la principale cause d'infertilité feminine à travers le monde, associé à un risqué élevé de comorbidités avec des conséquences économiques non négligeables. Ce syndrome est caractérisé par une oligo-anovulation, une hyperandrogénie, et un aspect échographique d'ovaires polykystiques. De plus, la plupart des femmes atteintes de SOPK présentent des concentrations élevées de LH suggérant une libération accrue de GnRH. De plus, les patientes SOPK ont habituellement des concentrations en Hormone Anti Müllerienne (AMH) 2 à 3 fois plus élevés que les femmes non atteintes.

Alors que l'origine exacte du SOPK demeure inconnue, des études de clustering familial et portant sur des jumeaux ou des ascendants de femmes atteintes du SOPK ont mis en évidence une forte composante héréditaire. Cependant, les gènes candidats identifiés n'expliquent qu'à peine 10% des cas de SOPK suggérant qu'une origine développementale et que des facteurs environnementaux tels que des modifications hormonales durant la vie fœtale pourrait être à l'origine du SOPK.

Dans cette étude, nous avons d'abord comparé les concentrations d'AMH dans un groupe de femmes atteintes de SOPK et chez des femmes témoins pendant la grossesse. Les concentrations d'AMH se sont révélées significativement plus élevées chez les SOPK par rapport aux témoins. Nous avons ensuite utilisé ces résultats cliniques pour développer un modèle animal murin de SOPK en exposant les souris gestantes à une concentration élevée d'AMH au cours d'une fenêtre temporelle spécifique. Nous avons montré que cette exposition fœtale conduisait à une cascade d'altérations affectant le cerveau maternel, les ovaires et le placenta, entrainant une reprogrammation du cerveau fœtal et induisant l'acquisition des principaux critères diagnostiques retrouvés dans le SOPK, à savoir l'hyperandrogénie, l'augmentation de la pulsalitié de la LH et de l'oligo-anovulation, ainsi qu'une augmentation persistante de l'activité électrique de la GnRH à l'âge adulte. De plus, nos résultats montrent que les conséquences à long terme d'une exposition courte à des niveaux élevés d'AMH pendant la gestation s'étendent au-delà de la première génération exposée et que les manifestations de type SOPK semblent être transmises d'une génération à l'autre chez les femelles.

De manière intéressante, en utilisant une approche pharmacologique, nous avons démontré que l'inhibition partielle de la voie de signalisation de la GnRH permettait de restaurer chez les animaux SOPK un phénotype neuroendocrinien normal, en rétablissant des concentrations hormonales normales, la cyclicité œstrale et leur morphologie ovarienne.

Enfin, nous avons cherché à comprendre comment une exposition précoce à un excès d'AMH affecterait les caractéristiques neuroendocriennes et reproductives de la progéniture mâle. Ici, nous avons démontré que le traitement par AMH en période prénatale modifiait la fonction de l'axe hypothalamo-hypophyso-gonadique (HPG) chez les mâles, qui ne parviennent pas à engager le pic de testostérone néonatal normalement observé chez les nouveau-nés mâles témoins, conduisant à une féminisation des circuits sexuellement dimorphiques cérébraux, à une augmentation de la LH, et finalement à une diminution drastique des niveaux de testostérone à

l'âge adulte, à des altérations sévères de la stéroïdogenèse et de la spermatogenèse ainsi qu'à un risque plus élevé de développer une cryptorchidie à l'âge adulte. Ainsi, il pourrait être intéressant de relier les résultats de cette étude au phénotype reproductif des garçons de femmes atteintes du SOPK, qui ont été exposés pendant la grossesse mais qui ne sont habituellement pas suivis plus tard à l'âge adulte.

Ensemble, ces résultats mettent en lumière l'origine *in utero* du de SOPK et semblent consolider le rôle prépondérant de l'AMH dans la physiopathologie du SOPK en tant qu'élément déclencheur. Il suggère également que des modifications hormonales survenant précocement Durant la vie intra-utérine peuvent affecter non seulement le fœtus féminin mais aussi le fœtus mâle et que ces altérations pourraient être transmises sur plusieurs générations.

Ces résultats indiquent que le modèle préclinique de souris PAMH est un excellent outil pour étudier à la fois les perturbations neuroendocriniennes du SOPK et la reprogrammation fœtale tout en offrant une piste thérapeutique afin d'améliorer la prise en charge des patientes atteintes.

Mots clés: SOPK, reprogrammation fœtale, AMH, GnRH, transmission transgénérationnelle.

Abbreviations

AC: Anterior Commissure

ACTH: adrenocorticotrophic hormone.

AGD: Ano-genital distance

AHA: Anterior hypothalamic area.

AMH: Anti-Müllerian Hormone

AVPV: Anteroventral periventricular nucleus

BMI: Body Mass Index.

BMP: Bone Morphogenic Protein

CAH: Congenital Adrenal Hyperplasia.

CC: Corpus Callosum.

CHH: Congenital hypogonadotropic hypogonadism.

CNS: Central Nervous System

DAX1: Dosage sensitive sex reversal, adrenal hypoplasia critical region, on chromosome X, gene 1

DHEAS: dehydroepiandrosterone sulfate

DHT: dihydrotestetrone

EGFR: epidermal growth factor receptor

E2: Estradiol

FAI: Free Androgen Index

FSH: Follicle stimulating hormone

FSH-R: Follicle stimulating hormone Receptor

FX: Fornix

GABA: Gamma aminobutyric acid

GC: Granulosa cells

GDF: Growth and Differentiation Factors

GnRH: Gonadotropin Releasing Hormone

GPCR: G protein-coupled receptor superfamily

GWAS: Genome-wide association study

HA: Hyperandrogenism

HCG: Human chorionic gonadotropin

HH: hypogonadotropic hypogonadism

HPG: Hypothalamic-Pituitary-Gonadal axis

IGFBP-1: insulin-like growth factor bindingprotein-1

INSL3: Insulin Like factor 3

KS: Kallmann syndrome

LH: Luteinizing hormone

LHR: Luteinizing hormone Receptor

ME: Median Eminence

MIS: Müllerian inhibiting substance

MS: Medial septum

NIH: National Institute of Health

NKB: Neurokinin B

nNOS: Neuronal nitric oxide synthase

OVLT: Organum Vasculosum of the Lamina Terminalis

PAMH: Prenatal AMH treatement

PCOS: Polycystic Ovary Syndrome

SCN: Suprahiasmatic Nucleus

SF-1: Steroidogenic Factor-1

SHBG: Sex Hormone-Binding Globulin

SOX9: SRY-related homolog box protein 9

SRY: Sex determining region on Y

StAR: Steroidogenic acute regulatory protein

TGFβ: Transforming growth factor beta

THADA: Thyroid adenoma associated

WT1: Wilms' tumour suppressor-1

"I am among those who think that science has great beauty. A scientist in his laboratory is not only a technician: he is also a child placed before natural phenomena which impress him like a fairy tale.."

- *Marie Curie*

Chapter 1

Hypothalamic- Pituitary- Gonadal axis

Hypothalamus - Pituitary - Gonads

Chapter One

1.1 Introduction

In 1973, Geoffrey Harris, a medical student, was the first to discover that the pituitary-gonadal axis is controlled by the central nervous system (CNS) (Fink 2015). Gonadotropin-releasing hormone (GnRH), a decapeptide, was isolated as the hypothalamic substance that regulates the synthesis and secretion of gonadotropins: Luteinizing Hormone (LH) and Follicle Stimulating Hormone (FSH), through the hypophysial portal circulation (Schally, Arimura et al. 1971).

1.1.1 Hypothalamus

"Les apparences sont trompeuses" is a French expression that I would apply to describe the hypothalamus, which, despite its small size in the brain, it is the most important integrator of vegetative and endocrine systems of the body. It is located under the thalamus and above the pituitary, which is connected to it by a stem, the pituitary stalk.

The hypothalamus controls diverse processes such as: Energy homeostasis, reproduction, sleep and circadian rhythms through various populations of specialized neurons are present in the hypothalamus. (Burbridge, Stewart et al. 2016), (Elmquist, Coppari et al. 2005). Among the hypothalamic neuronal populations are the Gonadotropin Releasing Hormone neurons which meticulously control the reproductive function in many species.

1.1.2 GnRH neurons

GnRH cells act as integrators of metabolic and reproductive signals, which come from both the central and the peripheral nervous system. They are considered the main orchestrators of the physiological events initiated from the hypothalamic region **(Figure 1)**. Their proper development, expression, and signaling is essential for sexual maturation and the normal functioning of the HPG axis in mammals (Cattanach, Iddon et al. 1977), (Mason, Hayflick et al. 1986), (Prevot 2011).

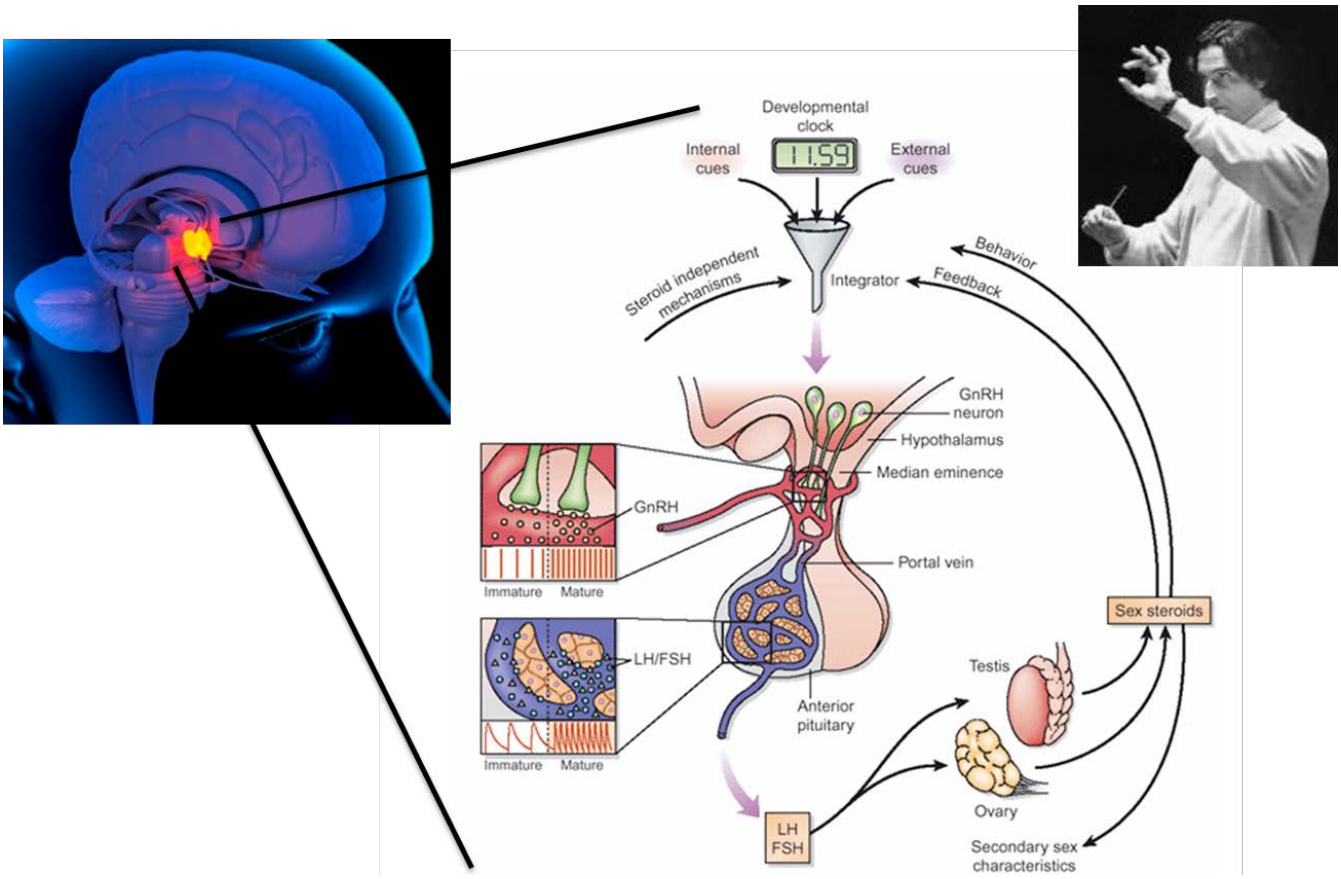

Figure 1: Hypothalamic-Pituitary-Gonadal axis (Sisk and Foster 2004)

1.1.3 Embryonic development and anatomical distribution of GnRH neurons

Unlike other neuronal populations, GnRH neurons are born outside the brain, they have the particularity to migrate during development, from the medial olfactory placode of developing nasal cavity through the nasal septum, along with vomeronasal axons and enter the forebrain with the nervus terminalis entering into the septal-preoptic area and hypothalamus (Schwanzel-Fukuda and Pfaff 1989), (Yoshida, Tobet et al. 1995, Casoni, Malone et al. 2016). In humans there are 1000-1500 GnRH neurons. A GnRH neuron in adults is composed of two denritic projections, extending a distance of 2-3 mm from their cell body. GnRH is released into capillaries of the hypophysial portal system and reaches the anterior pituitary gland and modulates its gonadotropin synthesis and secretion. If GnRH neurons fail to migrate in a proper manner, this would result in a hypogonadotropic hypogonadism (HH) and disrupts sexual maturation and altered fertility in mice and men (Wierman, Kiseljak-Vassiliades et al. 2011), (Malone, Papadakis et al. 2019).

It is well established that GnRH migration is modulated by various molecules. Indeed, following guidance cues given by extracellular molecules, receptor tyrosine kinases, chemokines and a series of neurotransmitters among others (Wray 2010), GnRH neurons migrate toward the forebrain (Tobet and Schwarting 2006, Wierman, Kiseljak-Vassiliades et al. 2011, Casoni, Malone et al. 2016) and subsequently continue the migration ventrally, along a branch of the vomeronasal nerve to reach the basal forebrain. Eventually, at postnatal day 0, GnRH neurons reach the hypothalamus, their final destination.

During postnatal development, GnRH neurons are subjected to a series of complex maturational events involving their morphological characteristics, neurosecretory pattern, and overall neuronal activity.

In females, during neonatal period, primordial follicles, which are present at postnatal day 7, develop into secondary follicles. At this stage, it is improbable that LH and FSH would exert direct actions on primordial follicles as functional gonadotropin receptors haven't developed yet (O'Shaughnessy, McLelland et al. 1997). Furthermore, in 1992 Rajah et al., showed that P7 GnRH deficient hypogonadal mice appear to have normal follicular development, thus, folliculogenesis does not require GnRH or LH/FSH development at this stage.

During the infantile period, a series of endocrine events stimulate the development of the pool of secondary follicles into preantral and antral follicles (McGee, Perlas et al. 1997) now responsive to FSH (O'Shaughnessy, McLelland et al. 1997).The surge of FSH at P12 is the first activation of the GnRH system and is required for proper maturation of the preantral follicles into antral follicles (McGee, Perlas et al. 1997); (McGee and Hsueh 2000)Small bursts of secretion of LH are noticed; however, they remain low and do not participate in the ovarian development during this stage (Dohler and Wuttke 1974, Zhang, Poutanen et al. 2001).

As the juvenile stage begin and infantile period comes to an end, FSH levels decrease while LH levels remain low. When juvenile stage nears its end, preovulatory levels of estradiol (E2) significantly increase to reach a peak around postnatal day 30 (Andrews, Mizejewski et al. 1981, Devillers, Petit et al. 2019) This increase in estradiol levels stimulates LH secretion, which acquires a particularly accelerated pulsatile pattern (Kimura and Kawakami 1982). This phenomenon is believed to involve

GnRH activation, evident by the increased GnRH pulse frequency occurring during the juvenile period (Sarkar and Fink 1979).

1.2 GnRH pulsatile secretion

Once the GnRH neurons have completed their migration to the hypothalamus during embryogenisis, secretion of GnRH by the hypothalamus increases in early postnatal life, leading to temporary activation of gonadal steroidogenesis, especially in males. Before the onset of puberty, the pulsatile GnRH release is suppressed which results in gonads remaining quiescent until the onset of puberty. This is when they respond to exogenous gonadotropin stimulation after re-awakening of pulsalite GnRH release.

GnRH secretion follows two modes: pulsatile and surge (Maeda, Ohkura et al. 2010)The surge mode occurs only in females. Pulsatile mode was first demonstrated in ovariectomised rhesus monkeys (Antunes, Carmel et al. 1978). This mode is the episodic release of GnRH, showing distinct pulses of GnRH secretion into circulation, with undetectable GnRH concentrations during inter-pulse intervals (Herbison 2018).

The activity of GnRH neurons is tightly coordinated, as they possess intrinsic electrical activity, dependent on intracellular signaling and mechanisms. The "GnRH pulse generator" is suggested to be located at the medial basal hypothalamus as the episodic multi-unit electric activity generates from there (Wilson, Kesner et al. 1984) and it relies on complex relations between neurons containing norepinephrine, dopamine, gamma aminobutyric acid (GABA) to state some. Glutamate and norepinephrine are stimulators of the reproductive axis, while GABA is an inhibitor. Regulation of GnRH pulsality is partly mediated by the Kisspeptin- Neurokinin B (NKB) -opioid pathway, by a mechanism whereby NKB and dynorphin act autosynaptically on kisspeptin neurons in the arcuate nucleus to synchronize and shape the pulsatile secretion of kisspeptin and drive the release of GnRH from fibers in the median eminence.(Navarro, Gottsch et al. 2009), (Ruka, Burger et al. 2013, Ezzat, Pereira et al. 2015) with which they colocalize (Kallo, Vida et al. 2012). The population of neuronal nitric oxide synthase (nNOS) neurons has also been shown to play a crucial role in the regulation of the GnRH system (Chachlaki, Malone et al. 2017)

1.3 GnRH receptors

The GnRH receptor is a member of the rhodopsin-like G protein-coupled receptor superfamily (GPCR). It is characterized by seven-transmembrane domain structure. In mammalian GnRH receptor, the cytoplasmic C-terminal tail is absent (Cheng and Leung 2005) which is present in non-mammalian GnRH receptors (Lethimonier, Madigou et al. 2004) . The human *GnRH* receptor gene is found on chromosome 4 and it consists of three exons separated by two introns (Kakar 1997). GnRH receptors and splice variants have been discovered in human pituitary and pituitary adenomas (Grosse, Schoneberg et al. 1997). The GnRH receptor has also been identified in the ovarian cancer cell lines, endometrial carcinoma cell lines, liver, heart, muscle, kidney, peripheral mononuclear cells, human corpus luteum, luteinized granulosa cells, melanoma, breast carcinoma and syncytiotrophoblast cell layers of human placenta (Cheng and Leung 2002). Another study has shown that GnRH and GnRH receptor mRNA are present in human testicular tissue (Bahk, Hyun et al. 1995).

GnRH regulates the expression of GnRH receptor in the pituitary. Decline in GnRH stimulation results in decline of GnRH receptors on pituitary gonadotrophs but subsequent exposure of the pituitary to GnRH restores the levels of receptors. This upregulation is differentially controlled by varying GnRH pulse frequencies and varies among species (Tsutsumi, Laws et al. 1995). In human ovarian cancer and peripheral blood mononuclear cells, GnRH performs a biphasic effect on GnRH receptor expression (Chen, Jeung et al. 1999, Kang, Choi et al. 2000). In contrast, GnRH receptor expression is downregulated with continuous exposure to GnRH, resulting in inhibition of LH and FSH synthesis and secretion.

GnRH receptor is suppressed by estradiol in the pituitary and extrapituitary tissues (Quinones-Jenab, Jenab et al. 1996, Cheng, Chow et al. 2003). Likewise, progesterone inhibits GnRH receptor expression in the pituitary (Laws, Beggs et al. 1990). On the other hand, activin stimulates GnRH receptor synthesis (Fernandez-Vazquez, Kaiser et al. 1996). Additionally, it was also discovered in rat testes that human chorionic gonadotropin (HCG) downregulates the GnRH receptor (Botte, Lerrant et al. 1999)but increases GnRH receptor gene transcription in choriocarcinoma JEG-3 cells (Cheng and Leung 2002); Thus, indicating a tissue specific effect.

It is important to highlight that the mutations of the GnRH receptor gene lead to idiopathic hypogonadotropic hypogonadism (HH) which is a rare disorder of sexual maturation characterized by gonadotropin deficiency with low sex steroid levels associated with low levels of FSH and LH (Topaloglu and Kotan 2016).

1.4 Gonadotropins

As mentioned above GnRH stimulates the synthesis and secretion of FSH and LH. These gonadotropins are heterodimeric glycoprotein hormones which act on gonads, i.e., ovaries and testes to control ovarian and testicular functions, respectively. In males, a high GnRH pulse induces secretion of LH (Constantin 2011)which in turn stimulates testosterone production of Leydig cells and plays a role in the maintenance of spermatogenesis through its paracrine action on Sertoli cells. Low pulse frequency promotes secretion of FSH. Before the onset of puberty, FSH stimulates Sertoli cell proliferation, defines the size of their population, the size of the testes and the quantity of spermatogenesis (Sharpe, McKinnell et al. 2003). Hence, the main action of FSH is, alongside testosterone, the augmentation of the sperm production (Huhtaniemi 2015). During the same time frame (prior to puberty), a plethora of inhibitory input is sent to GnRH neurons, allowing them to release very low concentrations of the GnRH peptide in the pituitary. Later during development, the increase in the GnRH pulsatile release from the hypothalamus is stimulated by a combination of excitatory and inhibitory inputs. This process is critical for the initiation of puberty (Plant 2015).

1.5 Establishment of GnRH afferent neuronal connections – the creation of a GnRH network

GnRH neuronal projections are already in place at birth, however, a mature neuronal network has yet to be formed. During the first 3 weeks of postnatal development, GnRH neuronal projections seem to continue to develop (Buchanan and Yellon 1993), (Heywood and Yellon 1997). By the second week of postnatal development, the axons of neurons that reside in the ARH have been evidenced to reach GnRH neuronal soma and they continue to expand throughout the infantile period (Bouret, Draper et al. 2004), (Caron, Ciofi et al. 2012). The maturation of ARH neuronal

projections coincides with the activation of the GnRH axis and simultaneous increase in circulating levels of FSH is observed at postnatal day 12 (Stiff, Bronson et al. 1974, Prevot, Rio et al. 2003). It is believed that the GnRH afferent connections received from the ARH axons contribute to the control of pulsatile GnRH release (Navarro, Gottsch et al. 2009),(Ruka, Burger et al. 2013, Ezzat, Pereira et al. 2015).Moreover, some studies have also raised the intriguing possibility that these ARH fibers could mediate the maturation of the gonadal negative feedback action on the GnRH system (Caron, Ciofi et al. 2012). Postnatally, along with ARH neuronal projections, other synaptic inputs are also established, such as ventromedial (VMH) and dorsomedial (DMG) hypothalamic areas **(Figure 2)** (Bouret, Draper et al. 2004).

Anteroventral and periventricular nucleus (AVPV) neurons have already established their projections to the GnRH neuronal soma in the preoptic area (POA) at birth. They are known to mediate gonadal positive feedback (Polston and Simerly 2006). It should be noted that during infantile period, synaptogenesis events are taking place which format the synaptic density and the number of dendritic spines of the GnRH neuronal population (Campbell, Han et al. 2005), (Cottrell, Campbell et al. 2006).

All of the events mentioned above certainly play an important role in the overall maturation of the GnRH neurons and their neuronal network, setting in motion the establishment of a mature and fully functional GnRH system that will orchestrate the initiation of puberty.

(i)

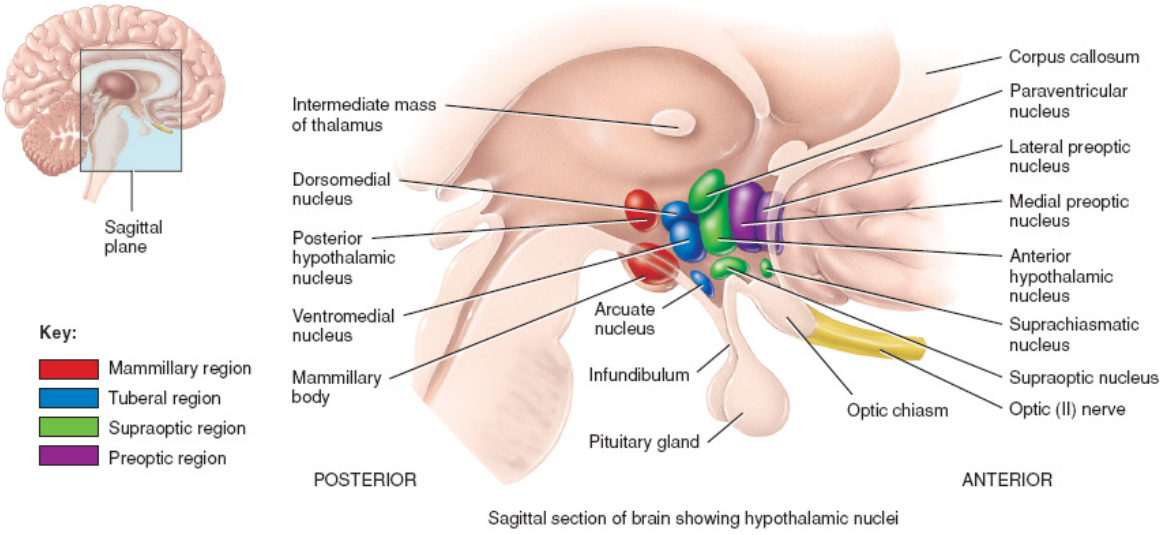

Sagittal section of brain showing hypothalamic nuclei

(ii)

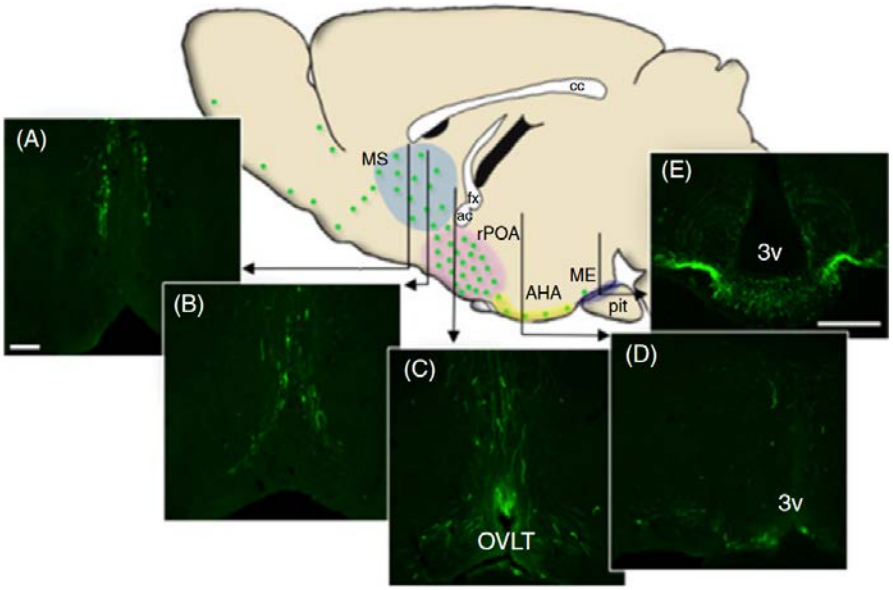

Figure 2: GnRH neurons distribution in the hypothalamus

(i) Schematic representation of the hypothalamic nuclei and **(ii)** GnRH distribution in the mouse brain. The GnRH neurons (Green) are found in a scattered distribution throughout the hypothalamus in **(A,B)** medial septum :MS ; **(C)** organum vasculosum of the lamina terminalis: OVLT ; **(D)** anterior hypothalamic area: AHA. GnRH neurons extend to the hypophysal portal vessels through **(E)** Median Eminence: ME to secrete the GnRH peptide in the pituitary. Scale bar= 100µm; fx: fornix, ac: anterior commissure, cc: corpus callosum. Figure adapted from (Campbell 2018)

1.6 Positive and negative feedbacks into the GnRH system

The secretion of estrogen occurs in the gonads during steroidogenesis, estrogen exert a dual effect on the hypothalamic GnRH secretion. During follicular phase, rising plasma estradiol levels result in a positive feedback action upon the GnRH network to stimulate the gonadotropin surge. However, during later stages of the cycle, estradiol suppresses GnRH secretion by exerting its negative feedback effect on the hypothalamic axis (Radovick, Levine et al. 2012) The surge of LH is induced when significantly high estrogen levels arrive in the hypothalamus during the preovulatory period (Christian and Moenter 2010). These high estradiol signals are responsible for the activation of GnRH neurons and consequently the secretion of GnRH peptide. This initiates a chain reaction that will eventually trigger ovulation (Moenter, Caraty et al. 1991). This stimulatory action of estrogen consists the "positive gonadal feedback", occurring during the late follicular phase in humans and in the afternoon of proestrus in rodents and (Herbison 1998), (Simerly 2002). The regions where this positive feedback takes place are following: anteroventral AVPV, preoptic area, and suprachiasmatic nucleus (SCN) (Radovick, Levine et al. 2012). A number of studies suggest that neurons that express the estrogen Receptor (ER-α) of the above region send direct inputs onto GnRH neurons which do not possess the ER-α to mediate the estrogenic positive feedback action. Kisspeptin neurons are believed to be one of these neuronal populations that are able to integrate positive estrogenic signals (Adachi, Yamada et al. 2007), (Clarkson, d'Anglemont de Tassigny et al. 2008, Mayer, Acosta-Martinez et al. 2010). Estrogen plasma levels, during the estrous cycle, inhibit GnRH secretion and maintain GnRH neuronal pulse in low frequency levels (Levine 1997); (Herbison 1998). It is still unclear through which mechanisms estradiol promotes its "negative feedback" action to retain GnRH pulse frequency and amplitude but there are propositions that it involves ER-α- containing neurons of the arcuate nucleus (AHN), as well as the ER-β-expressing neurons (Wersinger, Haisenleder et al. 1999), (Kwakowsky, Herbison et al. 2012).

The GnRH system is a complex, yet elegantly coordinated network. Hence, alterations in the migratory process or in the peptide secretion evoke heavy consequences on the reproductive function and eventually lead to some of the major reproductive disorders in humans:

- Congenital hypogonadotropic hypogonadism (CHH), a condition characterized by failure of sexual competence.
- Kallmann syndrome (KS), characterized by a combination of hypogonadotropic hypogonadism and a deficiency of sense of smell.
- And finally, yet importantly, the Polycystic Ovary Syndrome (PCOS), a reproductive disorder in we which an alteration of GnRH secretion and pulsatility is reported among other symptoms. In contrast with the first two disorders characterized by GnRH deficiency, PCOS is characterized by accelerated GnRH/LH secretion.

The next chapter of this thesis will be thus dedicated to the pathophysiology of PCOS and its main clinical and biological manifestations.

Chapter 2

Polycystic ovary syndrome:

A complex disorder with multiple faces

Chapter Two

2 Polycystic ovary syndrome

2.1 History of the polycystic ovary syndrome

"Giovane rustica, maritata, modicamente pingue, et infeconda, con due ovaie più grandi del normale, come uova di colomba, bernoccolute, lucenti et biancastre…"

Antonio Vallisneri, 1721

The first case description of the Polycystic Ovary Syndrome (PCOS) was provided by the Italian scientist Antonio Vallisneri who reported in 1721: " A young peasant woman, married, moderately lump and infertile, with ovaries larger than normal, like doves´ eggs, lumpy, shiny and whitish… " Many years later, Stein and Leventhal published in 1935 the case of seven women suffering from amenorrhea, hirsutism and obesity along with a particular ovarian aspect, with a thick, white, pearly cortex and small follicles, they probably did not suspect that they were describing for the first time a disorder which is now known as one the most complex and prevalent reproductive disorder affecting women worldwide.

PCOS is heterogeneous endocrinopathy with widely varying clinical manifestations. There is no single criterion for the diagnosis of this syndrome. Traditionally, the PCOS diagnosis was based on the histological examination of bilateral ovaries in women presenting anovulation, hirsutism or both (Goldzieher and Green 1962). However, other co-morbidities such as a metabolic syndrome including diabetes mellitus type 2, and depression are also associated with PCOS (Azziz, Carmina et al. 2016).

Due to the variability of clinical manifestations (both the phenotypic and metabolic spectrum of PCOS patients), a concise and consensual definition has long been lacking and is still very much at the heart of the debate today.

The first formal attempt to consolidate a clinical definition of PCOS emerged in 1990, during a conference sponsored by the National Institute of Health (NIH), when the majority of practitioners recommended that diagnostic criteria should include evidence of hyperandrogenism (clinical or biochemical) and ovulatory dysfunction in the absence of non-classic congenital adrenal hyperplasia (CAH).

The second definition (Rotterdam) was presented in 2003 by the Fertility and Embryology Association of Europe and America Fertility Society in Rotterdam conference in 2003 and has considered two criteria from the following three criteria as parameters for diagnosis of PCOS after having dismissed the other causes of hyperandrogenism (Rotterdam ESHRE/ASRM-Sponsored PCOS consensus workshop group, 2004):

1. Oligo-ovulation or chronic anovulation;
2. Biological and/or clinical hyperandrogenism;

3. Presence of polycystic ovaries on pelvic ultrasound (more than 12 follicles measuring 2 to 9 mm and ovarian volume greater than 10 mm).

Since 2003, no group of experts has been able to redefine the diagnostic criteria of this pathology despite great efforts of experts and the evolution of biological assay or imaging techniques. However, thanks to international clinical expertise and considerable joint efforts, international guidelines and recommendations have been established to improve the management and assessment of PCOS patients (Teede, Misso et al. 2018).

2.2 Physiopathology of PCOS

PCOS is a heterogeneous of symptoms which, gathered together, form a spectrum of a disorder with a mild presentation in some cases and a severe disturbance of reproductive, endocrine and metabolic function in other cases. In this introduction we will first highlight the major features of PCOS endocrinopathy before reporting the additional heterogeneous manifestations of the disorder which are not included in the diagnostic criteria but can typically be seen in PCOS patients.

2.2.1 Oligo-ovulation or chronic anovulation

The total number of follicles is determined early in life. Normal follicle development comprises initial recruitment, by which primordial follicles start to mature, and cyclic recruitment, which leads to the growth of a cohort of small antral follicles from which the dominant follicle, destined to ovulate, is subsequently selected.

Disorders of ovulation account for about 30% of infertility and often present with irregular periods (oligomenorrhoea) or an absence of periods (amenorrhoea). Polycystic Ovary Syndrome (PCOS) is the most common cause of chorionic anovulation and anovulatory infertility (Wood, Dumesic et al. 2007, Dumont, Robin et al. 2015) and ovarian dysfunction continues to be the main feature which makes this syndrome the major cause of anovulatory associated with infertility (Hamilton-Fairley and Taylor 2003);

Menstrual disturbances in PCOS generally present in the form of oligo-amenorrhea (fewer than eight episodes of menstrual bleeding per year or menses that occur at intervals greater than 35 days), (Franks, Adams et al. 1985, Dewailly, Gronier et al. 2011, Fauser, Tarlatzis et al. 2012). Therefore, PCOS is classified as type II b in the international classification of ovarian dysfunction **(Table1).**

Type	I	II a	II b	III
	Hypogonadotropic hypogonadism	**Idiopathic**	**PCOS**	**Primary ovarian insufficiency**
Clinical	Amenorrhea or oligomenorrhea	Isolated Oligomenorrhea	Oligomenorrhea hirsutism	Short cycles +/- Oligomenorrhea
FSH	N or ↘	N	N	↗
LH	N or ↘	N	N or ↗	↗
Estradiol		N	N or ↗	↘ or ↗
Androgens	N or ↘	N	N or ↗	↘
AMH	N or ↘	N	↗	↘
Ultrasound scan	Variable	Normal	PCO	Oligo-ovulatory

N : Normal

Table 1: World Health Organization classification of ovarian dysfunctions in 1973.

2.2.2 Hyperandrogenism

Hyperandrogenism is defined as an excessive secretion of the masculine sex steroids: testosterone, dihydrotestosterone, and their prohormones dehydroepiandrosterone sulfate (DHEAS), and androstenedione, this massive production of androgens induces a series of serious clinical and biologicals manifestations.

It is well established that ovaries and adrenal glands are under control of luteinizing hormone and adrenocorticotrophic hormone (ACTH), respectively, and contribute to the synthesis of sex steroids (Handa and Weiser 2014).

The adrenal cortex synthesizes all the three major androgens; dehydroepiandrosterone sulfate, androstenedione and testosterone, and this is the other major site of male androgen production, besides the ovaries.

At puberty, the ovaries start to be active by synthesizing hormones (especially androgens) on one hand and proceed with folliculogenesis on the other hand.

Excessive production of ovarian androgens is a hallmark of polycystic ovarian syndrome and increased levels of circulating androgens appear in most series studying the syndrome.

In the normal ovary, LH stimulate the theca cells to synthetize androgens which in turn are converted to estrogen by CYP19A1 (or P450aromatase), in granulosa cells **(Figure 3).** In PCOS conditions, activity of enzyme Cytochrome P450 c17 (CYP17A1), which converts progesterone to 17-hydroxyprogesterone and from 17- hydroxyprogesterone to androstenedione (A4) is exaggerated and a decreased activity of CYP19A1 favors androgen production in PCOS patients (Yang, Ruan et al. 2015).

Additionally, *In vivo* and *in vitro* studies show that theca cells of women with PCOS have a pronounced activity of converting androgen precursors into testosterone.(Nelson, Legro et al. 1999), Some other studies showed that alterations in steroidogenesis and gene expression of the involved enzymes include increased expression of cytochrome P450scc (CYP11A), but not StAR protein (steroidogenic acute regulatory protein) (Calvo, Asuncion et al. 2001).

Moreover, excessive LH secretion increases the synthesis of androgens by theca cells and results in thecal hyperplasia contributing to enhanced androgen production, disruption of follicle development and follicular atresia.

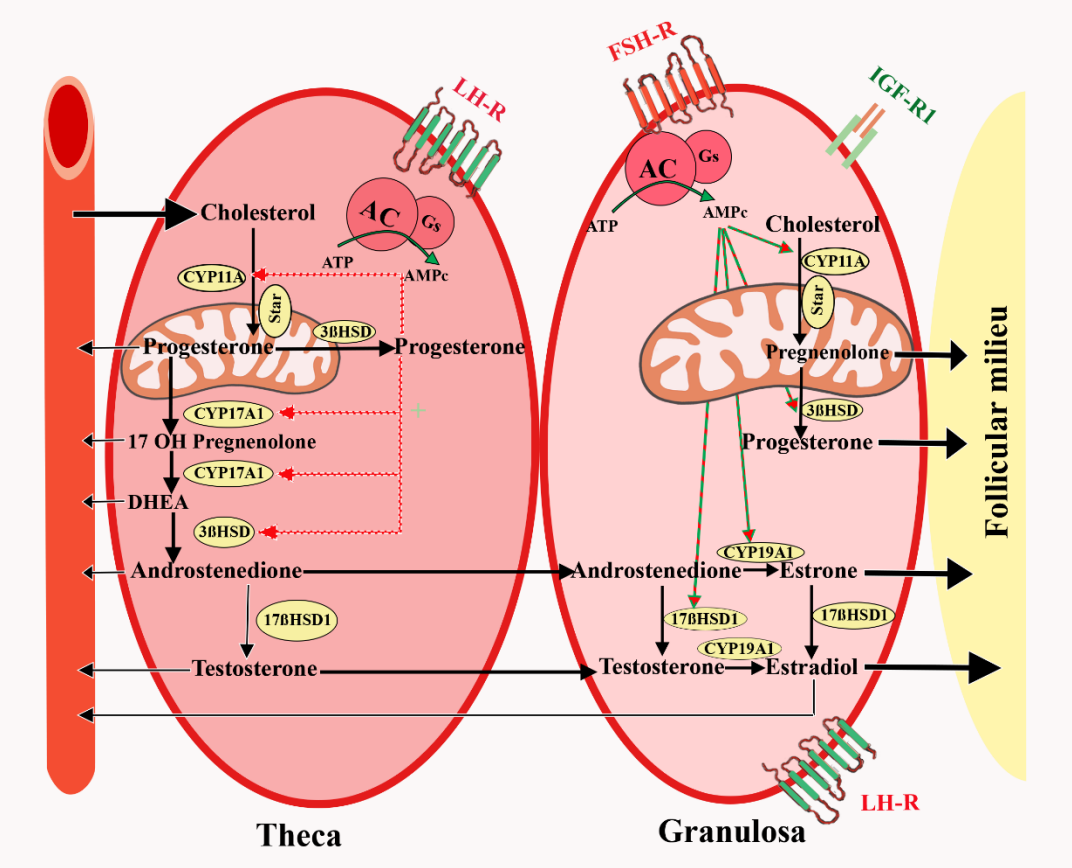

Figure 3: Biosynthesis of steroids in the ovary

Steroidogenesis requires the cooperation of two types of cells of the ovary: granulosa cells and thecal cells. Thecal cells respond to LH stimulation by producing androgens, these androgens are then converted into estrogens in the granulosa under the action of the FSH. At the end of the follicular stage, the granulosa cells express LH receptors which increases of the estrogen secretion.

A. Clinical signs of hyperandrogenism

The clinical hyperandrogenism manifests itself in different symptoms such as acne, seborrhea, androgenic alopecia and mainly hirsutism. This is a frequent reason for consultation given the aesthetic discomfort that it may originate. Clinically, this hyperpilosity is observed in androgen-

dependent zones: mainly in the face, thorax, back, inguinal hollows, inner and posterior faces of the thighs.

The score of Ferriman and Gallwey **(Figure 4)** (Ferriman and Gallwey 1961, Hatch, Rosenfield et al. 1981) allows to appreciate how severe is the impairment in a patient. It confirms the presence of "pathological" hirsutism when it is greater than 8. Androgens act on sex-specific areas of the body, converting small, straight, fair vellus hairs to larger, curlier, and darker terminal hairs.

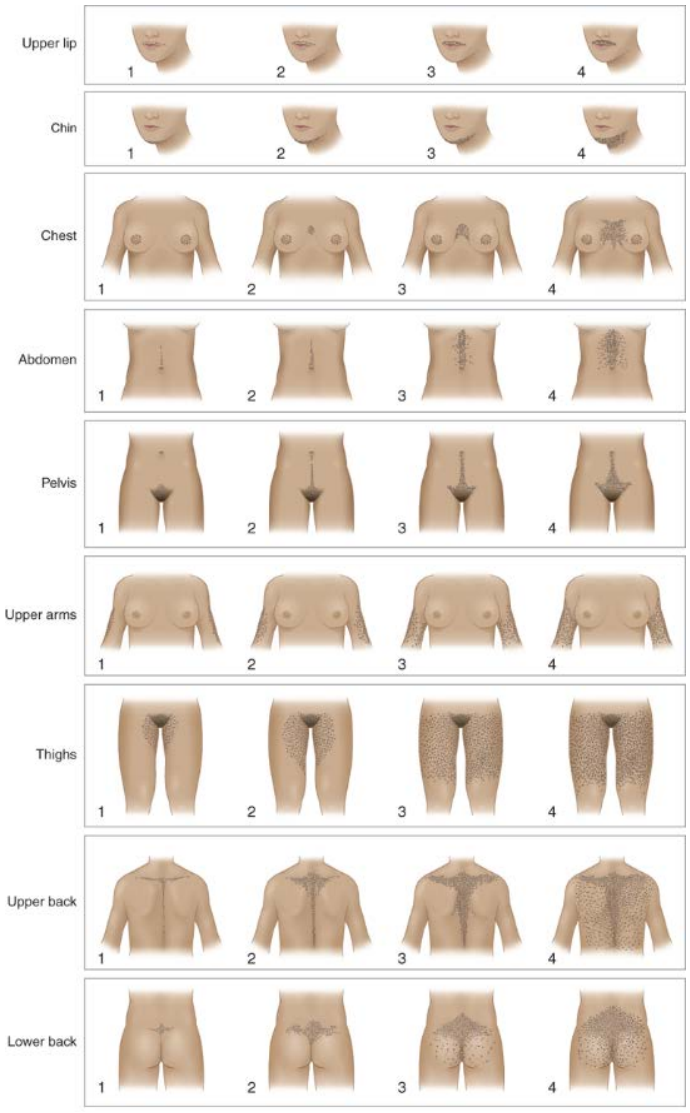

Figure 4: Ferriman and Gallwey score used to assess the degree of hirsutism.
Figure taken from: Hirsutism and virilization. Jameson JL, Fauci AS, Kasper DL, Hauser SL, Longo DL, Loscalzo J. Harrison's Principles of Internal Medicine- 20th edition.

B. Biological signs of hyperandrogenism

Biological signs of hyperandrogenism typically include an increase of free and total testosterone: testosterone circulates associated with Sex Hormone-Binding Globulin (SHBG) and other proteins such as albumin.

Moderate elevation of total testosterone (<1.2 ng/mL) is the most commonly used confirm the excess circulating androgens in PCOS patients. Nevertheless, it has been reported that the free testosterone dosage (Azziz, Carmina et al. 2009) or the use of free Androgen Index FAI) [Total Testosterone Ratio / SHBG x100] were more sensitive markers for highlighting biological hyperandrogenism (Cussons, Stuckey et al. 2005, Azziz, Carmina et al. 2009).

The lack of a reproducible and reliable dosing method for free testosterone however limits the use of this parameter to better appreciate the androgenic impregnation.

2.2.3 Polycystic appearing ovaries

Ultrasound scan has an important position in the diagnosis of PCOS as the same level as the precedent criteria. Transabdominal and transvaginal ultrasound examination methods correlate well, and both are acceptable tools for the diagnosis.

In healthy woman we can distinguish 5 to 10 small follicles of about 5 mm each visible on the ultrasound on each ovary at the beginning of the cycle **(Figure 5)**. Conversely, this number increases in PCOS patients to at least 20 follicles on each ovary, between 2 and 9mm in size.

The ovarian volume, which reflects both stromal hypertrophy and total follicular volume is also increased in PCOS patients, reaching more than 10 ml as compared to an average value of 6.31 ml in normal ovaries. (Buckett, Bouzayen et al. 1999)

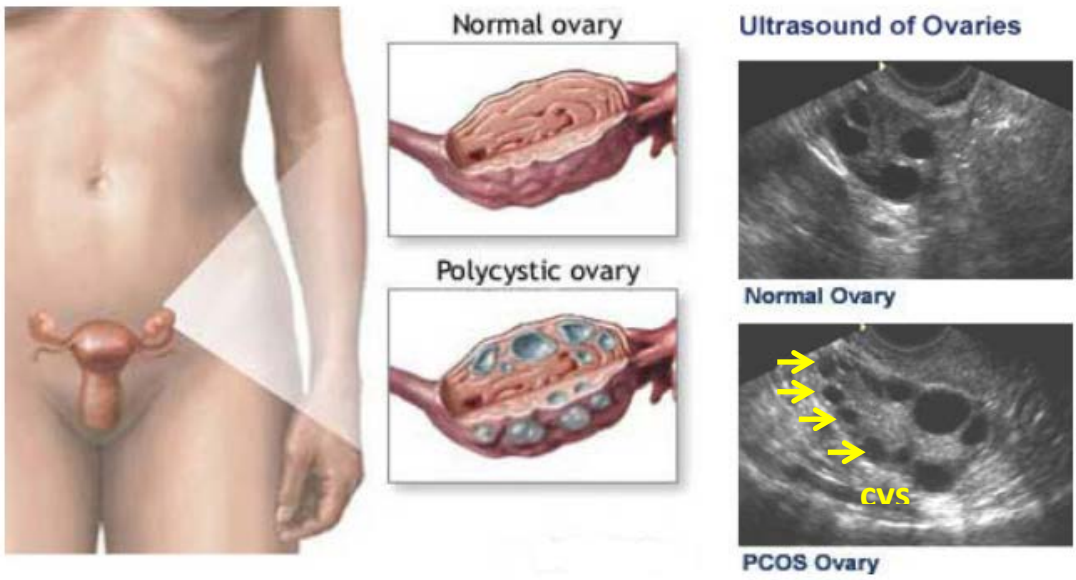

Figure 5: Illustration and ultrasound images of healthy ovaries in comparison with polycystic ovaries

It is important to highlight, that all criteria previously cited require the exclusion of other factors which cause clinical features of PCOS. These conditions include congenital adrenal hyperplasia, Cushing's disease, thyroid dysfunction and hyperprolactinemia (Azziz et al., 2006, Azziz et al., 2009, Rotterdam, 2004).

2.3 The other faces of PCOS

PCOS is the leading cause of infertility through anovulation, cycle disorders and hirsutism. Its prevalence in fertile women is estimated to be between 4- 21% (Ma, Li et al. 2010, Boyle, Cunningham et al. 2012, Lizneva, Suturina et al. 2016). Hence, the prevalence rates are variable in most studies which is justified by the ethnicity of the studied populations (Diamanti-Kandarakis, Kouli et al. 1999, Asuncion, Calvo et al. 2000, Azziz, Woods et al. 2004) (Boyle, Cunningham et al. 2012) but most importantly due to the inconsistency of the diagnostic criteria used, and the heterogeneity of the symptoms displayed by PCOS patients.

It has long been reported that PCOS has variable clinical phenotypes, biochemical and hormonal imbalances, cardiovascular complications, metabolic abnormalities, that are not part of Rotterdam's diagnostic criteria yet frequently observed in PCOS patients.

2.3.1 Hormonal imbalance

2.3.1.1 Alterations in gonadotropin secretion

A key characteristic of PCOS is inappropriate gonadotropin secretion. When compared with the follicular phase of the normal menstrual cycle, women with PCOS exhibit a disproportionately high LH secretion with relatively constant low FSH secretion. 40-60% PCOS women display an increase in LH plasma levels (Balen, Conway et al. 1995). In PCOS, the increase in LH is explained by an increased pulse frequency of the hypothalamic GnRH which may favor the production of the β-subunit of LH over the β-subunit of FSH and/or by increased pituitary sensitivity to GnRH stimulation which results in an elevated LH/FSH ratio increased in more than 75% of PCOS patients (McCartney, Eagleson et al. 2002) (Waldstreicher, Santoro et al. 1988, Taylor, McCourt et al. 1997). The increase in LH causes the ovaries to favor the production of androgens from the theca cells carrying LH receptors. The dosage of LH may vary depending on the time of the cycle, the body mass index (BMI) of the patient or the affinity of dosing kit used, which is why despite its informative value, its elevation is not essential for a diagnosis of PCOS (Dewailly, Hieronimus et al. 2010, Conway, Dewailly et al. 2014).

2.3.1.2 Increased AMH levels

Serum anti-müllerian hormone is synthesized by small antral follicles, which are precisely the ones seen in ultrasound (Jeppesen, Anderson et al. 2013). Most studies report an increase in circulating levels of AMH in PCOS patients, be 2 to 4 times higher in PCOS patients (Pigny, Merlen et al. 2003, Laven, Mulders et al. 2004, Park, Lawson et al. 2010). Interestingly, the circulating AMH levels correlate with the severity of the syndrome, through its direct action to control follicular development, blocking the follicles' maturation and assisting in the selection of a "dominant follicle", additionally, AMH behaves by its paracrine action on granulosa cells (GC) as a local inhibitor of FSH action (Jonard and Dewailly 2004).Some clinicians have concluded that AMH can be utilized as a diagnostic marker for ovarian hyperandrogenism (Dewailly et al., 2010).

Overall, most researchers agree that AMH should be considered as a marker for increased ovarian reserve (Rosenfield, Wroblewski et al. 2012). Some recent studies have reported that AMH levels are

not only increased during adulthood in PCOS women, but that this elevation in AMH levels is also observed during pregnancy in PCOS patients, whereas, AMH levels in pregnant healthy women (Tata, Mimouni et al. 2018), (Valdimarsdottir, Valgeirsdottir et al. 2019).

2.3.2 Metabolic complications

The association between abdominal obesity, hyperinsulinaemia and insulin resistance play a key role in the pathophysiology of PCOS and worsen both reproductive and long-term health of patients suffering from PCOS. Burghen et al. were first to highlight a link between PCOS and insulin resistance. They demonstrated that hyperandrogenism correlates with hyperinsulinemia in obese PCOS women (Burghen, Givens et al. 1980). Interestingly, it seems that there is chronological link between the onset of hyperandrogenism as well as dysovulation and the inception of the metabolic disturbances **(Figure 6),** not only in PCOS patients but also first-degree family members, (Yildiz, Yarali et al. 2003), this indicates that PCOS may be the presentation of a complex genetic trait disorder.

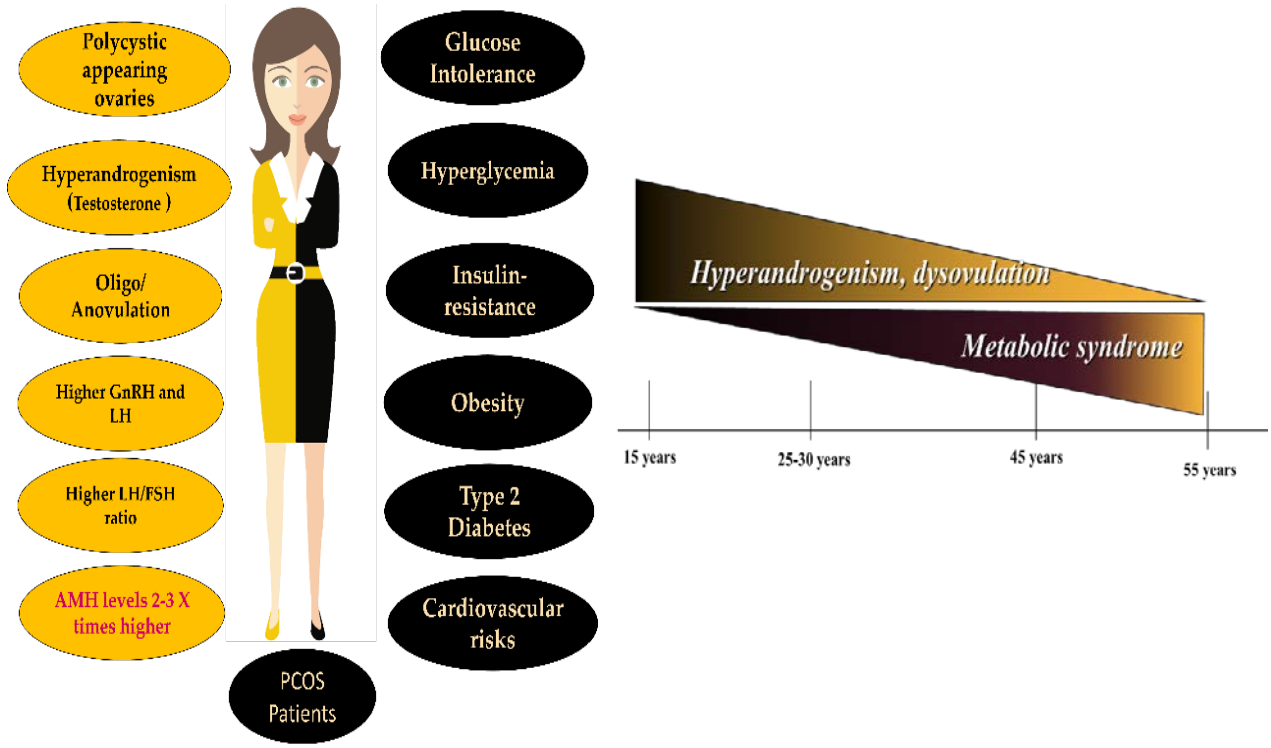

Figure 6: The close association in PCOS, between early age reproductive disorders and long-term metabolic disturbances.

2.3.2.1 Obesity

Evaluation of height and weight with calculation of Body Mass Index (BMI) along with the measurement of the waist circumference, are essential to look for overweight or obesity. Obesity is defined as excessive fat accumulation. According to BMI assessment we can distinguish the major classifications: Healthy: BMI of 18.5 to <25 kg/m^2; Overweight: BMI of 25 to 29 kg/m^2; Obese: BMI greater than 30 kg/m^2.

Nearly 50% of PCOS patients are clinically obese, although this varies with ethnicity (Carmina, Legro et al. 2003). However, the exact causative mechanism of this association remains unclear.

PCOS woman are predisposed to weight gain and in turn overweight seems to exacerbate the clinical manifestations of PCOS (Teede, Joham et al. 2013, Shorakae, Boyle et al. 2014).

Clinical investigations have reported that oligo-ovulation and anovulatory infertility are more frequent in obese PCOS patients in comparison with the lean ones (Teede, Joham et al. 2013). A correlation between the severity of the ovulatory impairment and increased BMI is observed in this syndrome (Teede, Joham et al. 2013).

Moreover, increased insulin resistance, glucose intolerance, hyperandrogenism and decreased SHBG levels are commonly observed in obese PCOS patients as compared to lean PCOS patients (Norman, Masters et al. 2001), (Rich-Edwards, Spiegelman et al. 2002). Likewise, complications during pregnancy and risk of miscarriages are also emphasized with obesity in PCOS conditions (Pasquali 2014).

2.3.2.2 Hyperinsulinemia

Increased secretion of insulin is an extra-ovarian factor aggravating hyperandrogenism in PCOS. Several studies have explored the mechanisms that could be implicated:

- At a gonadal level: during steroidogenesis, insulin has a direct stimulation action on androgen production by thecal cells by stimulating synthesis and/or activity of enzymes involved in ovarian steroidogenesis (Li, Chen et al. 2013).

- At a hepatic level: through its inhibitory properties on the synthesis of sex hormone binding globulin (SHBG) in the liver, favoring free circulating bioactive androgens in the circulation.

Hyperinsulinemia also decreases the synthesis of insulin-like growth factor bindingprotein-1 (IGFBP-1), allowing more IGF-1 to be available both locally and peripherally to stimulate ovarian steroidogenesis (Janssen, Stolk et al. 1998).

- At pituitary level: insulin seems to influence LH hypersecretion from pituitary by increasing LH pulse amplitude or potentiate the effects of LH on ovarian steroidogenesis, inducing hyperandrogenism (Allon, Leach et al. 2005), (Adashi, Hsueh et al. 1981).

2.3.2.3 Insulin resistance

Insulin resistance is defined as an impaired stimulation of glycogen formation in all major target tissues (skeletal muscle, adipose tissue, liver, kidney), and is frequently associated with PCOS. In fact, up to 90% of women with PCOS display an acute insulin resistance, surpassing the prediction obtained by their BMI (Dunaif, Segal et al. 1989). Even if, one would think that lean women would be spared from these metabolic complications, yet PCOS women with a lean phenotype also exhibit severe insulin resistance compared with BMI-matched control women (Dunaif 1999).
Insulin resistance causes compensatory hyperinsulinemia and putative origins of this IR in PCOS include abnormalities in the insulin receptor signaling and enhanced cytokine actions(Escobar-Morreale, Luque-Ramirez et al. 2011, Diamanti-Kandarakis and Dunaif 2012). Moreover, Andrisse et al. reported an enhanced insulin resistance of reproductive tissues (ovaries and pituitary) in presence of androgens in female rodents (Andrisse, Billings et al. 2018).

2.3.3 Cardiovascular pathology

While an association between PCOS and increased cardiovascular risk is still at the heart of the debate (Rizzo, Berneis et al. 2009, Papadakis, Kandaraki et al. 2017), strong findings show that postmenopausal PCOS women with a personal history of clinical hyperandrogenism or menstrual disorders have more cerebrovascular events as well as increased cardiovascular morbidity as compared to healthy women (Shaw, Bairey Merz et al. 2008) (Krentz, von Muhlen et al. 2007).

2.3.4 Pregnancy complications

Most PCOS women struggle to become pregnant and once they succeed to conceive, they often encounter complications during pregnancy and delivery (Legro, Castracane et al. 2004), (Wild 2002). Women with PCOS have a three times higher risk to miscarriage in the early months of pregnancy as compared to women without PCOS (Palomba, de Wilde et al. 2015).

A meta-analysis involving 720 PCOS women and 4505 controls, highlighted increased prevalence in PCOS women of gestational diabetes, gestational hypertension, preeclampsia and preterm births. In addition, the infants of PCOS women were more often admitted to a neonatal intensive care unit and the perinatal mortality was higher (Boomsma, Eijkemans et al. 2006).

2.3.5 Gynecological malignancies

Growing evidence show that endometrial cancer is considerably higher in women with PCOS (Wild, Pierpoint et al. 2000), (Haoula, Salman et al. 2012), (Dumesic and Lobo 2013). The chronic anovulation observed in PCOS conditions, could be involved in the onset of endometrial cancer, due to prolonged exposure to unopposed estrogens, leading to endometrial hyperplasia. However, other co-founding factors such as: progesterone dependent gene dysregulation, hyperandrogenism, hyperinsulinemia and/or LH hypersecretion could also contribute to a higher risk of endometrial cancer (Dumesic and Lobo 2013).

Nevertheless, there is insufficient evidence to implicate PCOS in the development of breast, vaginal, cervical or ovarian cancers.

2.3.6 Psychological disorders

PCOS is a life-long disease, not exclusively associated to reproductive and metabolic disturbances as it may also impact the quality of life and mental health of affected women.

An increased prevalence of depressive and anxiety symptoms has been reported in several studies (Barry, Kuczmierczyk et al. 2011, Dokras, Clifton et al. 2012) (Veltman-Verhulst, Boivin et al. 2012). Moreover, other studies indicate that women with PCOS and their children have a greater risk of autism (Cherskov, Pohl et al. 2018).

Chapter 3

Progress towards understanding PCOS etiology

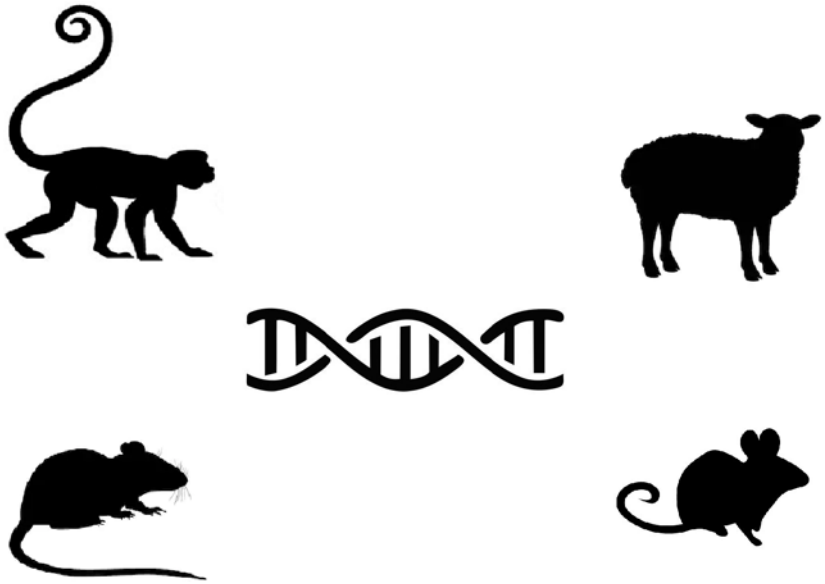

Chapter Three

The etiology of PCOS is not fully understood and the mechanisms underpinning the onset of disease in women remain elusive, however some studies suggest a genetic basis involved in the onset of the disease.

3.1 Genetic determinants & the genesis of PCOS

Phenotypic presentation of PCOS may be driven by heritable alleles and their association with environmental factors. In 1988 Hague et al., suggested PCOS as an autosomal dominant inheritance disorder with prevalence of 40-50% between first-degree family relatives (Hague, Adams et al. 1988). A study performed in an Australian monozygotic and dizygotic twin cohort led to question the autosomal dominant inheritance of PCOS as there was stark difference between hyperandrogenic and non-hyperandrogenic PCOS women (Jahanfar, Eden et al. 1995). A larger twin study using quantitative estimation of genetic influence showed a strong genetic contribution with a heritability rate of 79% for PCOS prevalence according to the Rotterdam criteria (Vink, Sadrzadeh et al. 2006). Therefore, it is unlikely that PCOS results from a single autosomal genetic determinant.

Genome-wide association studies (GWAS) may provide mechanistic values to understand the development of PCOS by attempting to give genetic associations. Eleven candidate genes were elucidated in chinese population by two initial large GWAS which analyzed risk loci for developing PCOS (Chen, Zhao et al. 2011, Shi and Vine 2012). PCOS association signals were found in DENND1A loci, which is involved in trafficking of endosomes and androgen production (Tee, Speek et al. 2016); Thyroid adenoma associated (THADA) gene intronic region, a gene linked with thyroid cancers, energy balance and risk for type 2 diabetes (Kloth, Belge et al. 2011); (Moraru, Cakan-Akdogan et al. 2017) and variants in FSH gene receptor (FSH-R), critical for folliculogenesis and fertility (Simoni, Tempfer et al. 2008).

In 2015, Day et al., published a comprehensive GWAS that further elucidated genetic genesis of PCOS and its neuroendocrine correlates. In this study, more than 5,000 Caucasian European women were evaluated and dense imputation of genotypes was used to identify association signals and draw mechanistic interpretations from the genetic data. Among the six genetic loci which were

discovered to be associated with PCOS were the epidermal growth factor receptor (EGFR) family members; and FSHB (beta subunit of FSH). Furthermore, this study shed a light on polymorphism which could lead to an alteration of FSH secretion and signaling, thus participating in neuroendocrine genesis of PCOS. It is important to note that EGFR family members are involved, not only, in LH-mediated steroidogenesis (Park, Su et al. 2004) and ovulation but also in brain circuitry development (Namba, Nagano et al. 2017). With the help of Mendelian randomization analysis, it was identified that body weight, insulin resistance and low levels of sex-hormone-binding globulin (SHBG) are among the risk factors of PCOS. The study also demonstrated a strong and positive association between the risk of having PCOS and delayed menopause, which suggested an attenuation of ovarian ageing in these women (Day, Hinds et al. 2015). This data linked with the hypotheses proposed earlier that a genetic predisposition to delayed reproductive senescence in PCOS would support the evolutionary paradox of being highly prevalent disease that impairs female reproductive competence (Abbott, Dumesic et al. 2002); (Casarini and Brigante 2014).

Despite a consensus on PCOS not being caused by one single determinant, there exists a strong association between exposure to environmental factors (such as: excess prenatal androgen) and the presentation of some of features of the disease after the onset of puberty. In human, *in utero* excess of androgen caused by congenital adrenal hyperplasia (CAH) and maternal Cushing's disease leads to clinical manifestation of PCOS in adulthood. Similarly, female offspring's of PCOS women, presenting higher levels of circulating testosterone during pregnancy than control subjects, show signs of ovarian and metabolic dysfunction during pubertal development and poses a higher risk of developing PCOS in adulthood (Crisosto, Codner et al. 2007), (Sir-Petermann, Codner et al. 2009) Furthermore, higher steroidogenic activity is exhibited in placental tissue of mothers with PCOS which in turn increases androstenedione levels and lowers P450 aromatase activity, which is critical in converting androgens into estrogens (Maliqueo, Lara et al. 2013). As a result, the altered placental steroidogenesis in PCOS women could sustain elevated intrauterine androgen levels during pregnancy and affect the development of female offspring. Taken altogether, the data leads to a prenatal androgen programming as potential mechanism to drive PCOS features later.

Two hypotheses exist on how the developmental programming generates the reproductive impairment of PCOS if the syndrome is thought to have *in utero* origin. The first one explains that

ovarian dysfunction as the initiator of the disease with the androgen imprinting in the ovaries triggering an abnormal secretion of testosterone with the onset of puberty (Gilling-Smith, Willis et al. 1994), (Rosenfield and Bordini 2010). High levels of testosterone may lead to modification of HPG axis to PCOS symptoms. The second explanation sets the brain as the primary site of PCOS. During perinatal life, hypothalamic circuits are highly responsive to sex steroid hormone modulation(McCarthy, Nugent et al. 2017). Consequently, prenatal androgen may act to alter the organization of components within GnRH the neuronal network and ultimately lead to abnormal GNRH/LH pulsality and ovulatory dysfunction (Blank, McCartney et al. 2006), (Moore and Campbell 2016). It is important to note that one hypothesis does not exclude the possibility of the other and that both could happen concomitantly in PCOS.

Various studies have shown that PCOS is hereditable (Azziz and Kashar-Miller 2000); and have underlined targeted genes, dividing them into three categories: genes encoding androgen production and metabolism, genes responsible for the secretion and action of insulin, and genes related to folliculogenesis. The first category involves genes that are linked to androgen secretion, such as LH and its receptor or genes that linked to androgen production like CYP19. The second group of genes is related to insulin and its receptor. Lastly, the third group of genes is linked to ovaries (Franks, Gharani et al. 2001). Other polymorphisms have been found in AMH and its receptor AMH type 2 in connection with follicle development (Georgopoulos, Karagiannidou et al. 2013).

The evidence of a genetic component is based on familial clustering (Legro, Driscoll et al. 1998), (Diamanti-Kandarakis, Kandarakis et al. 2006) and twin studies have shown two-fold increase in concordance of PCOS in genetically identical twins compared to non-identical twins (Vink, Sadrzadeh et al. 2006).The way PCOS is inherited remains unclear, despite numerous association studies (focusing on genes associated with synthesis and metabolism of androgens and insulin. Modern mapping techniques have managed to make some progress to identify targeting genes, two of which are: locus on chromosome 19p13.2, associated with high susceptibility to PCOS (Urbanek, Woodroffe et al. 2005) and fat-mass and obesity associated gene, whose polymorphism has have been found to be associated with PCOS (Barber, Bennett et al. 2008). However, these two candidate genes need to be studied further to be confirmed in larger studies and various populations.

There is a strong genetic component linked to PCOS which is evidenced by clustering PCOS in families as well as PCOS-like feature in male and female relatives of affected women (Goodarzi, Dumesic et al. 2011).Twin studies and linkage studies have been used to decipher the contribution of heritability in this multifactorial syndrome. Linkage studies have been carried out for 37 candidate genes and the results predicted strong association of follistatin and nominal association of *CYP11A1* gene in affected siblings with hyperandrogenemia and PCOS related traits. Furthermore, it was established by transmission disequilibrium test, by this same study, that there existed a strong genetic association of *D19S884* allelic marker near *INSR* gene with PCOS (Urbanek, Legro et al. 1999).

Numerous association studies were also carried out on candidate genes that are involved in pathways related to the etiology of the syndrome. The associated anomalies to this syndrome have pushed the research community to try and pinpoint the importance of genetic predisposition in manifestation of PCOS (Prapas, Karkanaki et al. 2009). Although, polymorphisms of genes involved in pathways such as gonadotropin regulation, insulin signaling, chronic inflammation, and energy homeostasis has been studied (Prapas, Karkanaki et al. 2009); however, the exact role of these susceptible genes has not yet been established. Single nucleotide polymorphisms (SNPs) have been able to uncover functional changes caused by modulation of gene expression or amino acid variation. Other approaches such as searching for candidate gene are helpful in reveal the impact of differential frequency distribution in healthy and diseased population. Although, this is possible in relatively smaller populations, thus, genome-wide association studies (GWAS) have revolutionized the study of PCOS genetics. Hyperandrogenism is a hallmark of the PCOS condition, therefore, various polymorphisms in genes involved in androgen synthesis, action, and bioavailability have been and are being studied.

CYP11A1 Gene. *CYP11A1* encodes the enzyme P450 cholesterol side-chain cleavage. The main function of this enzyme is that it catalyzes the rate limiting step of ovarian steroidogenesis: the conversion of cholesterol to pregnenolone (Miller 2002), (Pusalkar, Meherji et al. 2009) Two studies showed that theca cells derived from PCOS ovaries and propagated in long-term culture demonstrate increased CYP11A expression in comparison to normal theca cells (Nelson, Legro et al. 1999) (Wickenheisser, Biegler et al. 2012) Twenty families were chosen to perform a linkage study which showed involvement of *CYP11A* locus in PCOS development and consequently association of

5'UTR (TTTTA) pentanucleotide repeats in hirsute PCOS women (Gharani, Waterworth et al. 1997). This was further confirmed by another study from South India (Reddy, Deepika et al. 2014) United States (Daneshmand, Weitsman et al. 2002), Greece (Diamanti-Kandarakis, Bartzis et al. 2000) and nominally in women from United Kingdom (Gaasenbeek, Powell et al. 2004). In Chinese women, it was discovered that different allele combinations may increase or decrease the risk of PCOS (Wang, Wu et al. 2006).

However, there are studies that found no association between pentanucleotide repeat alleles with PCOS susceptibility in Spanish (San Millan, Sancho et al. 2001), Chinese (Li and Guijin 2005), 2005; (Hao, Bao et al. 2009) Argentinian (Perez, Cerrone et al. 2008), Indian (Pusalkar, Meherji et al. 2009) and Czech (Prazakova, Vankova et al. 2010) women with PCOS. A recent meta-analysis confirmed strong association of this (TTTTA) repeat polymorphism of *CYP11A* with increased risk of PCOS in Caucasian population (Shen, Li et al. 2014).

There are conflicting reports in regards to the association of these pentanucleotide repeats with PCOS related traits. Carriers of short alleles in women with PCOS have been reported to possess increased testosterone levels (Pusalkar, Meherji et al. 2009); (Diamanti-Kandarakis, Bartzis et al. 2000) while no effect of allele dose was seen on CYP11A transcription (Daneshmand, Weitsman et al. 2002) or serum androgen levels in another studies (Daneshmand, Weitsman et al. 2002); (Gaasenbeek, Powell et al. 2004); (Li and Guijin 2005).

A significant association was shown in Chinese women with PCOS with the polymorphism rs4077582 (Gao, Cao et al. 2010); (Zhang, Zhu et al. 2009) as well as altered testosterone and LH levels (Zhang, Zhu et al. 2009). The data from these studies implies *CYP11A* to be a promising genetic biomarker for PCOS.

CYP17 Gene. The *CYP17* gene encodes cytochrome P450 enzyme with 17-hydroxylase activity. This enzyme converts pregnenolone and progesterone into 17-hydroxypregnenolone and 17-hydroxyprogesterone, respectively. The lyase activity converts these steroids to dehydroepiandrosterone (DHEA) and 4-androstenedione (Prapas, Karkanaki et al. 2009).

The majority of studies have focused on a widely studied polymorphism in the promotor at −34 position (−34 T/C), which creates an additional Sp1 transcription factor binding site, thus

regulating expression of CYP17 and consequently androgen levels (Sharp, Cardy et al. 2004). A study showed significant association of this polymorphism with PCOS and male pattern baldness in a family-based study (Carey, Waterworth et al. 1994); however, these findings were not persistent when they increased the sample size (Gharani, Waterworth et al. 1996)), nor was this polymorphism found to be a significant factor for PCOS development in British (Techatraisak, Conway et al. 1997), Polish (Marszalek, Lacinski et al. 2001) American (Kahsar-Miller, Boots et al. 2004), Korean (Park, Lee et al. 2008) Chilean (Echiburu, Perez-Bravo et al. 2008) Chinese (Li, Gu et al. 2015), Thai (Techatraisak, Chayachinda et al. 2015) and Indian (Banerjee, Dasgupta et al. 2016) women with PCOS or even in Turkish adolescents (Unsal, Konac et al. 2009). A meta-analysis that took all studies into consideration revealed that this variant was not associated with risk of PCOS development when any genetic model or stratification by country or ethnicity was considered.

CYP19 Gene. This gene encodes aromatase P450 enzyme which is essential for synthesis of estrogen from androgens (Bulun, Takayama et al. 2004). In both lean and obese women with PCOS, reduced aromatase activity has been seen (Chen, Shen et al. 2015) which is further inhibited by hyperandrogenemia (Medeiros, Barbosa et al. 2015) Yang et al. have shown that decreased aromatase expression is associated with increased levels of testosterone in follicular fluid derived from PCOS women (Yang, Ruan et al. 2015).PCOS ovaries present promoter hypermethylation and reduced CYP19A1 mRNA and protein levels, which suggests repressed aromatase expression (Yu, Sun et al. 2013) Moreover, a study in Han Chinese women demonstrated that an intronic variant rs2414096 was significantly associated with increased risk of PCOS development and with increased estradiol to testosterone ratio (E2/T), FSH levels, and age of menarche (Jin, Sun et al. 2009). In adolescent girls in the UK carrying this polymorphism, it was observed that they possessed raised PCOS symptom score and changes in circulating estradiol and testosterone concentrations (Petry, Ong et al. 2005). There was no association of the rs2414096 polymorphism with PCOS or with alterations in hormonal and metabolic variables after a 6-month treatment regime of oral contraceptives in both ovulatory and anovulatory PCOS women (Maier and Spritzer 2012).The tetranucleotide repeat polymorphism (TTTA) in the fourth intron (Xita, Chatzikyriakidou et al. 2010) has been investigated. Results indicate that short allele repeats, predominantly consisting of seven repeats, are prevalent in Greek (Xita, Lazaros et al. 2010) (Xita, Georgiou et al. 2008) and Han Chinese

(Hao, Zhang et al. 2010) women with PCOS compared to healthy women without PCOS. These short repeat alleles were associated with hormonal parameters such as increased testosterone levels, high LH**:**FSH ratios (Xita, Chatzikyriakidou et al. 2010).

Chinese women with PCOS were shown to be carriers of 11 repeat alleles (Hao, Zhang et al. 2010); (Xu, Zhang et al. 2013) which in turn influence lipid metabolism (Hao, Zhang et al. 2010).Although the polymorphism, rs2470152, did not affect PCOS risk but the heterozygous TC genotype was found to be significantly associated with increased testosterone levels with decreased E2/T ratio, which suggested a role of this polymorphism in regulating aromatase activity (Zhang, Zhang et al. 2012). Arg264Cys, a missense polymorphism, increases aromatase activity and affects PCOS susceptibility (Wang, Li et al. 2011). However, the above findings indicate a definite role of this gene in PCOS outcome.

AR Gene. Located on chromosome X, the androgen receptor (AR) gene encodes the AR, which consists of a poorly conserved N terminal domain containing highly polymorphic CAG repeats (Peng, Xie et al. 2014). In a case study, it was reported that the enfant of a woman carrying a heterozygous *AR* gene mutation was diagnosed with androgen insensitivity syndrome suggesting plausible repercussions on reproductive outcomes associated with *AR* gene mutations (Nam, Kim et al. 2015) and not only with repeat lengths. The primary location of AR has been in the granulosa cells of preantral and antral follicles, theca interna cells of preantral follicles, and both theca and granulosa cells of dominant follicles (Walters, Allan et al. 2008). In Chinese and Caucasian populations, it has been ascertained that short *AR* CAG repeats are more frequent in PCOS cases and may possibly be linked to PCOS onset (Wang, Li et al. 2011); (Lin, Baracat et al. 2013)e; (Schuring, Welp et al. 2012) ; (Shah, Antoine et al. 2008) (Xia, Che et al. 2012) and perhaps contributing to the inherent hyperandrogenic phenotype commonly seen in women with PCOS by enhancing androgen sensitivity to even low circulating levels of testosterone and increasing AR activity, which promotes hirsutism, acne, and irregular cycles (Schuring, Welp et al. 2012); Anovulatory normoandrogenic PCOS women showed a significant trend towards short CAG repeat length indicating increased intrinsic androgen sensitivity (Mifsud, Ramirez et al. 2000).Moreover, it was found that Indian women showed comparatively shorter repeat lengths compared to Chinese women, implying that ethnic variation might play a possible role. No association of *AR* CAG repeat lengths with PCOS was

reported in Indian (Rajender, Carlus et al. 2013), Slovene (Ferk, Perme et al. 2008) Korean (Kim (Kim, Choung et al. 2008), and Croatian women (Skrgatic, Baldani et al. 2012). Some studies have indicated that CAG repeat lengths may also modify both testosterone and insulin resistance parameters in women with PCOS although, they have failed to show association with PCOS risk. It is interesting to note that this CAG repeat polymorphism was a significant predictor of serum circulating testosterone levels in Croatian (Skrgatic, Baldani et al. 2012), Brazilian (Ramos Cirilo, Rosa et al. 2012), Chinese (Peng, Xie et al. 2014) and Korean (Kim, Choung et al. 2008) women with PCOS. German women carrying short CAG repeats possessed increased testosterone which aggravated insulin resistance in these women suggesting a putative effect of CAG repeats as an underlying mechanism of hyperandrogenism induced insulin resistance (Mohlig, Jurgens et al. 2006). Meta-analyses, which have examined the relationship between CAG repeat lengths at *AR* and PCOS risk, have concluded that they may not be major determining factors in PCOS etiology (Rajender, Carlus et al. 2013), (Wang, Goodarzi et al. 2012). Collectively, the data from these studies suggest that *AR* polymorphisms may exacerbate the hyperandrogenic phenotype of women with PCOS.

SHBG Gene. Sex hormone binding globulin (SHBG), primarily synthesized in the liver, binds androgens and estrogen. This lowers the circulating steroid hormones and renders them biologically unavailable to target tissues (Hammond 2016). Chromosome 17 contains several polymorphisms in the SHBG and they have been shown to alter hepatic biosynthesis, plasma levels, and plasma clearance efficiency of SHBG, thus regulating the distribution of sex steroid hormones (Hammond 2016).

A woman showing severe SHBG deficiency helped uncover two novel coding region mutations. One of them resulted in truncated SHBG synthesis and the other to abnormal glycosylation; leading to extremely low levels of SHBG with elevated circulating free testosterone concentrations (Hogeveen, Cousin et al. 2002) . Xita et al., provided evidence for the hypothetical genetic contribution of SHBG polymorphisms which demonstrated an association between longer TAAAA repeats with late onset of menarche and decreased SHBG levels in hirsute French women (Cousin, Calemard-Michel et al. 2004). It was further shown that long TAAAA repeat alleles failed to be associated with PCOS risk in Croatian (Baldani, Skrgatic et al. 2015) Slovenian (Ferk, Teran et al. 2007), French (Cousin et al., 2004), and Chinese (Zhao, Chen et al. 2005) women; whereas, Greek women with PCOS had significantly

greater frequency of long repeat alleles compared to controls (Xita, Tsatsoulis et al. 2003). It has been established that there exists an inverse association between TAAAA repeat polymorphism alone (Cousin, Calemard-Michel et al. 2004), (Baldani, Skrgatic et al. 2015), (Ferk, Teran et al. 2007), (Xita, Tsatsoulis et al. 2003) or coupled with short AR CAG repeats (Xita, Georgiou et al. 2008) and SHBG serum levels. Greek women with PCOS having long SHBG alleles coupled with short CYP19 alleles resulted in low SHBG levels and increased testosterone levels with raised FAI, DHEAS and T/E2 ratios (Xita, Georgiou et al. 2008).

A recent study discovered that in Bahraini women, haplotypes spanning six polymorphisms were associated with either increased or decreased PCOS susceptibility (Abu-Hijleh, Gammoh et al. 2016). This study rekindled interest in SHBG gene polymorphisms in PCOS susceptibility.

StAR Gene. Located on chromosome 8, it encodes the steroidogenic acute regulatory protein which binds to and facilitates uptake of cholesterol into mitochondria of cells for steroidogenesis. Despite its function, a pilot study carried out in Iranian women investigated seven known polymorphisms but showed no conclusive association with PCOS risk (Nazouri, Khosravifar et al. 2015).

HSD17B5 Gene. In theca cells and adrenal glands, the enzyme type 17β-hydroxysteroid dehydrogenase type 5 (HSD17B5) is vital in converting androstenedione to testosterone (Ju, Wu et al. 2015). Revealed for the first time by Qin et al., the −71A/G polymorphism in the promoter region was studied for its prevalence in a population of ethnically diverse PCOS women. It was found that this polymorphism is associated with PCOS susceptibility in Caucasian but not in African American women with PCOS (Qin, Ehrmann et al. 2006). Furthermore, this variant modulated testosterone biosynthesis and thus plasma testosterone levels (Qin, Ehrmann et al. 2006). However, subsequent studies failed to find this association (Marioli, Saltamavros et al. 2009) in women with PCOS. Another intronic polymorphism rs12529 in Chinese women affected testosterone levels but PCOS risk remained unchanged.

INSL3 Gene. Insulin-like factor 3 (INSL3) is localized in the thecal cells and corpus luteum of the ovary. The role of INSL3-RXFP2 signaling in maintaining androgen production by theca cells was established by Glister et al. (Glister, Satchell et al. 2013) It has been reported recently that women

with PCOS have increased serum INSL3 levels (Anand-Ivell, Tremellen et al. 2013), (Gambineri, Patton et al. 2011) (Szydlarska, Grzesiuk et al. 2012) implicating *INSL3* polymorphisms may have an important role in modulating ovarian steroidogenesis and hence contribute to the pathogenesis of PCOS. Additionally, Shaikh et al. led a first a case-control association study, investigated the link between *INSL3* polymorphisms and its haplotypes with PCOS susceptibility and its related traits in a well characterized cohort of Indian women with PCOS (Shaikh, Dadachanji et al. 2016). In this study, they showed that the A/G polymorphism present in exon 1 of *INSL3: rs6523* was significantly associated with PCOS susceptibility.

However, despite intensive investigations , the genes identified only account for 10% of the 70% estimated heritability implying that environmental factors such as androgen excess could be involved in the onset of PCOS pathology.

3.2 Animal models: A strong tool to study PCOS

Throughout the history of modern medicine, from the rabies vaccine to gene therapy scientists have relied on animal models to understand diseases and allowed preventive and therapeutic strategies to be tested. Prenatal life and early childhood are critical periods marked by the influence of environmental factors in mammals. During these phases of development, the brain undergoes significant growth and remodeling, and has a particular vulnerability to external conditions and interference.

As mentioned above the pathogenesis of PCOS is multifactorial and mechanisms underlying its occurrence remain unclear. In humans, higher testosterone levels, have been found in the umbilical vein in female infants born to mothers with PCOS (Barry, Kay et al. 2010)

Therefore, this part will be dedicated to reviewing the current animal models used to study the physiopathology of PCOS and which mainly rely on the prenatal administration of dihydrotestosterone (DHT) to induce the emergence of PCOS-like traits.

3.2.1 Developmental programming: role of intrauterine androgenization in the pathogenesis of PCOS

A- Non-human primates:

Rhesus monkey or *Macaca mulatta* is an ideal model to PCOS due to the shared physiological characteristics between primates and the well-conserved genetics (Abbott, Nicol et al., 2013) (Abbott, Dumesic et al., 1998).

Monkeys are precocious and mono-ovulatory species just as humans, presenting complete intrauterine ovarian development. When evidence arose of elevated intrauterine androgen levels in CAH induced ovulatory dysfunction, HA and LH hyper-secretion in female offspring, it was suggested that that non-human primates also be studied (Abbott, Dumesic et al. 1998). When pregnant rhesus monkeys are exposed to testosterone from gestation day (GD) 40 to GD 60, the female offspring presented PCOS features such as anovulation, increased LH secretion, polycystic ovaries and HA (Abbott, Dumesic et al. 1998). (Dumesic, Abbott et al. 1997); (Eisner, Barnett et al. 2002)et al. 2002). It is important to note that rhesus monkeys can naturally be hyperandrogenic and develop PCOS-like features. Abbott et al., revealed that prevalence of female monkeys who present PCOS-like features in a laboratory population was close to findings in humans (~15%). Furthermore, they showed that these hyperandrogenic rhesus monkeys exhibit high serum concentration of LH and AMH and they are positively associated with infertility (Abbott, Rayome et al. 2017). The results from this study lead us to conclude that neuroendcroine, metabolic and ovarian features of PCOS can be recapitulated in non-primate models. Alas, the generation of these animal models is time consuming, costly and provides poor availability of transgenic lines, thus, these models have limited use in research.

B- Sheep

Similar to humans, sheep are monoovulatory animals and are a valuable model for the study of PCOS. Anovulation, cystic-like ovarian morphology and HA can be recapitulated by the early (30-90 GD) or mid (69-90 GD) gestation prenatal testosterone exposure (Birch, Padmanabhan et al. 2003) Elevated LH pulse frequency was seen in PNA sheep model, along with increased response to intermittent treatment of exogenous GnRH (Manikkam, Thompson et al. 2008) which

recapitulates the neuroendocrine impairment of PCOS. PNA sheep model has also shown to display disruption of LH surge and impaired progesterone and estradiol negative feedback on GnRH/LH release (Padmanabhan and Veiga-Lopez 2013)

This model gives ample opportunity to study the cardinal features of PCOS, however, it can be remarked that a high degree of virilization of the external genitalia in PNA female sheep is observed (Roland, Nunemaker et al. 2010), raising the question whether this is modeling a masculinization of PCOS or the brain. For the sheep model as well, the costs, lack of specific transgenic animals, long gestational length and seasonal aspects of breeding are few of the hurdles which make the use of this model limited.

C- Rodents

In rats and mice, during late pregnancy, prenatal exposure of testosterone or dihydrotestetrone (DHT) evokes some PCOS-like features. Foecking et al. demonstrated that in rats, 1 mg/day of testosterone or DHT during GD 21-23 is able to increase LH secretion frequency, eliminate the LH surge and attenuate progesterone receptor expression in the POA and in adulthood (Foecking, Szabo et al. 2005). An increase to 3 mg/day of prenatal testosterone or DHT during the same period results in higher testosterone levels, irregular estrous cyclicity, ovarian dysfunction, and high LH frequency and amplitude (Wu, Li et al. 2010). Furthermore, a prenatal dose of 5 mg/day of testosterone during the same gestational period induces PCOS characteristics such as increased body weight, hyperinsulinemia and dyslipidemia in adults (Demissie, Lazic et al. 2008). The data from these studies suggest that differential intrauterine androgen environment might be the key to the heterogeneous manifestation of PCOS. Anxiety-like behavior was further seen in PNA female rats, which is associated with disrupted AR signaling in the amygdale (Hu, Richard et al. 2015) This is evidence that PNA rats are suitable models for PCOS associated neurological disease investigation such as depression and anxiety.

Similarly, mice and transgenic mice technology has been a vital genetic tool used to understand and define PCOS pathogenesis. Mice prenatally exposed to DHT with a dose of 250 µg/day during late pregnancy (GD 16-18) generates female off-springs who as adult female mice display ovarian dysfunction, increased testosterone plasma levels, and impaired steroid-mediated negative

feedback mechanisms, similar to the women with PCOS (Sullivan and Moenter 2004) (Moore, Prescott et al. 2013). This neuroendocrine disruption further causes problems during adulthood as it is associated with increase of dendritic spine density in GnRH neurons (Moore, Prescott et al. 2013), suggestive of enhanced afferent synaptic inputs onto the GnRH neurons. Aberrations within the hypothalamic circuits controlling GnRH/LH secretion were also observed in PNA mice (Moore, Prescott et al. 2013),(Moore, Prescott et al. 2015). The mild metabolic phenotype of PNA mice and their leanness demonstrates increased fasting glucose levels, early form of islet dysfunction in the pancreas and adipocyte hypertrophy (Roland, Nunemaker et al. 2010); (Caldwell, Middleton et al. 2014). This particular lean, PCOS modeling provides a unique opportunity to eliminate specific factors that might contribute to the reproductive impairment in PCOS without the secondary influence of hyperinsulinemia or increased body weight.

Chapter 4

Anti-Müllerian Hormone (AMH)

Chapter Four

4 Anti-Müllerian Hormone (AMH)

4.1 How was AMH discovered?

In 1947, Alfred Jost suggested that a testicular factor regulated the sexual differentiation of the gonads. He observed that Müllerian ducts of the rabbit would independently differentiate into the female reproductive system (Jost 1947) He performed gonadectomy on sexually undifferentiated rabbits and he grafted either ovarian or testicular tissue inside rabbits and observed the development of the undifferentiated rabbit into correct female or male genitalia, respectively. It was, however, with the implantation of testosterone proprionate crystal alone following gonadectomy; that he noticed that Wolffian ducts developed but there was no regression of the Müllerian ducts. This led him to conclude that testosterone alone was responsible for gonadal differentiation. Jost called this factor "hormone inhibitrice" or "inhibiteur müllerien", today known as, Anti-Müllerian Hormone (AMH) or Müllerian inhibiting substance (MIS).

4.2 AMH gene and protein

The AMH gene is highly conserved through evolution. It is present in almost all mammals. The human AMH gene is positioned on chromosome 19, band p13.3 (Cohen-Haguenauer, Picard et al. 1987), the mouse AMH gene on chromosome 10 (King, Lee et al. 1991) and in cattle on chromosome 7 (Gao and Womack 1997). The AMH gene is 4Kb long and characterised by a high GC content. Among the 5 exons forming the AMH gene, studies show that 2-5 exons are recognized as the highest degree of homogeneity in all species.

In humans, the *AMH* gene encodes a pre-protein of 560 amino acids. The N-terminal domain is devoid of intrinsic activity, whereas the C-terminal domain possesses the biological activity which causes the regression of Müllerian ducts (Wilson, di Clemente et al. 1993). Once the first 40 amino acids are cleaved, the result is a 140 kDa glycoprotein, composed of two monomers of 70 kDa, belonging to the TGFβ superfamily (Figure 7). It was discovered in 1978 by several investigators

(Picard, Tran et al. 1978)It is primarily secreted by Sertoli cells of the testes (embryonic, neonatal and postnatal) (Donahoe, Ito et al. 1977) and granulosa cells of ovaries (Vigier, Picard et al. 1984), AMH must be cleaved into two N-terminal and one C-terminal dimmers to acquire its biological function, giving rise to 110 kDa N-terminal homodimer composed of two 57kDa subunits and an active 25kDa C-terminal.

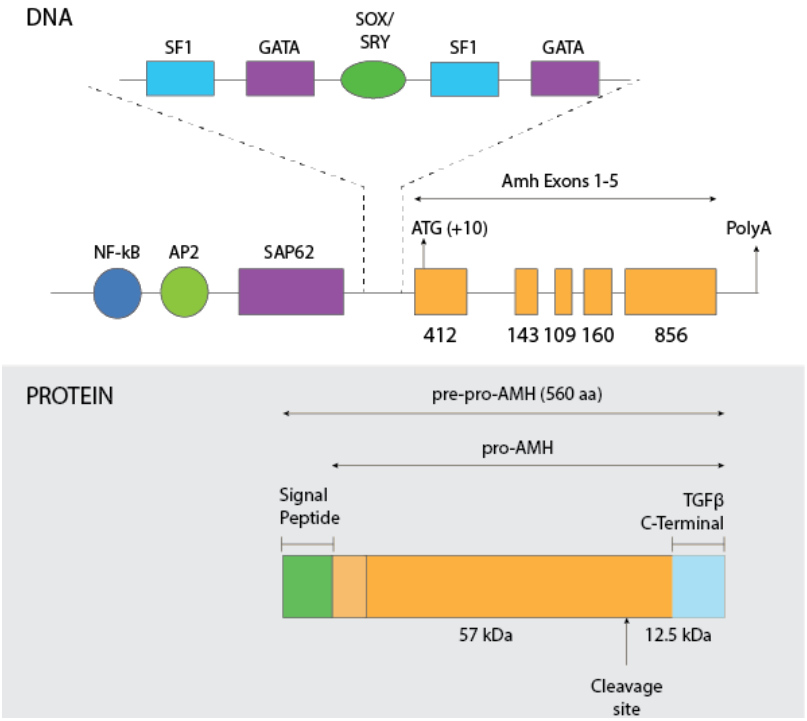

Figure 7: AMH gene and protein.

Structure of AMH gene presenting the exons and introns. Structure of AMH protein. Formation of mature AMH requires proteolytic cleavage from pre-pro-hormone to form the mature form that is detectable within blood. (Figure taken with the permission of Samuel Malone)

4.3 Regulation of AMH promoter

A strict temporal regulation of AMH is required for the differentiation of male and female phenotypes. The promotor is located 434bp downstream of stop codon Sap62, splicesosome protein (Dresser, Hacker et al. 1995). Using *in vivo* models, several regulators have been identified for the AMH promotor: activators, in males, responsible for initiating expression in the embryonic gonad whilst repressors of AMH in females in the embryonic gonad.

There are several activators of AMH promoter:

SRY. Haqq et al., unveiled the role of SRY (Sex determining region on Y) in inducing AMH expression. *AMH* expression is visible in mice 20h after the initial expression of *SRY*. However, they showed that SRY acts indirectly to activate the AMH expression. (Haqq, King et al. 1994)

SOX9. SRY-related homolog box protein 9 or SOX9, belongs to the SOXE family of transcription factors, expressed in the testes during mammalian differentiation (Schepers, Wilson et al. 2003). It is expressed in both male and female embryos at embryonic day10. It is upregulated in the embryonic male gonad and falls to undetectable levels in the female gonad. This increase in SOX9 expression initiates Sertoli cells to express AMH and sexual development, thus being an activator of AMH expression.

SF-1. Steroidogenic Factor-1 or SF-1, is expressed in mice in the genital ridges at embryonic day 9. The expression is upregulated in foetal testes and downregulated in the ovaries as sexual differentiation begins, thus, suggesting it might play a role in regulating *AMH* activity. The AMH promoter contains a conserved 20 bp motif, capable of binding to SF-1 *in vitro* (Arango, Lovell-Badge et al. 1999) and SF-1 is required for the upregulation of *AMH* transcription.

GATA4. Prenatal Sertoli cells and granulose cells express GATA4. It transactivates the AMH promotor in granulosa cells (Anttonen, Ketola et al. 2003). The GATA binding site on AMH promotor suggests that GATA4 directly regulates AMH expression (Tremblay and Viger 1999).

WT1. Wilms' tumour suppressor-1 or WT1, is a transcription factor containing zinc fingers and DNA binding domain. The synergistic action of WT1 and SF-1 are required for normal gonad formation (Kreidberg, Sariola et al. 1993, Luo, Ikeda et al. 1994). *In vitro*, it's been shown that an isoform of WT1 interacts with SF-1 to upregulate AMH promoter (Nachtigal, Hirokawa et al. 1998)

Dax1. Dosage sensitive sex reversal, adrenal hypoplasia critical region, on chromosome X, gene 1 or Dax1, is one of the repressors of *AMH* promotor which is present in the ovaries and absent in the testes in developing gonads and acts as a dominant-negative regulator of SF-1 (Burris, Guo et al. 1995),(Clipsham and McCabe 2003).

4.4 AMH signalling pathway

4.4.1 Transforming Growth Factor β (TGFβ) family

AMH belongs to the divergent superfamily of TGF. In humans, there are more than 30 signalling proteins which include activins, TGFβ, bone morphogenic proteins (BMPs), nodals, or growth and differentiation factors (GDFs). Their functions during development are indispensible and heterogeneous as seen in mutant mice that display embryonic mortality or show abnormal phenotype when lacking different TGF family members (Kaartinen, Voncken et al. 1995, Sanford, Ormsby et al. 1997).It is implicated in different and varied physiological processes such as: development, proliferation and cellular differentiation (Watabe and Miyazono 2009).

The superfamily of ligands can be phylogenetically divided into two main groups: the TGF-β/Activin and BMP/growth and differentiation factor (GDF) branches (de Caestecker, 2004). The TGF-β members are synthesized as a dimeric complex containing a preproprotein comprising N-terminal signal peptide, a large proregion, and a smaller biologically active mature region, the C-terminal (Massague 1990). After dimerization this complex is directed by the signal peptide in the RE/Golgi where the pro-region undergo posttranslational processing for activation (Kingsley 1994, Massague 1998), is cleaved by furin-like endoproteinase, but remains attached by non-covalent bounds.

4.4.2 TGF receptors

TGF receptors are transmembrane serine-threonine kinase receptors which require association of two different types of receptor class, resulting in a complex formation. Type I receptors are the Activin-like Kinases (ALKs), whereas, the type II receptors are named after the ligands they bind. The number of known ligands in the TGFβ superfamily is greater than the number of known receptors. This signifies that numerous receptors are common and implicated in different signalling pathways. The type II receptor kinases are constitutively phosphorylated (Luo and Lodish 1997)and the ligands that bind to the receptor form the tetrameric complex. The signal is then propagated downstream by Smad proteins.

AMH binds exclusively to the type II receptor, AMHR2 (Mishina, Rey et al. 1996). AMHR2 interacts with three type I receptors of Activin like kinase (ALK) family – AcvR1 (Activin receptor 1: ALK2), BMPR1a (Bone morphogenic protein receptor 1A: ALK3) and BMPR1b (Bone morphogenic protein receptor 1B: ALK6).

4.5 AMH receptors

AMH action is mediated by a heterodimeric receptor formed by AMH type 2 receptor (AMHR2) and AMH type 1 receptor (Jamin, Arango et al. 2003). The binding of AMH to AMHR2 leads to the recruitment of AMH type 1 receptor to form a complex which phosphorylates its serine-threonine kinase domain. This activated AMH type 1 receptor phosphorylates a receptor-regulated SMAD (R-Smad), associating with Smad4 and moving into the nucleus where they control transcription (Massague 1998).

In 1994, *AMHR2* gene was located on chromosome 12 in humans and on chromosome 15 in mice. The genetic sequence comprises of 11 exons in which exons 1-3 encode the extracellular domain, exon 4 the transmembrane domain and exons 5-11 encode the intracellular domain. The mRNA encodes a protein of 82 kDa comprising of 573 amino acids.

It is most likely that the mechanism through which AMH interacts with AMHR2 is distinct from other members of the TGFβ family (di Clemente, Jamin et al. 2010). It has been anticipated that once the full-length AMH is cleaved, it results in a conformational change in the C-terminal domain which facilitates the receptor binding. The binding of AMHR2 induces the dissociation of the pro-region by a negative allosteric interaction between the receptor and the pro-region binding sites on C-terminal dimer (Figure 8). Prenatally, AMHR2 expression pattern reflects AMH profile. It is expressed by the mesenchymal cells surrounding the Müllerian ducts during embryonic development(Baarends, van Helmond et al. 1994, di Clemente, Wilson et al. 1994), (Teixeira, He et al. 1996). It has also been found in foetal testes (Baarends, van Helmond et al. 1994). Postnatally, AMHR2 is expressed in the endometrium (Wang, Protheroe et al. 2009)breast (Segev, Hoshiya et al.

2001)prostrate (Hoshiya, Gupta et al. 2003) and the gonads of both sexes (Teixeira, Maheswaran et al. 2001) indicating that the main role of this receptor is to mediate the action of AMH. During development AMHR2 positive cells migrate and change their phenotype in response to AMH signal, thus causing the regression of Müllerian ducts (Zhan, Fujino et al. 2006). In the ovaries, to regulate follicular development and maturation, AMHR2 signals the paracrine action of AMH.

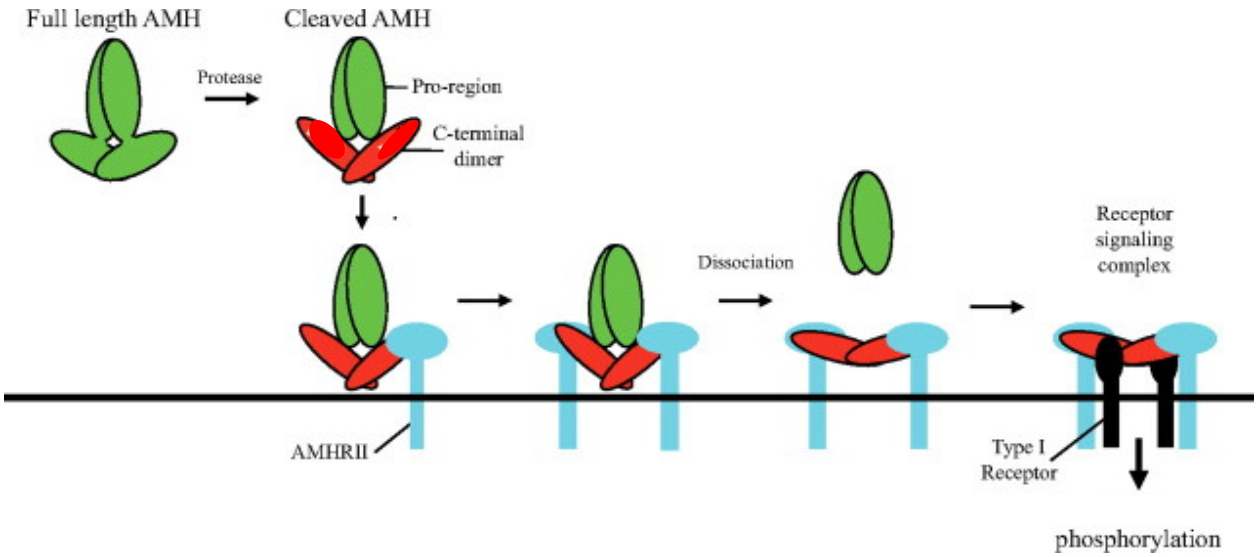

Figure 8: Model of AMH-AMHR2 signalling

The exact mechanism of AMH with its receptor currently remains unknown. The team of Nathalie di Clemente has proposed the above model of receptor-ligand. Once the full-length AMH is cleaved, there comes about a conformational change in the C-terminal domain, which allows binding of AMRH2. This induces dissociation of the pro-region through a negative allosteric interaction between the receptor- and pro-region-binding sites on the C-terminal dimer. Figure taken from (di Clemente, Jamin et al. 2010).

4.5.1 AMH type 1 Receptor

4.5.1.1 Alk6

The first AMH type 1 receptor to be discovered was ALK6 (Gouedard, Chen et al. 2000), as it was able to interact with AMHR2 (Imbeaud, Faure et al. 1995) in an AMH dependent manner. Low levels of Alk6 mRNA were found in urogenital ridges of both sexes, in the epithelial cells layer of the

Müllerian duct and in adult gonads. It has been shown that Alk6 is important for AMH action in the ovary but not required for Müllerian duct regression during male sexual differentiation (Monsivais, Matzuk et al. 2017).

4.5.1.2 Alk2

Alk2 expression is more stringent than Alk6 because it overlaps with AMHR2 perfectly. In fact, Alk2 is expressed in all AMH target tissues early in development, whereas Alk6 is expressed only at the level of the epithelium of the Müllerian duct(Zhan, Fujino et al. 2006), like the urogenital ridge (Wang et al., 2005), gonads at different embryonic stages (Visser, Olaso et al. 2001)and mesenchymal cells adjacent to the Müllerian duct.

4.5.1.3 Alk3

Alk3 interacts weakly with AMHR2 (Clarke, Hoshiya et al. 2001)and it has been reported that lack of expression of Alk3 in the developing gonads leads to PMDS in mice (Jamin, Arango et al. 2002). Moreover, AMH seems to spatiotemporally regulate Alk3 because its expression appears later when Alk2 decreases. Furthermore, it is restricted to the mesenchyme, suggesting sequential role in Müllerian duct regression (Zhan, Fujino et al. 2006).

4.6 AMH actions on gonadal development

4.6.1 Development of the embryonic gonad

During embryonic development, each individual possesses both female and male reproductive ducts. These undifferentiated ducts have the potential to differentiate into male or female reproductive systems. For normal female development, the Wolffian ducts must regress and Müllerian (paramesonephric) ducts must develop. These will give rise to the uterus, upper part of vagina and oviducts. Whereas, for normal male development, Müllerian ducts must regress and Wolffian (mesonephric) ducts must develop; giving rise to seminal vesicles, epididymus, vas deferens and ejaculatory ducts(Kobayashi and Behringer 2003, Cunha, Robboy et al. 2018).

4.6.2 Sexual differentiation of the male gonad

The dimorphic sex determination starts, in humans, at 7 weeks after conception. It is determined by the genetic sex in most mammals, with the presence of Y chromosome, containing the sex determining region (SRY) gene and AMH (Figure 9). *SRY* gene sets off the correct biochemical events in testes to produce specific hormones that will lead to sexual differentiation (Page, Mosher et al. 1987), (Skaletsky, Kuroda-Kawaguchi et al. 2003). In females lack of Y chromosome and presence of AMH causes the regression of Wolffian ducts (Nef and Parada 2000) (Cunha, Robboy et al. 2018) around 8-9 weeks of gestation in humans.

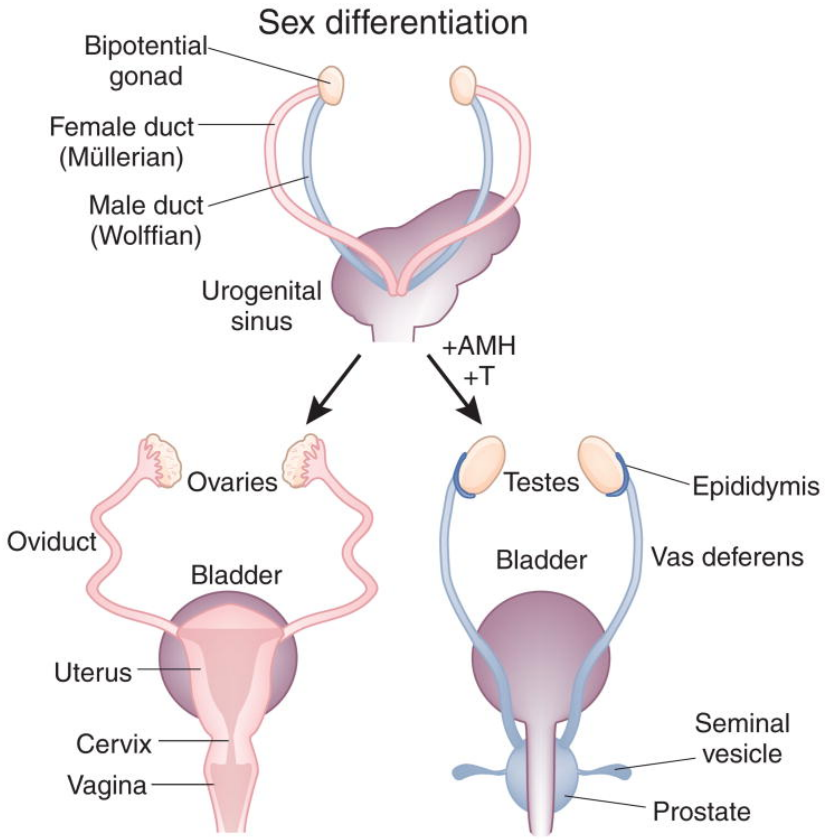

Figure 9. Mammalian sex differentiation.

A bilateral pair of Müllerian and Wolffian ducts are present in all mammals. The Y chromosome in males stimulates the expression of testosterone and AMH from testes act on Müllerian ducts and results in their regression. In the absence of Y chromosome, there's no secretion of testosterone and AMH, female gonadal development occurs with the degeneration of Wolffian ducts. Figure taken from Matzuk & Lamb, Nature Medicine 2008. (Matzuk and Lamb 2008).

4.6.3 Persistent Müllerian Duct Syndrome (PMDS)

AMH signalling is central to the development of correct male genitalia. This is demonstrated by mutations affecting the function of AMH or AMH receptors, known to cause Persistent Müllerian Duct Syndrome (PMDS). Approximately, 45% of the cases of PMDS are caused by mutations of *AMH* gene (type 1) and 40% are caused by mutations of *AMHR2* gene type 2. This syndrome is characterised by the retention of Müllerian duct derivatives (the uterus, fallopian tubes and upper part of the vagina) phenotypically and karyotypically (46XY) in male patients (Josso and Clemente, 2003;Behringer et al., 1994; Mishina et al., 1996; Belville et al., 1999; Belville et al., 2004; Orvis et al., 2008). On the surface, PMDS patients do not exhibit any anomalies as they have normal development of external genitalia and secondary sexual characteristics (Renu et al., 2010).

4.6.4 Postnatal roles of AMH

4.6.4.1 AMH actions in female reproductive function

AMH is secreted by the granulosa cells of small antral and pre-antral follicles to regulate early follicular development (Sahmay, Aydin et al. 2014). AMH continues to be expressed in the growing follicles in the ovary until they have reached the size and differentiation state at which they are to be selected for dominance by the action of pituitary FSH (van Houten, Themmen et al. 2010) and gradually decreases at the following stages of follicular development. Hence, serum level of AMH reflects the size of the primordial follicle pool and is considered as a marker of the ovarian reserve.

AMH regulates ovarian function in cyclic females by preventing premature stimulating hormone (FSH)-mediated follicular growth and steroidogenesis **(Figure 10)** By experimentally manipulating FSH and E2 levels in infantile mice, Devillier et al., have shown that high FSH concentrations lower Amh expression in early antral follicles, while E2 has no effect. The team noticed decrease in FSH mediated expression of Cyp19a1 aromatase when they treated infantile ovaries in organotypic cultures with AMH. Thus, infatile elevation in FSH levels suppresses Amh expression in early antral

follicles, in this manner favouring Cyp19a1 aromatase expression and E2 production (Devillers, Petit et al. 2019).

This data in correlation with recent discoveries indicates that AMH can act on hypothalamus as well as the pituitary, increasing gondaotropin levels, suggesting that AMH plays the role of critical regulator of gonadotrope axis during infantile period, thus contributing to adult reproductive function (Devillers, Petit et al. 2019).

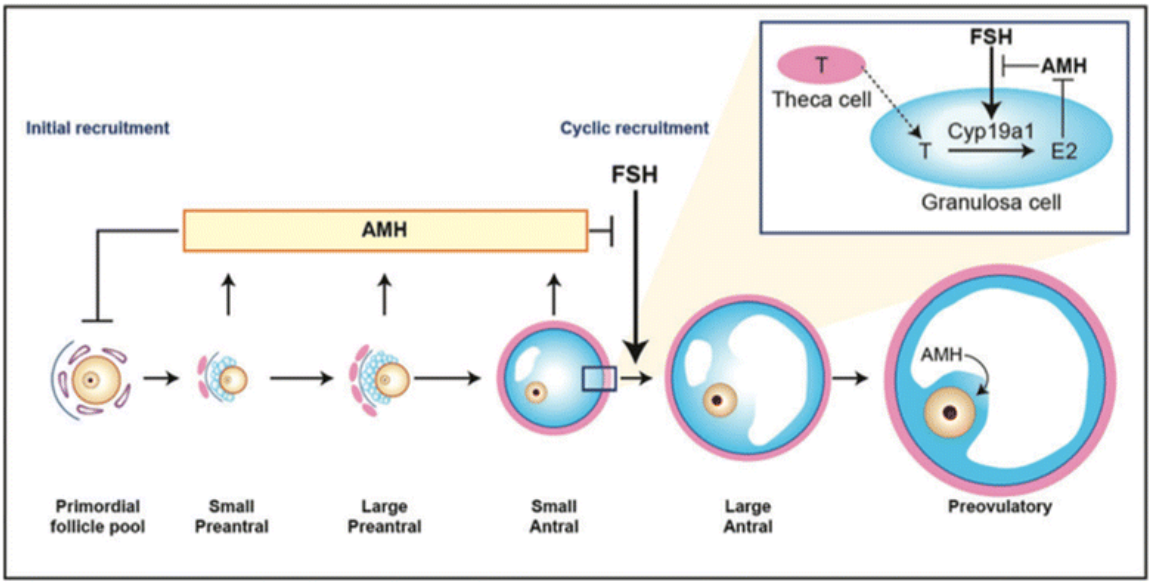

Figure10: AMH actions in the ovary.

Gonadal role of AMH. AMH is produced by the small growing follicles in the postnatal ovary (arrows) and has two sites of actions. It inhibits initial follicle recruitment and inhibits FSH-dependent growth and selection of preantral and small antral follicles. Figure taken from (van Houten, Themmen et al. 2010).

Levels of circulating AMH are good indicators of ovarian reserve (van Rooij, Broekmans et al. 2002)Clinically, a correlation has been observed between basal levels of AMH and Polycystic Ovary Syndrome (PCOS) which has led to the role of AMH in follicular development (Peñarrubia, Fábregues et al. 2005, La Marca, Sighinolfi et al. 2010). Primary follicles of females with PCOS secrete an abnormally high level of AMH which results in a reduced suppression of androgen production and secretion coupled to arrested follicular maturation. AMH secreted by primary and growing small antral follicles acts as an inhibiting factor for further follicular recruitment and development in

humans and rodents. Furthermore, a recent study showed that AMH levels parallel fluctuations in antral follicle count through menstrual cycle (Depmann, van Disseldorp et al. 2016).

4.6.4.2 AMH actions in male reproductive function

In males, AMH is produced by differentiated Sertoli cells, causing the regression of Müllerian ducts (Tran, Muesy-Dessole et al. 1977). AMHR2, secreted by Sertoli and Leydig cells indicates a potential paracrine role in regulating male gonadal function (Arango, Kobayashi et al. 2008)Indeed, high levels of AMHR2 result in decreased expression of testosterone secretion (Racine, Rey et al. 1998). Along with this, AMH triggers a decrease in luteinizing hormone Receptor (LHR) expression, further decreasing testosterone secretion. Physiologically, at puberty in males, AMH levels reduce whereas testosterone levels increase and spermatogenesis is initiated (Rey 2005). However, it is important to remember that this is only true for postnatal life due to androgen mediated decrease in AMH levels (Chemes, Rey et al. 2008, Boukari, Meduri et al. 2009).

4.7 Emerging extra-gonadal roles of AMH

Gonadotropin releasing hormone plays a key role for the onset of puberty and reproduction. It is released into the pituitary blood vessel from where it travels to the anterior pituitary. The production and release of gonadotropins LH and FSH is under its control. These gonadotropins, in turn, stimulate gametogenesis and production of sex steroids in the gonads (Christian and Moenter 2010).

GnRH-secreting neurons are neuroendocrine cells originating in the nasal placode outside of the nervous system during embryonic development and migrate to the hypothalamus (Wray, Grant et al. 1989), (Schwanzel-Fukuda and Pfaff 1989). This process is evolutionarily conserved in mammals(Wray, Grant et al. 1989),(Schwanzel-Fukuda and Pfaff 1989) including humans (Schwanzel-Fukuda, Crossin et al. 1996), (Casoni, Malone et al. 2016). A disruption of the migration of GnRH neurons or a defect in GnRH synthesis and secretion results in a rare endocrine disorder congenital

hypogonadotropic hypogonadisms (CHH). CHH is characterised by absence of incompleteness of puberty, which leads to infertility (Boehm, Bouloux et al. 2015).

Strictly in females, another AMH action is observed, occurring only before puberty. This AMH action is essentially a preferential secretion and adenohypophyseal gene expression of gonadotropin FSH *in vivo* in rats (Garrel, Racine et al. 2016). Garrel et al., additionally, demonstrate that GnRH is a regulator of AMHR2 expression in humans, highlighting the importance of AMH signalling in the regulation of gonadotrope function. Using perifused murine LbetaT2 gonadotrope cells, the team showed that Amhr2 expression is differentially regulated by GnRH pulse frequency with an induction under high GnRH pulsatility (Garrel, Denoyelle et al. 2019).

Erg1 (short proximal region of the promotor) was identified as a new transcription factor controlling hAMHR2 expression as it mediates basal and GnRH-dependent activity of the promoter. This was achieved by using site-directed mutagenesis of Erg1 motif and siRNA mediated-knockdown of Egr1. Furthermore, FOXO1 was recognized as FOXO1 as a negative regulator of basal and GnRH-dependent AMHR2 expression in gonadotrope cells, using a constitutively active mutant of FOXO1 (Garrel, Denoyelle et al. 2019)

Mature neurons in the adult brain express high levels of AMH receptors in males and females(Wang, Protheroe et al. 2009). In 2016, Cimino et al. discovered a novel neuroendocrine action of AMH. They reported a direct action of AMH on GnRH neuronal activity and demonstrated that AMHR2 is expressed in a part of the hypothalamic gonadotropin-releasing hormone neurons in mice and humans **(Figure 11)** and responds to exogenous AMH by induces neuronal activity and GnRH secretion.(Cimino, Casoni et al. 2016) This, further, results in an increase in LH secretions, equivalent to levels required to produce an ovulatory surge. In 80% of PCOS females, a notable rise in LH levels is observed (Taylor, McCourt et al. 1997) indicating that the pulse frequency of GnRH is persistently accelerated in this syndrome.

It's been shown that GnRH neurons express AMHR2 since early foetal development to adulthood and that AMH stimulates GnRH neuronal activity and hormone secretion in mature GnRH cells (Cimino, Casoni et al. 2016).

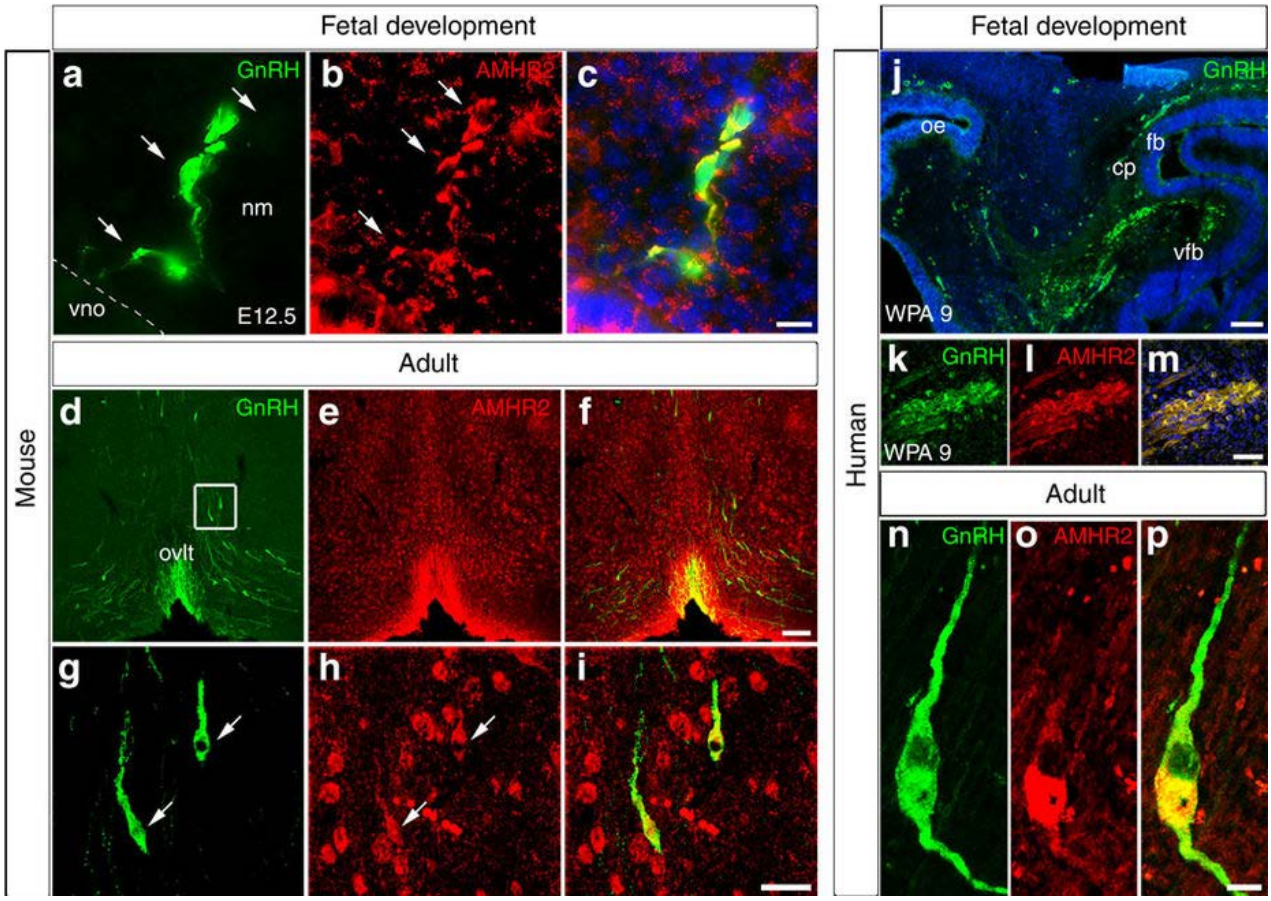

Figure 11. AMHR2 is expressed in mouse and human GnRH neurons.

(A-C) Confocal images of murine GnRH neurons (green) at E12.5 expressing AMHR2. (red) with Hoechst as a nuclear counterstain (blue). (D-I) Images from the adult OVLT showing GnRH and AMHR2 localisation. (J-M) Confocal images of a human foetus at 8 gestational weeks stained for GnRH and AMHR2. (N-P) Images from an adult human showing GnRH neurons also express AMHR2 postnatally. Figure taken from (Cimino, Casoni et al. 2016).

Furthermore, Malone et al. identified four heterozygous loss-of-function mutations in AMH and AMHR2 in a cohort of 136 CHH patients (Malone, Papadakis et al. 2019). They demonstrated that GnRH cells also express AMH during their migratory process (in mice and human fetuses) and maintain this expression until adulthood. This study also demonstrates that AMH is a potent stimulator of GnRH cell motility. Invalidation of AMHR2 signalling, pharmacologically or genetically, alters GnRH migration leading to a reduced size of this neuronal population in adult brains, altered ovulation and fertility

References

Abbott, D. H., D. A. Dumesic, J. R. Eisner, R. J. Colman and J. W. Kemnitz (1998). "Insights into the development of polycystic ovary syndrome (PCOS) from studies of prenatally androgenized female rhesus monkeys." Trends Endocrinol Metab **9**(2): 62-67.

Abbott, D. H., D. A. Dumesic and S. Franks (2002). "Developmental origin of polycystic ovary syndrome - a hypothesis." J Endocrinol **174**(1): 1-5.

Abbott, D. H., B. H. Rayome, D. A. Dumesic, K. C. Lewis, A. K. Edwards, K. Wallen, M. E. Wilson, S. E. Appt and J. E. Levine (2017). "Clustering of PCOS-like traits in naturally hyperandrogenic female rhesus monkeys." Hum Reprod **32**(4): 923-936.

Abu-Hijleh, T. M., E. Gammoh, A. S. Al-Busaidi, Z. H. Malalla, S. Madan, N. Mahmood and W. Y. Almawi (2016). "Common Variants in the Sex Hormone-Binding Globulin (SHBG) Gene Influence SHBG Levels in Women with Polycystic Ovary Syndrome." Ann Nutr Metab **68**(1): 66-74.

Adachi, S., S. Yamada, Y. Takatsu, H. Matsui, M. Kinoshita, K. Takase, H. Sugiura, T. Ohtaki, H. Matsumoto, Y. Uenoyama, H. Tsukamura, K. Inoue and K. Maeda (2007). "Involvement of anteroventral periventricular metastin/kisspeptin neurons in estrogen positive feedback action on luteinizing hormone release in female rats." J Reprod Dev **53**(2): 367-378.

Adashi, E. Y., A. J. Hsueh and S. S. Yen (1981). "Insulin enhancement of luteinizing hormone and follicle-stimulating hormone release by cultured pituitary cells." Endocrinology **108**(4): 1441-1449.

Allon, M. A., R. E. Leach, J. Dunbar and M. P. Diamond (2005). "Effects of chronic hyperandrogenism and/or administered central nervous system insulin on ovarian manifestation and gonadotropin and steroid secretion." Fertility and Sterility **83**(4): 1319-1326.

Anand-Ivell, R., K. Tremellen, Y. Dai, K. Heng, M. Yoshida, P. G. Knight, G. E. Hale and R. Ivell (2013). "Circulating insulin-like factor 3 (INSL3) in healthy and infertile women." Hum Reprod **28**(11): 3093-3102.

Andrews, W. W., G. J. Mizejewski and S. R. Ojeda (1981). "Development of estradiol-positive feedback on luteinizing hormone release in the female rat: a quantitative study." Endocrinology **109**(5): 1404-1413.

Andrisse, S., K. Billings, P. Xue and S. Wu (2018). "Insulin signaling displayed a differential tissue-specific response to low-dose dihydrotestosterone in female mice." Am J Physiol Endocrinol Metab **314**(4): E353-e365.

Anttonen, M., I. Ketola, H. Parviainen, A. K. Pusa and M. Heikinheimo (2003). "FOG-2 and GATA-4 Are coexpressed in the mouse ovary and can modulate mullerian-inhibiting substance expression." Biol Reprod **68**(4): 1333-1340.

Antunes, J. L., P. W. Carmel, E. M. Housepian and M. Ferin (1978). "Luteinizing hormone-releasing hormone in human pituitary blood." J Neurosurg **49**(3): 382-386.

Arango, N. A., A. Kobayashi, Y. Wang, S. P. Jamin, H. H. Lee, G. D. Orvis and R. R. Behringer (2008). "A mesenchymal perspective of Mullerian duct differentiation and regression in Amhr2-lacZ mice." Mol Reprod Dev **75**(7): 1154-1162.

Arango, N. A., R. Lovell-Badge and R. R. Behringer (1999). "Targeted mutagenesis of the endogenous mouse Mis gene promoter: in vivo definition of genetic pathways of vertebrate sexual development." Cell **99**(4): 409-419.

Asuncion, M., R. M. Calvo, J. L. San Millan, J. Sancho, S. Avila and H. F. Escobar-Morreale (2000). "A prospective study of the prevalence of the polycystic ovary syndrome in unselected Caucasian women from Spain." J Clin Endocrinol Metab **85**(7): 2434-2438.

Azziz, R., E. Carmina, Z. Chen, A. Dunaif, J. S. Laven, R. S. Legro, D. Lizneva, B. Natterson-Horowtiz, H. J. Teede and B. O. Yildiz (2016). "Polycystic ovary syndrome." Nat Rev Dis Primers **2**: 16057.

Azziz, R., E. Carmina, D. Dewailly, E. Diamanti-Kandarakis, H. F. Escobar-Morreale, W. Futterweit, O. E. Janssen, R. S. Legro, R. J. Norman, A. E. Taylor and S. F. Witchel (2009). "The Androgen Excess and PCOS Society criteria for the polycystic ovary syndrome: the complete task force report." Fertil Steril **91**(2): 456-488.

Azziz, R. and M. D. Kashar-Miller (2000). "Family history as a risk factor for the polycystic ovary syndrome." J Pediatr Endocrinol Metab **13 Suppl 5**: 1303-1306.

Azziz, R., K. S. Woods, R. Reyna, T. J. Key, E. S. Knochenhauer and B. O. Yildiz (2004). "The prevalence and features of the polycystic ovary syndrome in an unselected population." J Clin Endocrinol Metab **89**(6): 2745-2749.

Baarends, W. M., M. J. van Helmond, M. Post, P. J. van der Schoot, J. W. Hoogerbrugge, J. P. de Winter, J. T. Uilenbroek, B. Karels, L. G. Wilming, J. H. Meijers and et al. (1994). "A novel member of the transmembrane serine/threonine kinase receptor family is specifically expressed in the gonads and in mesenchymal cells adjacent to the mullerian duct." Development **120**(1): 189-197.

Bahk, J. Y., J. S. Hyun, S. H. Chung, H. Lee, M. O. Kim, B. H. Lee and W. S. Choi (1995). "Stage specific identification of the expression of GnRH mRNA and localization of the GnRH receptor in mature rat and adult human testis." J Urol **154**(5): 1958-1961.

Baldani, D. P., L. Skrgatic, J. Z. Cerne, S. K. Oguic, B. M. Gersak and K. Gersak (2015). "Association between serum levels and pentanucleotide polymorphism in the sex hormone binding globulin gene and acardiovascular risk factors in females with polycystic ovary syndrome." Mol Med Rep **11**(5): 3941-3947.

Balen, A. H., G. S. Conway, G. Kaltsas, K. Techatrasak, P. J. Manning, C. West and H. S. Jacobs (1995). "Polycystic ovary syndrome: the spectrum of the disorder in 1741 patients." Hum Reprod **10**(8): 2107-2111.

Banerjee, U., A. Dasgupta, A. Khan, M. K. Ghosh, P. Roy, J. K. Rout, P. Roy and S. Dhara (2016). "A cross-sectional study to assess any possible linkage of C/T polymorphism in CYP17A1 gene with insulin resistance in non-obese women with polycystic ovarian syndrome." Indian J Med Res **143**(6): 739-747.

Barber, T. M., A. J. Bennett, C. J. Groves, U. Sovio, A. Ruokonen, H. Martikainen, A. Pouta, A. L. Hartikainen, P. Elliott, C. M. Lindgren, R. M. Freathy, K. Koch, W. H. Ouwehand, F. Karpe, G. S. Conway, J. A. Wass, M. R. Jarvelin, S. Franks and M. I. McCarthy (2008). "Association of variants in the fat mass and obesity associated (FTO) gene with polycystic ovary syndrome." Diabetologia **51**(7): 1153-1158.

Barry, J. A., A. R. Kay, R. Navaratnarajah, S. Iqbal, J. E. Bamfo, A. L. David, M. Hines and P. J. Hardiman (2010). "Umbilical vein testosterone in female infants born to mothers with polycystic ovary syndrome is elevated to male levels." J Obstet Gynaecol **30**(5): 444-446.

Barry, J. A., A. R. Kuczmierczyk and P. J. Hardiman (2011). "Anxiety and depression in polycystic ovary syndrome: a systematic review and meta-analysis." Hum Reprod **26**(9): 2442-2451.

Birch, R. A., V. Padmanabhan, D. L. Foster, W. P. Unsworth and J. E. Robinson (2003). "Prenatal programming of reproductive neuroendocrine function: fetal androgen exposure produces progressive disruption of reproductive cycles in sheep." Endocrinology **144**(4): 1426-1434.

Blank, S. K., C. R. McCartney and J. C. Marshall (2006). "The origins and sequelae of abnormal neuroendocrine function in polycystic ovary syndrome." Hum Reprod Update **12**(4): 351-361.

Boehm, U., P. M. Bouloux, M. T. Dattani, N. de Roux, C. Dode, L. Dunkel, A. A. Dwyer, P. Giacobini, J. P. Hardelin, A. Juul, M. Maghnie, N. Pitteloud, V. Prevot, T. Raivio, M. Tena-Sempere, R. Quinton and J. Young (2015). "Expert consensus document: European Consensus Statement on congenital hypogonadotropic hypogonadism--pathogenesis, diagnosis and treatment." Nat Rev Endocrinol **11**(9): 547-564.

Boomsma, C. M., M. J. Eijkemans, E. G. Hughes, G. H. Visser, B. C. Fauser and N. S. Macklon (2006). "A meta-analysis of pregnancy outcomes in women with polycystic ovary syndrome." Hum Reprod Update **12**(6): 673-683.

Botte, M. C., Y. Lerrant, A. Lozach, A. Berault, R. Counis and M. L. Kottler (1999). "LH down-regulates gonadotropin-releasing hormone (GnRH) receptor, but not GnRH, mRNA levels in the rat testis." J Endocrinol **162**(3): 409-415.

Boukari, K., G. Meduri, S. Brailly-Tabard, J. Guibourdenche, M. L. Ciampi, N. Massin, L. Martinerie, J. Y. Picard, R. Rey, M. Lombes and J. Young (2009). "Lack of androgen receptor expression in Sertoli cells accounts for the absence of anti-Mullerian hormone repression during early human testis development." J Clin Endocrinol Metab **94**(5): 1818-1825.

Bouret, S. G., S. J. Draper and R. B. Simerly (2004). "Formation of projection pathways from the arcuate nucleus of the hypothalamus to hypothalamic regions implicated in the neural control of feeding behavior in mice." J Neurosci **24**(11): 2797-2805.

Boyle, J. A., J. Cunningham, K. O'Dea, T. Dunbar and R. J. Norman (2012). "Prevalence of polycystic ovary syndrome in a sample of Indigenous women in Darwin, Australia." Med J Aust **196**(1): 62-66.

Buchanan, K. L. and S. M. Yellon (1993). "Developmental study of GnRH neuronal projections to the medial basal hypothalamus of the male Djungarian hamster." J Comp Neurol **333**(2): 236-245.

Buckett, W. M., R. Bouzayen, K. L. Watkin, T. Tulandi and S. L. Tan (1999). "Ovarian stromal echogenicity in women with normal and polycystic ovaries." Hum Reprod **14**(3): 618-621.

Bulun, S. E., K. Takayama, T. Suzuki, H. Sasano, B. Yilmaz and S. Sebastian (2004). "Organization of the human aromatase p450 (CYP19) gene." Semin Reprod Med **22**(1): 5-9.

Burbridge, S., I. Stewart and M. Placzek (2016). "Development of the Neuroendocrine Hypothalamus." Compr Physiol **6**(2): 623-643.

Burghen, G. A., J. R. Givens and A. E. Kitabchi (1980). "Correlation of hyperandrogenism with hyperinsulinism in polycystic ovarian disease." J Clin Endocrinol Metab **50**(1): 113-116.

Burris, T. P., W. Guo, T. Le and E. R. McCabe (1995). "Identification of a putative steroidogenic factor-1 response element in the DAX-1 promoter." Biochem Biophys Res Commun **214**(2): 576-581.

Caldwell, A. S., L. J. Middleton, M. Jimenez, R. Desai, A. C. McMahon, C. M. Allan, D. J. Handelsman and K. A. Walters (2014). "Characterization of reproductive, metabolic, and endocrine features of polycystic ovary syndrome in female hyperandrogenic mouse models." Endocrinology **155**(8): 3146-3159.

Calvo, R. M., M. Asuncion, D. Telleria, J. Sancho, J. L. San Millan and H. F. Escobar-Morreale (2001). "Screening for mutations in the steroidogenic acute regulatory protein and steroidogenic factor-1 genes, and in CYP11A and dosage-sensitive sex reversal-adrenal hypoplasia gene on the X chromosome, gene-1 (DAX-1), in hyperandrogenic hirsute women." J Clin Endocrinol Metab **86**(4): 1746-1749.

Campbell, R. E. (2018). Morphology of the Adult GnRH Neuron. The GnRH Neuron and its Control**:** 121-148.

Campbell, R. E., S. K. Han and A. E. Herbison (2005). "Biocytin filling of adult gonadotropin-releasing hormone neurons in situ reveals extensive, spiny, dendritic processes." Endocrinology **146**(3): 1163-1169.

Carey, A. H., D. Waterworth, K. Patel, D. White, J. Little, P. Novelli, S. Franks and R. Williamson (1994). "Polycystic ovaries and premature male pattern baldness are associated with one allele of the steroid metabolism gene CYP17." Hum Mol Genet **3**(10): 1873-1876.

Carmina, E., R. S. Legro, K. Stamets, J. Lowell and R. A. Lobo (2003). "Difference in body weight between American and Italian women with polycystic ovary syndrome: influence of the diet." Hum Reprod **18**(11): 2289-2293.

Caron, E., P. Ciofi, V. Prevot and S. G. Bouret (2012). "Alteration in neonatal nutrition causes perturbations in hypothalamic neural circuits controlling reproductive function." J Neurosci **32**(33): 11486-11494.

Casarini, L. and G. Brigante (2014). "The polycystic ovary syndrome evolutionary paradox: a genome-wide association studies-based, in silico, evolutionary explanation." J Clin Endocrinol Metab **99**(11): E2412-2420.

Casoni, F., S. A. Malone, M. Belle, F. Luzzati, F. Collier, C. Allet, E. Hrabovszky, S. Rasika, V. Prevot, A. Chedotal and P. Giacobini (2016). "Development of the neurons controlling fertility in humans: new insights from 3D imaging and transparent fetal brains." Development **143**(21): 3969-3981.

Cattanach, B. M., C. A. Iddon, H. M. Charlton, S. A. Chiappa and G. Fink (1977). "Gonadotrophin-releasing hormone deficiency in a mutant mouse with hypogonadism." Nature **269**(5626): 338-340.

Chachlaki, K., S. A. Malone, E. Qualls-Creekmore, E. Hrabovszky, H. Munzberg, P. Giacobini, F. Ango and V. Prevot (2017). "Phenotyping of nNOS neurons in the postnatal and adult female mouse hypothalamus." J Comp Neurol **525**(15): 3177-3189.

Chemes, H. E., R. A. Rey, M. Nistal, J. Regadera, M. Musse, P. Gonzalez-Peramato and A. Serrano (2008). "Physiological androgen insensitivity of the fetal, neonatal, and early infantile testis is explained by the

ontogeny of the androgen receptor expression in Sertoli cells." J Clin Endocrinol Metab **93**(11): 4408-4412.

Chen, H. F., E. B. Jeung, M. Stephenson and P. C. Leung (1999). "Human peripheral blood mononuclear cells express gonadotropin-releasing hormone (GnRH), GnRH receptor, and interleukin-2 receptor gamma-chain messenger ribonucleic acids that are regulated by GnRH in vitro." J Clin Endocrinol Metab **84**(2): 743-750.

Chen, J., S. Shen, Y. Tan, D. Xia, Y. Xia, Y. Cao, W. Wang, X. Wu, H. Wang, L. Yi, Q. Gao and Y. Wang (2015). "The correlation of aromatase activity and obesity in women with or without polycystic ovary syndrome." Journal of Ovarian Research **8**(1): 11.

Chen, Z. J., H. Zhao, L. He, Y. Shi, Y. Qin, Y. Shi, Z. Li, L. You, J. Zhao, J. Liu, X. Liang, X. Zhao, J. Zhao, Y. Sun, B. Zhang, H. Jiang, D. Zhao, Y. Bian, X. Gao, L. Geng, Y. Li, D. Zhu, X. Sun, J. E. Xu, C. Hao, C. E. Ren, Y. Zhang, S. Chen, W. Zhang, A. Yang, J. Yan, Y. Li, J. Ma and Y. Zhao (2011). "Genome-wide association study identifies susceptibility loci for polycystic ovary syndrome on chromosome 2p16.3, 2p21 and 9q33.3." Nat Genet **43**(1): 55-59.

Cheng, C. K., B. K. Chow and P. C. Leung (2003). "An activator protein 1-like motif mediates 17beta-estradiol repression of gonadotropin-releasing hormone receptor promoter via an estrogen receptor alpha-dependent mechanism in ovarian and breast cancer cells." Mol Endocrinol **17**(12): 2613-2629.

Cheng, C. K. and P. C. Leung (2005). "Molecular biology of gonadotropin-releasing hormone (GnRH)-I, GnRH-II, and their receptors in humans." Endocr Rev **26**(2): 283-306.

Cheng, K. W. and P. C. Leung (2002). "Human chorionic gonadotropin-activated cAMP pathway regulates human placental GnRH receptor gene transcription in choriocarcinoma JEG-3 cells." J Clin Endocrinol Metab **87**(7): 3291-3299.

Cherskov, A., A. Pohl, C. Allison, H. Zhang, R. A. Payne and S. Baron-Cohen (2018). "Polycystic ovary syndrome and autism: A test of the prenatal sex steroid theory." Translational Psychiatry **8**(1): 136.

Christian, C. A. and S. M. Moenter (2010). "The neurobiology of preovulatory and estradiol-induced gonadotropin-releasing hormone surges." Endocr Rev **31**(4): 544-577.

Cimino, I., F. Casoni, X. Liu, A. Messina, J. Parkash, S. P. Jamin, S. Catteau-Jonard, F. Collier, M. Baroncini, D. Dewailly, P. Pigny, M. Prescott, R. Campbell, A. E. Herbison, V. Prevot and P. Giacobini (2016). "Novel role for anti-Mullerian hormone in the regulation of GnRH neuron excitability and hormone secretion." Nat Commun **7**: 10055.

Clarke, T. R., Y. Hoshiya, S. E. Yi, X. Liu, K. M. Lyons and P. K. Donahoe (2001). "Müllerian Inhibiting Substance Signaling Uses a Bone Morphogenetic Protein (BMP)-Like Pathway Mediated by ALK2 and Induces Smad6 Expression." Molecular Endocrinology **15**(6): 946-959.

Clarkson, J., X. d'Anglemont de Tassigny, A. S. Moreno, W. H. Colledge and A. E. Herbison (2008). "Kisspeptin-GPR54 signaling is essential for preovulatory gonadotropin-releasing hormone neuron activation and the luteinizing hormone surge." J Neurosci **28**(35): 8691-8697.

Clipsham, R. and E. R. McCabe (2003). "DAX1 and its network partners: exploring complexity in development." Mol Genet Metab **80**(1-2): 81-120.

Cohen-Haguenauer, O., J. Y. Picard, M. G. Mattéi, S. Serero, N. Van Cong, M. F. de Tand, D. Guerrier, M. C. Hors-Cayla, N. Josso and J. Frézal (1987). "Mapping of the gene for anti-Müllerian hormone to the short arm of human chromosome 19." Cytogenetic and Genome Research **44**(1): 2-6.

Constantin, S. (2011). "Physiology of the gonadotrophin-releasing hormone (GnRH) neurone: studies from embryonic GnRH neurones." J Neuroendocrinol **23**(6): 542-553.

Conway, G., D. Dewailly, E. Diamanti-Kandarakis, H. F. Escobar-Morreale, S. Franks, A. Gambineri, F. Kelestimur, D. Macut, D. Micic, R. Pasquali, M. Pfeifer, D. Pignatelli, M. Pugeat and B. O. Yildiz (2014). "The polycystic ovary syndrome: a position statement from the European Society of Endocrinology." Eur J Endocrinol **171**(4): P1-29.

Cottrell, E. C., R. E. Campbell, S. K. Han and A. E. Herbison (2006). "Postnatal remodeling of dendritic structure and spine density in gonadotropin-releasing hormone neurons." Endocrinology **147**(8): 3652-3661.

Cousin, P., L. Calemard-Michel, H. Lejeune, G. Raverot, N. Yessaad, A. Emptoz-Bonneton, Y. Morel and M. Pugeat (2004). "Influence of SHBG gene pentanucleotide TAAAA repeat and D327N polymorphism on serum sex hormone-binding globulin concentration in hirsute women." J Clin Endocrinol Metab **89**(2): 917-924.

Crisosto, N., E. Codner, M. Maliqueo, B. Echiburu, F. Sanchez, F. Cassorla and T. Sir-Petermann (2007). "Anti-Mullerian hormone levels in peripubertal daughters of women with polycystic ovary syndrome." J Clin Endocrinol Metab **92**(7): 2739-2743.

Cunha, G. R., S. J. Robboy, T. Kurita, D. Isaacson, J. Shen, M. Cao and L. S. Baskin (2018). "Development of the human female reproductive tract." Differentiation **103**: 46-65.

Cussons, A. J., B. G. Stuckey, J. P. Walsh, V. Burke and R. J. Norman (2005). "Polycystic ovarian syndrome: marked differences between endocrinologists and gynaecologists in diagnosis and management." Clin Endocrinol (Oxf) **62**(3): 289-295.

Daneshmand, S. d., S. R. Weitsman, A. Navab, A. J. Jakimiuk and D. A. Magoffin (2002). "Overexpression of theca-cell messenger RNA in polycystic ovary syndrome does not correlate with polymorphisms in the cholesterol side-chain cleavage and 17α-hydroxylase/C₁₇₋₂₀ lyase promoters." Fertility and Sterility **77**(2): 274-280.

Day, F. R., D. A. Hinds, J. Y. Tung, L. Stolk, U. Styrkarsdottir, R. Saxena, A. Bjonnes, L. Broer, D. B. Dunger, B. V. Halldorsson, D. A. Lawlor, G. Laval, I. Mathieson, W. L. McCardle, Y. Louwers, C. Meun, S. Ring, R. A. Scott, P. Sulem, A. G. Uitterlinden, N. J. Wareham, U. Thorsteinsdottir, C. Welt, K. Stefansson, J. S. E. Laven, K. K. Ong and J. R. B. Perry (2015). "Causal mechanisms and balancing selection inferred from genetic associations with polycystic ovary syndrome." Nat Commun **6**: 8464.

Demissie, M., M. Lazic, E. M. Foecking, F. Aird, A. Dunaif and J. E. Levine (2008). "Transient prenatal androgen exposure produces metabolic syndrome in adult female rats." Am J Physiol Endocrinol Metab **295**(2): E262-268.

Depmann, M., J. van Disseldorp, S. L. Broer, M. J. Eijkemans, J. S. Laven, J. A. Visser, Y. B. de Rijke, B. W. Mol and F. J. Broekmans (2016). "Fluctuations in anti-Mullerian hormone levels throughout the menstrual cycle parallel fluctuations in the antral follicle count: a cohort study." Acta Obstet Gynecol Scand **95**(7): 820-828.

Devillers, M. M., F. Petit, V. Cluzet, C. M. Francois, F. Giton, G. Garrel, J. Cohen-Tannoudji and C. J. Guigon (2019). "FSH inhibits AMH to support ovarian estradiol synthesis in infantile mice." J Endocrinol **240**(2): 215-228.

Devillers, M. M., F. Petit, V. Cluzet, C. M. Francois, F. Giton, G. Garrel, J. Cohen-Tannoudji and C. J. Guigon (2019). "[Ovarian estradiol production during mini-puberty: importance of the cross-talk between FSH and AMH]." Med Sci (Paris) **35**(3): 201-203.

Dewailly, D., H. Gronier, E. Poncelet, G. Robin, M. Leroy, P. Pigny, A. Duhamel and S. Catteau-Jonard (2011). "Diagnosis of polycystic ovary syndrome (PCOS): revisiting the threshold values of follicle count on ultrasound and of the serum AMH level for the definition of polycystic ovaries." Hum Reprod **26**(11): 3123-3129.

Dewailly, D., S. Hieronimus, P. Mirakian and J. N. Hugues (2010). "Polycystic ovary syndrome (PCOS)." Ann Endocrinol (Paris) **71**(1): 8-13.

di Clemente, N., S. P. Jamin, A. Lugovskoy, P. Carmillo, C. Ehrenfels, J. Y. Picard, A. Whitty, N. Josso, R. B. Pepinsky and R. L. Cate (2010). "Processing of anti-mullerian hormone regulates receptor activation by a mechanism distinct from TGF-beta." Mol Endocrinol **24**(11): 2193-2206.

di Clemente, N., C. Wilson, E. Faure, L. Boussin, P. Carmillo, R. Tizard, J. Y. Picard, B. Vigier, N. Josso and R. Cate (1994). "Cloning, expression, and alternative splicing of the receptor for anti-Mullerian hormone." Mol Endocrinol **8**(8): 1006-1020.

Diamanti-Kandarakis, E., M. I. Bartzis, A. T. Bergiele, T. C. Tsianateli and C. R. Kouli (2000). "Microsatellite polymorphism (tttta)(n) at -528 base pairs of gene CYP11alpha influences hyperandrogenemia in patients with polycystic ovary syndrome." Fertil Steril **73**(4): 735-741.

Diamanti-Kandarakis, E. and A. Dunaif (2012). "Insulin resistance and the polycystic ovary syndrome revisited: an update on mechanisms and implications." Endocr Rev **33**(6): 981-1030.

Diamanti-Kandarakis, E., H. Kandarakis and R. S. Legro (2006). "The role of genes and environment in the etiology of PCOS." Endocrine **30**(1): 19-26.

Diamanti-Kandarakis, E., C. R. Kouli, A. T. Bergiele, F. A. Filandra, T. C. Tsianateli, G. G. Spina, E. D. Zapanti and M. I. Bartzis (1999). "A survey of the polycystic ovary syndrome in the Greek island of Lesbos: hormonal and metabolic profile." J Clin Endocrinol Metab **84**(11): 4006-4011.

Dohler, K. D. and W. Wuttke (1974). "Serum LH, FSH, prolactin and progesterone from birth to puberty in female and male rats." Endocrinology **94**(4): 1003-1008.

Dokras, A., S. Clifton, W. Futterweit and R. Wild (2012). "Increased prevalence of anxiety symptoms in women with polycystic ovary syndrome: systematic review and meta-analysis." Fertil Steril **97**(1): 225-230.e222.

Donahoe, P. K., Y. Ito, J. M. Price and W. H. Hendren, 3rd (1977). "Mullerian inhibiting substance activity in bovine fetal, newborn and prepubertal testes." Biol Reprod **16**(2): 238-243.

Dresser, D. W., A. Hacker, R. Lovell-Badge and D. Guerrier (1995). "The genes for a spliceosome protein (SAP62) and the anti-Mullerian hormone (AMH) are contiguous." Hum Mol Genet **4**(9): 1613-1618.

Dumesic, D. A., D. H. Abbott, J. R. Eisner and R. W. Goy (1997). "Prenatal exposure of female rhesus monkeys to testosterone propionate increases serum luteinizing hormone levels in adulthood." Fertil Steril **67**(1): 155-163.

Dumesic, D. A. and R. A. Lobo (2013). "Cancer risk and PCOS." Steroids **78**(8): 782-785.

Dumont, A., G. Robin, S. Catteau-Jonard and D. Dewailly (2015). "Role of Anti-Müllerian Hormone in pathophysiology, diagnosis and treatment of Polycystic Ovary Syndrome: a review." Reprod Biol Endocrinol **13**: 137.

Dunaif, A. (1999). "Insulin action in the polycystic ovary syndrome." Endocrinol Metab Clin North Am **28**(2): 341-359.

Dunaif, A., K. R. Segal, W. Futterweit and A. Dobrjansky (1989). "Profound peripheral insulin resistance, independent of obesity, in polycystic ovary syndrome." Diabetes **38**(9): 1165-1174.

Echiburu, B., F. Perez-Bravo, M. Maliqueo, F. Sanchez, N. Crisosto and T. Sir-Petermann (2008). "Polymorphism T --> C (-34 base pairs) of gene CYP17 promoter in women with polycystic ovary syndrome is associated with increased body weight and insulin resistance: a preliminary study." Metabolism **57**(12): 1765-1771.

Eisner, J. R., M. A. Barnett, D. A. Dumesic and D. H. Abbott (2002). "Ovarian hyperandrogenism in adult female rhesus monkeys exposed to prenatal androgen excess." Fertil Steril **77**(1): 167-172.

Elmquist, J. K., R. Coppari, N. Balthasar, M. Ichinose and B. B. Lowell (2005). "Identifying hypothalamic pathways controlling food intake, body weight, and glucose homeostasis." J Comp Neurol **493**(1): 63-71.

Escobar-Morreale, H. F., M. Luque-Ramirez and F. Gonzalez (2011). "Circulating inflammatory markers in polycystic ovary syndrome: a systematic review and metaanalysis." Fertil Steril **95**(3): 1048-1058.e1041-1042.

Ezzat, A., A. Pereira and I. J. Clarke (2015). "Kisspeptin is a component of the pulse generator for GnRH secretion in female sheep but not the pulse generator." Endocrinology **156**(5): 1828-1837.

Fauser, B. C., B. C. Tarlatzis, R. W. Rebar, R. S. Legro, A. H. Balen, R. Lobo, E. Carmina, J. Chang, B. O. Yildiz, J. S. Laven, J. Boivin, F. Petraglia, C. N. Wijeyeratne, R. J. Norman, A. Dunaif, S. Franks, R. A. Wild, D. Dumesic and K. Barnhart (2012). "Consensus on women's health aspects of polycystic ovary syndrome (PCOS): the Amsterdam ESHRE/ASRM-Sponsored 3rd PCOS Consensus Workshop Group." Fertil Steril **97**(1): 28-38.e25.

Ferk, P., M. P. Perme, N. Teran and K. Gersak (2008). "Androgen receptor gene (CAG)n polymorphism in patients with polycystic ovary syndrome." Fertil Steril **90**(3): 860-863.

Ferk, P., N. Teran and K. Gersak (2007). "The (TAAAA)n microsatellite polymorphism in the SHBG gene influences serum SHBG levels in women with polycystic ovary syndrome." Hum Reprod **22**(4): 1031-1036.

Fernandez-Vazquez, G., U. B. Kaiser, C. T. Albarracin and W. W. Chin (1996). "Transcriptional activation of the gonadotropin-releasing hormone receptor gene by activin A." Mol Endocrinol **10**(4): 356-366.

Ferriman, D. and J. D. Gallwey (1961). "Clinical assessment of body hair growth in women." J Clin Endocrinol Metab **21**: 1440-1447.

Fink, G. (2015). "60 YEARS OF NEUROENDOCRINOLOGY: MEMOIR: Harris' neuroendocrine revolution: of portal vessels and self-priming." J Endocrinol **226**(2): T13-24.

Foecking, E. M., M. Szabo, N. B. Schwartz and J. E. Levine (2005). "Neuroendocrine consequences of prenatal androgen exposure in the female rat: absence of luteinizing hormone surges, suppression of progesterone receptor gene expression, and acceleration of the gonadotropin-releasing hormone pulse generator." Biol Reprod **72**(6): 1475-1483.

Franks, S., J. Adams, H. Mason and D. Polson (1985). "Ovulatory disorders in women with polycystic ovary syndrome." Clin Obstet Gynaecol **12**(3): 605-632.

Franks, S., N. Gharani and M. McCarthy (2001). "Candidate genes in polycystic ovary syndrome." Hum Reprod Update **7**(4): 405-410.

Gaasenbeek, M., B. L. Powell, U. Sovio, L. Haddad, N. Gharani, A. Bennett, C. J. Groves, K. Rush, M. J. Goh, G. S. Conway, A. Ruokonen, H. Martikainen, A. Pouta, S. Taponen, A. L. Hartikainen, S. Halford, M. R. Jarvelin, S. Franks and M. I. McCarthy (2004). "Large-scale analysis of the relationship between CYP11A promoter variation, polycystic ovarian syndrome, and serum testosterone." J Clin Endocrinol Metab **89**(5): 2408-2413.

Gambineri, A., L. Patton, O. Prontera, F. Fanelli, W. Ciampaglia, G. E. Cognigni, U. Pagotto and R. Pasquali (2011). "Basal insulin-like factor 3 levels predict functional ovarian hyperandrogenism in the polycystic ovary syndrome." J Endocrinol Invest **34**(9): 685-691.

Gao, G. H., Y. X. Cao, L. Yi, Z. L. Wei, Y. P. Xu and C. Yang (2010). "[Polymorphism of CYP11A1 gene in Chinese patients with polycystic ovarian syndrome]." Zhonghua Fu Chan Ke Za Zhi **45**(3): 191-196.

Gao, Q. and J. E. Womack (1997). "A genetic map of bovine chromosome 7 with an interspecific hybrid backcross panel." Mamm Genome **8**(4): 258-261.

Garrel, G., C. Denoyelle, D. L'Hote, J. Y. Picard, J. Teixeira, U. B. Kaiser, J. N. Laverriere and J. Cohen-Tannoudji (2019). "GnRH Transactivates Human AMH Receptor Gene via Egr1 and FOXO1 in Gonadotrope Cells." Neuroendocrinology **108**(2): 65-83.

Garrel, G., C. Racine, D. L'Hote, C. Denoyelle, C. J. Guigon, N. di Clemente and J. Cohen-Tannoudji (2016). "[Anti-Mullerian hormone: a new regulator of pituitary gonadotrope cells. Involvement in sexual dimorphism of gonadotrope activity before puberty]." Med Sci (Paris) **32**(12): 1076-1078.

Georgopoulos, N. A., E. Karagiannidou, V. Koika, N. D. Roupas, A. Armeni, D. Marioli, E. Papadakis, C. K. Welt and D. Panidis (2013). "Increased frequency of the anti-mullerian-inhibiting hormone receptor 2

(AMHR2) 482 A>G polymorphism in women with polycystic ovary syndrome: relationship to luteinizing hormone levels." J Clin Endocrinol Metab **98**(11): E1866-1870.

Gharani, N., D. M. Waterworth, S. Batty, D. White, C. Gilling-Smith, G. S. Conway, M. McCarthy, S. Franks and R. Williamson (1997). "Association of the steroid synthesis gene CYP11a with polycystic ovary syndrome and hyperandrogenism." Hum Mol Genet **6**(3): 397-402.

Gharani, N., D. M. Waterworth, R. Williamson and S. Franks (1996). "5' polymorphism of the CYP17 gene is not associated with serum testosterone levels in women with polycystic ovaries." J Clin Endocrinol Metab **81**(11): 4174.

Gilling-Smith, C., D. S. Willis, R. W. Beard and S. Franks (1994). "Hypersecretion of androstenedione by isolated thecal cells from polycystic ovaries." J Clin Endocrinol Metab **79**(4): 1158-1165.

Glister, C., L. Satchell, R. A. Bathgate, J. D. Wade, Y. Dai, R. Ivell, R. Anand-Ivell, R. J. Rodgers and P. G. Knight (2013). "Functional link between bone morphogenetic proteins and insulin-like peptide 3 signaling in modulating ovarian androgen production." Proc Natl Acad Sci U S A **110**(15): E1426-1435.

Goldzieher, J. W. and J. A. Green (1962). "The polycystic ovary. I. Clinical and histologic features." J Clin Endocrinol Metab **22**: 325-338.

Goodarzi, M. O., D. A. Dumesic, G. Chazenbalk and R. Azziz (2011). "Polycystic ovary syndrome: etiology, pathogenesis and diagnosis." Nat Rev Endocrinol **7**(4): 219-231.

Gouedard, L., Y. G. Chen, L. Thevenet, C. Racine, S. Borie, I. Lamarre, N. Josso, J. Massague and N. di Clemente (2000). "Engagement of bone morphogenetic protein type IB receptor and Smad1 signaling by anti-Mullerian hormone and its type II receptor." J Biol Chem **275**(36): 27973-27978.

Grosse, R., T. Schoneberg, G. Schultz and T. Gudermann (1997). "Inhibition of gonadotropin-releasing hormone receptor signaling by expression of a splice variant of the human receptor." Mol Endocrinol **11**(9): 1305-1318.

Hague, W. M., J. Adams, S. T. Reeders, T. E. Peto and H. S. Jacobs (1988). "Familial polycystic ovaries: a genetic disease?" Clin Endocrinol (Oxf) **29**(6): 593-605.

Hamilton-Fairley, D. and A. Taylor (2003). "Anovulation." Bmj **327**(7414): 546-549.

Hammond, G. L. (2016). "Plasma steroid-binding proteins: primary gatekeepers of steroid hormone action." J Endocrinol **230**(1): R13-25.

Handa, R. J. and M. J. Weiser (2014). "Gonadal steroid hormones and the hypothalamo-pituitary-adrenal axis." Front Neuroendocrinol **35**(2): 197-220.

Hao, C. F., H. C. Bao, N. Zhang, H. F. Gu and Z. J. Chen (2009). "Evaluation of association between the CYP11alpha promoter pentannucleotide (TTTTA)n polymorphism and polycystic ovarian syndrome among Han Chinese women." Neuro Endocrinol Lett **30**(1): 56-60.

Hao, C. F., N. Zhang, Q. Qu, X. Wang, H. F. Gu and Z. J. Chen (2010). "Evaluation of the association between the CYP19 Tetranucleotide (TTTA)n polymorphism and polycystic ovarian syndrome(PCOS) in Han Chinese women." Neuro Endocrinol Lett **31**(3): 370-374.

Haoula, Z., M. Salman and W. Atiomo (2012). "Evaluating the association between endometrial cancer and polycystic ovary syndrome." Human Reproduction **27**(5): 1327-1331.

Haqq, C. M., C. Y. King, E. Ukiyama, S. Falsafi, T. N. Haqq, P. K. Donahoe and M. A. Weiss (1994). "Molecular basis of mammalian sexual determination: activation of Mullerian inhibiting substance gene expression by SRY." Science **266**(5190): 1494-1500.

Hatch, R., R. L. Rosenfield, M. H. Kim and D. Tredway (1981). "Hirsutism: implications, etiology, and management." Am J Obstet Gynecol **140**(7): 815-830.

Herbison, A. E. (1998). "Multimodal influence of estrogen upon gonadotropin-releasing hormone neurons." Endocr Rev **19**(3): 302-330.

Herbison, A. E. (2018). "The Gonadotropin-Releasing Hormone Pulse Generator." Endocrinology **159**(11): 3723-3736.

Heywood, S. G. and S. M. Yellon (1997). "Gonadotropin-releasing hormone neural projections to the systemic vasculature during sexual maturation and delayed puberty in the male Djungarian hamster." Biol Reprod **57**(4): 873-878.

Hogeveen, K. N., P. Cousin, M. Pugeat, D. Dewailly, B. Soudan and G. L. Hammond (2002). "Human sex hormone-binding globulin variants associated with hyperandrogenism and ovarian dysfunction." J Clin Invest **109**(7): 973-981.

Hoshiya, Y., V. Gupta, D. L. Segev, M. Hoshiya, J. L. Carey, L. M. Sasur, T. T. Tran, T. U. Ha and S. Maheswaran (2003). "Mullerian Inhibiting Substance induces NFkB signaling in breast and prostate cancer cells." Mol Cell Endocrinol **211**(1-2): 43-49.

Hu, M., J. E. Richard, M. Maliqueo, M. Kokosar, R. Fornes, A. Benrick, T. Jansson, C. Ohlsson, X. Wu, K. P. Skibicka and E. Stener-Victorin (2015). "Maternal testosterone exposure increases anxiety-like behavior and impacts the limbic system in the offspring." Proc Natl Acad Sci U S A **112**(46): 14348-14353.

Huhtaniemi, I. (2015). "A short evolutionary history of FSH-stimulated spermatogenesis." Hormones (Athens) **14**(4): 468-478.

Imbeaud, S., E. Faure, I. Lamarre, M. G. Mattei, N. di Clemente, R. Tizard, D. Carre-Eusebe, C. Belville, L. Tragethon, C. Tonkin, J. Nelson, M. McAuliffe, J. M. Bidart, A. Lababidi, N. Josso, R. L. Cate and J. Y. Picard (1995). "Insensitivity to anti-mullerian hormone due to a mutation in the human anti-mullerian hormone receptor." Nat Genet **11**(4): 382-388.

Jahanfar, S., J. A. Eden, P. Warren, M. Seppala and T. V. Nguyen (1995). "A twin study of polycystic ovary syndrome." Fertil Steril **63**(3): 478-486.

Jamin, S. P., N. A. Arango, Y. Mishina, M. C. Hanks and R. R. Behringer (2002). "Requirement of Bmpr1a for Müllerian duct regression during male sexual development." Nature Genetics **32**(3): 408-410.

Jamin, S. P., N. A. Arango, Y. Mishina, M. C. Hanks and R. R. Behringer (2003). "Genetic studies of the AMH/MIS signaling pathway for Mullerian duct regression." Mol Cell Endocrinol **211**(1-2): 15-19.

Janssen, J. A., R. P. Stolk, H. A. Pols, D. E. Grobbee, F. H. de Jong and S. W. Lamberts (1998). "Serum free IGF-I, total IGF-I, IGFBP-1 and IGFBP-3 levels in an elderly population: relation to age and sex steroid levels." Clin Endocrinol (Oxf) **48**(4): 471-478.

Jeppesen, J. V., R. A. Anderson, T. W. Kelsey, S. L. Christiansen, S. G. Kristensen, K. Jayaprakasan, N. Raine-Fenning, B. K. Campbell and C. Yding Andersen (2013). "Which follicles make the most anti-Mullerian hormone in humans? Evidence for an abrupt decline in AMH production at the time of follicle selection." Mol Hum Reprod **19**(8): 519-527.

Jin, J. L., J. Sun, H. J. Ge, Y. X. Cao, X. K. Wu, F. J. Liang, H. X. Sun, L. Ke, L. Yi, Z. W. Wu and Y. Wang (2009). "Association between CYP19 gene SNP rs2414096 polymorphism and polycystic ovary syndrome in Chinese women." BMC Med Genet **10**: 139.

Jonard, S. and D. Dewailly (2004). "The follicular excess in polycystic ovaries, due to intra-ovarian hyperandrogenism, may be the main culprit for the follicular arrest." Hum Reprod Update **10**(2): 107-117.

Jost, A. (1947). "The age factor in the castration of male rabbit fetuses." Proc Soc Exp Biol Med **66**(2): 302.

Ju, R., W. Wu, J. Fei, Y. Qin, Q. Tang, D. Wu, Y. Xia, J. Wu and X. Wang (2015). "Association analysis between the polymorphisms of HSD17B5 and HSD17B6 and risk of polycystic ovary syndrome in Chinese population." Eur J Endocrinol **172**(3): 227-233.

Kaartinen, V., J. W. Voncken, C. Shuler, D. Warburton, D. Bu, N. Heisterkamp and J. Groffen (1995). "Abnormal lung development and cleft palate in mice lacking TGF-beta 3 indicates defects of epithelial-mesenchymal interaction." Nat Genet **11**(4): 415-421.

Kahsar-Miller, M., L. R. Boots, A. Bartolucci and R. Azziz (2004). "Role of a CYP17 polymorphism in the regulation of circulating dehydroepiandrosterone sulfate levels in women with polycystic ovary syndrome." Fertil Steril **82**(4): 973-975.

Kakar, S. S. (1997). "Molecular structure of the human gonadotropin-releasing hormone receptor gene." Eur J Endocrinol **137**(2): 183-192.

Kallo, I., B. Vida, L. Deli, C. S. Molnar, E. Hrabovszky, A. Caraty, P. Ciofi, C. W. Coen and Z. Liposits (2012). "Co-localisation of kisspeptin with galanin or neurokinin B in afferents to mouse GnRH neurones." J Neuroendocrinol **24**(3): 464-476.

Kang, S. K., K. C. Choi, K. W. Cheng, P. S. Nathwani, N. Auersperg and P. C. Leung (2000). "Role of gonadotropin-releasing hormone as an autocrine growth factor in human ovarian surface epithelium." Endocrinology **141**(1): 72-80.

Kim, J. J., S. H. Choung, Y. M. Choi, S. H. Yoon, S. H. Kim and S. Y. Moon (2008). "Androgen receptor gene CAG repeat polymorphism in women with polycystic ovary syndrome." Fertil Steril **90**(6): 2318-2323.

Kimura, F. and M. Kawakami (1982). "Episodic lh secretion in the immature male and female rat as assessed by sequential blood sampling." Neuroendocrinology **35**(2): 128-132.

King, T. R., B. K. Lee, R. R. Behringer and E. M. Eicher (1991). "Mapping anti-mullerian hormone (Amh) and related sequences in the mouse: identification of a new region of homology between MMU10 and HSA19p." Genomics **11**(2): 273-283.

Kingsley, D. M. (1994). "The TGF-beta superfamily: new members, new receptors, and new genetic tests of function in different organisms." Genes Dev **8**(2): 133-146.

Kloth, L., G. Belge, K. Burchardt, S. Loeschke, W. Wosniok, X. Fu, R. Nimzyk, S. A. Mohamed, N. Drieschner, V. Rippe and J. Bullerdiek (2011). "Decrease in thyroid adenoma associated (THADA) expression is a marker of dedifferentiation of thyroid tissue." BMC Clin Pathol **11**: 13.

Kobayashi, A. and R. R. Behringer (2003). "Developmental genetics of the female reproductive tract in mammals." Nat Rev Genet **4**(12): 969-980.

Kreidberg, J. A., H. Sariola, J. M. Loring, M. Maeda, J. Pelletier, D. Housman and R. Jaenisch (1993). "WT-1 is required for early kidney development." Cell **74**(4): 679-691.

Krentz, A. J., D. von Muhlen and E. Barrett-Connor (2007). "Searching for polycystic ovary syndrome in postmenopausal women: evidence of a dose-effect association with prevalent cardiovascular disease." Menopause **14**(2): 284-292.

Kwakowsky, A., A. E. Herbison and I. M. Abraham (2012). "The role of cAMP response element-binding protein in estrogen negative feedback control of gonadotropin-releasing hormone neurons." J Neurosci **32**(33): 11309-11317.

La Marca, A., G. Sighinolfi, D. Radi, C. Argento, E. Baraldi, A. C. Artenisio, G. Stabile and A. Volpe (2010). "Anti-Mullerian hormone (AMH) as a predictive marker in assisted reproductive technology (ART)." Hum Reprod Update **16**(2): 113-130.

Laven, J. S., A. G. Mulders, J. A. Visser, A. P. Themmen, F. H. De Jong and B. C. Fauser (2004). "Anti-Mullerian hormone serum concentrations in normoovulatory and anovulatory women of reproductive age." J Clin Endocrinol Metab **89**(1): 318-323.

Laws, S. C., M. J. Beggs, J. C. Webster and W. L. Miller (1990). "Inhibin increases and progesterone decreases receptors for gonadotropin-releasing hormone in ovine pituitary culture." Endocrinology **127**(1): 373-380.

Legro, R. S., V. D. Castracane and R. P. Kauffman (2004). "Detecting insulin resistance in polycystic ovary syndrome: purposes and pitfalls." Obstet Gynecol Surv **59**(2): 141-154.

Legro, R. S., D. Driscoll, J. F. Strauss, 3rd, J. Fox and A. Dunaif (1998). "Evidence for a genetic basis for hyperandrogenemia in polycystic ovary syndrome." Proc Natl Acad Sci U S A **95**(25): 14956-14960.

Lethimonier, C., T. Madigou, J. A. Munoz-Cueto, J. J. Lareyre and O. Kah (2004). "Evolutionary aspects of GnRHs, GnRH neuronal systems and GnRH receptors in teleost fish." Gen Comp Endocrinol **135**(1): 1-16.

Levine, J. E. (1997). "New concepts of the neuroendocrine regulation of gonadotropin surges in rats." Biol Reprod **56**(2): 293-302.

Li, H., Y. Chen, L. Y. Yan and J. Qiao (2013). "Increased expression of P450scc and CYP17 in development of endogenous hyperandrogenism in a rat model of PCOS." Endocrine **43**(1): 184-190.

Li, L., Z. P. Gu, Q. M. Bo, D. Wang, X. S. Yang and G. H. Cai (2015). "Association of CYP17A1 gene -34T/C polymorphism with polycystic ovary syndrome in Han Chinese population." Gynecol Endocrinol **31**(1): 40-43.

Li, T. and Z. Guijin (2005). "Role of the pentanucleotide (tttta)n polymorphisms ofCYP11α gene in the pathogenesis of hyperandrogenism in chinese women with polycystic ovary syndrome." Journal of Huazhong University of Science and Technology [Medical Sciences] **25**(2): 212-214.

Lin, L. H., M. C. Baracat, G. A. Maciel, J. M. Soares, Jr. and E. C. Baracat (2013). "Androgen receptor gene polymorphism and polycystic ovary syndrome." Int J Gynaecol Obstet **120**(2): 115-118.

Lizneva, D., L. Suturina, W. Walker, S. Brakta, L. Gavrilova-Jordan and R. Azziz (2016). "Criteria, prevalence, and phenotypes of polycystic ovary syndrome." Fertility and Sterility **106**(1): 6-15.

Luo, K. and H. F. Lodish (1997). "Positive and negative regulation of type II TGF-beta receptor signal transduction by autophosphorylation on multiple serine residues." Embo j **16**(8): 1970-1981.

Luo, X., Y. Ikeda and K. L. Parker (1994). "A cell-specific nuclear receptor is essential for adrenal and gonadal development and sexual differentiation." Cell **77**(4): 481-490.

Ma, Y. M., R. Li, J. Qiao, X. W. Zhang, S. Y. Wang, Q. F. Zhang, L. Li, B. B. Tu and X. Zhang (2010). "Characteristics of abnormal menstrual cycle and polycystic ovary syndrome in community and hospital populations." Chin Med J (Engl) **123**(16): 2185-2189.

Maeda, K., S. Ohkura, Y. Uenoyama, Y. Wakabayashi, Y. Oka, H. Tsukamura and H. Okamura (2010). "Neurobiological mechanisms underlying GnRH pulse generation by the hypothalamus." Brain Res **1364**: 103-115.

Maier, P. S. and P. M. Spritzer (2012). "Aromatase gene polymorphism does not influence clinical phenotype and response to oral contraceptive pills in polycystic ovary syndrome women." Gynecol Obstet Invest **74**(2): 136-142.

Maliqueo, M., H. E. Lara, F. Sanchez, B. Echiburu, N. Crisosto and T. Sir-Petermann (2013). "Placental steroidogenesis in pregnant women with polycystic ovary syndrome." Eur J Obstet Gynecol Reprod Biol **166**(2): 151-155.

Malone, S. A., G. E. Papadakis, A. Messina, N. E. H. Mimouni, S. Trova, M. Imbernon, C. Allet, I. Cimino, J. Acierno, D. Cassatella, C. Xu, R. Quinton, G. Szinnai, P. Pigny, L. Alonso-Cotchico, L. Masgrau, J. D. Marechal, V. Prevot, N. Pitteloud and P. Giacobini (2019). "Defective AMH signaling disrupts GnRH neuron development and function and contributes to hypogonadotropic hypogonadism." Elife **8**.

Manikkam, M., R. C. Thompson, C. Herkimer, K. B. Welch, J. Flak, F. J. Karsch and V. Padmanabhan (2008). "Developmental programming: impact of prenatal testosterone excess on pre- and postnatal gonadotropin regulation in sheep." Biol Reprod **78**(4): 648-660.

Marioli, D. J., A. D. Saltamavros, V. Vervita, V. Koika, G. Adonakis, G. Decavalas, K. B. Markou and N. A. Georgopoulos (2009). "Association of the 17-hydroxysteroid dehydrogenase type 5 gene polymorphism (-71A/G HSD17B5 SNP) with hyperandrogenemia in polycystic ovary syndrome (PCOS)." Fertil Steril **92**(2): 648-652.

Marszalek, B., M. Lacinski, N. Babych, E. Capla, J. Biernacka-Lukanty, A. Warenik-Szymankiewicz and W. H. Trzeciak (2001). "Investigations on the genetic polymorphism in the region of CYP17 gene encoding 5'-UTR in patients with polycystic ovarian syndrome." Gynecol Endocrinol **15**(2): 123-128.

Mason, A. J., J. S. Hayflick, R. T. Zoeller, W. S. Young, 3rd, H. S. Phillips, K. Nikolics and P. H. Seeburg (1986). "A deletion truncating the gonadotropin-releasing hormone gene is responsible for hypogonadism in the hpg mouse." Science **234**(4782): 1366-1371.

Massague, J. (1990). "Transforming growth factor-alpha. A model for membrane-anchored growth factors." J Biol Chem **265**(35): 21393-21396.

Massague, J. (1998). "TGF-beta signal transduction." Annu Rev Biochem **67**: 753-791.

Matzuk, M. M. and D. J. Lamb (2008). "The biology of infertility: research advances and clinical challenges." Nat Med **14**(11): 1197-1213.

Mayer, C., M. Acosta-Martinez, S. L. Dubois, A. Wolfe, S. Radovick, U. Boehm and J. E. Levine (2010). "Timing and completion of puberty in female mice depend on estrogen receptor alpha-signaling in kisspeptin neurons." Proc Natl Acad Sci U S A **107**(52): 22693-22698.

McCarthy, M. M., B. M. Nugent and K. M. Lenz (2017). "Neuroimmunology and neuroepigenetics in the establishment of sex differences in the brain." Nat Rev Neurosci **18**(8): 471-484.

McCartney, C. R., C. A. Eagleson and J. C. Marshall (2002). "Regulation of gonadotropin secretion: implications for polycystic ovary syndrome." Semin Reprod Med **20**(4): 317-326.

McGee, E. A. and A. J. Hsueh (2000). "Initial and cyclic recruitment of ovarian follicles." Endocr Rev **21**(2): 200-214.

McGee, E. A., E. Perlas, P. S. LaPolt, A. Tsafriri and A. J. Hsueh (1997). "Follicle-stimulating hormone enhances the development of preantral follicles in juvenile rats." Biol Reprod **57**(5): 990-998.

Medeiros, S. F., J. S. Barbosa and M. M. Yamamoto (2015). "Comparison of steroidogenic pathways among normoandrogenic and hyperandrogenic polycystic ovary syndrome patients and normal cycling women." J Obstet Gynaecol Res **41**(2): 254-263.

Mifsud, A., S. Ramirez and E. L. Yong (2000). "Androgen receptor gene CAG trinucleotide repeats in anovulatory infertility and polycystic ovaries." J Clin Endocrinol Metab **85**(9): 3484-3488.

Miller, W. L. (2002). "Androgen biosynthesis from cholesterol to DHEA." Molecular and Cellular Endocrinology **198**(1): 7-14.

Mishina, Y., R. Rey, M. J. Finegold, M. M. Matzuk, N. Josso, R. L. Cate and R. R. Behringer (1996). "Genetic analysis of the Mullerian-inhibiting substance signal transduction pathway in mammalian sexual differentiation." Genes Dev **10**(20): 2577-2587.

Moenter, S. M., A. Caraty, A. Locatelli and F. J. Karsch (1991). "Pattern of gonadotropin-releasing hormone (GnRH) secretion leading up to ovulation in the ewe: existence of a preovulatory GnRH surge." Endocrinology **129**(3): 1175-1182.

Mohlig, M., A. Jurgens, J. Spranger, K. Hoffmann, M. O. Weickert, H. W. Schlosser, T. Schill, G. Brabant, A. Schuring, A. F. Pfeiffer, J. Gromoll and C. Schofl (2006). "The androgen receptor CAG repeat modifies

the impact of testosterone on insulin resistance in women with polycystic ovary syndrome." Eur J Endocrinol **155**(1): 127-130.

Monsivais, D., M. M. Matzuk and S. A. Pangas (2017). "The TGF-β Family in the Reproductive Tract." Cold Spring Harb Perspect Biol **9**(10).

Moore, A. M. and R. E. Campbell (2016). "The neuroendocrine genesis of polycystic ovary syndrome: A role for arcuate nucleus GABA neurons." J Steroid Biochem Mol Biol **160**: 106-117.

Moore, A. M., M. Prescott and R. E. Campbell (2013). "Estradiol negative and positive feedback in a prenatal androgen-induced mouse model of polycystic ovarian syndrome." Endocrinology **154**(2): 796-806.

Moore, A. M., M. Prescott, C. J. Marshall, S. H. Yip and R. E. Campbell (2015). "Enhancement of a robust arcuate GABAergic input to gonadotropin-releasing hormone neurons in a model of polycystic ovarian syndrome." Proc Natl Acad Sci U S A **112**(2): 596-601.

Moraru, A., G. Cakan-Akdogan, K. Strassburger, M. Males, S. Mueller, M. Jabs, M. Muelleder, M. Frejno, B. P. Braeckman, M. Ralser and A. A. Teleman (2017). "THADA Regulates the Organismal Balance between Energy Storage and Heat Production." Dev Cell **41**(1): 72-81.e76.

Nachtigal, M. W., Y. Hirokawa, D. L. Enyeart-VanHouten, J. N. Flanagan, G. D. Hammer and H. A. Ingraham (1998). "Wilms' tumor 1 and Dax-1 modulate the orphan nuclear receptor SF-1 in sex-specific gene expression." Cell **93**(3): 445-454.

Nam, H., C. H. Kim, M. Y. Cha, J. M. Kim, B. M. Kang and H. W. Yoo (2015). "Polycystic ovary syndrome woman with heterozygous androgen receptor gene mutation who gave birth to a child with androgen insensitivity syndrome." Obstet Gynecol Sci **58**(2): 179-182.

Namba, H., T. Nagano, E. Jodo, S. Eifuku, M. Horie, H. Takebayashi, Y. Iwakura, H. Sotoyama, N. Takei and H. Nawa (2017). "Epidermal growth factor signals attenuate phenotypic and functional development of neocortical GABA neurons." J Neurochem **142**(6): 886-900.

Navarro, V. M., M. L. Gottsch, C. Chavkin, H. Okamura, D. K. Clifton and R. A. Steiner (2009). "Regulation of gonadotropin-releasing hormone secretion by kisspeptin/dynorphin/neurokinin B neurons in the arcuate nucleus of the mouse." J Neurosci **29**(38): 11859-11866.

Nazouri, A. S., M. Khosravifar, A. A. Akhlaghi, M. Shiva and P. Afsharian (2015). "No relationship between most polymorphisms of steroidogenic acute regulatory (StAR) gene with polycystic ovarian syndrome." Int J Reprod Biomed (Yazd) **13**(12): 771-778.

Nef, S. and L. F. Parada (2000). "Hormones in male sexual development." Genes Dev **14**(24): 3075-3086.

Nelson, V. L., R. S. Legro, J. F. Strauss, 3rd and J. M. McAllister (1999). "Augmented androgen production is a stable steroidogenic phenotype of propagated theca cells from polycystic ovaries." Mol Endocrinol **13**(6): 946-957.

Norman, R. J., L. Masters, C. R. Milner, J. X. Wang and M. J. Davies (2001). "Relative risk of conversion from normoglycaemia to impaired glucose tolerance or non-insulin dependent diabetes mellitus in polycystic ovarian syndrome." Hum Reprod **16**(9): 1995-1998.

O'Shaughnessy, P. J., D. McLelland and M. W. McBride (1997). "Regulation of luteinizing hormone-receptor and follicle-stimulating hormone-receptor messenger ribonucleic acid levels during development in the neonatal mouse ovary." Biol Reprod **57**(3): 602-608.

Padmanabhan, V. and A. Veiga-Lopez (2013). "Sheep models of polycystic ovary syndrome phenotype." Mol Cell Endocrinol **373**(1-2): 8-20.

Page, D. C., R. Mosher, E. M. Simpson, E. M. Fisher, G. Mardon, J. Pollack, B. McGillivray, A. de la Chapelle and L. G. Brown (1987). "The sex-determining region of the human Y chromosome encodes a finger protein." Cell **51**(6): 1091-1104.

Palomba, S., M. A. de Wilde, A. Falbo, M. P. H. Koster, G. B. La Sala and B. C. J. M. Fauser (2015). "Pregnancy complications in women with polycystic ovary syndrome." Human Reproduction Update **21**(5): 575-592.

Papadakis, G., E. Kandaraki, O. Papalou, A. Vryonidou and E. Diamanti-Kandarakis (2017). "Is cardiovascular risk in women with PCOS a real risk? Current insights." Minerva Endocrinol **42**(4): 340-355.

Park, A. S., M. A. Lawson, S. S. Chuan, S. E. Oberfield, K. M. Hoeger, S. F. Witchel and R. J. Chang (2010). "Serum anti-mullerian hormone concentrations are elevated in oligomenorrheic girls without evidence of hyperandrogenism." J Clin Endocrinol Metab **95**(4): 1786-1792.

Park, J. M., E. J. Lee, S. Ramakrishna, D. H. Cha and K. H. Baek (2008). "Association study for single nucleotide polymorphisms in the CYP17A1 gene and polycystic ovary syndrome." Int J Mol Med **22**(2): 249-254.

Park, J. Y., Y. Q. Su, M. Ariga, E. Law, S. L. Jin and M. Conti (2004). "EGF-like growth factors as mediators of LH action in the ovulatory follicle." Science **303**(5658): 682-684.

Pasquali, R. (2014). "Reproductive endocrinology: Maternal and fetal insulin levels at birth in women with PCOS." Nat Rev Endocrinol **10**(7): 382-384.

Peñarrubia, J., F. Fábregues, D. Manau, M. Creus, G. Casals, R. Casamitjana, F. Carmona, J. A. Vanrell and J. Balasch (2005). "Basal and stimulation day 5 anti-Müllerian hormone serum concentrations as predictors of ovarian response and pregnancy in assisted reproductive technology cycles stimulated with gonadotropin-releasing hormone agonist–gonadotropin treatment." Human Reproduction **20**(4): 915-922.

Peng, C. Y., X. Y. Long and G. X. Lu (2010). "Association of AR rs6152G/A gene polymorphism with susceptibility to polycystic ovary syndrome in Chinese women." Reprod Fertil Dev **22**(5): 881-885.

Peng, C. Y., H. J. Xie, Z. F. Guo, Y. L. Nie, J. Chen, J. M. Zhou and J. Yin (2014). "The association between androgen receptor gene CAG polymorphism and polycystic ovary syndrome: a case-control study and meta-analysis." J Assist Reprod Genet **31**(9): 1211-1219.

Perez, M. S., G. E. Cerrone, H. Benencia, N. Marquez, E. De Piano and G. D. Frechtel (2008). "[Polymorphism in CYP11alpha and CYP17 genes and the etiology of hyperandrogenism in patients with polycystic ovary syndrome]." Medicina (B Aires) **68**(2): 129-134.

Petry, C. J., K. K. Ong, K. F. Michelmore, S. Artigas, D. L. Wingate, A. H. Balen, F. de Zegher, L. Ibanez and D. B. Dunger (2005). "Association of aromatase (CYP 19) gene variation with features of hyperandrogenism in two populations of young women." Hum Reprod **20**(7): 1837-1843.

Picard, J. Y., D. Tran and N. Josso (1978). "Biosynthesis of labelled anti-mullerian hormone by fetal testes: evidence for the glycoprotein nature of the hormone and for its disulfide-bonded structure." Mol Cell Endocrinol **12**(1): 17-30.

Pigny, P., E. Merlen, Y. Robert, C. Cortet-Rudelli, C. Decanter, S. Jonard and D. Dewailly (2003). "Elevated serum level of anti-mullerian hormone in patients with polycystic ovary syndrome: relationship to the ovarian follicle excess and to the follicular arrest." J Clin Endocrinol Metab **88**(12): 5957-5962.

Plant, T. M. (2015). "Neuroendocrine control of the onset of puberty." Front Neuroendocrinol **38**: 73-88.

Polston, E. K. and R. B. Simerly (2006). "Ontogeny of the projections from the anteroventral periventricular nucleus of the hypothalamus in the female rat." J Comp Neurol **495**(1): 122-132.

Prapas, N., A. Karkanaki, I. Prapas, I. Kalogiannidis, I. Katsikis and D. Panidis (2009). "Genetics of polycystic ovary syndrome." Hippokratia **13**(4): 216-223.

Prazakova, S., M. Vankova, O. Bradnova, P. Lukasova, J. Vcelak, K. Dvorakova, K. Vondra, J. Vrbikova and B. Bendlova (2010). "[(TTTTA), polymorphism in the promoter of the CYP11A1 gene in the pathogenesis of polycystic ovary syndrome]." Cas Lek Cesk **149**(11): 520-525.

Prevot, V. (2011). "GnRH neurons directly listen to the periphery." Endocrinology **152**(10): 3589-3591.

Prevot, V., C. Rio, G. J. Cho, A. Lomniczi, S. Heger, C. M. Neville, N. A. Rosenthal, S. R. Ojeda and G. Corfas (2003). "Normal female sexual development requires neuregulin-erbB receptor signaling in hypothalamic astrocytes." J Neurosci **23**(1): 230-239.

Pusalkar, M., P. Meherji, J. Gokral, S. Chinnaraj and A. Maitra (2009). "CYP11A1 and CYP17 promoter polymorphisms associate with hyperandrogenemia in polycystic ovary syndrome." Fertility and Sterility **92**(2): 653-659.

Qin, K., D. A. Ehrmann, N. Cox, S. Refetoff and R. L. Rosenfield (2006). "Identification of a functional polymorphism of the human type 5 17beta-hydroxysteroid dehydrogenase gene associated with polycystic ovary syndrome." J Clin Endocrinol Metab **91**(1): 270-276.

Quinones-Jenab, V., S. Jenab, S. Ogawa, T. Funabashi, G. D. Weesner and D. W. Pfaff (1996). "Estrogen regulation of gonadotropin-releasing hormone receptor messenger RNA in female rat pituitary tissue." Brain Res Mol Brain Res **38**(2): 243-250.

Racine, C., R. Rey, M. G. Forest, F. Louis, A. Ferre, I. Huhtaniemi, N. Josso and N. di Clemente (1998). "Receptors for anti-mullerian hormone on Leydig cells are responsible for its effects on steroidogenesis and cell differentiation." Proc Natl Acad Sci U S A **95**(2): 594-599.

Radovick, S., J. E. Levine and A. Wolfe (2012). "Estrogenic regulation of the GnRH neuron." Front Endocrinol (Lausanne) **3**: 52.

Rajender, S., S. J. Carlus, S. K. Bansal, M. P. Negi, N. Sadasivam, M. N. Sadasivam and K. Thangaraj (2013). "Androgen receptor CAG repeats length polymorphism and the risk of polycystic ovarian syndrome (PCOS)." PLoS One **8**(10): e75709.

Ramos Cirilo, P. D., F. E. Rosa, M. F. Moreira Ferraz, C. A. Rainho, A. Pontes and S. R. Rogatto (2012). "Genetic polymorphisms associated with steroids metabolism and insulin action in polycystic ovary syndrome." Gynecol Endocrinol **28**(3): 190-194.

Reddy, K. R., M. L. Deepika, K. Supriya, K. P. Latha, S. S. Rao, V. U. Rani and P. Jahan (2014). "CYP11A1 microsatellite (tttta)n polymorphism in PCOS women from South India." J Assist Reprod Genet **31**(7): 857-863.

Rey, R. (2005). "Anti-Mullerian hormone in disorders of sex determination and differentiation." Arq Bras Endocrinol Metabol **49**(1): 26-36.

Rich-Edwards, J. W., D. Spiegelman, M. Garland, E. Hertzmark, D. J. Hunter, G. A. Colditz, W. C. Willett, H. Wand and J. E. Manson (2002). "Physical activity, body mass index, and ovulatory disorder infertility." Epidemiology **13**(2): 184-190.

Rizzo, M., K. Berneis, G. Spinas, G. B. Rini and E. Carmina (2009). "Long-term consequences of polycystic ovary syndrome on cardiovascular risk." Fertility and Sterility **91**(4): 1563-1567.

Roland, A. V., C. S. Nunemaker, S. R. Keller and S. M. Moenter (2010). "Prenatal androgen exposure programs metabolic dysfunction in female mice." J Endocrinol **207**(2): 213-223.

Rosenfield, R. L. and B. Bordini (2010). "Evidence that obesity and androgens have independent and opposing effects on gonadotropin production from puberty to maturity." Brain Res **1364**: 186-197.

Rosenfield, R. L., K. Wroblewski, V. Padmanabhan, E. Littlejohn, M. Mortensen and D. A. Ehrmann (2012). "Antimullerian hormone levels are independently related to ovarian hyperandrogenism and polycystic ovaries." Fertil Steril **98**(1): 242-249.

Ruka, K. A., L. L. Burger and S. M. Moenter (2013). "Regulation of arcuate neurons coexpressing kisspeptin, neurokinin B, and dynorphin by modulators of neurokinin 3 and kappa-opioid receptors in adult male mice." Endocrinology **154**(8): 2761-2771.

Sahmay, S., Y. Aydin, M. Oncul and L. M. Senturk (2014). "Diagnosis of Polycystic Ovary Syndrome: AMH in combination with clinical symptoms." J Assist Reprod Genet **31**(2): 213-220.

San Millan, J. L., J. Sancho, R. M. Calvo and H. F. Escobar-Morreale (2001). "Role of the pentanucleotide (tttta)(n) polymorphism in the promoter of the CYP11a gene in the pathogenesis of hirsutism." Fertil Steril **75**(4): 797-802.

Sanford, L. P., I. Ormsby, A. C. Gittenberger-de Groot, H. Sariola, R. Friedman, G. P. Boivin, E. L. Cardell and T. Doetschman (1997). "TGFbeta2 knockout mice have multiple developmental defects that are non-overlapping with other TGFbeta knockout phenotypes." Development **124**(13): 2659-2670.

Sarkar, D. K. and G. Fink (1979). "Mechanism of the first spontaneous gonadotrophin surge and that induced by pregnant mare serum and effects of neonatal androgen in rats." J Endocrinol **83**(3): 339-354.

Schally, A. V., A. Arimura, A. J. Kastin, H. Matsuo, Y. Baba, T. W. Redding, R. M. Nair, L. Debeljuk and W. F. White (1971). "Gonadotropin-releasing hormone: one polypeptide regulates secretion of luteinizing and follicle-stimulating hormones." Science **173**(4001): 1036-1038.

Schepers, G., M. Wilson, D. Wilhelm and P. Koopman (2003). "SOX8 is expressed during testis differentiation in mice and synergizes with SF1 to activate the Amh promoter in vitro." J Biol Chem **278**(30): 28101-28108.

Schuring, A. N., A. Welp, J. Gromoll, M. Zitzmann, B. Sonntag, E. Nieschlag, R. R. Greb and L. Kiesel (2012). "Role of the CAG repeat polymorphism of the androgen receptor gene in polycystic ovary syndrome (PCOS)." Exp Clin Endocrinol Diabetes **120**(2): 73-79.

Schwanzel-Fukuda, M., K. L. Crossin, D. W. Pfaff, P. M. Bouloux, J. P. Hardelin and C. Petit (1996). "Migration of luteinizing hormone-releasing hormone (LHRH) neurons in early human embryos." J Comp Neurol **366**(3): 547-557.

Schwanzel-Fukuda, M. and D. W. Pfaff (1989). "Origin of luteinizing hormone-releasing hormone neurons." Nature **338**(6211): 161-164.

Segev, D. L., Y. Hoshiya, A. E. Stephen, M. Hoshiya, T. T. Tran, D. T. MacLaughlin, P. K. Donahoe and S. Maheswaran (2001). "Mullerian inhibiting substance regulates NFkappaB signaling and growth of mammary epithelial cells in vivo." J Biol Chem **276**(29): 26799-26806.

Shah, N. A., H. J. Antoine, M. Pall, K. D. Taylor, R. Azziz and M. O. Goodarzi (2008). "Association of androgen receptor CAG repeat polymorphism and polycystic ovary syndrome." J Clin Endocrinol Metab **93**(5): 1939-1945.

Shaikh, N., R. Dadachanji, P. Meherji, N. Shah and S. Mukherjee (2016). "Polymorphisms and haplotypes of insulin-like factor 3 gene are associated with risk of polycystic ovary syndrome in Indian women." Gene **577**(2): 180-186.

Sharp, L., A. H. Cardy, S. C. Cotton and J. Little (2004). "CYP17 gene polymorphisms: prevalence and associations with hormone levels and related factors. a HuGE review." Am J Epidemiol **160**(8): 729-740.

Sharpe, R. M., C. McKinnell, C. Kivlin and J. S. Fisher (2003). "Proliferation and functional maturation of Sertoli cells, and their relevance to disorders of testis function in adulthood." Reproduction **125**(6): 769-784.

Shaw, L. J., C. N. Bairey Merz, R. Azziz, F. Z. Stanczyk, G. Sopko, G. D. Braunstein, S. F. Kelsey, K. E. Kip, R. M. Cooper-DeHoff, B. D. Johnson, V. Vaccarino, S. E. Reis, V. Bittner, T. K. Hodgson, W. Rogers and C. J. Pepine (2008). "Withdrawn: Postmenopausal Women with a History of Irregular Menses and Elevated Androgen Measurements at High Risk for Worsening Cardiovascular Event-Free Survival: Results from the National Institutes of Health—National Heart, Lung, and Blood Institute Sponsored Women's Ischemia Syndrome Evaluation." The Journal of Clinical Endocrinology & Metabolism **93**(4): 1276-1284.

Shen, W., T. Li, Y. Hu, H. Liu and M. Song (2014). "Common polymorphisms in the CYP1A1 and CYP11A1 genes and polycystic ovary syndrome risk: a meta-analysis and meta-regression." Arch Gynecol Obstet **289**(1): 107-118.

Shi, D. and D. F. Vine (2012). "Animal models of polycystic ovary syndrome: a focused review of rodent models in relationship to clinical phenotypes and cardiometabolic risk." Fertil Steril **98**(1): 185-193.

Shorakae, S., J. Boyle and H. Teede (2014). "Polycystic ovary syndrome: a common hormonal condition with major metabolic sequelae that physicians should know about." Intern Med J **44**(8): 720-726.

Simerly, R. B. (2002). "Wired for reproduction: organization and development of sexually dimorphic circuits in the mammalian forebrain." Annu Rev Neurosci **25**: 507-536.

Simoni, M., C. B. Tempfer, B. Destenaves and B. C. Fauser (2008). "Functional genetic polymorphisms and female reproductive disorders: Part I: Polycystic ovary syndrome and ovarian response." Hum Reprod Update **14**(5): 459-484.

Sir-Petermann, T., E. Codner, V. Perez, B. Echiburu, M. Maliqueo, A. Ladron de Guevara, J. Preisler, N. Crisosto, F. Sanchez, F. Cassorla and S. Bhasin (2009). "Metabolic and reproductive features before and during puberty in daughters of women with polycystic ovary syndrome." J Clin Endocrinol Metab **94**(6): 1923-1930.

Sisk, C. L. and D. L. Foster (2004). "The neural basis of puberty and adolescence." Nat Neurosci **7**(10): 1040-1047.

Skaletsky, H., T. Kuroda-Kawaguchi, P. J. Minx, H. S. Cordum, L. Hillier, L. G. Brown, S. Repping, T. Pyntikova, J. Ali, T. Bieri, A. Chinwalla, A. Delehaunty, K. Delehaunty, H. Du, G. Fewell, L. Fulton, R. Fulton, T. Graves, S. F. Hou, P. Latrielle, S. Leonard, E. Mardis, R. Maupin, J. McPherson, T. Miner, W. Nash, C. Nguyen, P. Ozersky, K. Pepin, S. Rock, T. Rohlfing, K. Scott, B. Schultz, C. Strong, A. Tin-Wollam, S. P. Yang, R. H. Waterston, R. K. Wilson, S. Rozen and D. C. Page (2003). "The male-specific region of the human Y chromosome is a mosaic of discrete sequence classes." Nature **423**(6942): 825-837.

Skrgatic, L., D. P. Baldani, J. Z. Cerne, P. Ferk and K. Gersak (2012). "CAG repeat polymorphism in androgen receptor gene is not directly associated with polycystic ovary syndrome but influences serum testosterone levels." J Steroid Biochem Mol Biol **128**(3-5): 107-112.

Stiff, M. E., F. H. Bronson and M. H. Stetson (1974). "Plasma gonadotropins in prenatal and prepubertal female mice: disorganization of pubertal cycles in the absence of a male." Endocrinology **94**(2): 492-496.

Sullivan, S. D. and S. M. Moenter (2004). "Prenatal androgens alter GABAergic drive to gonadotropin-releasing hormone neurons: implications for a common fertility disorder." Proc Natl Acad Sci U S A **101**(18): 7129-7134.

Szydlarska, D., W. Grzesiuk, A. Trybuch, A. Kondracka, I. Kowalik and E. Bar-Andziak (2012). "Insulin-like factor 3 -- a new hormone related to polycystic ovary syndrome?" Endokrynol Pol **63**(5): 356-361.

Tata, B., N. E. H. Mimouni, A. L. Barbotin, S. A. Malone, A. Loyens, P. Pigny, D. Dewailly, S. Catteau-Jonard, I. Sundstrom-Poromaa, T. T. Piltonen, F. Dal Bello, C. Medana, V. Prevot, J. Clasadonte and P. Giacobini (2018). "Elevated prenatal anti-Mullerian hormone reprograms the fetus and induces polycystic ovary syndrome in adulthood." Nat Med **24**(6): 834-846.

Taylor, A. E., B. McCourt, K. A. Martin, E. J. Anderson, J. M. Adams, D. Schoenfeld and J. E. Hall (1997). "Determinants of abnormal gonadotropin secretion in clinically defined women with polycystic ovary syndrome." J Clin Endocrinol Metab **82**(7): 2248-2256.

Techatraisak, K., C. Chayachinda, T. Wongwananuruk, C. Dangrat, S. Indhavivadhana, M. Rattanachaiyanont and W. Thongnoppakhun (2015). "No association between CYP17 -34T/C polymorphism and insulin resistance in Thai polycystic ovary syndrome." J Obstet Gynaecol Res **41**(9): 1412-1417.

Techatraisak, K., G. S. Conway and G. Rumsby (1997). "Frequency of a polymorphism in the regulatory region of the 17 alpha-hydroxylase-17,20-lyase (CYP17) gene in hyperandrogenic states." Clin Endocrinol (Oxf) **46**(2): 131-134.

Tee, M. K., M. Speek, B. Legeza, B. Modi, M. E. Teves, J. M. McAllister, J. F. Strauss, 3rd and W. L. Miller (2016). "Alternative splicing of DENND1A, a PCOS candidate gene, generates variant 2." Mol Cell Endocrinol **434**: 25-35.

Teede, H. J., A. E. Joham, E. Paul, L. J. Moran, D. Loxton, D. Jolley and C. Lombard (2013). "Longitudinal weight gain in women identified with polycystic ovary syndrome: results of an observational study in young women." Obesity (Silver Spring) **21**(8): 1526-1532.

Teede, H. J., M. L. Misso, M. F. Costello, A. Dokras, J. Laven, L. Moran, T. Piltonen and R. J. Norman (2018). "Recommendations from the international evidence-based guideline for the assessment and management of polycystic ovary syndrome." Fertil Steril **110**(3): 364-379.

Teixeira, J., W. W. He, P. C. Shah, N. Morikawa, M. M. Lee, E. A. Catlin, P. L. Hudson, J. Wing, D. T. Maclaughlin and P. K. Donahoe (1996). "Developmental expression of a candidate mullerian inhibiting substance type II receptor." Endocrinology **137**(1): 160-165.

Teixeira, J., S. Maheswaran and P. K. Donahoe (2001). "Mullerian inhibiting substance: an instructive developmental hormone with diagnostic and possible therapeutic applications." Endocr Rev **22**(5): 657-674.

Tobet, S. A. and G. A. Schwarting (2006). "Minireview: Recent Progress in Gonadotropin-Releasing Hormone Neuronal Migration." Endocrinology **147**(3): 1159-1165.

Topaloglu, A. K. and L. D. Kotan (2016). "Genetics of Hypogonadotropic Hypogonadism." Endocr Dev **29**: 36-49.

Tran, D., N. Muesy-Dessole and N. Josso (1977). "Anti-Mullerian hormone is a functional marker of foetal Sertoli cells." Nature **269**(5627): 411-412.

Tremblay, J. J. and R. S. Viger (1999). "Transcription factor GATA-4 enhances Mullerian inhibiting substance gene transcription through a direct interaction with the nuclear receptor SF-1." Mol Endocrinol **13**(8): 1388-1401.

Tsutsumi, M., S. C. Laws, V. Rodic and S. C. Sealfon (1995). "Translational regulation of the gonadotropin-releasing hormone receptor in alpha T3-1 cells." Endocrinology **136**(3): 1128-1136.

Unsal, T., E. Konac, E. Yesilkaya, A. Yilmaz, A. Bideci, H. Ilke Onen, P. Cinaz and A. Menevse (2009). "Genetic polymorphisms of FSHR, CYP17, CYP1A1, CAPN10, INSR, SERPINE1 genes in adolescent girls with polycystic ovary syndrome." J Assist Reprod Genet **26**(4): 205-216.

Urbanek, M., R. S. Legro, D. A. Driscoll, R. Azziz, D. A. Ehrmann, R. J. Norman, J. F. Strauss, 3rd, R. S. Spielman and A. Dunaif (1999). "Thirty-seven candidate genes for polycystic ovary syndrome: strongest evidence for linkage is with follistatin." Proc Natl Acad Sci U S A **96**(15): 8573-8578.

Urbanek, M., A. Woodroffe, K. G. Ewens, E. Diamanti-Kandarakis, R. S. Legro, J. F. Strauss, 3rd, A. Dunaif and R. S. Spielman (2005). "Candidate gene region for polycystic ovary syndrome on chromosome 19p13.2." J Clin Endocrinol Metab **90**(12): 6623-6629.

Valdimarsdottir, R., H. Valgeirsdottir, A. K. Wikstrom, T. K. Kallak, E. Elenis, O. Axelsson, K. Ubhayasekhera, J. Bergquist, T. T. Piltonen, P. Pigny, P. Giacobini and I. S. Poromaa (2019). "Pregnancy and neonatal complications in women with polycystic ovary syndrome in relation to second-trimester anti-Mullerian hormone levels." Reprod Biomed Online **39**(1): 141-148.

van Houten, E. L., A. P. Themmen and J. A. Visser (2010). "Anti-Mullerian hormone (AMH): regulator and marker of ovarian function." Ann Endocrinol (Paris) **71**(3): 191-197.

van Rooij, I. A. J., F. J. M. Broekmans, E. R. te Velde, B. C. J. M. Fauser, L. F. J. M. M. Bancsi, F. H. d. Jong and A. P. N. Themmen (2002). "Serum anti-Müllerian hormone levels: a novel measure of ovarian reserve." Human Reproduction **17**(12): 3065-3071.

Veltman-Verhulst, S. M., J. Boivin, M. J. Eijkemans and B. J. Fauser (2012). "Emotional distress is a common risk in women with polycystic ovary syndrome: a systematic review and meta-analysis of 28 studies." Hum Reprod Update **18**(6): 638-651.

Vigier, B., J. Y. Picard, D. Tran, L. Legeai and N. Josso (1984). "Production of anti-Mullerian hormone: another homology between Sertoli and granulosa cells." Endocrinology **114**(4): 1315-1320.

Vink, J. M., S. Sadrzadeh, C. B. Lambalk and D. I. Boomsma (2006). "Heritability of Polycystic Ovary Syndrome in a Dutch Twin-Family Study." The Journal of Clinical Endocrinology & Metabolism **91**(6): 2100-2104.

Visser, J. A., R. Olaso, M. Verhoef-Post, P. Kramer, A. P. Themmen and H. A. Ingraham (2001). "The serine/threonine transmembrane receptor ALK2 mediates Mullerian inhibiting substance signaling." Mol Endocrinol **15**(6): 936-945.

Waldstreicher, J., N. F. Santoro, J. E. Hall, M. Filicori and W. F. Crowley, Jr. (1988). "Hyperfunction of the hypothalamic-pituitary axis in women with polycystic ovarian disease: indirect evidence for partial gonadotroph desensitization." J Clin Endocrinol Metab **66**(1): 165-172.

Walters, K. A., C. M. Allan and D. J. Handelsman (2008). "Androgen actions and the ovary." Biol Reprod **78**(3): 380-389.

Wang, H., Q. Li, T. Wang, G. Yang, Y. Wang, X. Zhang, Q. Sang, H. Wang, X. Zhao, Q. Xing, J. Shi, L. He and L. Wang (2011). "A common polymorphism in the human aromatase gene alters the risk for polycystic ovary syndrome and modifies aromatase activity in vitro." Mol Hum Reprod **17**(6): 386-391.

Wang, P. Y., A. Protheroe, A. N. Clarkson, F. Imhoff, K. Koishi and I. S. McLennan (2009). "Müllerian inhibiting substance contributes to sex-linked biases in the brain and behavior." Proc Natl Acad Sci U S A **106**(17): 7203-7208.

Wang, R., M. O. Goodarzi, T. Xiong, D. Wang, R. Azziz and H. Zhang (2012). "Negative association between androgen receptor gene CAG repeat polymorphism and polycystic ovary syndrome? A systematic review and meta-analysis." Mol Hum Reprod **18**(10): 498-509.

Wang, Y., X. Wu, Y. Cao, L. Yi and J. Chen (2006). "A microsatellite polymorphism (tttta)n in the promoter of the CYP11a gene in Chinese women with polycystic ovary syndrome." Fertility and Sterility **86**(1): 223-226.

Watabe, T. and K. Miyazono (2009). "Roles of TGF-beta family signaling in stem cell renewal and differentiation." Cell Res **19**(1): 103-115.

Wersinger, S. R., D. J. Haisenleder, D. B. Lubahn and E. F. Rissman (1999). "Steroid feedback on gonadotropin release and pituitary gonadotropin subunit mRNA in mice lacking a functional estrogen receptor alpha." Endocrine **11**(2): 137-143.

Wickenheisser, J. K., J. M. Biegler, V. L. Nelson-DeGrave, R. S. Legro, J. F. Strauss, III and J. M. McAllister (2012). "Cholesterol Side-Chain Cleavage Gene Expression in Theca Cells: Augmented Transcriptional Regulation and mRNA Stability in Polycystic Ovary Syndrome." PLOS ONE **7**(11): e48963.

Wierman, M. E., K. Kiseljak-Vassiliades and S. Tobet (2011). "Gonadotropin-releasing hormone (GnRH) neuron migration: initiation, maintenance and cessation as critical steps to ensure normal reproductive function." Front Neuroendocrinol **32**(1): 43-52.

Wild, R. A. (2002). "Long-term health consequences of PCOS." Hum Reprod Update **8**(3): 231-241.

Wild, S., T. Pierpoint, H. Jacobs and P. McKeigue (2000). "Long-term consequences of polycystic ovary syndrome: Results of a 31 year follow-up study." Human Fertility **3**(2): 101-105.

Wilson, C. A., N. di Clemente, C. Ehrenfels, R. B. Pepinsky, N. Josso, B. Vigier and R. L. Cate (1993). "Mullerian inhibiting substance requires its N-terminal domain for maintenance of biological activity, a novel finding within the transforming growth factor-beta superfamily." Mol Endocrinol **7**(2): 247-257.

Wilson, R. C., J. S. Kesner, J. M. Kaufman, T. Uemura, T. Akema and E. Knobil (1984). "Central electrophysiologic correlates of pulsatile luteinizing hormone secretion in the rhesus monkey." Neuroendocrinology **39**(3): 256-260.

Wood, J. R., D. A. Dumesic, D. H. Abbott and J. F. Strauss, 3rd (2007). "Molecular abnormalities in oocytes from women with polycystic ovary syndrome revealed by microarray analysis." J Clin Endocrinol Metab **92**(2): 705-713.

Wray, S. (2010). "From nose to brain: development of gonadotrophin-releasing hormone-1 neurones." J Neuroendocrinol **22**(7): 743-753.

Wray, S., P. Grant and H. Gainer (1989). "Evidence that cells expressing luteinizing hormone-releasing hormone mRNA in the mouse are derived from progenitor cells in the olfactory placode." Proc Natl Acad Sci U S A **86**(20): 8132-8136.

Wu, X. Y., Z. L. Li, C. Y. Wu, Y. M. Liu, H. Lin, S. H. Wang and W. F. Xiao (2010). "Endocrine traits of polycystic ovary syndrome in prenatally androgenized female Sprague-Dawley rats." Endocr J **57**(3): 201-209.

Xia, Y., Y. Che, X. Zhang, C. Zhang, Y. Cao, W. Wang, P. Xu, X. Wu, L. Yi, Q. Gao and Y. Wang (2012). "Polymorphic CAG repeat in the androgen receptor gene in polycystic ovary syndrome patients." Mol Med Rep **5**(5): 1330-1334.

Xita, N., A. Chatzikyriakidou, I. Stavrou, C. Zois, I. Georgiou and A. Tsatsoulis (2010). "The (TTTA)n polymorphism of aromatase (CYP19) gene is associated with age at menarche." Hum Reprod **25**(12): 3129-3133.

Xita, N., I. Georgiou, L. Lazaros, V. Psofaki, G. Kolios and A. Tsatsoulis (2008). "The synergistic effect of sex hormone-binding globulin and aromatase genes on polycystic ovary syndrome phenotype." Eur J Endocrinol **158**(6): 861-865.

Xita, N., L. Lazaros, I. Georgiou and A. Tsatsoulis (2010). "CYP19 gene: a genetic modifier of polycystic ovary syndrome phenotype." Fertil Steril **94**(1): 250-254.

Xita, N., A. Tsatsoulis, A. Chatzikyriakidou and I. Georgiou (2003). "Association of the (TAAAA)n repeat polymorphism in the sex hormone-binding globulin (SHBG) gene with polycystic ovary syndrome and relation to SHBG serum levels." J Clin Endocrinol Metab **88**(12): 5976-5980.

Xu, P., X. L. Zhang, G. B. Xie, C. W. Zhang, S. M. Shen, X. X. Zhang, Y. X. Cao, W. J. Wang, Y. N. Che, Y. J. Xia, X. K. Wu, L. Yi, Q. Gao and Y. Wang (2013). "The (TTTA)n polymorphism in intron 4 of CYP19 and the polycystic ovary syndrome risk in a Chinese population." Mol Biol Rep **40**(8): 5041-5047.

Yang, F., Y. C. Ruan, Y. J. Yang, K. Wang, S. S. Liang, Y. B. Han, X. M. Teng and J. Z. Yang (2015). "Follicular hyperandrogenism downregulates aromatase in luteinized granulosa cells in polycystic ovary syndrome women." Reproduction **150**(4): 289-296.

Yildiz, B. O., H. Yarali, H. Oguz and M. Bayraktar (2003). "Glucose intolerance, insulin resistance, and hyperandrogenemia in first degree relatives of women with polycystic ovary syndrome." J Clin Endocrinol Metab **88**(5): 2031-2036.

Yoshida, K., S. A. Tobet, J. E. Crandall, T. P. Jimenez and G. A. Schwarting (1995). "The migration of luteinizing hormone-releasing hormone neurons in the developing rat is associated with a transient, caudal projection of the vomeronasal nerve." J Neurosci **15**(12): 7769-7777.

Yu, Y. Y., C. X. Sun, Y. K. Liu, Y. Li, L. Wang and W. Zhang (2013). "Promoter methylation of CYP19A1 gene in Chinese polycystic ovary syndrome patients." Gynecol Obstet Invest **76**(4): 209-213.

Yuan, C., C. Gao, Y. Qian, Y. Liu, S. W. Jiang, Y. Cui and J. Liu (2015). "Polymorphism of CAG and GGN repeats of androgen receptor gene in women with polycystic ovary syndrome." Reprod Biomed Online **31**(6): 790-798.

Zhan, Y., A. Fujino, D. T. MacLaughlin, T. F. Manganaro, P. P. Szotek, N. A. Arango, J. Teixeira and P. K. Donahoe (2006). "Mullerian inhibiting substance regulates its receptor/SMAD signaling and causes mesenchymal transition of the coelomic epithelial cells early in Mullerian duct regression." Development **133**(12): 2359-2369.

Zhang, C. W., X. L. Zhang, Y. J. Xia, Y. X. Cao, W. J. Wang, P. Xu, Y. N. Che, X. K. Wu, L. Yi, Q. Gao and Y. Wang (2012). "Association between polymorphisms of the CYP11A1 gene and polycystic ovary syndrome in Chinese women." Mol Biol Rep **39**(8): 8379-8385.

Zhang, F. P., M. Poutanen, J. Wilbertz and I. Huhtaniemi (2001). "Normal prenatal but arrested postnatal sexual development of luteinizing hormone receptor knockout (LuRKO) mice." Mol Endocrinol **15**(1): 172-183.

Zhang, H. Y., F. F. Zhu, J. Xiong, X. B. Shi and S. X. Fu (2009). "Characteristics of different phenotypes of polycystic ovary syndrome based on the Rotterdam criteria in a large-scale Chinese population." Bjog **116**(12): 1633-1639.

Zhao, J. L., Z. J. Chen, Y. R. Zhao, L. X. Zhao, L. C. Wang, Y. Li, R. Tang and Y. H. Shi (2005). "[Study on the (TAAAA)n repeat polymorphism in sex hormone-binding globulin gene and the SHBG serum levels in putative association with the glucose metabolic status of Chinese patients suffering from polycystic ovarian syndrome in Shandong province]." Zhonghua Yi Xue Yi Chuan Xue Za Zhi **22**(6): 644-647.

Chapter 5:

Elevated prenatal Anti-Müllerian Hormone reprograms the fetus and induces polycystic ovary syndrome in adulthood

Chapter Five (Thesis on article)

Elevated prenatal Anti-Müllerian Hormone reprograms the fetus and induces polycystic ovary syndrome in adulthood

Brooke Tata [1,2,§], Nour El Houda Mimouni [1,2,§], Anne-Laure Barbotin [1,3], Samuel A. Malone [1,2,] , Anne Loyens[1,2], Pascal Pigny [2,4], Didier Dewailly [1,2,5], Sophie Catteau-Jonard [1,2,5], Inger Sundström-Poromaa [6], Terhi T. Piltonen[7], Vincent Prevot [1,2], Jerome Clasadonte [1,2*] and Paolo Giacobini [1,2*]

(Tata, Mimouni et al, *Nature Medicine, 2018)*

https://doi.org: 10.1038/s41591-018-0035-5

1 Jean-Pierre Aubert Research Center (JPArC), Laboratory of Development and Plasticity of the Neuroendocrine Brain, Inserm, UMR-S 1172, Lille, France

2 University of Lille, FHU 1,000 Days for Health, School of Medicine, Lille, France

3 CHU Lille, Institut de Biologie de la Reproduction-Spermiologie-CECOS, Lille, France

4 Laboratoire de Biochimie & Hormonologie, Centre de Biologie Pathologie, Centre Hospitalier Régional Universitaire, CHU de Lille, Lille, France

5 Service de Gynécologie Endocrinienne et Médecine de la Reproduction, Hôpital Jeanne de Flandre, CHU de Lille, Lille, France

6 Department of Women's and Children's Health, Uppsala University, Uppsala, Sweden

7 Department of Obstetrics and Gynecology, Oulu University Hospital, Oulu, Finland; University of Oulu and Medical Research Center Oulu, Oulu, Finland.

Correspondence should be addressed to Paolo Giacobini (paolo.giacobini@inserm.fr)

§ The authors equally contributed to this work

* The authors co-supervised this work

Abstract

Polycystic ovary syndrome (PCOS) is the main cause of female infertility worldwide with high comorbidity and economic burden. Most women with PCOS exhibit higher levels of circulating luteinizing hormone, suggestive of heightened gonadotropin-releasing hormone (GnRH) release, and Anti-Müllerian Hormone (AMH) as compared to healthy women. Although the prevalence of the syndrome among women is as high as 18%, the origin of PCOS is yet unknown. Herein, we measured AMH in a cohort of pregnant PCOS and control women revealing that AMH is significantly more elevated in pregnant women with PCOS than in controls. We then treated dams with AMH and followed the neuroendocrine phenotype of their female progeny postnatally. This treatment engages maternal neuroendocrine driven testosterone excess and diminishes placental metabolism of testosterone to estradiol, leading to a fetal programming of the exposed offspring into exhibiting a PCOS-like reproductive and neuroendocrine phenotype in adulthood. GnRH neurons are persistently hyperactivated in these animals and GnRH antagonist treatment completely restored their neuroendocrine phenotype, highlighting a critical role for GnRH/GnRH receptor signaling in the neuroendocrine dysfunctions of PCOS and offering new therapeutic perspectives.

Introduction

Polycystic ovary syndrome (PCOS) is the most common female reproductive disorder, affecting 10-18% of women worldwide (Norman, Dewailly et al. 2007, March, Moore et al. 2010, Goodarzi, Dumesic et al. 2011, Jayasena and Franks 2014). The syndrome is underpinned by excessive ovarian and/or adrenal androgen secretion, oligo-anovulation and many cases also with insulin resistance.

In non-pregnant women with PCOS, serum levels of Anti-Mullerian Hormone (AMH) are 2-3 –fold higher than in women without polycystic ovaries (PCO) or PCOS (Cook, Siow et al. 2002, Pigny, Jonard et al. 2006), and the severity of the reproductive dysfunction is positively correlated with AMH levels (Pigny, Merlen et al. 2003, Pellatt, Hanna et al. 2007).

The pathophysiology of PCOS also extends to hypothalamic neuronal dysregulation and increased risks for metabolic derangements (Wild, Carmina et al. 2010, Dumesic and Lobo 2013). Indeed, 50-70% of women with PCOS are overweight or obese and have an increased risk of developing type 2 diabetes mellitus and cardiovascular disease (Goodarzi, Dumesic et al. 2011). Moreover, most PCOS women exhibit increased luteinizing hormone (LH) suggestive of rapid hypothalamic gonadotropin-releasing hormone (GnRH) secretion (Goodarzi, Dumesic et al. 2011, Cimino, Casoni et al. 2016). Whether this defect is primary or secondary to other changes in PCOS remains unclear but recent evidence has shown that GnRH neurons express AMH receptors and that exogenous AMH potently increases GnRH neurons firing and GnRH release in murine living tissue explants (Cimino, Casoni et al. 2016).

Familial clustering and twin studies have shown that PCOS has a strong heritable component (McAllister, Legro et al. 2015). However, the mutations that have been identified so far do not account for the high prevalence of all cases, implying that fetal environmental factors likely play important roles in the onset of this disease (Sir-Petermann, Maliqueo et al. 2007). The lack of a defined PCOS pathogenic mechanism has hindered the progress toward a cure for this syndrome.

Here, we showed that an early imbalance in the AMH-dependent gonad/brain/placental dialogue can be a preparatory and aggravating event predisposing the onset of PCOS.

AMH levels were previously found to be low during pregnancy in women with normal fertility (La Marca, Giulini et al. 2005, Koninger, Kauth et al. 2013). We thus sought to examine AMH levels in a cohort of pregnant PCOS and control women and revealed that AMH concentrations are significantly higher in PCOS as compared to healthy women. Next, using mouse models, we showed that exposure to excess AMH during pregnancy engages maternal neuroendocrine driven testosterone excess and diminishes placental metabolism of testosterone to estradiol, leading to a fetal programming of the exposed offspring into exhibiting a PCOS-like reproductive and neuroendocrine phenotype in adulthood. Female offspring recapitulated the major PCOS neuroendocrine reproductive features, namely elevation in testosterone and LH levels, associated with oligo-anovulation and impaired fertility. Moreover, prenatal AMH-treated (PAMH) female offspring exhibited an increase in the excitatory appositions onto GnRH neurons and heightened GnRH neuronal activity in adulthood. Prenatal GnRH antagonist treatment prevents the transgenerational transmission of the disease and postnatal GnRH antagonist treatment restored the neuroendocrine phenotype of PCOS-like animals.

Results

AMH levels during pregnancy are higher in women with PCOS than in controls

The comparisons of serum AMH levels in 63 control women (age 27-39 years old) and 66 patients with PCOS (age 27-39 years old) at gestational week 16-19, confirmed with ultrasound, (**Fig. 1a, Supplementary table 1**) revealed significant differences in AMH median values between these populations, with AMH concentrations being higher in pregnant PCOS women than in control women (**Fig. 1b**). This difference was not attributable to differences in age between the two groups (**Supplementary table 1**).

When we analysed this sample stratified by body mass index (BMI), and classified women as lean or obese (lean BMI $\leq$ 25 kg/m^2, obese BMI $\geq$30 kg/m^2), we found that AMH was still significantly higher in women with PCOS as compared to the control group, regardless of BMI, even though the difference was more striking in the lean women than in the obese (**Fig. 1c**).

Interestingly, when we compared women with PCOS, stratified by BMI as well as hyperandrogenism (normoandrogenic vs. hyperandrogenic, the latter defined as either biochemical or clinical hyperandrogenism), we detected a significant difference between lean normo- and hyperandrogenic women with PCOS, with AMH being more elevated in hyperandrogenic lean PCOS women than in normoandrogenic women (**Fig. 1d**). No difference between normo- and hyperandrogenic obese women with PCOS was detected (**Fig. 1d**).

We then analysed the control and PCOS groups stratified by age (age 27-34 years and age > 34 years), and found higher AMH levels in both PCOS age groups compared with their respective control women (**Fig. 1e**).

Our results show that serum AMH levels are higher in PCOS pregnant women than in control women, regardless of their age and BMI.

Prenatal AMH-treatment triggers the neuroendocrine disturbances of PCOS in the offspring

In order to test whether prenatal exposure to elevated AMH might lead to PCOS later in life, we treated pregnant female mice with PBS or recombinant AMH at the end of gestation and studied the neuroendocrine reproductive features of the female offspring at adulthood (**Fig. 2a**).

We injected daily intraperitoneally (i.p.) pregnant mice with PBS (Control) or with the bioactive form of AMH (human recombinant AMH_C, 0.12 mg/Kg/d; prenatal AMH_C-treated, PAMH) (Cimino, Casoni et al. 2016) during the same temporal window (E16.5-E18.5) that was previously used to generate prenatal androgen-treated mice, PNA (Sullivan and Moenter 2004, Moore, Prescott et al. 2013, Moore, Prescott et al. 2015) (**Fig. 2a**). We chose this temporal window for the treatment because it lies beyond the developmental stages during which gonadal and genital tract differentiation takes place in mice (E12.5-E14.5), which therefore excludes any morphogenetic effects that exogenous AMH could have (Orvis and Behringer 2007). PAMH offspring exhibited delayed vaginal opening (VO), delayed puberty onset (**Supplementary Fig. 1a, b**), severely disrupted estrous cyclicity (oligo-anovulation; **Fig. 2b, c**) and no difference in body weight (**Supplementary Fig. 1d**). PAMH mice rarely entered the preovulatory stage of the estrous cycle and displayed prolonged time in metestrus/diestrus as compared to the control female offspring

(**Fig. 2b**; metestrus/diestrus: M/D, estrus: E, proestrus: P). Ovarian histology of PAMH animals showed abnormalities consistent with their anovulatory phenotype, with the presence of fewer post-ovulation corpora lutea and less late antral follicles as compared to control animals (**Fig. 2d, e**). Additionally, PAMH adult female mice showed impaired fertility as indicated by a significant delay in their first litter, fewer litters and fewer pups per litter produced over a 3-month period (**Fig. 2f**).

In order to test whether this disruptive effect of prenatal AMH treatment is eventually mediated by GnRH binding to the GnRH receptor, we treated pregnant mice with AMH_C along with a GnRH antagonist, at a concentration previously validated in animal works (Cetrorelix acetate, 0.5 mg/Kg/day) (Cimino, Casoni et al. 2016), from E16.5 to E18.5. Cetrorelix is known to specifically saturate GnRH receptors at the level of the anterior pituitary (Halmos, Schally et al. 1996, Pinski, Lamharzi et al. 1996) thus decreasing the GnRH-mediated release of LH and FSH, with an effect more pronounced on LH secretion (Duijkers, Klipping et al. 1998).

Prenatal GnRH antagonist treatment prevented the appearance of the ovulatory and fertility defects in postnatal offspring (PAMH + GnRH antag; **Fig. 2b, c, f**).

To determine whether AMH treatment affects the levels of circulating testosterone in PAMH animals, we first measured the ano-genital (ano-vaginal) distance, which reflects androgenic impregnation, from postnatal day 30 (P30) to P60 (**Fig. 3a**). The PAMH female offspring displayed a significantly longer ano-genital distance than did the control female offspring (**Fig. 3a**) and this phenotype was also completely reversed by the prenatal co-treatment of AMH with the GnRH antagonist (**Fig. 3a**). Accordingly, plasma testosterone (T) and LH levels, measured at diestrus, were markedly elevated in PAMH compared to control and PAMH+GnRH antagonist mice (**Fig. 3b, c**). We then evaluated LH pulsatility by serial blood sampling in intact (non-gonadectomized) female mice at diestrus (**Fig. 3d**) and found that PAMH animals had a significantly higher LH pulse frequency as compared to control and AMH+GnRH antagonist treatment groups (**Fig. 3e, f**). This is suggestive of an alteration in the hypothalamic network activity of the offspring caused by late-gestational exposure to AMH excess.

These data show that the PAMH mouse model displays the cardinal PCOS neuroendocrine clinical features, including hyperandrogenism, LH elevation, sporadic ovulation, altered ovarian morphology and fertility defects. However, PAMH animals did not present weight alterations, indicating that this model is most representative of the lean PCOS phenotype.

Circulating AMH is presumed to be a mixture of proprotein (proAMH) and a complex of the NH2- and COOH-terminal peptides ($AMH_{N,C}$) (Pankhurst and McLennan 2013, Pankhurst, Chong et al. 2016), that can bind to AMHR2 and initiate signalling (MacLaughlin, Hudson et al. 1992, di Clemente, Jamin et al. 2010). We thus sought to investigate whether prenatal exposure to proAMH (140 kDa) would recapitulate the same PCOS-like traits observed upon injection of the bioactive form of AMH (AMH_C; 23.4 kDa).

We injected pregnant mice daily with PBS (Control) or with the proAMH (AMH, 0.12 mg/Kg/d) from E16.5 to E18.5 and studied the neuroendocrine phenotype of the offspring postnatally. Phenotypic characterization of these animals (**Supplementary Fig. 1**) show that prenatal exposure to proAMH mirrors the same PCOS neuroendocrine features observed in PAMH mice.

Peripherally administered AMH enters the adult brain and acts centrally by inducing GnRH neuronal activation

We speculated that peripherally administered AMH could impinge on the maternal GnRH neurons, which express AMHR2 (Cimino, Casoni et al. 2016), leading to their activation. In order to test that, we quantified the number of active GnRH neurons ($GnRH^+/Fos^+$) 90 minutes after i.p. delivery of AMH_C (**Supplementary Fig. 2a-d**). Indeed, a single AMH injection significantly increased the total number of Fos^+ nuclei in the hypothalamic OVLT (organum vasculosum laminae terminalis; **Supplementary Fig. 2 a-c**) as well as the proportion of GnRH neurons expressing Fos in the same regions (**Supplementary Fig. 2 a, b, d**). These results show that peripheral AMH can act centrally by inducing GnRH neuronal activation.

Next, we studied whether blood-borne AMH could enter the maternal brain and/or the fetal brain. For this purpose, we intravenously administered fluorescently-labeled bioactive AMH to E16.5

pregnant mice 2 min before sacrifice and subsequently harvested respectively the brains of the dams, the placentae and the heads of the fetuses (**Supplementary Fig. 2 e-i**). At this short interval, fluorescent AMH was detectable in the maternal brains at the level of the ME, where it diffuses out of the highly permeable, fenestrated endothelial cells, into the external layer of the ME, where GnRH terminals are located (**Supplementary Fig. 2 f**).

3D analysis of fluorescent AMH in tissue-cleared intact placentae collected from these animals indicated the presence of AMH in the maternal side but not in the fetal side of the placenta, indicating that AMH cannot cross the placental barrier (**Supplementary Fig. 2h**), as confirmed by the lack of fluorescent AMH in the corresponding fetal brains (**Supplementary Fig. 2i**).

We also verified whether Cetrorelix injected i.p. could access the maternal and, eventually, the fetal brain. Pregnant mice were treated either with Cetrorelix (0.5 mg/Kg/day) or PBS from E16.5 to E18.5; maternal and fetal brains were harvested one day later. Mass-spectrometry analyses…revealed the presence of the GnRH antagonist in the brains of the dams injected with Cetrorelix as well as in their fetal brains (values here….). TO BE COMPLETED BY CLAUDIO MEDANA…

Peripheral AMH causes gestational hyperandrogenism through a brain-ovarian-placental crosstalk

Since LH secretion is an indirect measurement of GnRH neuronal secretion, we measured LH in pregnant mice one day after vehicle (PBS), AMH or AMH + GnRH antagonist treatment (E19.5; **Fig. 3g**). During pregnancy serum LH levels are known to be almost undetectable as a consequence of the progesterone break. Unexpectedly, circulating LH levels were found to be 5 times higher in AMH-treated pregnant mice as compared to the control group (**Fig. 3g**). Such increase was prevented by the prenatal co-treatment of AMH with the GnRH antagonist (**Fig. 3g**). To assess whether the rise in LH levels would also be associated with an elevation in circulating T, caused by GnRH-driven maternal pituitary hypersecretion of LH driving ovarian testosterone synthesis, we then measured circulating T levels in the three animal groups (**Fig. 3g**). AMH-treated pregnant females showed a robust elevation in T, whereas control and AMH + GnRH antag dams displayed very low T levels

(**Fig. 3g**). We next measured circulating estradiol (E2) and progesterone (P) in those treatment groups and found a robust decrease of both hormones in the AMH-treated dams as compared to the vehicle-treated and AMH + GnRH antag-treated dams (**Fig. 3g**). These data indicate that late gestational exposure to high AMH is sufficient to generate in dams heightened LH and T levels and diminished E2 and P concentrations in a GnRH-dependent manner.

Since the placenta expresses AMHR2 both in humans (Novembri, Funghi et al. 2015) and in mice (**Fig. 3h**), and because we found high T and low E2 levels in AMH-treated dams, we examined if AMH treatment could alter aromatase expression in the murine placenta, possibly affecting the conversion of T into E2. We performed qPCR for the enzyme P450 aromatase (*CYP19A1*) gene in the placentae harvested from pregnant mice at the end of the treatment period (**Fig. 3h**). AMH treatment significantly lowered placental aromatase expression (**Fig. 3h**). Intriguingly, GnRH antag treatment prevented the AMH-driven inhibition of *CYP19A1* mRNA (**Fig. 3h**). We thus investigated the expression of *GnRH*, GnRH receptor (*GnRHR*) and LH receptor (*LHR*) transcripts in the placentae collected from those animals (**Supplementary Fig. 3**). All genes were found to be expressed in the placenta of the different treatment groups. However, while the expression of *GnRH* and *GnRHR* was unchanged among treatment groups, *LHR* expression was found to be significantly higher in the AMH-treated dams and to be normalized by the GnRH antag (**Supplementary Fig. 3**). We next quantified placental expression of *CYP11A1* and *HSD3B1*, two other key steroidogenic enzymes involved in onset of steroidogenesis and derivation of progesterone, respectively. We did not find any difference in the expression of *CYP11A1* among treatment groups but we found greatly diminished *HSD3B1* expression in the placentae of AMH-treated- as compared to control dams (**Fig. 3h**). In addition, GnRH antag-treatment prevented the downregulation of *HSD3B1* gene expression, indicating normalization of the GnRH/LH-driven maternal steroidogenesis.

As T is an anabolic hormone, we monitored whether dams increased their body weight and fat deposition as a consequence of the AMH treatment (**Supplementary Fig. 4a-c**). We did not find any changes in body weight, subcutaneous fat mass and perigonadal fat mass in E19.5 dams injected for 3 days with vehicle, AMH or AMH + GnRH antag (**Supplementary Fig. 4a-c**).

Finally, since P and E2 are vital to placental sufficiency and both hormones were greatly diminished in AMH-treated dams, we monitored whether there were any changes in litters lost, litter size, birthweights of pups when dams experienced diminished placental aromatase and *HSD3B1* expression (**Supplementary Fig. 4d-f**). Indeed, we found a significant increase in the number of aborted fetuses/litter and smaller litters when dams where treated with AMH as compared to vehicle- and AMH + GnRH antag-treated dams (**Supplementary Fig. 4d-e**). We did not observe any changes in the body weights of pups at birth (**Supplementary Fig. 4f**).

PAMH female offspring exhibit a masculinization of the brain

Perinatal gonadal steroids are primarily responsible for the sexual differentiation of the brain by triggering irreversible mechanisms (Simerly 2002, McCarthy, Arnold et al. 2012). We therefore analyzed whether the gestational, AMH-dependent maternal hyperandrogenism might interfere with the establishment of brain sexual dimorphism in the offspring and contribute to the establishment of the adult PAMH phenotype. In most vertebrate species, gonadal T secretion occurs in a sexually dimorphic pattern during the first hours following birth (0-4 hours at P0), being elevated in newborn males but not in females (Corbier, Edwards et al. 1992). We therefore measured T levels 2 hr post-partum in control males and females as well as in PAMH female pups. This showed that T was markedly elevated in both control males and newborn PAMH females as compared to the control female pups (**Fig. 4a**). Interestingly, the neonatal T surge observed in PAMH female pups was completely prevented by the prenatal GnRH antag treatment (**Fig. 4a**). Similarly to T, a short-lived (1–12 h post-partum) surge in circulating LH is detected exclusively in newborn males in rodent as well as in primate species (Herbison 2016). We thus measured serum LH in the pups and showed that LH was significantly more elevated in control male and PAMH female pups as compared to control females (**Fig. 4a**). Also in this case, the prenatal GnRH antag treatment prevented the LH neonatal surge of PAMH female pups (**Fig. 4a**).

To investigate whether the perinatal hyperandrogenism of the PAMH females could lead to long-term consequences in the organization of those brain areas, we analyzed three highly steroid-

sensitive features of well-known sexually dimorphic brain regions in adult control males (prenatal PBS-treated), control females (prenatal PBS-treated) and PAMH females (**Fig. 4b**, **Supplementary Fig. 5**). The established markers of developmental androgenization were the female-dominant (low androgen context) tyrosine hydroxylase (TH) neuron population in the anteroventral periventricular nucleus (AVPV) (Simerly 1989) and kisspeptin neuron population in the rostral periventricular area of the third ventricle (RP3V) of the hypothalamus (Clarkson and Herbison 2006) and the male-dominant (high androgen context) vasopressin (VP) expression in the bed nucleus of the stria terminalis (BnST) and the medial amygdaloid nucleus (MeA) (De Vries and Panzica 2006). As previously documented (Simerly 1989, Clarkson and Herbison 2006), we counted a higher number of TH neurons in the AVPV of control females versus control males (**Fig. 4c**) as well as a greater proportion of kisspeptin neurons in the RP3V of control females (**Supplementary Fig. 5**). Importantly, PAMH female mice exhibited a male-like number of TH and kisspeptin cells in these regions (**Fig. 4c**, **Supplementary Fig. 5**). A similar signature of androgenization was observed in the male-like VP expression in the BnST and MeA of PAMH females that displayed higher numbers of vasopressin-immunoreactive cells than control females, however without reaching the control male values (**Fig. 4d**).

These results show that PAMH female offspring exhibit a masculinization of both the neonatal T and LH surge, followed by a marked masculinization of the sexually dimorphic brain regions that regulate reproduction.

In utero exposure to excess AMH permanently alters the GnRH neuronal afferent network and the GnRH neuronal activity in the offspring

Given that GnRH neurons represent the final common pathway in the neural control of fertility, a crucial point was to determine whether the marked hormonal and morphological signatures of androgenization detected in the PAMH animals were accompanied by protracted changes in GnRH neuronal morphology and electrical activity during adult life. Using *GnRH-GFP* mice and 3D-reconstruction analysis, we identified increased spine density both on the soma and along the primary dendrite (over the proximal 45 μm distance) in PAMH female mice compared with controls during diestrus (**Fig. 5a-e, Supplementary movie 1 and 2**). We next analyzed whether this

increased spine density was correlated with increased Glutamatergic or GABAergic appositions. By counting the number of the vesicular glutamate transporter 2 (vGluT2)-immunoreactive (ir) puncta (associated with the primary dendrite of GnRH cells), we found no significant differences in the number of appositions of vGluT2 of PAMH compared to control female mice at diestrus (**Supplementary Fig. 6a-c**). However, when we counted the vesicular GABA Transporter (vGaT)-ir puncta on GnRH cell soma and proximal dendrite, we detected a significant increase in the number of vGaT appositions onto GnRH cells of PAMH compared to control, female diestrous mice (**Fig. 5f-h**). Although principally recognized as an inhibitory neurotransmitter in the adult brain, there is now a consensus that GABA is excitatory in adult GnRH neurons (Sullivan and Moenter 2004, Herbison and Moenter 2011). In order to test whether the elevated hypothalamic excitatory appositions onto GnRH neurons in our preclinical model of PCOS effectively translates into an increased neuronal activity, we performed whole-cell current-clamp recordings of GnRH-GFP neurons in acute coronal brain slices containing the preoptic area (POA). The recordings were done in animals sacrificed at diestrus, when GnRH secretion into the portal circulation is low (**Fig. 5i-m**). GnRH neurons from PAMH mice showed a robust, significant three-fold increase in their spontaneous action potential firing rate, as compared with controls (**Fig. 5i-k**). The average resting membrane potential (RMP) and average input resistance (R_{in}) of GnRH neurons were similar in control and PAMH mice (**Fig. 5l, m**). Since R_{in} and the membrane capacitance (C_m) did not differ significantly among groups (mean ± s.e.m.; Control: 41.348 ± 5.121 pF, n = 6; PAMH: 39.893 ± 3.921 pF, n = 7; Student's *t*-test: $P = 0.823$, t = 0.229), we can assume that the change in GnRH neuronal firing in PAMH animals compared to control animals is not due to modifications of passive electrical membrane properties.

GnRH antagonist treatment of adult PAMH mice normalizes their neuroendocrine phenotype.

Since our results uncovered a persistent hyperactivation of GnRH neurons in PAMH female animals, we reasoned that partially competing with natural GnRH for binding to membrane receptors on gonadotropes and thus decreasing the rate of LH and FSH release would ameliorate the PCOS-like phenotype observed in these mice.

To assess that, we analyzed estrous cyclicity of PAMH female mice, over 90 days, before, during and after i.p. injections of increasing doses of GnRH antagonist (0.05 mg/Kg, 0.5 mg/Kg and 5 mg/Kg

Cetrorelix acetate/per injection; **Fig. 6a**). We monitored daily vaginal cytology of PAMH animals throughout this time: before the beginning of the treatments, during the Cetrorelix administrations and during the recovery times (discontinuation of treatment; **Fig. 6a**).

As shown in **Figure 2**, PAMH mice display prolonged time in metestrus/diestrus as compared to the control female offspring. Therefore, we initially monitored estrous cyclicity and LH concentrations in PAMH mice for 12 days before the beginning of Cetrorelix treatment to ascertain that the animals included in the experimental paradigm displayed the typical PCOS-like neuroendocrine alterations. Subsequently, in order to normalize the GnRH action on the pituitary (partial inhibition of GnRH receptor), we injected these mice i.p. every second day, for 12 days, with Cetrorelix acetate at the dose of 0.05 and 0.5 mg/Kg, respectively (**Fig. 6a**). Tail-blood samples were collected for LH measurements twice during the GnRH antagonist treatment and once during the 10 days recovery time (no treatment), that followed each administration period.

To attain a complete blockade of GnRH receptor and suppression of LH secretion, we finally administered daily 5 mg/Kg Cetrorelix acetate over 12 days (**Fig. 6a**).

As expected, PAMH mice were oligo-anovulatory, displaying only about 25% of completed estrous cycles during 12 days as compared to control mice (**Fig. 6b**). Notably, normal estrous cyclicity was restored only when animals were injected with 0.5 mg/Kg of GnRH antagonist but not with the lowest or highest doses of the antagonist (0.05 mg/Kg and 5 mg/Kg Cetrorelix acetate; **Fig. 6b**).

LH concentrations were also measured in PAMH and Control mice before the beginning of the treatments (Cetrorelix acetate for the PAMH group and PBS for the Control group), at day 2 and day 6 of each treatment and 4 days after the last injection (recovery time; **Fig. 6c**). The time-course and dose-effect experiments showed that the aberrant mean LH values initially observed in PAMH mice were normalized following the GnRH antagonist treatment at the 0.5 mg/Kg dose only (**Fig. 6c, d**). Serum LH levels following the injections with 0.05 mg/Kg Cetrorelix acetate were found to be significantly greater than in Control animals, whereas they were significantly suppressed when mice were treated with the highest dose at 5 mg/Kg (**Fig. 6c, d**). As in clinical practice, the effects of

Cetrorelix on LH were reversible few days after discontinuation of treatment, independently by the dose of the injected drug (**Fig. 6c**).

After having identified the concentration of the GnRH antagonist which corrected the serum LH levels and estrous cyclicity in adult PCOS-like animals (0.05 mg/Kg), we performed the rest of the experiments with this dose (**Fig. 6e-i**). We monitored the % of time that animals spent in each stage of the estrous cycle (Metestrus/Diestrus, M/D; Estrus, E; Proestrus, P) and we showed that the GnRH antagonist restored ovulation of PAMH animals (**Fig. 6e**).

The aberrant T concentrations and LH pulsatility observed in PAMH mice were also normalized following the Cetrorelix treatment (**Fig. 6g-i**). These data show that postnatal GnRH antagonist treatment can rescue the major PCOS-like traits of PAMH mice: oligo-anovulation, hyperandrogenism, increased LH concentrations and LH pulsatility.

Material and Methods

Study population: human patients

Blood samples were derived from the population-based Uppsala Biobank of Pregnant Women, where blood samples are collected in conjunction with routine ultrasound screening during gestational weeks 16-19. Gestational age was determined according to the ultrasound-based estimated date of birth. Eligible women were 18 years or older and without blood-borne disease. In Sweden, all pregnant women are invited to a routine ultrasound examination, and approximately 97% of the pregnant population participate, hence, the Biobank subjects likely represent a population-based sample. Invitation to participate in the Biobank is random, with 70% of respondents accepting participation, it is estimated that the Biobank covers approximately half of the pregnant population of Uppsala County {Granfors, 2013 #538} Upon inclusion, brief demographic data are collected, including ongoing chronic disorders, ongoing medication, smoking, height and weight. Following written informed consent, a plasma sample is collected. The sample was centrifuged within two hours and stored at -80°C.

By September 2013, 160 women with PCOS had donated a blood sample to the biobank, and from these blood samples, 32 normal-weight and 34 obese women with PCOS were selected for the present study based on their age (27-39 years old). PCOS was diagnosed according to Rotterdam criteria, i.e. presence of 2 of the following criteria: 1) polycystic ovaries on transvaginal ultrasound, 2) oligoamenorrhea 3) hyperandrogenism (either biochemical or clinical). Hyperandrogenism was defined as pre-pregnancy hyperandrogenism: either elevated testosterone, or elevated free androgen index (testosterone/sex hormone binding globulin > 0.05) or pre-pregnancy hirsutism as judged at the time of diagnosis. All women with PCOS had normal prolactin levels and thyroid function. Based on the initial, pre-pregnancy, diagnostic work-up, each woman was further phenotyped as hyperandrogenic PCOS (with signs of biochemical and/or clinical hyperandrogenism) or normoandrogenic PCOS. The medical records of all women with PCOS were scrutinized to ensure a correct diagnosis of PCOS, and to obtain information on obstetric and perinatal outcomes.

For each woman with PCOS an age- and BMI matched healthy control was chosen. Each control had donated blood samples during the same week as the respective case and were healthy according to the self-report. The medical records of the controls were reviewed to ensure than none had been

diagnosed with PCOS or female factor infertility previously. Three blood samples from the controls could not be retrieved; hence 63 healthy controls were available for analysis. All women gave written informed consent for inclusion and the study has been approved by the Independent Ethical Review Board of Uppsala, Sweden.

AMH levels during pregnancy

Serum AMH levels were measured on samples stored at -80°C using the fully automated Acces Dxi sandwich immunoassay (B13127, Beckman Coulter). This assay measures the proAMH and the cleaved $AMH_{N,C}$ complex and uses recombinant human AMH as a calibrator. The limit of quantification of the assay is 0.57 pmol/L. Its intra- and inter-assay imprecision is < 5%. Results are expressed in pmol/L.

Animals

Timed-pregnant female wild-type C57BL/6J (B6) (Charles River, USA) and transgenic *Gnrh-Gfp* {Spergel, 1999 #539} were group-housed under specific pathogen-free conditions in a temperature-controlled room (21-22°C) with a 12-h light/dark cycle and *ad libitum* access to food and water. Standard diet (9.5mm Pelleted RM3, Special Diets Services, France) was given to all mice during breeding, lactation and growth of young stock. Nutritional profile of the standard diet RM3 is the following: Protein 22.45%, Fat 4.2%, Fiber 4.42%, Ash 8%, Moisture 10%, Nitrogen free extract 50.4%; Calories: 3.6 kcal/gr.

Mice were randomly assigned to groups at the time of purchase or weaning to minimize any potential bias. No data sets were excluded from analyses.

C57BLl/6J *Gnrh-Gfp* transgenic mice have been previously characterized {Spergel, 1999 #539}. Animal studies were approved by the Institutional Ethics Committees of Care and Use of Experimental Animals of the University of Lille (France; Ethical protocol number: APAFIS#2617-2015110517317420 v5). All experiments were performed in accordance with the guidelines for animal use specified by the European Council Directive of 22 September 2010 (2010/63/EU). The sample size, sex and age of the animals used is specified in the text and/or figure legends.

Genotyping

Tail biopsies were used to isolate genomic DNA to identify the sex of embryos and mice at birth using Ube1 primers: Ube1 (forward), 5'CACCTGCACGTTGCCCTT-3' and Ube1 (reverse), 5'TGGATGGTGTGGCCAATG-3'. Males were identified with two bands marking both X (252 bp) and Y (334 bp) chromosomes and females with a single band representing only the X chromosome at 252 bp. *Gnrh-Gfp* transgenic animals were genotyped as previously described {Spergel, 1999 #539}.

Prenatal anti-Müllerian Hormone (PAMH) treatment

Timed-pregnant adult (3-4 months) C57BL6/J (B6) dams were injected daily intraperitoneally (i.p.) from embryonic day (E) 16.5 to 18.5 with 200 μL of a solution containing respectively: 1) 0.01 M phosphate buffered saline (PBS, pH 7.4, prenatal control-treated), 2) PBS with 0.12 $mgKg^{-1}$/d human anti-Müllerian hormone (AMH) (AMH_C, R&D Systems, rhMIS 1737-MS-10, prenatal AMH (PAMH)-treated), 3) PBS with 0.12 $mgKg^{-1}$/d AMH and 0.5 $mgKg^{-1}$ of the GnRH antagonist, cetrorelix acetate (Sigma, Cat #C5249; PAMH + GnRH antag-treated), 4) 0.5 $mgKg^{-1}$/d of cetrorelix acetate in PBS (prenatal GnRH antag-treated), and 5) PBS with 0.12 $mgKg^{-1}$/d proAMH (Origene Technologies, Cat #TP308397; prenatal proAMH-treated, PproAMH).

Gnrh-Gfp adult females (P60-P90) were paired with males and checked for copulatory plugs, indicating day 1 of gestation. Pregnant *Gnrh-Gfp* dams were given either 200μl i.p. injections of PBS (control-treated) or 0.12 $mgKg^{-1}$/d AMHc in PBS from E16.5, E17.5 and E18.5. PAMH-*Gnrh-Gfp* and Control-*Gnrh-Gfp* offspring were weaned, genotyped and phenotyped during postnatal life.

Assessment of phenotype, estrous cycle and fertility

Control, PAMH, PAMH+GnRH antag, GnRH antag, and PproAMH female offspring were weaned at post-natal day P21 and checked for vaginal opening (VO) and time of first estrus. Anogenital distance (AGD) and body mass (grams, g) were measured at different ages during post-natal development (P30, 35, 40, 50 and 60). At VO and in adulthood (P60), vaginal smears were performed daily for 16 consecutive days (4-cycles) for analysis of age of first estrus and estrous cyclicity. Vaginal cytology was analyzed under an inverted microscope to identify the specific day of the estrous cycle.

The reproductive competency of these animals was determined by pairing the following mice: Control females mated with untreated C57BL6J (B6) wild-type males, PAMH females mated with PAMH males, PAMH+GnRH antag females mated with PAMH+GnRH antag males, and GnRH antag females mated with GnRH antag males for a period of 3 months. Unexperienced males and primiparous females, selected from at least three different litters, were used for the 90-days mating protocol test.

Number of pups/litter (number of pups), fertility index (number of litters per females over 3 months), and time to first litter (number of days to first litter after pairing) were quantified per treatment and pairing.

Postnatal GnRH antagonist treatment in PAMH mice and assessment of phenotype and hormone levels.

PAMH adult female offspring were cycled for 12-days before GnRH antagonist treatments. Vaginal cytology was analyzed under an inverted microscope to record the specific day of the estrous cycle. Animals were injected intraperitoneally (i.p.) with 200μL of a solution containing 0.01M phosphate buffered saline (PBS, pH 7.4) with Cetrorelix acetate at 0.05 and 0.5 mg/Kg, every second day, or daily with Cetrorelix acetate at the dose of 5 mg/Kg. Tail-blood samples were collected for LH measurements twice before the beginning of the treatments, and at day 2 and 6 of each treatment as well as 4 days after the last injection (no treatment). Estrous cyclicity was monitored every day at the same time of day for the 12 days during postnatal GnRH antagonist treatments.

Ovarian histology

Ovaries were collected from 3-4-month-old diestrus mice, immersion-fixed in 4% PFA solution and stored at 4°C. Paraffin-embedded ovaries were sectioned at a thickness of 5 μm (histology facility, University of Lille 2, France) and stained with hematoxylin-eosin (Sigma Aldrich, Cat # GHS132, HT1103128). Sections were examined throughout the ovary. Total numbers of large antral follicles (containing a single large antrum), atretic and cysts-like follicles (large fluid-filled cysts with an attenuated granulosa cell layer, dispersed theca cell layer, and an oocyte lacking connection to the granulosa cells), and corpora lutea (CL) were classified and quantified as previously reported

{Caldwell, 2017 #540}. To avoid repetitive counting, each follicle was only counted in the section where the oocyte's nucleolus was visible. Using an ocular scale, follicles were classified by diameter into preantral, large growing (200–400 μm) and cystic follicles (> 400 μm). To avoid repetitive counting, CL were counted every 100 μm by comparing the section with the preceding and following sections. CL were characterized by a still present central cavity, filled with blood and follicular fluid remnants or by prominent polyhedral to round luteal cells.

Perfusions

Adult mice (P60-P90) were anesthetized with i.p. injections of 100 mg/kg of ketamine-HCl and 10 mg/kg xylazine-HCl and perfused transcardially with 20ml of saline, followed by 100 ml of 4% PFA in 0.1M phosphate buffer (PB) (4% PFA/0.1M PB; pH 7.6). Brains were collected, post-fixed in the same fixative for 2h at 4 °C, cryoprotected overnight in PB/Sucrose 30% at 4°C, embedded in OCT-embedding medium (Tissue-Tek), frozen and stored at -80°C until cryosectioning.

Immunohistochemistry

Tissues were cryosectioned coronally (Leica cryostat) at 35μm for free-floating immunohistochemistry (IHC). Sections were blocked in an incubation solution of Tris-buffered saline (TBS 0.05M, pH 7.6), 0.25% bovine serum albumin (BSA; Sigma, A9418), 0.3% Triton X-100 (TBS-T; Sigma, T8787) with 10% normal donkey serum (NDS; D9663; Sigma) for 2h at room temperature before incubation with the following different primary antisera (depending on experiment) for 72h at 4°C: guinea pig anti-GnRH (EH#1018; 1:10,000){Hrabovszky, 2010 #349}{Casoni, 2016 #37}, a generous gift from E. Hrabovszky (Laboratory of Endocrine Neurobiology, Institute of Experimental Medicine of the Hungarian Academy of Sciences, Budapest, Hungary), rabbit anti-GFP (Abcam ab6556; 1:1000), mouse monoclonal anti-vesicular GABA Transporter, vGaT) antibody (Synaptic Systems #131001; 1:500), guinea pig anti-vesicular glutamate transporter 2 (vGluT2) (Synaptic Systems #135404; 1:500), monoclonal mouse anti-Tyrosine Hydroxylase (TH) antibody (Millipore MAB318; 1:3000), guinea pig anti-(Arg^8)-Vasopressin (Peninsula Laboratories #T-5048; 1:2500), rabbit anti-cFos (Santa Cruz Biotechnology #sc-52; 1:5000), and a rabbit anti-kisspeptin (A. Caraty #566 1:10,000, Institut National de la Recherche Agronomique){Clarkson, 2014 #542}. After TBS

rinses, immunoreactivity (i.r) was revealed using the corresponding secondary antibodies (Life Technologies, Molecular Probes, Invitrogen) all 1:400, [Alexa-Fluor 488-conjugated #A21206; Alexa-Fluor 647-conjugated #A31573, #A31571; Alexa-Fluor 568-conjugated #A10042, #A10037] for 90 min in incubation solution at RT. After TBS washes, sections were incubated with 0.02% Hoechst (H3569; Invitrogen) in TBS-T for 15-mins at RT and mounted on gelatin-coated slides and coverslipped with mowiol medium (Sigma #81381).

Sections were examined using an Axio Imager. Z1 ApoTome microscope (Carl Zeiss, Germany) equipped with a motorized stage and an AxioCam MRm camera (Zeiss). For confocal observation and analyses, an inverted laser scanning Axio observer microscope (LSM 710, Zeiss) with an EC Plan NeoFluor ×100/1.4 numerical aperture oil-immersion objective (Zeiss) was used with an argon laser exciting at 488nm and helium laser exciting at 543nm (Imaging Core Facility of IFR114, of the University of Lille 2, France).

3D rendering and movies of GnRH neurons were generated using Imaris ×64 software (7.6.1, Bitplane).

Immunohistochemical analysis

Assessment of Fos-GnRH co-expression

Adult C57BL6/J (B6) females in diestrus were given i.p. injections of a solution containing 200µL of 0.01M PBS, pH 7.4 or PBS with 0.12 $mgKg^{-1}/d$ AMH_C at 10:00. 90-min after injection, each mouse was anaesthetized and perfused transcardially as described above (*Perfusions*). Brains were collected, post-fixed in the same fixative for 2h at 4°C, embedded in OCT-embedding medium, frozen and cryosectioned coronally (Leica cryostat) at 35µm for free-floating IHC. Sections were processed for dual-label Fos-GnRH IHC.

Analysis of the double-labeled tissue was undertaken by counting the number of single-labeled and dual-labeled GnRH neurons in the preoptic area (POA: OVLT), with 2-3 brain sections representing the POA counted per mouse. Sections were scanned using a 20× objective to image Fos-GnRH double positively labelled cells for quantification. Activated neurons were identified as expressing Fos in the nucleus of the GnRH i.r. cell. The number of GnRH neurons co-expressing Fos was quantified and grouped to produce a mean percentage of the co-expression of GnRH-Fos in both

PBS- and AMH-treated groups. The data from each mouse were then grouped to provide the median percentage ± interquartile range (IQR).

For the analysis of the total Fos-i.r cells in the POA, the same sections described above were examined using a 10 × objective. The total number of Fos positive cells per POA (OVLT) section in each treatment was quantified using the particle analysis program from Fiji (NIH); the total number of Fos-positive cells in the OVLT were quantified and averaged across OVLT sections from each animal and treatment.

Analysis of sexually dimorphic brain nuclei

For single-labeled Tyrosine Hydroxylase (TH) IHC, the number of TH-i.r cell bodies located within anteroventral periventricular nuclei were counted. For single-labeled Vasopressin (VP) IHC, the number of VP-i.r cell bodies located within the bed nucleus stria terminalis (BNST) and Medial Amygdala (MeA) were counted. For both TH and VP single-labeled IHC, each section containing the AVPV or the BNST and MeA were analyzed in each sex, mouse and treatment (3-5 sections per mouse). For single-labeled kisspeptin IHC, the number of kisspeptin-i.r cell bodies were counted in the rostral periventricular area of the third ventricle (RP3V), which comprises the anteroventral periventricular nucleus (AVPV) and the preoptic periventricular nucleus. Two brain sections at each level of the RP3V were analyzed per mouse, and the number of kisspeptin positive cells counted and combined to produce the mean number of kisspeptin neurons per section for the RP3V of each mouse.

The mean number of TH-, VP- and Kiss-i.r neurons counted per section for the sexually dimorphic brain regions of each mouse and treatment were then grouped to provide the mean ± s.e.m. values for the experimental groups.

Assessment of GnRH neuron spine density

Coronal brain sections from adult (P60-90) female Control-*Gnrh-Gfp* and PAMH-*Gnrh-Gfp* animals were analyzed for GnRH neuron spine density.

Ten GFP-i.r GnRH neurons located within the rPOA were randomly chosen from adult (P60-P90) diestrus Control-*Gnrh-Gfp* (*n*=5) and PAMH-*Gnrh-Gfp* female mice (*n*=5) and were imaged using a

LSM 710, Zeiss upright confocal laser scanning microscope equipped with LSM 710 software. For each GnRH-GFP cell, a stack of images at 0.25μm intervals were collected using a 100× objective and 2× digital zoom function throughout the entire depth of the GFP-i.r neuron. Images containing the cell body and initial portion of the primary dendrite were collected and soma and dendritic spine density were determined. Spines were identified as protrusions from the somata or dendrite and defined as being less than 5μm in length from the soma or proximal dendrite (the dendrite with the greatest circumference extending from the GnRH soma). GnRH neuron soma spine density was expressed as the number of spines per μm relative to the soma circumference. Spine density was quantified every 15μm along the entire length of the proximal GnRH dendrite (0-45μm) as 45μm was the longest length of the proximal dendritic that could be imaged before the dendrite exited the section. Spine density was expressed as the number of spines/μm.

Analysis of vGaT or vGluT2 appositions on Gnrh-Gfp neurons

Coronal brain sections from adult (P60-90) female Control-*Gnrh-Gfp* and PAMH-*Gnrh-Gfp* animals were analyzed for GnRH neuron spine and vGaT or vGluT2 density. Between 8-10 GFP/vGaT or GFP/vGluT2 double labeled neurons located within the rPOA from Control;*Gnrh-Gfp* and PAMH;*Gnrh-Gfp* adult (P60-P90) diestrus female mice were imaged using the same criteria above. A z-series stack of images using a 100× objective was generated to estimate the density of vGaT or vGluT2 appositions. A contact was defined when there were no black pixels between the primary *Gnrh-Gfp* dendritic spine and vGaT or vGluT2 positive terminals. For each image, the number of vGaT- or vGluT2-labeled puncta directly opposed to GFP-labeled neuronal soma and dendrite (up to 45μm along the GnRH primary dendrite) were counted and combined to provide the mean values for each cell. The primary GFP-i.r dendrite could not be followed for more than 45μm from the cell body, therefore we determined the number of vGaT appositions every 15μm until the dendrite exited the section. Data are presented as vGaT or vGluT2 appositions/μm.

Fluorescent AMH assays

Recombinant bioactive AMH (AMH_C, R&D Systems, rhMIS 1737-MS-10) was tagged with a fluorescent dye (d2; MW: approx. 800 Da, max light output at 665nm) by Cisbio Bioassays (Codolet,

France) as previously described for other hormones{Balland, 2014 #543}, {Schaeffer, 2013 #519}, {Xu, 2017 #545}. Fluorescently-labeled bioactive AMH (2.5 nmoles/animal; Cisbio Bioassays) was injected into the jugular vein of pregnant mice (E16.5), anesthetized with ketamine/xylazine, and mice sacrificed 2 min later. Dams' brains, fetal brains and placentae were collected and immersion-fixed in 4% PFA overnight at 4 °C. Brains were cryoprotected overnight in PB/Sucrose 30% at 4°C, embedded in OCT-embedding medium, frozen and stored at -80 °C until cryosectioning. Placentae were processed for iDisco tissue-clearing as described below.

Cetrorelix measurement in biological samples

Sample preparation for nano-HPLC-HRMS analysis

Timed-pregnant adult (3-4 months) C57BL6/J (B6) dams were injected daily i.p. from embryonic day (E) 16.5 to 18.5 with 200µL of a solution containing respectively: 1) 0.01M phosphate buffered saline (PBS, pH 7.4, prenatal control-treated), 2) PBS with 0.5 $mgKg^{-1}$ of the GnRH antagonist, cetrorelix acetate (GnRH antag-treated). At E19.5, dams were anesthetized with ketamine/xylazine, and sacrificed by cervical dislocation. Dams' brains and fetal brains were collected, snap-frozen in liquid nitrogen and stored at -80 °C until nano-HPLC-HRMS experiments. Murine maternal and embryo brain samples were prepared adapting the procedure described. Briefly, brains were weighted, homogenized with 1% formic acid in cold acetonitrile and incubated for 15 min at -20°C. After centrifugation, the supernatant was freeze-dried and reconstituted with 3% acetic acid and 1% trifluoroacetic acid (TFA). all solvents sourced from Sigma-Aldrich Merck. The reconstituted sample was purified with a solid phase extraction using a Phenomenex polymeric reversed phase cartridge (Strata-X 33µm Polymeric Reversed Phase, 60 mg/3mL, Phenomenex, Bologna, Italy). The cartridges were equilibrated with a methanol and water solution of acetic acid and TFA (96:3:1 v/v), loaded with sample, washed with a 70:30 solution of water solution with acetic acid and TFA (96:3:1 v/v) and methanol, and eluted with a 90:10 solution of methanol and 3% acetic acid. The eluted solution was gently dried under stream on nitrogen and reconstituted with 0.1% formic acid. When brains were homogenized, an internal standard (ganirelix, empirical formula $C_{80}H_{113}ClN_{18}O_{13}$) was added to obtain a final concentration of 100ng/ml.

Nano-HPLC-HRMS analysis parameters

A Dionex Ultimate 3000 (Thermo Scientific, Milan, Italy) nano-HPLC instrument coupled to a Orbitrap Fusion (Thermo Scientific, Milan, Italy) high resolution hybrid mass analyzer was used.

Seperation was achieved with an EASY-Spray PepMap® column (C18, 2µm, 100Å, 75µm × 500mm, Thermo Scientific, Milan, Italy) using formic acid 0.1% in water (solvent A) and in acetonitrile:water 8:2 (solvent B) as mobile phases (ultrapure solvents for nano-LC, Sigma-Aldrich, Milan, Italy). The gradient conditions were as follow: 5% B for 5 min isocratic, up to 100% B in 30 min and reconditioned for at least 20 min. The first 5 minutes of isocratic flow was mandatory for the preconcentration step on a µ-precolumn (C18 PepMap 100, 300µm i.d. × 5 mm, Thermo Scientific, Milan, Italy), and water with 0.1% formic acid and 0.05% TFA. The injection volume was 1 µL and the flow rate 300 nL/min.

The column was equipped with a nanoESI source and the capillary voltage was 2000V in positive ion mode. The ion transfer tube temperature was 275°C and the pressure was standard (0.008 Torr). Full scan spectra were acquired in the range of *m/z* 350-2000. MS^n spectra were acquired in the range between the ion trap cut-off and precursor ion *m/z* values. CID collision energy was selected for each analyte to allow the survival of 5-10% of the chosen precursor ion. High resolution spectra were acquired with a resolution of 60000 (FWHM) and the mass accuracy of recorded ions (vs. calculated) was ± 5ppm units (without internal calibration).

Tissue clearing

We used iDisco clearing protocol, as previously described {Renier, 2014 #547}. Samples were washed in PBS (twice for 1h), followed by 50% methanol in PBS (1h), 80% methanol (1h) and 100% methanol (2x 1h). Next, samples were bleached in ice cold 5% H_2O_2 in 20% DMSO/methanol at 4°C overnight. Next, samples were washed in methanol (2x 1h), in 20% DMSO/methanol (2x 1h), 80% methanol (1h), 50% methanol (1h), PBS (2x 1h), and stored in PBS at 4°C until processing. Samples were then incubated at RT on a rotating wheel at 12 rpm in a solution containing: 20% MeOH, 40% MeOH, 60% MeOH, 80% MethOH, 100% MeOH, 100% MeOH; 1h each. Delipidation was achieved with an overnight incubation in DCM/Methanol (2:1), followed by a 30-min wash in 100% DCM (Dichloromethane; Sigma-Aldrich). Samples were cleared in dibenzylether (DBE; Sigma-Aldrich) for

2h at RT on constant agitation and in the dark. Finally, samples were moved into fresh DBE and stored in glass tube in the dark and at RT until imaging. 3D imaging was performed as previously described [72,73]. An ultramicroscope (LaVision BioTec) using InspectorPro software (LaVision BioTec) was used to perform imaging. The light sheet was generated by a laser (wavelength 488 or 561nm, Coherent Sapphire Laser, LaVision BioTec) and two cylindrical lenses. A binocular stereomicroscope (MXV10, Olympus) with a 2× objective (MVPLAPO, Olympus) was used at different magnifications (1.6×, 4×, 5×, and 6.3×). Samples were placed in an imaging reservoir made of 100% quartz (LaVision BioTec) filled with DBE and illuminated from the side by the laser light. A PCO Edge SCMOS CCD camera (2,560 × 2,160 pixel size, LaVision BioTec) was used to acquire images. The step size between each image was fixed at 2μm.

Pulsatile LH measurements

Diestrus female adult mice were habituated with daily handling for 3–weeks. Blood samples (5μl) were taken from the tail at 10-min intervals for 2h (between 10:00and 12:00) during diestrus, diluted in 45μl PBS-Tween (0.05%) and immediately frozen and kept at -80°C. LH levels were determined by the previously described sensitive LH sandwich ELISA. A 96-well high-affinity binding microplate (Corning) was coated with 50μl of capture antibody (monoclonal antibody, anti-bovine LHβ subunit, 518B7; L. Sibley; University of California, UC Davis) at a final dilution of 1:1000 (in Na_2CO_3/$NaHCO_3$, 0.1M, pH 9.6) and incubated overnight at 4°C. Wells were incubated with 200μl blocking buffer (5% (w/v) skim milk powder in 1 X PBS-T pH 7.4 [0.01M PBS, 0.05% Tween 20 (Sigma #P9416)] for 2hr at RT. A standard curve was generated using a two-fold serial dilution of mouse LH (reference preparation, AFP-5306A; National Institute of Diabetes and Digestive and Kidney Diseases National Hormone and Pituitary Program (NIDDK-NHPP) in 0.25% (w/v) BSA (Sigma, A9418) in PBS-T. The LH standards and blood samples were incubated with 50μl of detection antibody (rabbit LH antiserum, AFP240580Rb; NIDDK-NHPP) at a final dilution of 1:10,000 for 1.5h at RT. Each well containing bound substrate was incubated with 50μl of horseradish peroxidase-conjugated antibody (goat anti-rabbit; Vector Laboratories, PI-1000) at a final dilution of 1:10,000. After a 1.5h incubation, 100μl 1-Step™ Ultra TMB-Elisa Substrate Solution (ThermoFisher Scientific, Cat #34028) was added to each well and left at RT for 10 min. The reaction was halted by the addition of 50μl of

3M HCL to each well, and absorbance read at 490nm. Pulses were confirmed using DynPeak {Steyn, 2013 #549}.

LH and T ELISA Assays

LH levels were determined by a sandwich ELISA, as described previously{Vidal, 2012 #550}, using the mouse LH–RP reference provided by A.F. Parlow (National Hormone and Pituitary Program, Torrance, CA). Plasma T levels were analyzed using a commercial ELISA (Demeditec Diagnostics, GmnH, DEV9911) {Moore, 2015 #505} according to the manufacturers' instructions.

LH and T measurement in pregnant mice

Timed-pregnant female C57BL6/J (B6) dams were treated with i.p. injections of 200μL of PBS or 0.12 $mgKg^{-1}$/d AMH in PBS from E16.5-E18.5. At E19.5, pregnant-treated dams were decapitated and trunk blood was harvested in sterile Eppendorf tubes and left on ice until centrifugation. Plasma was collected after centrifugation of blood samples at 3000 *g* for 15 mins at 4°C and stored at -80° C until use. Mean T and LH levels were determined as described above.

LH and T measurement in P0 mice

Timed-pregnant C57BL6/J (B6) dams were given i.p injections of 200 μL PBS or 0.12 $mgKg^{-1}$/d AMH in PBS from E16.5-E18.5. Dams were allowed to deliver naturally. Pups were harvested 2h after birth. Tail biopsies of pups were taken to determine the sex of each animal (*see Genotyping*). Trunk blood and was collected from P0 males, control females and PAMH female pups for analysis of circulating testosterone and LH levels. Plasma was collected after centrifugation of blood samples at 3000*g* for 15 mins at 4°C and stored at -80° C until use. T and LH levels were determined as described above.

Quantitative RT-PCR analyses

E19.5 placental tissue from female control and PAMH embryos was isolated for total RNA was using Trizol (ThermoFisher Scientific, Cat #15596026) and the RNeasy Lipid Tissue Mini Kit (Qiagen; Cat # 74804) using the manufacturer's instructions. For gene expression analyses, mRNAs obtainHSD3ed from E19.5 placental tissue were reverse transcribed using SuperScript® IV Reverse Transcriptase

(Life Technologies). Real-time PCR was carried out on Applied Biosystems 7900HT Fast Real-Time PCR system using exon-boundary-specific TaqMan® Gene Expression Assays (Applied Biosystems): *Amhr2* (AMHR2- *Mm00513847_m1*); *Cyp19a1* (Cyp19a1-*Mm00484049_m1); Cyp11a1* (Cyp11a1-*Mm00490735_m1*); *Hsd3b1* (Hsd3b1-*Mm01261921_mH*); *Gnrh* (Gnrh-*Mm01315604_m1*); *Gnrhr* (Gnrhr-*Mm00439143_m1*); *Lhr* (Lhcgr-*Mm00442931_m1*). Control housekeeping genes*: ActB (*ActB-*Mm00607939_s1); Gapdh (*GAPDH**-Mm99999915_g1***).

Quantitative RT-PCR was performed using TaqMan® Low-Density Arrays (Applied Biosystems) on an Applied Biosystems thermocycler using the manufacturer's recommended cycling conditions. Gene expression data were analyzed using SDS 2.4.1 and Data Assist 3.01 software (Applied Biosystems), with *ActB* and *Gapdh* as control house-keeping mRNA following a standardized procedure. Values are expressed relative to control values, as appropriate, set at 1.

Brain slice electrophysiology preparation and recordings

Gnrh-Gfp adult females (3-4 months) were paired with adult *Gnrh-Gfp* males (3-4 months) and checked for copulatory plugs. Pregnant *Gnrh-Gfp* dams were given 200µl i.p. injections of PBS or 0.12 $mgKg^{-1}$/d AMH in PBS on days 16.5, 17.5 and 18.5 of gestation. Adult (3-4 months) female diestrus Control;*Gnrh-Gfp* and PAMH;*Gnrh-Gfp* offspring were anaesthetized with isoflurane, and, after decapitation, the brain was rapidly removed and put in ice-cold oxygenated (O_2 95% / CO_2 5%) artificial cerebrospinal fluid (ACSF) containing the following (in mM): 120 NaCl, 3.2 KCl, 1 NaH_2PO_4, 26 $NaHCO_3$, 1 $MgCl_2$, 2 $CaCl_2$, 10 glucose, pH 7.4 (with O_2 95% / CO_2 5%). After removal of the cerebellum, the brain was glued and coronal slices (150µm thickness) were cut throughout the septum and preoptic area using a vibratome (VT1200S; Leica). Before recording, slices were incubated at 34ºC for a recovery period of 1h. After recovery, slices were placed in a submerged recording chamber (32.8ºC; Warner Instruments) and continuously perfused (2ml/min) with oxygenated ACSF. *GFP*-positive GnRH neurons in the hypothalamic preoptic area were visually identified with a ×40 objective magnification in an upright Leica DM LFSA microscope under a FITC filter and their cell body observed by using IR-differential interference contrast. Whole-cell patch-clamp recordings were performed in current-clamp with bridge mode by using a Multiclamp 700B amplifier (Molecular Devices). Data were filtered at 1kHz and sampled at 5kHz with Digidata 1440A

interface and pClamp 10 software (Molecular Devices). Pipettes (from borosilicate capillaries; World Precision Instruments) of resistance of 6-8 MΩ when filled with an internal solution containing the following (in mM): 140 K-gluconate, 10 KCl, 1 EGTA, 2 Mg-ATP and 10 HEPES, pH 7.3 with KOH. Bridge balance was adjusted to compensate for pipette resistance. All recordings were analyzed with Clampfit 10 (Molecular Devices). Junction potentials were determined to allow correction of membrane potential values. Electrical membrane properties were measured in current-clamp mode by applying a series of current pulses from – 60 to + 60 pA (1s, 10pA increments). Input resistance (R_{in}) was determined by measuring the slope of the linear portion of the current-voltage curve. Recordings were terminated if R_{in} changed more than 10% between the beginning and the end of the recording. Membrane capacitance (C_m) was calculated using the equation $\tau=RC$, where τ=time constant, R=resistance, and C=capacitation. Membrane time constant was estimated by fitting a single exponential to the charging curve (Clampfit 10; Molecular Devices) generated from a hyperpolarizing current pulse (1s, 10pA) from rest.

Statistical analyses

All analyses were performed using Prism 7 (Graphpad Software, San Diego, CA) and assessed for normality (Shapiro–Wilk test) and variance, when appropriate. Sample sizes were chosen according to standard practice in the field. The investigators were not blinded to the group allocation during the experiments. However, analyses were performed by two independent investigators in a blinded fashion. For each experiment, replicates are described in the figure legends.

For AMH measurement during pregnancy, as AMH levels were found not to be normally distributed in the study population, results are reported as median and 25^{th}-75^{th} percentile range. All comparisons between PCOS and control patients were performed using the nonparametric Mann-Whitney *U* test. The significance level was set at $P < 0.05$.

For animal studies, data were compared using an unpaired two-tailed Student's *t*-test or a one-way ANOVA for multiple comparisons followed by Tukey's multiple comparison *post-hoc* test. Data analyses for percentages were performed using either a Mann-Whitney *U* test (comparison between two experimental groups) or Kruskal-Wallis test (comparison between three or more experimental groups) followed by a Dunn's *post hoc* analysis. The number of biologically independent

experiments, sample size, *P* values, age and sex of the animals are all indicated in the main text or figure legends. All experimental data are indicated as mean ± s.e.m or as the 25th–75th percentile, line at median. The significance level was set at $P < 0.05$. Symbols in figures correspond to the following significance levels: * $P < 0.05$, ** $P < 0.001$, *** $P < 0.0001$.

Discussion

Serum AMH levels have been shown to decrease with age both in healthy women and in women with PCOS, although they remain always 2- to 3-fold higher and elevated until 40 years of age in PCOS subjects (Piltonen, Morin-Papunen et al. 2005). On the other hand, AMH levels were previously found to be very low during pregnancy in women without decreased fertility (La Marca, Giulini et al. 2005, Koninger, Kauth et al. 2013) and it has been assumed that this would be also the case for PCOS individuals. Herein, we provide compelling evidences showing that pregnant women with PCOS have significantly higher circulating AMH levels than control pregnant women, independently of their BMI and age. Our data complement the above findings and add up that AMH levels in women with PCOS remain high until late reproductive age also during gestation.

Notably, most women with PCOS are hyperandrogenic during pregnancy (Sir-Petermann, Maliqueo et al. 2002, Sir-Petermann, Maliqueo et al. 2007), yet the cause of this remains enigmatic. Here, we found a positive relationship between AMH levels and hyperandrogenism in pregnant lean women with PCOS but not in obese PCOS pregnant patients. We do not know whether a causal-relationship between AMH and T might exist during gestation in humans. However, our results in mice demonstrate that AMH has a programming effect leading to gestational and perinatal hyperandrogenism and subsequent changes in the HPG axis and hormone levels of both the dams and the progeny.

Our data show for the first time that peripheral bioactive AMH (AMH_C) can access the maternal brain, at the level of the ME, and act centrally by inducing GnRH neuronal activation, as demonstrated by the increase in $GnRH^+/Fos^+$ neurons shortly after peripheral administration of AMH. Circumventricular organs, like the ME and the OVLT, contain highly permeable, fenestrated endothelial cells, that allow the free passage of molecules below 35 kDa (Schaeffer, Langlet et al. 2013). Therefore, circulating AMH_C can have direct access to GnRH dendrites and terminals, which express AMHR2 both in mice and humans (Cimino, Casoni et al. 2016), and that extend outside the blood-brain barrier in the OVLT (Herde, Geist et al. 2011) and in the ME.

The AMH in blood is generally presumed to be the bioactive cleaved AMH_C (Ragin, Donahoe et al. 1992), although recent studies suggested that human blood might contain mainly proAMH and

$AMH_{N,C}$ (Pankhurst and McLennan 2013, Pankhurst, Chong et al. 2016). Whether the $AMH_{N,C}$ undergoes some further cleavage, in proximity of the ME, remains to be fully investigated. However, the fact that peripheral administration of either proAMH or AMH_C leads to overlapping phenotypes in the offspring supports the latter hypothesis.

Several animal models of PCOS rely on the prenatal administration of dihydrotestosterone (DHT) to induce the emergence of the PCOS-like traits (Roland and Moenter 2014, Moore and Campbell 2017), even though pregnant women do not have DHT in their circulation. Although there are no animal models that can perfectly recapitulate all PCOS clinical features, we have now generated one of the most relevant PCOS mouse model, from a clinical perspective. In fact, our model is based on an AMH-driven gestational hyperandrogenism, which is then responsible for the pathophysiological alterations leading to the acquisitions of PCOS cardinal defects in the offspring. This fits well with previous studies demonstrating that gestational hyperandrogenism in monkeys, either occurring naturally or induced by T treatment, induces PCOS-like reproductive and metabolic traits in adulthood (Abbott, Nicol et al. 2013, Abbott, Rayome et al. 2017).

Our findings highlight a novel pathophysiological mechanism whereby exposure to AMH excess during pregnancy leads to a cascade of alterations touching the maternal brain, the ovaries and the placenta, and resulting into a strong elevation of maternal LH and T, and by a drop of P and E2. The maternal androgenization is most likely the result of a dual action of AMH on the dams: 1) central action and exacerbation of GnRH/LH-driven ovarian steroidogenesis and 2) peripheral action and inhibition of placental aromatase and *HSD3b1* expression, leading respectively to an increase in T bioavailability and a drop of circulating P levels. The 50% reduction in P levels detected in AMH-treated dams could significantly lower the break of P on LH secretion and further increase T production by theca cells (**Supplementary Fig. 7**).

These findings are in line with clinical investigations, which identified lower placental aromatase expression in women with PCOS (Maliqueo, Lara et al. 2013), implying that a dysregulation of P450 aromatase activity in pregnant women with PCOS might occur and be partly attributable to elevated levels of circulating AMH.

The robust drop of plasmatic P and E2 detected in AMH-treated pregnant mice most likely compromises their placental function, thus explaining the higher incidence of aborted fetuses observed in these animals (**Supplementary Fig. 7**). Interestingly, numerous clinical reports indicate that women with PCOS have increased risk of poor pregnancy outcomes (Katulski, Czyzyk et al. 2015), most likely due to placental dysfunctions, and lower maternal E2 levels (Maliqueo, Sundstrom Poromaa et al. 2015). However, whether women with PCOS also have lower levels of P during pregnancy is currently unknown and deserve further investigation.

Here, we also showed for the first time that the AMH-driven gestational hyperandrogenism triggers the masculinization of the brain in female offspring (**Supplementary Fig. 7**). In the developing male brain the appropriate exposure of androgens *in utero* is known to contribute to establishing sexually dimorphic brain circuitry controlling reproductive physiological processes (Lenz and McCarthy 2010). Interestingly, PAMH female animals exhibit a masculinization of both the neonatal T and LH surge, followed by a marked masculinization of the sexually dimorphic brain regions that regulate reproduction. Notably, the neonatal T and LH surges of PAMH female pups were corrected by prenatal GnRH antagonist administration, strongly indicating that the neonatal consequences of the gestational AMH treatments are programmed *in utero* and not neonatally.

Since GnRH neurons do not express androgen receptor or estrogen receptor alpha (ERα) (Huang and Harlan 1993), we propose that steroid hormone receptor activation should occur in upstream neuronal afferents. Indeed, we provided evidences indicating that hyperandrogenism during critical periods of development leads to increased GABAergic appositions to GnRH neurons and to a persistent GnRH neuronal hyperactivity in adulthood. The alterations in VGaT, observed in PAMH animals, phenocopy those of PNA mice (Sullivan and Moenter 2004, Moore, Prescott et al. 2015), and support a modified afferent synaptic input to GnRH neurons. Since GABAergic inputs are known to excite GnRH neurons (DeFazio and Moenter 2002, Herbison and Moenter 2011), we can postulate the hypothesis that elevated excitatory innervation of GnRH neurons might be responsible for the increase in the GnRH/LH pulse frequency that we described in PAMH adult females. Such hyperactivation of GnRH neurons (Chang 2007) is most likely responsible for the LH-driven ovarian androgen production over FSH release, which consequently leads to anovulation. Most women who

are diagnosed with PCOS exhibit high-frequency LH secretion, which is suggestive of rapid GnRH pulsatility (Goodarzi, Dumesic et al. 2011). This is the case for 95% of the metabolically healthy PCOS women, who present high LH levels, but not for obese PCOS patients (Rebar, Judd et al. 1976, Chang, Mandel et al. 1982, Pastor, Griffin-Korf et al. 1998, Huang, Tien et al. 2015).

It should be noted that both the PNA mice, described before (Sullivan and Moenter 2004, Roland, Nunemaker et al. 2010, Moore, Prescott et al. 2013), and the PAMH animals, described in this study, did not present any weight alterations, indicating that these models are most representative of the "lean" PCOS condition, characterized by elevated circulating LH. Such findings are highly compatible with recently improved understanding of a leaner PCOS phenotype *per se* in the general population. Indeed, studies in referral PCOS populations (studied in the clinical environment) versus medically unselected populations have suggested that patients with PCOS diagnosed in the referral setting had a greater BMI and prevalence of obesity than women with PCOS detected in the medically unselected population (Ezeh, Yildiz et al. 2013, Azziz 2016, Lizneva, Kirubakaran et al. 2016).

While it is clear that the weight of PAMH mice is unaffected, further study is needed to clarify whether other metabolic parameters known to be altered in hyperandrogenic lean PCOS women (Dumesic, Akopians et al. 2016) such as glucose tolerance, insulin resistance or intra-abdominal fat storage, might be also altered in these animals.

Management strategies aimed at treating PCOS have met only limited success and alternative and preventive therapies are therefore urgently needed.

Here, we showed that the prenatal co-treatment of AMH with the GnRH antagonist prevented the appearance of PCOS-like neuroendocrine traits in the offspring, thus demonstrating a critical role for GnRH in the prenatal programming of the disease. Moreover, we also showed that postnatal GnRH antagonist treatment of adult PAMH mice, at a concentration that only partially compete with endogenous GnRH for binding to membrane receptors on gonadotropes, restores their ovulation and normalizes LH secretion/pulsatility as well as androgen levels. Given that GnRH antagonists are largely used in the clinic, with no adverse secondary effects, pharmacological antagonism aimed at tempering GnRH/LH secretion is an attractive therapeutic strategy to restore ovulation and fertility in PCOS individuals characterized by normal body mass composition and high LH levels.

ACKNOWLEDGMENTS

We thank M. Tardivel (microscopy core facility), M.-H. Gevaert (histology core facility), D. Taillieu and J. Devassine (animal core facility) and the BICeL core facility of the Lille University School of Medicine for expert technical assistance. We are deeply indebted to Dr. Philippe Ciofi (U1215, Neurocentre Magendie, Institut National de la Santé et de la Recherche Médicale, Bordeaux, France) for his helpful feedbacks and discussion of the data.

This work was supported by: the Institut National de la Santé et de la Recherche Médicale (INSERM), France [grant number U1172]; the Centre Hospitalier Régional Universitaire, CHU de Lille, France (Bonus H to P.G. and Ph.D. fellowship to N.E.H.M.); ERC-2016-CoG to P.G. (725149_REPRODAMH); Agence Nationale de la Recherche (ANR), France [ANR-14-CE12-0015-01 RoSes and GnRH to P.G.]; Bourse France *L'Oréal-UNESCO Pour les Femmes et la Science* to B.K.T; Horizon 2020 Marie Sklodowska-Curie actions – European Research Fellowship (H2020-MSCA-IF-2014) to J.C.

FIGURE 1

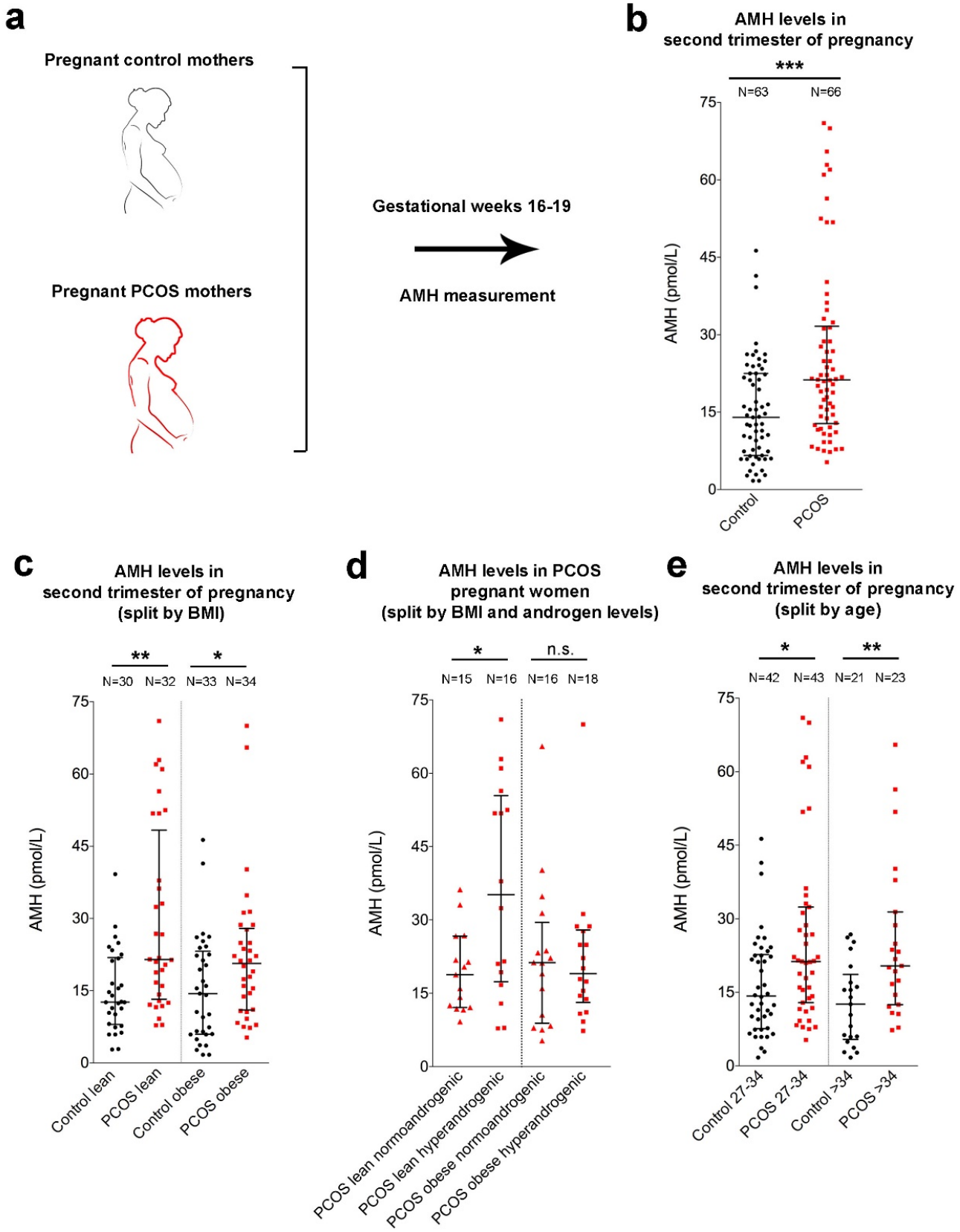
a
Pregnant control mothers
Pregnant PCOS mothers
Gestational weeks 16-19
AMH measurement
b
AMH levels in second trimester of pregnancy
***
N=63
N=66
AMH (pmol/L)
Control
PCOS
c
AMH levels in second trimester of pregnancy (split by BMI)
**
*
N=30
N=32
N=33
N=34
AMH (pmol/L)
Control lean
PCOS lean
Control obese
PCOS obese
d
AMH levels in PCOS pregnant women (split by BMI and androgen levels)
*
n.s.
N=15
N=16
N=16
N=18
AMH (pmol/L)
PCOS lean normoandrogenic
PCOS lean hyperandrogenic
PCOS obese normoandrogenic
PCOS obese hyperandrogenic
e
AMH levels in second trimester of pregnancy (split by age)
*
**
N=42
N=43
N=21
N=23
AMH (pmol/L)
Control 27-34
PCOS 27-34
Control >34
PCOS >34

Figure 1. AMH levels during the second trimester of gestation are higher in PCOS women than control women. (**a**) Blood samples were derived from 63 control and 66 PCOS pregnant women at gestational week 16-19 and AMH concentration was measure by ELISA. (**b**) Scatter-plot showing the circulating AMH levels in control pregnant women and in PCOS pregnant patients. (**c**) Scatter-plot showing the circulating AMH levels in control pregnant women and in PCOS pregnant patients stratified by the body mass index (BMI) of the patients and classified it into lean and obese subjects. (**d**) Scatter-plot showing the circulating AMH levels in PCOS pregnant patients stratified by their BMI and androgen levels (normoandrogenic or with signs of biochemical and/or clinical hyperandrogenism). (**e**) Scatter-plot showing the circulating AMH levels in control pregnant women and in PCOS pregnant patients stratified by their age. The horizontal line in each plot corresponds to the median value. The vertical line represents the 25^{th} – 75^{th} percentile range. Comparisons between groups, matched by BMI, androgen levels and age, were performed using unpaired nonparametric two-tailed Mann-Whitney *U* test. * $P < 0.05$, ** $P < 0.005$, *** $P < 0.0005$. Data were combined from two independent experiments.

FIGURE 2

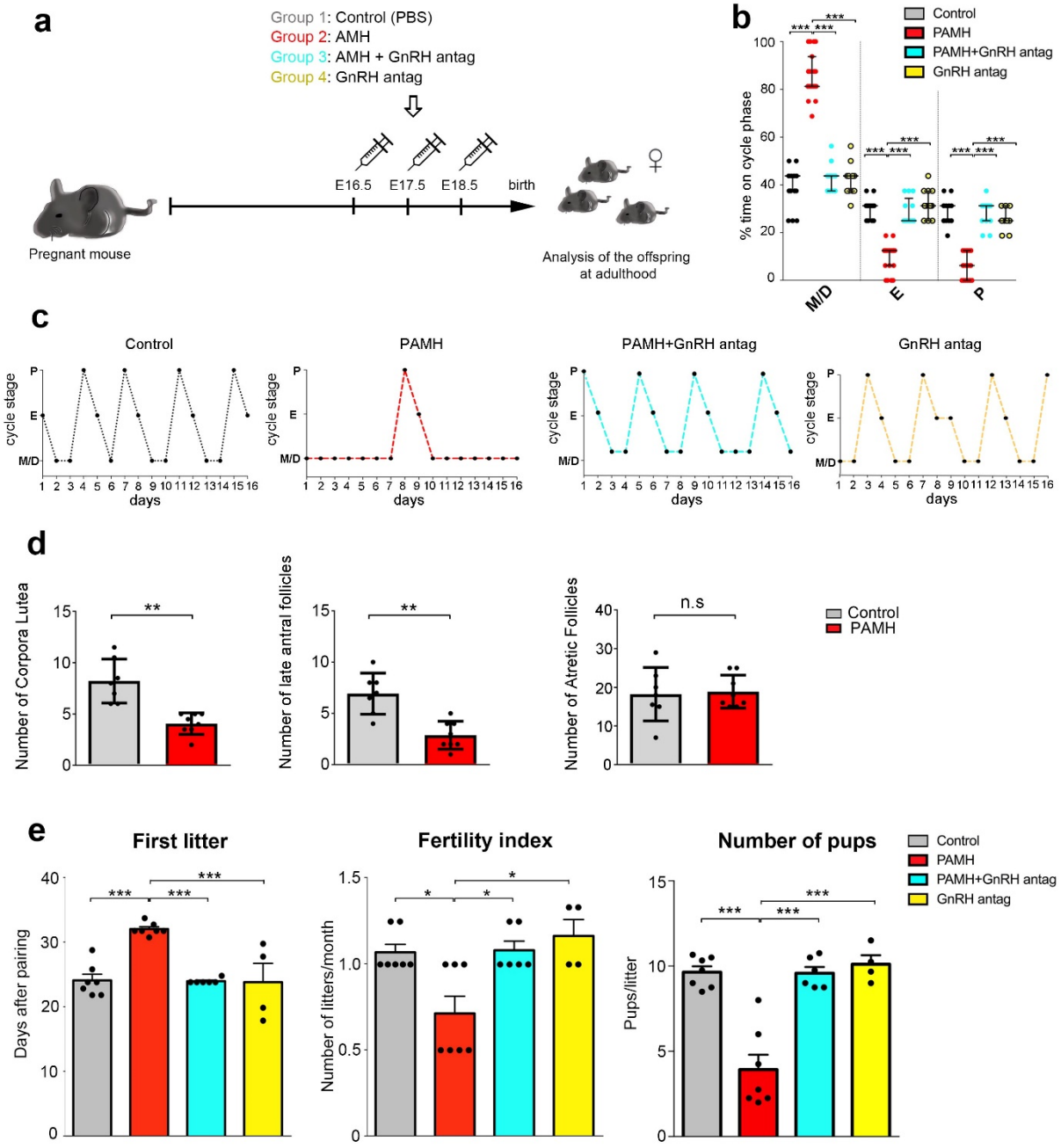

Figure 2. Prenatal AMH treatment disrupts estrous cyclicity, ovarian morphology and fertility in adult offspring. (a) Schematic of experimental design whereby pregnant dams were subjected to different treatments by intraperitoneal (i.p.) injections during the late gestational period (embryonic days (E) 16.5 - E18.5). Pregnant dams (P90-P120; *n* = 34) were treated with i.p. injections of four different treatments, listed in the figure. The offspring were designated as follows: Control,

(PBS-treated); PAMH (Prenatal recombinant AMHc-treated); PAMH+GnRH antag, (AMHc plus Cetrorelix acetate); GnRH antag (Cetrorelix acetate alone). (b) Quantitative analysis of ovarian cyclicity in adult (P60-P90) offspring mice (control, n = 15; PAMH, n = 19; PAMH+GnRH antag, n = 13; GnRH antag, n = 11). Vaginal cytology was assessed for 16 days. The horizontal line in each scatter plot corresponds to the median value. The vertical line represents the 25^{th} – 75^{th} percentile range. Comparisons between treatment groups were performed using Kruskal-Wallis test followed by Dunn's *post hoc* analysis test; *** P < 0.0001. Data were combined from three independent experiments. (**c**) Representation of estrous cyclicity in one female mouse of each of the four treatments during 16 consecutive days (4-cycles). (**d**) Quantitative analysis of corpora lutea, late antral follicles and atretic follicles in the ovaries of control (n = 7, age: P90) and PAMH mice (n = 8, age: P90). Data are represented as mean ± s.e.m (two-tailed Student's t-test; corpora lutea, $t_{(13)}$ = 4.879, **P < 0.001; late antral follicles, $t_{(13)}$ =4.637, ** P < 0.001; atretic follicles, $t_{(13)}$ =0.226, P = 0.82). Data were combined from two independent experiments. (**e**) Fertility tests of the adult offspring mice (P90). Matings were performed for 90 days. Control females were paired with control males (n = 7), PAMH females were paired with PAMH males (n = 7), PAMH+GnRH antag females were paired with PAMH+GnRH antag males (n = 6), and GnRH antag females were paired with GnRH antag males (n = 8). Female PAMH mice exhibit impaired fertility. Data are represented as mean ± s.e.m. Statistics were computed with one-way ANOVA followed by Tukey's multiple comparison *post hoc* test. *P < 0.05, **P < 0.001 and ***P < 0.0001. Data of fertility tests were combined from two independent experiments.

FIGURE 3

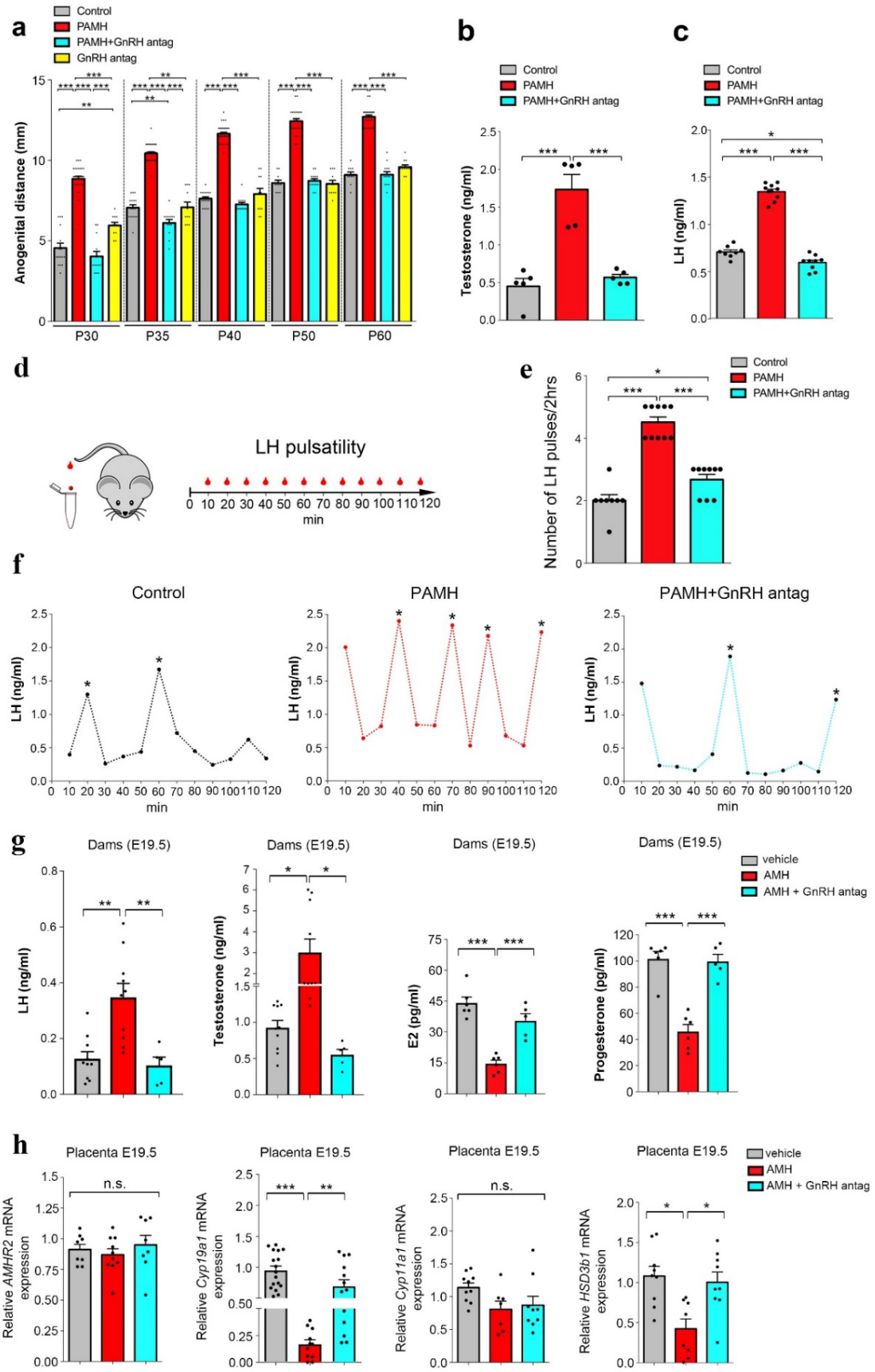
a
Control
PAMH
PAMH+GnRH antag
GnRH antag
Anogenital distance (mm)
P30
P35
P40
P50
P60
b
Testosterone (ng/ml)
c
LH (ng/ml)
d
LH pulsatility
0 10 20 30 40 50 60 70 80 90 100 110 120
min
e
Number of LH pulses/2hrs
f
Control
PAMH
PAMH+GnRH antag
LH (ng/ml)
min
g
Dams (E19.5)
vehicle
AMH
AMH + GnRH antag
LH (ng/ml)
Testosterone (ng/ml)
E2 (pg/ml)
Progesterone (pg/ml)
h
Placenta E19.5
n.s.
Relative AMHR2 mRNA expression
Relative Cyp19a1 mRNA expression
Relative Cyp11a1 mRNA expression
Relative HSD3b1 mRNA expression

Figure 3. Prenatal AMH treatment leads to hyperandrogenism and elevation in LH secretion/pulsatility. (**a**) Anogenital distance (AGD) was measured over post-natal days (P) 30, 35, 40, 50, and 60 in adult female control (*n* = 10-16), PAMH (*n* = 24-32), PAMH+GnRH antag (*n* = 13), and GnRH antag (*n* = 11) mice. Data were combined from three independent experiments. **(b)** Plasma testosterone concentration was measured by ELISA in adult females (P60) in diestrus: control group control (*n* = 5), PAMH mice (*n* = 5) and PAMH+GnRH antag (*n* = 5) littermates. **(c)** Plasma LH level was measured by sandwich ELISA in adult females (P60-P90) in diestrus female littermates. Data were combined from three independent experiments (control, *n* = 8; PAMH, *n* = 10; PAMH+GnRH antag, *n* = 9). Data in **b** and **c** were combined from two independent experiments. (**d**) Schematic representation of tail-tip blood sampling in adult diestrus female mice (3-4 months old). (**e**) Tail blood was collected every 10 min for 2 h and LH level measured from 10 a.m-12 p.m in adult (P60) diestrus females (Control, *n* = 8; PAMH, *n* = 10; PAMH+GnRH antag, *n* = 9). Data were combined from three independent experiments. (**f**) Representative graphs for LH pulsatility over 2-hr in one female adult (P60) mouse of each treatment. Asterisks in (**f**) indicate the number of LH pulses/2-hr. (**g**) Dams were injected from E16.5 to E18.5 with either PBS (vehicle, *n* = 9-11), AMH (*n* = 8-10), AMH + GnRH antag (*n* = 5) and trunk blood was collected at E19.5 for hormonal measurements by ELISA. Data were combined from at least two independent experiments. (**h**) Real-time PCR analysis of expression levels of *Amhr2*, *Cyp191a* (cytochrome P450 family 19A1, aromatase), *Cyp11a1* (cytochrome P450 family 11A1), *Hsd3b1* (3beta-hydroxysteroid dehydrogenase/delta(5)-delta(4)isomerase type I or hydroxy-delta-5-steroid dehydrogenase) mRNA in the placenta of E19.5 dams. Dams were injected i.p. from E16.5 to E18.5 with either PBS (vehicle, *n* = 8-17), AMH (*n* = 7-11), or AMH + GnRH antag (*n* = 8-13). Data were combined from three independent experiments.

Throughout, data are displayed as mean ± s.e.m. Statistics were computed with one-way ANOVA followed by Tukey's multiple comparison *post hoc* test. **P* < 0.05, ***P* < 0.001 and ****P* < 0.0001.

FIGURE 4

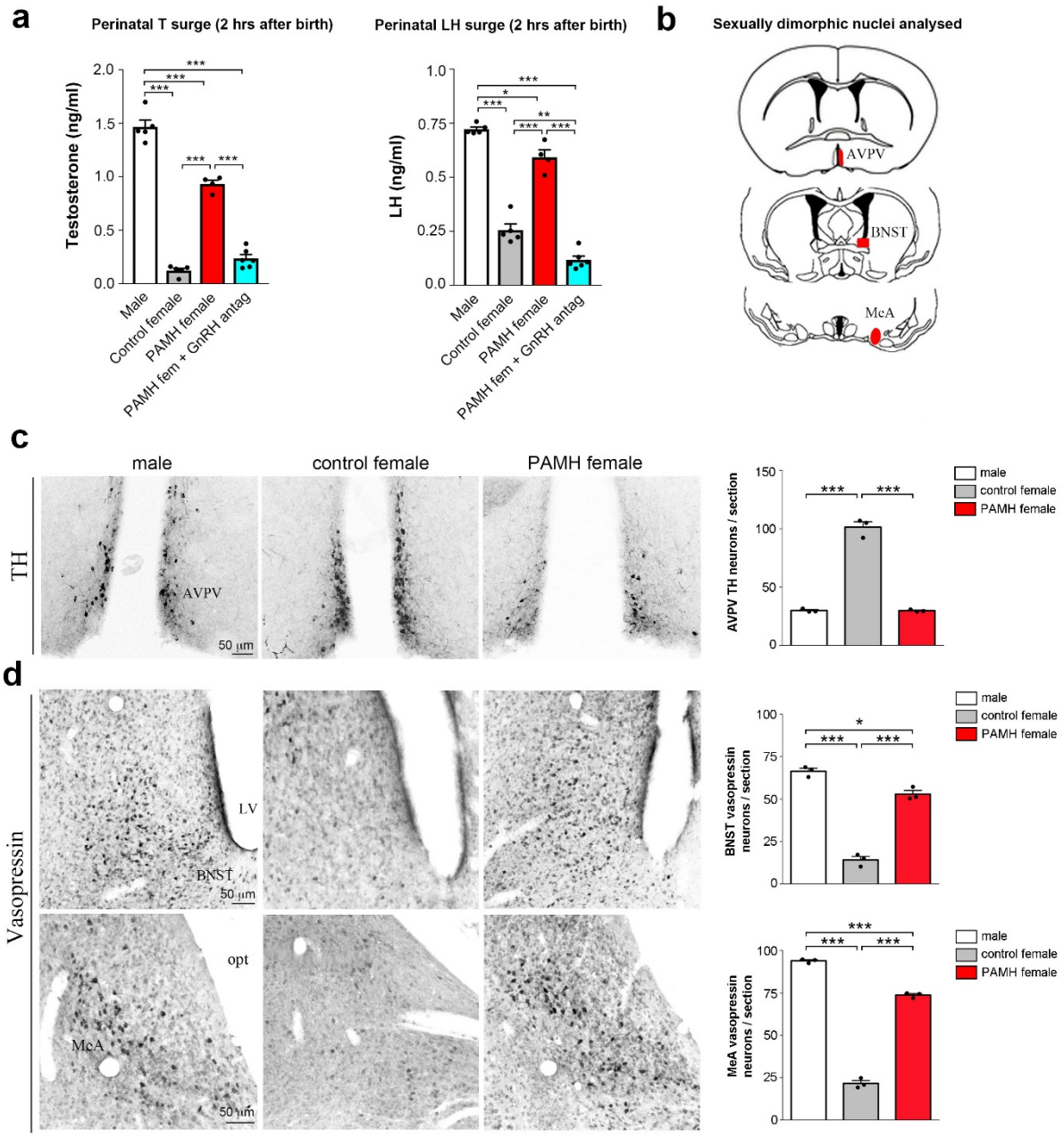

Figure 4. Prenatal AMH treatment increases perinatal T levels in females and masculinizes their brain. (**a**) Plasma T and LH levels were measured in pups 2 hours after birth (males, *n* = 5; control females, *n* = 5; PAMH females, *n* = 4; PAMH females + GnRH antag, *n* = 6). (**b**) Schematic representation depicting the analyzed sexual dimorphic neuroanatomical regions of the brain (denoted in red) expressing Vasopressin (VP) and Tyrosine Hydroxylase (TH). (**c**) Photomicrographs of TH-immunoreactive neurons in the anteroventral periventricular nucleus (AVPV) of a male, control

female and PAMH female at P60. TH immunoreactive (-ir) neurons in the AVPV were quantified in these animal groups (n = 3 per sex and treatment). (**d**) Photomicrographs of VP-immunoreactive neurons in the bed nucleus of the stria terminalis (BNST) and medial amygdala (MeA) of a male, control female and PAMH female at P60. VP–ir neurons in the BNST and MeA were quantified in these animal groups (n = 3 per sex and treatment). Throughout, data are displayed as mean ± s.e.m. Statistics were computed with one-way ANOVA followed by Tukey's multiple comparison *post hoc* test. *P < 0.05, **P < 0.001 and ***P < 0.0001. Experiments were replicated three times with comparable results.

FIGURE 5

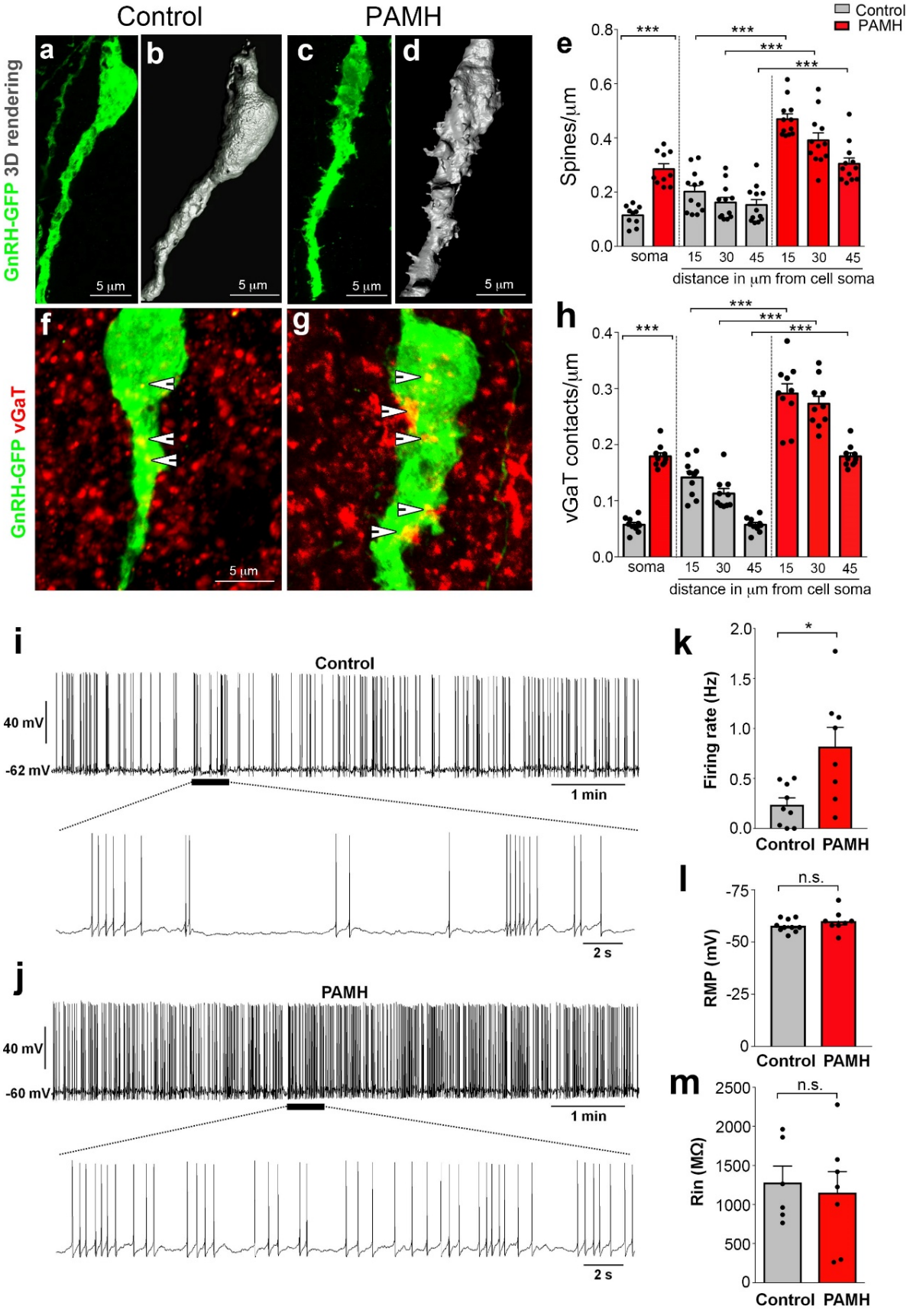
Control
PAMH
GnRH-GFP 3D rendering
GnRH-GFP vGaT
5 µm
Control
PAMH
Spines/µm
soma
15 30 45 15 30 45
distance in µm from cell soma
vGaT contacts/µm
***
i
Control
40 mV
-62 mV
1 min
2 s
j
PAMH
40 mV
-60 mV
1 min
2 s
k
Firing rate (Hz)
*
Control PAMH
l
RMP (mV)
n.s.
Control PAMH
m
Rin (MΩ)
n.s.
Control PAMH

Figure 5. PAMH/*GnRH-GFP* mice exhibit higher GnRH dendritic spine density, increased GABAergic appositions to GnRH neurons and elevated firing frequency of GnRH neurons in adulthood. (**a-d**) Projected confocal images and 3D reconstruction of *GnRH-GFP* neurons from an adult (P60) female diestrus control (**a, b**) and a PAMH (**c, d)** female diestrus mouse. (**e**) The GnRH dendritic spine density was analyzed in adult (P60) diestrus control and PAMH/*GnRH-GFP* females. Two sections with the largest number of GnRH neurons (rPOA containing the OVLT) where chosen from each animal, where the full extent of GFP-labeled GnRH neurons (*n* = 10-12 neurons from 3 animals per treatment group) were imaged and analyzed using confocal microscopy. Spine density was quantified for the soma and each 15 µm portion of the primary GnRH neuronal dendrite. (**f, g**) Projected confocal images of a GFP-immunoreactive GnRH neuron (green) surrounded by vGaT-immunoreactive (red) puncta in an adult diestrus control (**f**) and PAMH female mouse (**g**). Points where the vGaT signal was considered to be immediately adjacent to the GnRH neuron are indicated by arrowheads. (**h**) Quantification of the number of vGaT-immunoreactive puncta adjacent to GnRH neuron soma and along the primary GnRH neuronal dendrite is expressed as vGaT appositions/µm. vGaT contacts were defined as positive when vGaT immunolabeling was directly apposed onto the GnRH neuronal dendrites without any black pixels between the GnRH dendritic spine. (**i-m**) Spontaneous electrical activity and membrane properties of GnRH neurons recorded in acute brain slices from control and PAMH *GnRH-GFP* female diestrus mice. (**i**) Whole-cell current-clamp recording showing the typical spontaneous burst firing of a GnRH neuron from control mouse. The bottom trace shows an expanded time scale of that recording. (**j**) Same experiment as in (**i**) but in a GnRH neuron from PAMH mouse. (**k**) Average firing rate of GnRH neurons recorded from control (*n* = 9 cells from 4 animals) and PAMH mice (*n* = 8 cells from 4 animals). (**l**) Average resting membrane potential (RMP) of GnRH neurons recorded from control (*n* =10 cells from 4 animals, age P90-P120) and PAMH mice (*n* = 8 cells from 4 animals, age P90-P120) was not significantly different between both groups (two-tailed Student's *t*-test, $t_{(16)}$ = 1.143, *P* = 0.2700, ns). (**m**) Average input resistance (R_{in}) of GnRH neurons recorded from control (*n* = 6 cells from 4 animals, age P90-P120) and PAMH mice (*n* = 7 cells from 4 animals, age P90-P120) was not found significantly different between both groups (two-tailed Student's *t*-test, $t_{(11)}$ = 0.3685, *P* = 0.7195, ns, not significant). Throughout, data are displayed as mean ± s.e.m. Statistics were computed with two-tailed Student's *t*-test. **P* < 0.05, ***P* < 0.001 and ****P* < 0.0001. Experiments were replicated three times with comparable results. OVLT, organum vasculosum lamina terminalis; rPOA, rostral Preoptic Area.

FIGURE 6

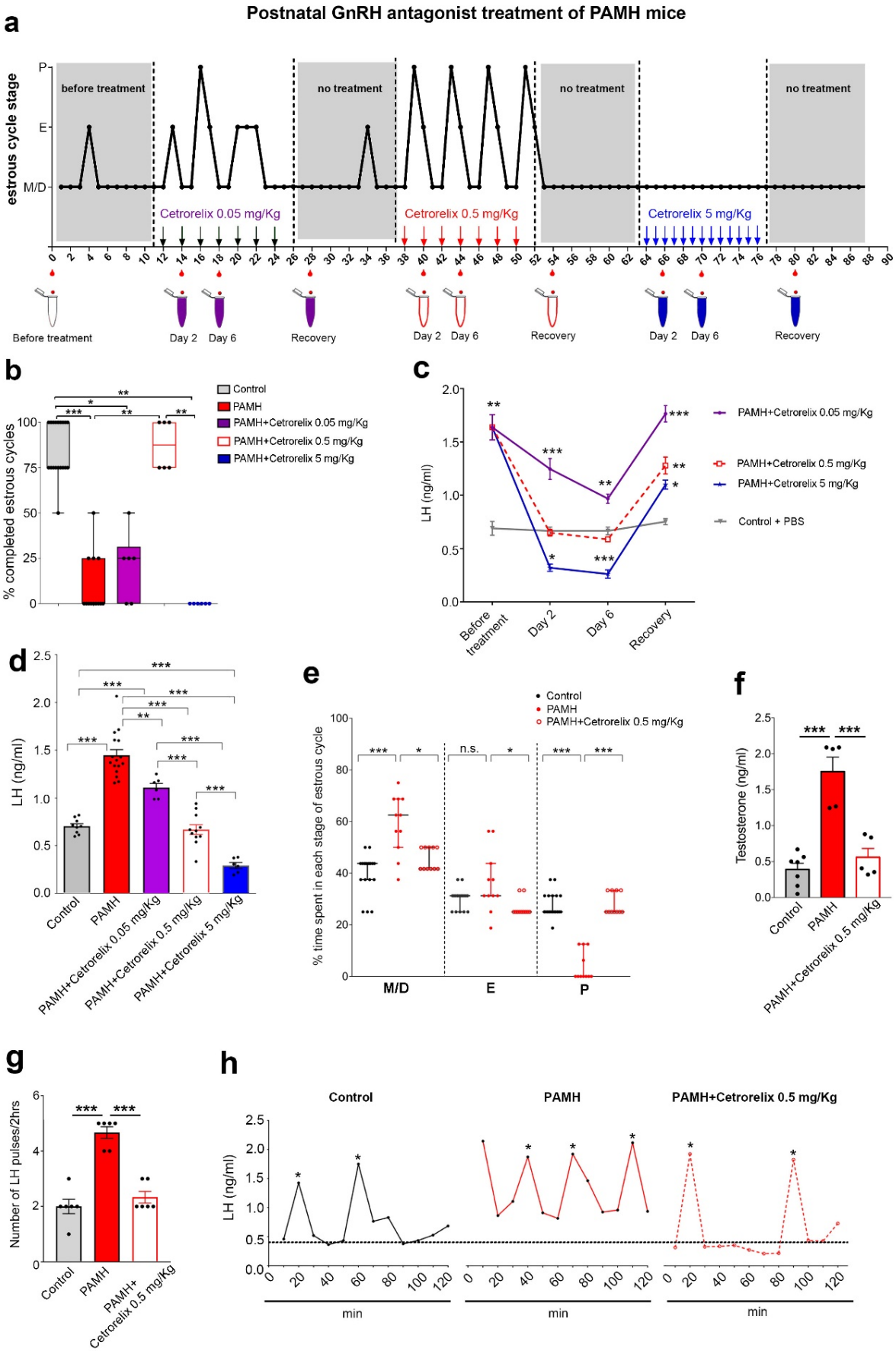
a
Postnatal GnRH antagonist treatment of PAMH mice
estrous cycle stage
P
E
M/D
before treatment
no treatment
no treatment
no treatment
Cetrorelix 0.05 mg/Kg
Cetrorelix 0.5 mg/Kg
Cetrorelix 5 mg/Kg
Before treatment
Day 2
Day 6
Recovery
Day 2
Day 6
Recovery
Day 2
Day 6
Recovery
b
% completed estrous cycles
Control
PAMH
PAMH+Cetrorelix 0.05 mg/Kg
PAMH+Cetrorelix 0.5 mg/Kg
PAMH+Cetrorelix 5 mg/Kg
c
LH (ng/ml)
PAMH+Cetrorelix 0.05 mg/Kg
PAMH+Cetrorelix 0.5 mg/Kg
PAMH+Cetrorelix 5 mg/Kg
Control + PBS
Before treatment
Day 2
Day 6
Recovery
d
LH (ng/ml)
Control
PAMH
PAMH+Cetrorelix 0.05 mg/Kg
PAMH+Cetrorelix 0.5 mg/Kg
PAMH+Cetrorelix 5 mg/Kg
e
% time spent in each stage of estrous cycle
Control
PAMH
PAMH+Cetrorelix 0.5 mg/Kg
n.s.
M/D
E
P
f
Testosterone (ng/ml)
Control
PAMH
PAMH+Cetrorelix 0.5 mg/Kg
g
Number of LH pulses/2hrs
Control
PAMH
PAMH+ Cetrorelix 0.5 mg/Kg
h
Control
PAMH
PAMH+Cetrorelix 0.5 mg/Kg
LH (ng/ml)
min
min
min

Figure 6. Postnatal GnRH antagonist treatment of PAMH mice restores the PCOS-like neuroendocrine phenotype. (**a**) Schematic of experimental design whereby vaginal cytology (estrous cyclicity) in PAMH adult mice (P90, *n* = 6) was analyzed during 3 months, before and after postnatal intraperitoneal (i.p.) injections with 0.05, 0.5 and 5 mg/Kg Cetrorelix acetate. The Y axis refers to the different stages of the estrous cycle: Metaestrus/Diestrus (M/D), Estrus (E) and Proestrus (P). The X axis represents the time-course of the experiments (days). Animals were injected i.p. every second day, for 12 days, with Cetrorelix acetate at the dose of 0.05 and 0.5 mg/Kg, and every day with Cetrorelix acetate at the dose of 5 mg/Kg. Tail-blood samples were collected for LH measurements twice before the beginning of the treatments, and at day 2 and 6 of each treatment as well as 4 days after the last injection (no treatment), that followed each administration period. (**b**) Quantitative analysis of the % of completed estrous cycles in control (PBS-treated, *n* = 19), PAMH (*n* = 13), and PAMH mice postnatally treated with the three doses of GnRH antagonist (PAMH+Cetrorelix 0.05 mg/Kg, PAMH+Cetrorelix 0.5 mg/Kg, PAMH+Cetrorelix 5 mg/Kg; *n* = 6 each). The horizontal line in each scatter plot corresponds to the median value. The vertical line represents the 25^{th} – 75^{th} percentile range. Comparisons between treatment groups were performed using nonparametric Kruskal-Wallis test followed by Dunn's *post hoc* analysis test. (**c**) Time course of serum LH measured on days 0 (before treatment), 2 and 6 of the treatment and 4 days after discontinuation of the treatment (recovery time). Treatment groups (*n* = 6 for each Cetrorelix treatment group and *n* = 3 for the Control) are indicated in the figure. Data were combined from two independent experiments. (**d**) Mean LH levels were measured in diestrus adult (P60-P120) control mice (*n* = 9), PAMH (*n* = 16), PAMH+Cetrorelix 0.05 mg/Kg (*n* = 6), PAMH+Cetrorelix 0.5 mg/Kg (*n* = 11), PAMH+Cetrorelix 5 mg/Kg (*n* = 6). Data were combined from three independent experiments. (**e**) Scatter plot representing the percentage (%) of time spent in each estrous cycle. The horizontal line in each scatter plot corresponds to the median value. The vertical line represents the 25^{th} – 75^{th} percentile range. The percentage (%) of time spent in each estrous cycle was quantified in control (*n* = 19), PAMH (*n* = 11) and PAMH+Cetrorelix 0.5 mg/Kg (*n* = 11) mice (age: P60-P90), as described above. Comparisons between treatment groups were performed using Kruskal-Wallis test followed by Dunn's *post hoc* analysis test. Data were combined from three independent experiments. (**f**) Mean T levels were measured by ELISA in diestrus adult control (*n* = 7), PAMH (*n* = 5) and PAMH+Cetrorelix 0.5 mg/Kg (*n* = 5) animals. (**g**) Tail blood was collected every 10 min for 2 h and LH level measured from 10 a.m-12 p.m in adult (P90) diestrus females (Control, *n* = 6; PAMH, *n* = 6; PAMH+Cetrorelix 0.5 mg/Kg, *n* = 6). (**h**) Representative graphs for LH pulsatility over 2-hr in

one female adult (P90) mouse of each treatment. Asterisks in (**h**) indicate the number of LH pulses/2-hr. The dotted line refers to the control LH baseline value.

Values in **c**, **d**, **f**, **g** are represented as the mean ± s.e.m. Statistics in **c**, **d**, **f**, **g** were computed with one-way ANOVA followed by Tukey's multiple comparison post hoc test. $*P < 0.05$, $**P < 0.001$ and $***P < 0.0001$. Experiments were replicated three times with similar results.

	Control lean (N=30)	**PCOS lean (N=32)**	**Control obese (N=33)**	**PCOS obese (N=34)**	***P* value**
Ethnic group	Caucasian (N=30)	Caucasian (N=32)	Caucasian (N=30 of 33)	Caucasian (N=34)	nd
Gestational age (weeks)	16-19	16-19	16-19	16-19	nd
Age (years) of pregnant patients	32 (IQR 28.75-35.25)	31.5 (IQR 29.25-35.00)	32 (IQR 29.5-36.00)	33 (IQR 30.75-37.00)	0.5241
BMI in first trimester (Kg/m^2)	22.4[a] (IQR 20.42-23.44)	21.91[a] (IQR 20.56-23.17)	32.47[b] (IQR 30.62-33.89)	32.37[b] (IQR 29.82-34.29)	*a* vs *b* < 0.0001
Gestational length (days)	280 (IQR 272-286)	278 (IQR 270.3-289)	282 (IQR 273.5-289)	279 (IQR 269.8-287)	0.7225
Birthweight (g)	3675 (IQR 3300-3900)	3510 (IQR 3210-3778)	3620 (IQR 3285-4125)	3670 (IQR 3255-4175)	0.3536
IVF	3 out of 31	10 out of 32	0 out of 33	5 out of 34	nd

SUPPLEMENTARY TABLE 1

Demographic table of pregnant control and PCOS patients. Blood samples were derived from the population-based Uppsala Biobank of Pregnant Women, where blood samples are collected in conjunction with the routine ultrasound screening in gestational week 16- 19.

When applicable, the Kruskal-Wallis test followed by Dunn's *post hoc* analysis was used to analyze differences between study groups. The significance level was set at $P < 0.05$.

Abbreviations: IQR, Interquartile ranges; BMI, body mass index; IVF, *in vitro* fertilization.

SUPPLEMENTARY FIGURE 1

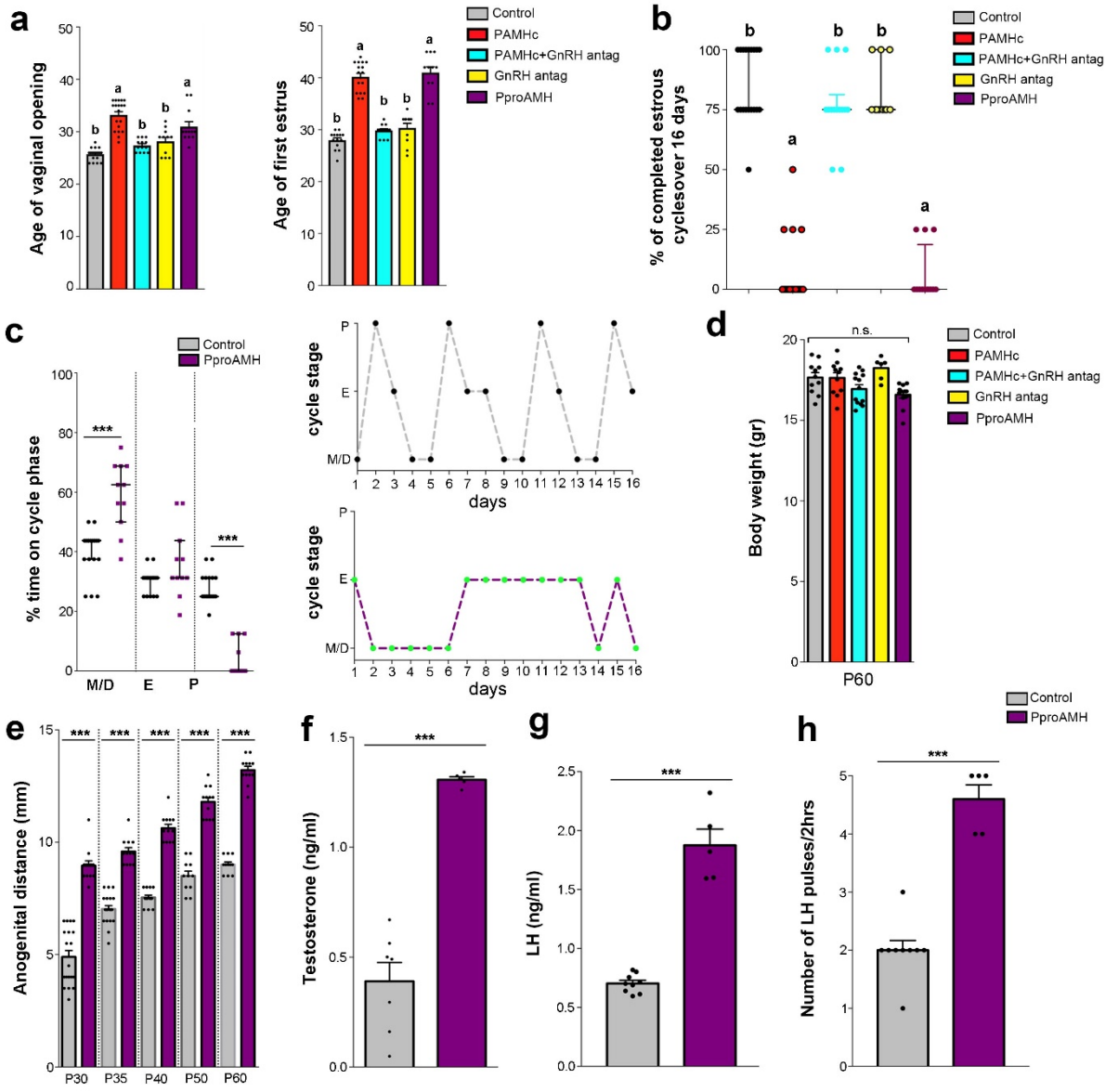

Supplementary Figure 1. Prenatal proprotein AMH (proAMH) treatment induces PCOS-like phenotype in the offspring.

(**a-b**) Parameters of vaginal opening and estrous cyclicity in the following prenatally treated offspring: Control (PBS-treated, *n* = 19); PAMHc (prenatal AMH C-terminal-treated, *n* = 17-19), PAMHc+GnRH antag (prenatal AMH C-terminal-treated with cetrorelix acetate, *n* = 13), GnRH antag (cetrorelix acetate-treated, *n* = 11), and PproAMH (prenatal proprotein AMH-treated, *n* = 12). **(a)** Differences in time of vaginal opening and age of first estrus were assessed by one-way ANOVA and

Tukey's multiple comparison *post hoc* test. Treatment groups defined as *a* significantly different from groups defined as *b*. Data were combined from three independent experiments. (**b**) Scatter plot representing the percentage (%) of completed estrous cycles over 16 days (4 cycles) in female offspring aged P60-P90. The horizontal line in each scatter plot corresponds to the median value. The vertical line represents the 25^{th} – 75^{th} percentile range. Comparisons between treatment groups were performed using Kruskal-Wallis test followed by a Dunn's multiple comparison *post-hoc* analysis. Treatment groups defined as *a* significantly different from groups defined as *b*. (**c**) Scatter plot representing the percentage (%) of time spent in each estrous cycle respectively in control (n = 19) and PproAMH mice (n = 11). M/D: Metestrus/Diestrus phase, P: Proestrus, E: Estrus. The horizontal line in each scatter plot corresponds to the median value. The vertical line represents the 25^{th} – 75^{th} percentile range. Comparisons between treatment groups were performed using two-tailed Mann-Whitney *U* test for each cycle stage. Right panel in **c** is a representation of estrous cyclicity in one female control and one female PproAMH mouse during 16 consecutive days compared to control females. (**d**) Body weight (gr) was measured in female control (PBS treated, n = 11), PAMHc (AMH C-terminal treated, n = 11), PAMHc + GnRH antag (n = 12), GnRH antag alone (n = 6) and PproAMH (proprotein AMH treated, n = 12) offspring and compared using one-way ANOVA and Tukey's multiple comparison *post hoc* analyses. (**e**) Anogenital distance (AGD) was measured over post-natal days (P) 30, 35, 40, 50, and 60 in adult female control (n = 11-19) and PproAMH (n =12) mice. (**f**) Plasma T levels was measured in adult control (n = 7) and PproAMH females (n = 5) in diestrus at P60. (**g**) Plasma LH level was measured in adult females (P60) in control (n = 9) and PproAMH (n = 5) littermates at diestrus. (**h**) Tail blood was collected every 10 min for 2 h and LH levels measured from 10 a.m-12 p.m in adult (P60) diestrus females for LH pulsatility over 2-hr in control (n = 9) and PproAMH (n = 5) mice. Values in **a** and **d-h** are represented as the mean ± s.e.m. Statistics in **e-h** were computed with with two-tailed Student's *t*-test. Asterisks represent significant statistical differences: * $P < 0.05$, ** $P < 0.005$, *** $P < 0.0001$. Data shown here were combined from at least three independent experiments.

SUPPLEMENTARY FIGURE 2

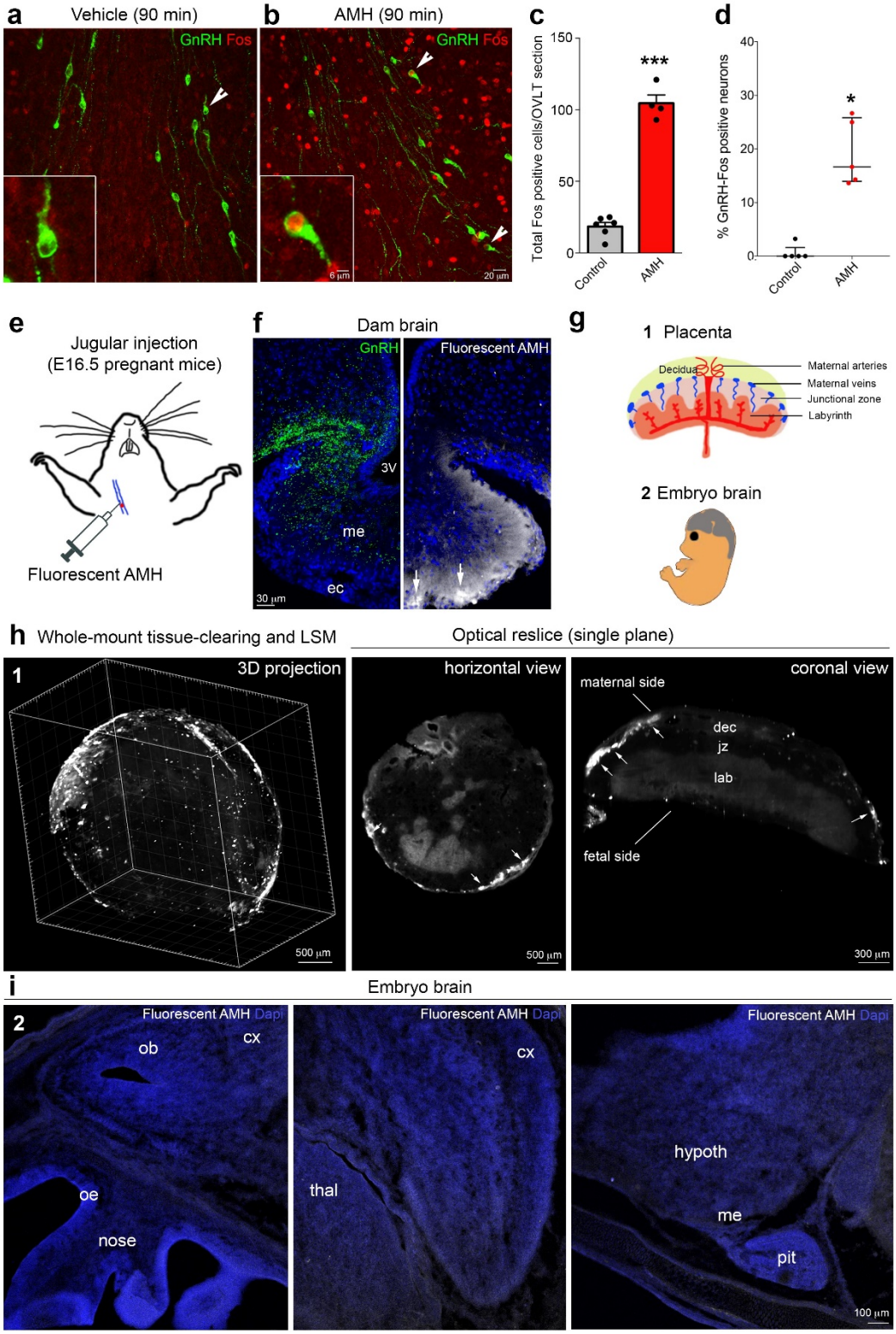

Supplementary Figure 2. Passage into the brain and action of peripherally-injected AMH. Female mice (P60-90) were injected (i.p.) with PBS or AMH_C in diestrus and sacrificed 90 min later. (**a, b**) Representative confocal images depicting the OVLT after dual-immunolabeling for GnRH (green) and Fos (red) in PBS-treated (**a**) and AMH-treated mice (**b**). Arrows point to double-labeled Fos-GnRH neurons. (**c**) The total number of Fos positive cells was quantified in the OVLT sections of control (n = 6) and AMH-treated animals (n = 4). Control females exhibit less Fos immunoreactive cells/OVLT section as compared to AMH-treated mice (Unpaired Student's t-test $t_{(8)} = 14.57$, *** $P < 0.0001$). (**d**) Scatter plot representing the percentage (%) of GnRH neurons expressing Fos in the OVLT sections. The horizontal line in each scatter plot corresponds to the median value. The vertical line represents the 25^{th} – 75^{th} percentile range. Comparisons between treatment groups (n = 5 per animal group) were performed using Mann-Whitney U test, * $P = 0.007$. OVLT, organum vasculosum laminae terminalis. Data shown in **a**-**d** were combined from two independent experiments. (**e-i**) Fluorescently-labeled bioactive AMH (2.5 nmoles/animal) was injected into the jugular vein of E16.5 pregnant mice (n = 4; **e**). Animals were sacrificed 2 min later to assess AMH passage into the dam's brains (**f**), placentae (**g**) and fetal brains (**i**). (**f**) Representative photomicrographs showing GnRH-immunopositive nerve terminals (green, left panel) and fluorescent AMH (white, right panel) in the median eminence (me), which lies outside the blood-brain-barrier (BBB). Note the diffusion of AMH, 2 mins after jugular administration, from the site of access into the me (arrows; permeable fenestrated endothelial cells: ec) and spreading in the external layer of the me. (**g**) Schematic representation of the other two organs, namely placenta (1) and fetal brain (2), where the passage of fluorescent AMH was also investigated. (**h**) 3D analysis of fluorescent AMH in the intact placenta. Panels are Light-Sheet Microscopy (LSM) images of a representative solvent-cleared placenta. The displayed 3D-projection, horizontal view and the lateral view, show the presence of fluorescent AMH (white) in the decidua at the level of the maternal veins (arrows) but not in the fetal side of the placenta, indicating that AMH cannot pass through the placental barrier. Data shown here were replicated in three independent experiments. (**i**) Representative sagittal section of the head of an E16.5 embryo harvested from a dam injected with fluorescent AMH, which shows the lack of AMH passage into the fetal brain. Data shown here were replicated in 4 independent experiments. In Figures **f** and **i** cell nuclei are counterstained with DAPI. Dec: decidua; jz: junctional zone; lab:

labyrinth; oe: olfactory epithelium; ob: olfactory bulb; cx: cortex; thal: thalamus; hypoth: hypothalamus; pit: pituitary.

SUPPLEMENTARY FIGURE 3

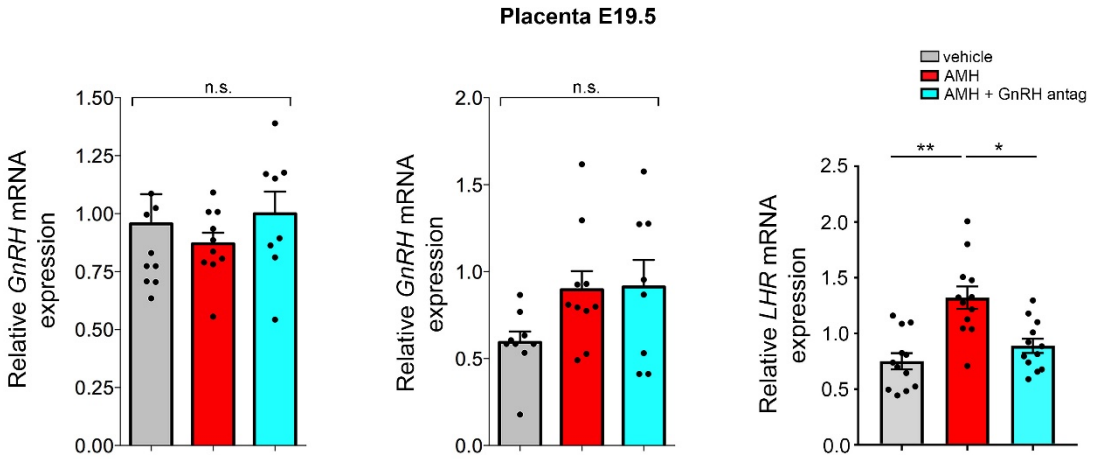

Supplementary Figure 3. Prenatal AMH treatment increases LH receptor expression in the placenta. Real-time PCR analysis of expression levels of *GnRH*, *GnRHR* (GnRH receptor) and *LHR* (LH receptor) mRNA in the placenta of E19.5 dams. Dams were injected i.p. from E16.5 to E18.5 with either PBS (vehicle, n = 9-12), AMH (n = 10-12), or AMH + GnRH antag (n = 8-12). Data were combined from three independent experiments. Throughout, data are displayed as mean ± s.e.m. Statistics were computed with one-way ANOVA followed by Tukey's multiple comparison *post hoc* test. *P < 0.05, **P < 0.001; n.s.: not significant (P > 0.05).

SUPPLEMENTARY FIGURE 4

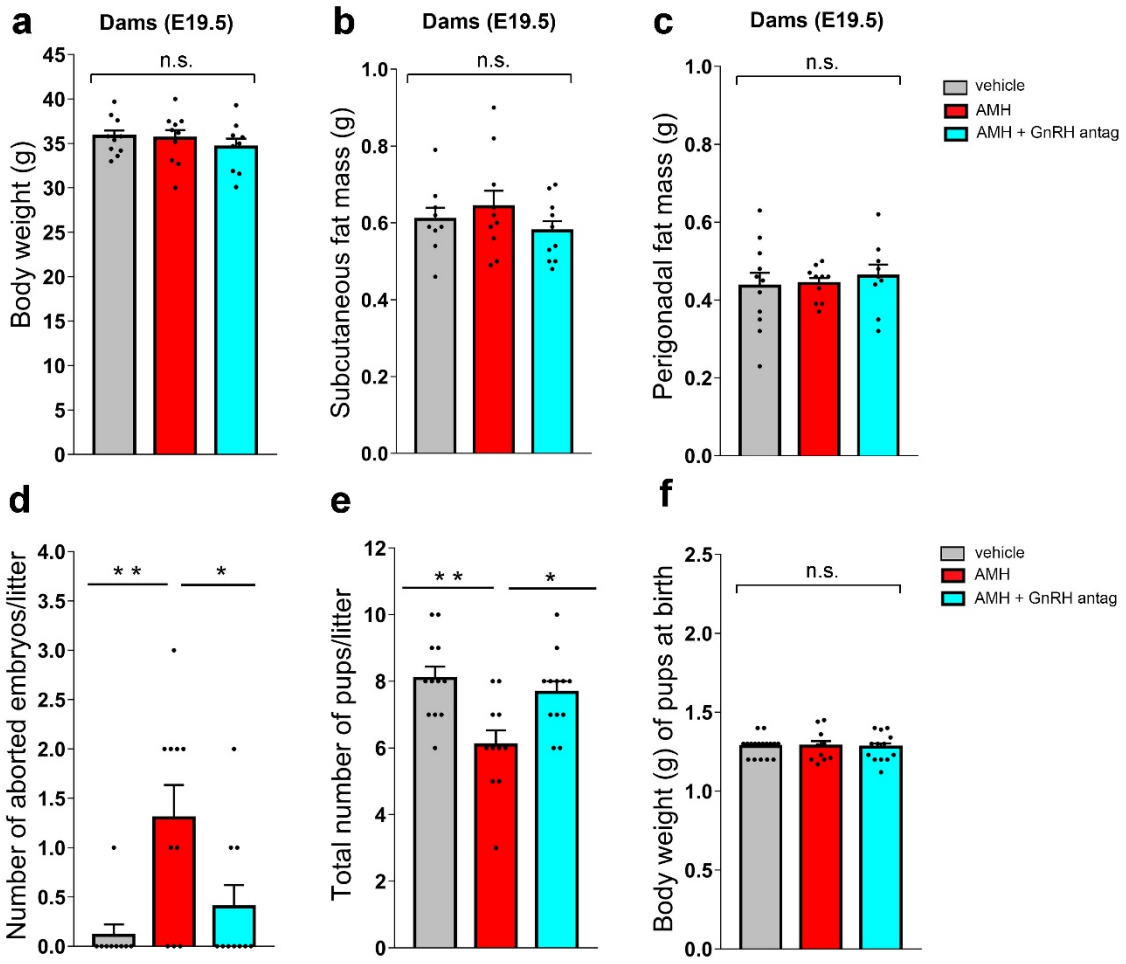

Supplementary Figure 4. Prenatal AMH treatment does not alter body weight of the dams and pups at birth but increases litter loss. Dams were injected from E16.5 to E18.5 with either PBS (vehicle, *n* = 8-11), AMH (*n* = 10), AMH + GnRH antag (*n* = 8-10). Body weight (grams: g; **a**), subcutaneous fat mass (**b**) and perigonadal fat mass (**c**) was measured in dams at gestational day 19.5. (**d**) Dams were injected from E16.5 to E18.5 with either PBS (vehicle, *n* = 9), AMH (*n* = 9), AMH + GnRH antag (*n* = 9). Dams were sacrificed one day later and the number of aborted embryos per litter was calculated. (**e**, **f**) Dams were injected from E16.5 to E18.5 with either PBS (vehicle, *n* = 12), AMH (*n* = 11), AMH + GnRH antag (*n* = 12). The number of pups per litter (**e**) and the weight of the pups at birth (**f**) was calculated. Values are represented as the mean ± s.e.m. Statistics were computed with one-way ANOVA followed by Tukey's multiple comparison post hoc test. **P* < 0.05, ***P* < 0.001; n.s.: not significant (*P* > 0.05). Data were combined from three independent experiments.

SUPPLEMENTARY FIGURE 5

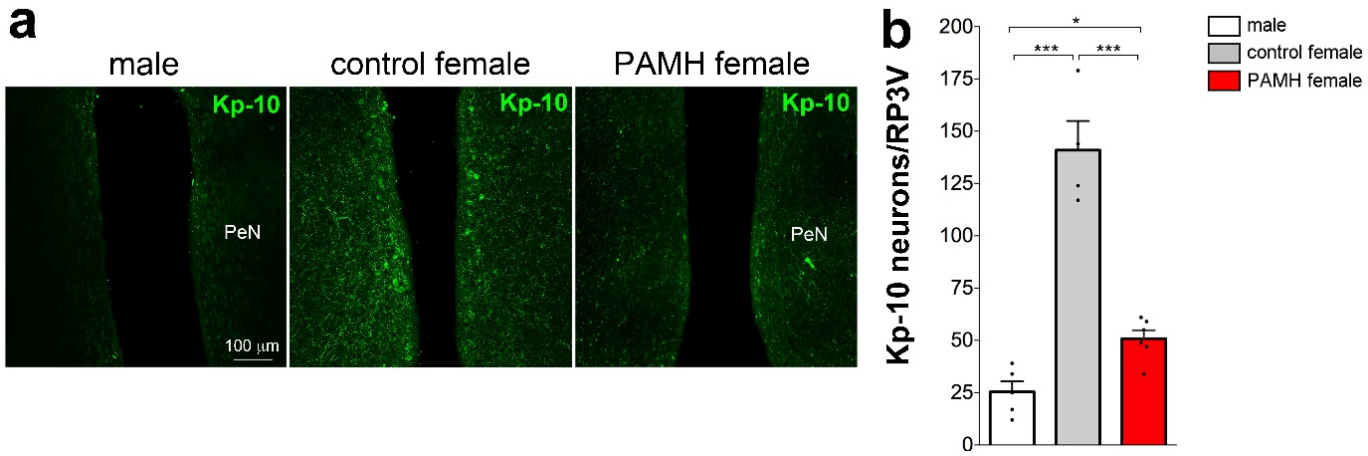

Supplementary Figure 5. Early androgenization of PAMH female mice obliterates sexually dimorphic Kisspeptin expression in the RP3V. (**a**) Representative coronal sections of the hypothalamic preoptic periventricular nucleus (PeN) immunostained for kisspeptin at P60. Note the sex differences in kisspeptin immunoreactivity in the adult control male (left) and female (center) brains, whereas no sex differences were observed between the male brain and adult PAMH female brain (right), which points to a masculinization of the PAMH female brain. (**b**) Kisspeptin immunoreactive (-ir) neurons in the rostral periventricular area of the third ventricle (RP3V) were quantified in these animal groups at P60 (control male, prenatal PBS injected: $n = 5$; control female, prenatal PBS injected: $n = 4$; PAMH female, prenatal AMH treated: $n = 6$). Data are displayed as mean ± s.e.m. Statistics were computed with one-way ANOVA followed by Tukey's multiple comparison *post hoc* test. $^{*}P < 0.05$ and $^{***}P < 0.0001$. Experiments were replicated twice with comparable results.

SUPPLEMENTARY FIGURE 6

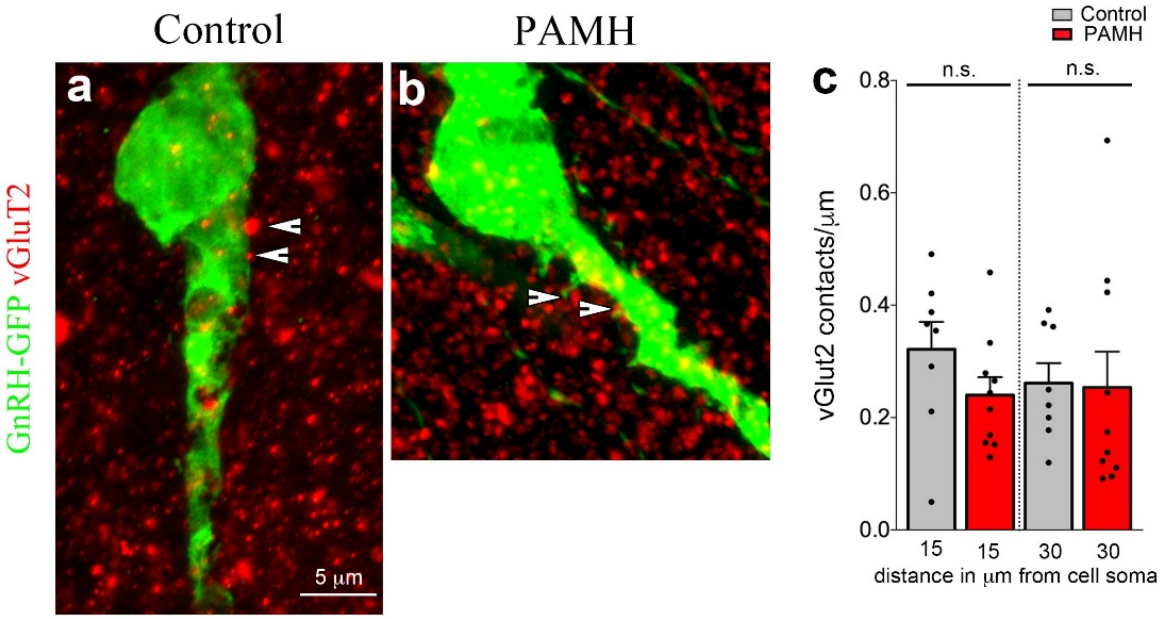

Supplementary Figure 6. The glutamatergic appositions onto GnRH neurons do not differ between control and PAMH mice. (**a, b**) Projected confocal images of a GFP-immunoreactive GnRH neuron (green) surrounded by vGluT2-immunoreactive (red) puncta in an adult (P60) diestrus control (**a**) and a PAMH female mouse (**b**). Points where the vGluT2 signal was considered to be immediately adjacent to the GnRH neuron are indicated by arrowheads. (**b**) Quantification of the number of vGluT2-immunoreactive puncta adjacent to GnRH neuron soma and along the primary GnRH neuronal dendrite is expressed as vGluT2 appositions/µm. The number of vGluT2 appositions/µm is comparable in PAMH/*GnRH-GFP* females (n = 10 neurons from 3 animals) as compared with Control/*GnRH-GFP* females (n = 8 neurons from 3 animals) along the first 30 µm length of the GnRH dendrite (0-30 µm; two-tailed Student's t-test: 15 µm, $t_{(16)}$ = 1.45; P = 0.16; 30 µm, $t_{(16)}$ = 0.09, P = 0.92). Data are represented as mean ± s.e.m.

SUPPLEMENTARY FIGURE 7

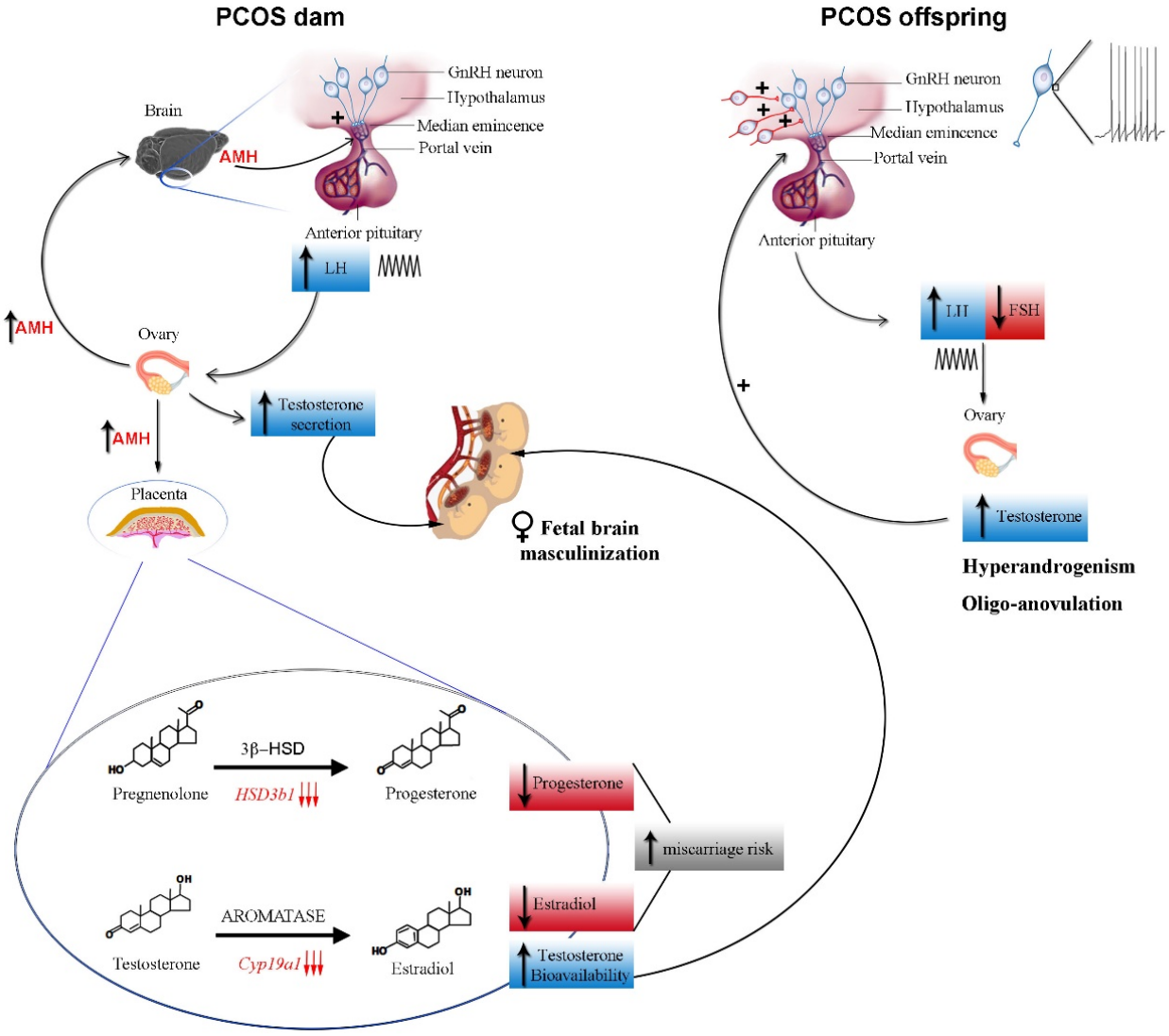

Supplementary Figure 7. Schematic representation of the proposed mechanism of action of AMH in the prenatal programming of PCOS.

Prenatal exposure to elevated AMH levels (left panel) leads to increased GnRH/LH pulsatility in dams, driving gestational steroidogenesis and hyperandrogenism. The maternal androgenization is further exacerbated by inhibition of aromatase expression in the placenta leading to an increase in testosterone bioavailability. The AMH-dependent inhibition of placental *HSD3b1* expression is followed by a significant reduction in circulating progesterone levels, which together with the reduction in E2 concentration, might be associated to an increased risk of miscarriage due to placental insufficiency and to an impaired progesterone negative feedback on LH secretion. The

elevated levels of T trigger a cascade of events in the offspring, which converge into the masculinization of the brain sexually dimorphic nuclei and altered hypothalamic wiring. In adult female PCOS offspring, the increase in excitatory synaptic input to GnRH drives a persistent rise in the GnRH neuronal firing activity. Finally, the constitutive hyperactivity of GnRH neurons stimulates ovarian androgen production and impairs folliculogenesis and ovulation, contributing to the vicious circle of PCOS.

References

Abbott, D. H., L. E. Nicol, J. E. Levine, N. Xu, M. O. Goodarzi and D. A. Dumesic (2013). "Nonhuman primate models of polycystic ovary syndrome." Mol Cell Endocrinol **373**(1-2): 21-28.

Abbott, D. H., B. H. Rayome, D. A. Dumesic, K. C. Lewis, A. K. Edwards, K. Wallen, M. E. Wilson, S. E. Appt and J. E. Levine (2017). "Clustering of PCOS-like traits in naturally hyperandrogenic female rhesus monkeys." Hum Reprod **32**(4): 923-936.

Azziz, R. (2016). "Introduction: Determinants of polycystic ovary syndrome." Fertil Steril **106**(1): 4-5.

Chang, R. J. (2007). "The reproductive phenotype in polycystic ovary syndrome." Nat Clin Pract Endocrinol Metab **3**(10): 688-695.

Chang, R. J., F. P. Mandel, J. K. Lu and H. L. Judd (1982). "Enhanced disparity of gonadotropin secretion by estrone in women with polycystic ovarian disease." J Clin Endocrinol Metab **54**(3): 490-494.

Cimino, I., F. Casoni, X. Liu, A. Messina, J. Parkash, S. P. Jamin, S. Catteau-Jonard, F. Collier, M. Baroncini, D. Dewailly, P. Pigny, M. Prescott, R. Campbell, A. E. Herbison, V. Prevot and P. Giacobini (2016). "Novel role for anti-Mullerian hormone in the regulation of GnRH neuron excitability and hormone secretion." Nat Commun **7**: 10055.

Clarkson, J. and A. E. Herbison (2006). "Postnatal development of kisspeptin neurons in mouse hypothalamus; sexual dimorphism and projections to gonadotropin-releasing hormone neurons." Endocrinology **147**(12): 5817-5825.

Cook, C. L., Y. Siow, A. G. Brenner and M. E. Fallat (2002). "Relationship between serum mullerian-inhibiting substance and other reproductive hormones in untreated women with polycystic ovary syndrome and normal women." Fertil Steril **77**(1): 141-146.

Corbier, P., D. A. Edwards and J. Roffi (1992). "The neonatal testosterone surge: a comparative study." Arch Int Physiol Biochim Biophys **100**(2): 127-131.

De Vries, G. J. and G. C. Panzica (2006). "Sexual differentiation of central vasopressin and vasotocin systems in vertebrates: different mechanisms, similar endpoints." Neuroscience **138**(3): 947-955.

DeFazio, R. A. and S. M. Moenter (2002). "Estradiol feedback alters potassium currents and firing properties of gonadotropin-releasing hormone neurons." Mol Endocrinol **16**(10): 2255-2265.

di Clemente, N., S. P. Jamin, A. Lugovskoy, P. Carmillo, C. Ehrenfels, J. Y. Picard, A. Whitty, N. Josso, R. B. Pepinsky and R. L. Cate (2010). "Processing of anti-mullerian hormone regulates receptor activation by a mechanism distinct from TGF-beta." Mol Endocrinol **24**(11): 2193-2206.

Duijkers, I. J., C. Klipping, W. N. Willemsen, D. Krone, E. Schneider, G. Niebch and R. Hermann (1998). "Single and multiple dose pharmacokinetics and pharmacodynamics of the gonadotrophin-releasing hormone antagonist Cetrorelix in healthy female volunteers." Hum Reprod **13**(9): 2392-2398.

Dumesic, D. A., A. L. Akopians, V. K. Madrigal, E. Ramirez, D. J. Margolis, M. K. Sarma, A. M. Thomas, T. R. Grogan, R. Haykal, T. A. Schooler, B. L. Okeya, D. H. Abbott and G. D. Chazenbalk (2016).

"Hyperandrogenism Accompanies Increased Intra-Abdominal Fat Storage in Normal Weight Polycystic Ovary Syndrome Women." J Clin Endocrinol Metab **101**(11): 4178-4188.

Dumesic, D. A. and R. A. Lobo (2013). "Cancer risk and PCOS." Steroids **78**(8): 782-785.

Ezeh, U., B. O. Yildiz and R. Azziz (2013). "Referral bias in defining the phenotype and prevalence of obesity in polycystic ovary syndrome." J Clin Endocrinol Metab **98**(6): E1088-1096.

Goodarzi, M. O., D. A. Dumesic, G. Chazenbalk and R. Azziz (2011). "Polycystic ovary syndrome: etiology, pathogenesis and diagnosis." Nat Rev Endocrinol **7**(4): 219-231.

Halmos, G., A. V. Schally, J. Pinski, M. Vadillo-Buenfil and K. Groot (1996). "Down-regulation of pituitary receptors for luteinizing hormone-releasing hormone (LH-RH) in rats by LH-RH antagonist Cetrorelix." Proc Natl Acad Sci U S A **93**(6): 2398-2402.

Herbison, A. E. (2016). "Control of puberty onset and fertility by gonadotropin-releasing hormone neurons." Nat Rev Endocrinol **12**(8): 452-466.

Herbison, A. E. and S. M. Moenter (2011). "Depolarising and hyperpolarising actions of GABA(A) receptor activation on gonadotrophin-releasing hormone neurones: towards an emerging consensus." J Neuroendocrinol **23**(7): 557-569.

Herde, M. K., K. Geist, R. E. Campbell and A. E. Herbison (2011). "Gonadotropin-releasing hormone neurons extend complex highly branched dendritic trees outside the blood-brain barrier." Endocrinology **152**(10): 3832-3841.

Huang, C. C., Y. J. Tien, M. J. Chen, C. H. Chen, H. N. Ho and Y. S. Yang (2015). "Symptom patterns and phenotypic subgrouping of women with polycystic ovary syndrome: association between endocrine characteristics and metabolic aberrations." Hum Reprod **30**(4): 937-946.

Huang, X. and R. E. Harlan (1993). "Absence of androgen receptors in LHRH immunoreactive neurons." Brain Res **624**(1-2): 309-311.

Jayasena, C. N. and S. Franks (2014). "The management of patients with polycystic ovary syndrome." Nat Rev Endocrinol **10**(10): 624-636.

Katulski, K., A. Czyzyk, A. Podfigurna-Stopa, A. R. Genazzani and B. Meczekalski (2015). "Pregnancy complications in polycystic ovary syndrome patients." Gynecol Endocrinol **31**(2): 87-91.

Koninger, A., A. Kauth, B. Schmidt, M. Schmidt, G. Yerlikaya, S. Kasimir-Bauer, R. Kimmig and C. Birdir (2013). "Anti-Mullerian-hormone levels during pregnancy and postpartum." Reprod Biol Endocrinol **11**: 60.

La Marca, A., S. Giulini, R. Orvieto, V. De Leo and A. Volpe (2005). "Anti-Mullerian hormone concentrations in maternal serum during pregnancy." Hum Reprod **20**(6): 1569-1572.

Lenz, K. M. and M. M. McCarthy (2010). "Organized for sex - steroid hormones and the developing hypothalamus." Eur J Neurosci **32**(12): 2096-2104.

Lizneva, D., R. Kirubakaran, K. Mykhalchenko, L. Suturina, G. Chernukha, M. P. Diamond and R. Azziz (2016). "Phenotypes and body mass in women with polycystic ovary syndrome identified in referral versus unselected populations: systematic review and meta-analysis." Fertil Steril **106**(6): 1510-1520 e1512.

MacLaughlin, D. T., P. L. Hudson, A. L. Graciano, M. K. Kenneally, R. C. Ragin, T. F. Manganaro and P. K. Donahoe (1992). "Mullerian duct regression and antiproliferative bioactivities of mullerian inhibiting substance reside in its carboxy-terminal domain." Endocrinology **131**(1): 291-296.

Maliqueo, M., H. E. Lara, F. Sanchez, B. Echiburu, N. Crisosto and T. Sir-Petermann (2013). "Placental steroidogenesis in pregnant women with polycystic ovary syndrome." Eur J Obstet Gynecol Reprod Biol **166**(2): 151-155.

Maliqueo, M., I. Sundstrom Poromaa, E. Vanky, R. Fornes, A. Benrick, H. Akerud, S. Stridsklev, F. Labrie, T. Jansson and E. Stener-Victorin (2015). "Placental STAT3 signaling is activated in women with polycystic ovary syndrome." Hum Reprod **30**(3): 692-700.

March, W. A., V. M. Moore, K. J. Willson, D. I. Phillips, R. J. Norman and M. J. Davies (2010). "The prevalence of polycystic ovary syndrome in a community sample assessed under contrasting diagnostic criteria." Hum Reprod **25**(2): 544-551.

McAllister, J. M., R. S. Legro, B. P. Modi and J. F. Strauss, 3rd (2015). "Functional genomics of PCOS: from GWAS to molecular mechanisms." Trends Endocrinol Metab **26**(3): 118-124.

McCarthy, M. M., A. P. Arnold, G. F. Ball, J. D. Blaustein and G. J. De Vries (2012). "Sex differences in the brain: the not so inconvenient truth." J Neurosci **32**(7): 2241-2247.

Moore, A. M. and R. E. Campbell (2017). "Polycystic ovary syndrome: Understanding the role of the brain." Front Neuroendocrinol.

Moore, A. M., M. Prescott and R. E. Campbell (2013). "Estradiol negative and positive feedback in a prenatal androgen-induced mouse model of polycystic ovarian syndrome." Endocrinology **154**(2): 796-806.

Moore, A. M., M. Prescott, C. J. Marshall, S. H. Yip and R. E. Campbell (2015). "Enhancement of a robust arcuate GABAergic input to gonadotropin-releasing hormone neurons in a model of polycystic ovarian syndrome." Proc Natl Acad Sci U S A **112**(2): 596-601.

Norman, R. J., D. Dewailly, R. S. Legro and T. E. Hickey (2007). "Polycystic ovary syndrome." Lancet **370**(9588): 685-697.

Novembri, R., L. Funghi, C. Voltolini, G. Belmonte, S. Vannuccini, M. Torricelli and F. Petraglia (2015). "Placenta expresses anti-Mullerian hormone and its receptor: Sex-related difference in fetal membranes." Placenta **36**(7): 731-737.

Orvis, G. D. and R. R. Behringer (2007). "Cellular mechanisms of Mullerian duct formation in the mouse." Dev Biol **306**(2): 493-504.

Pankhurst, M. W., Y. H. Chong and I. S. McLennan (2016). "Relative levels of the proprotein and cleavage-activated form of circulating human anti-Mullerian hormone are sexually dimorphic and variable during the life cycle." Physiol Rep **4**(9).

Pankhurst, M. W. and I. S. McLennan (2013). "Human blood contains both the uncleaved precursor of anti-Mullerian hormone and a complex of the NH2- and COOH-terminal peptides." Am J Physiol Endocrinol Metab **305**(10): E1241-1247.

Pastor, C. L., M. L. Griffin-Korf, J. A. Aloi, W. S. Evans and J. C. Marshall (1998). "Polycystic ovary syndrome: evidence for reduced sensitivity of the gonadotropin-releasing hormone pulse generator to inhibition by estradiol and progesterone." J Clin Endocrinol Metab **83**(2): 582-590.

Pellatt, L., L. Hanna, M. Brincat, R. Galea, H. Brain, S. Whitehead and H. Mason (2007). "Granulosa cell production of anti-Mullerian hormone is increased in polycystic ovaries." J Clin Endocrinol Metab **92**(1): 240-245.

Pigny, P., S. Jonard, Y. Robert and D. Dewailly (2006). "Serum anti-Mullerian hormone as a surrogate for antral follicle count for definition of the polycystic ovary syndrome." J Clin Endocrinol Metab **91**(3): 941-945.

Pigny, P., E. Merlen, Y. Robert, C. Cortet-Rudelli, C. Decanter, S. Jonard and D. Dewailly (2003). "Elevated serum level of anti-mullerian hormone in patients with polycystic ovary syndrome: relationship to the ovarian follicle excess and to the follicular arrest." J Clin Endocrinol Metab **88**(12): 5957-5962.

Piltonen, T., L. Morin-Papunen, R. Koivunen, A. Perheentupa, A. Ruokonen and J. S. Tapanainen (2005). "Serum anti-Mullerian hormone levels remain high until late reproductive age and decrease during metformin therapy in women with polycystic ovary syndrome." Hum Reprod **20**(7): 1820-1826.

Pinski, J., N. Lamharzi, G. Halmos, K. Groot, A. Jungwirth, M. Vadillo-Buenfil, S. S. Kakar and A. V. Schally (1996). "Chronic administration of the luteinizing hormone-releasing hormone (LHRH) antagonist cetrorelix decreases gonadotrope responsiveness and pituitary LHRH receptor messenger ribonucleic acid levels in rats." Endocrinology **137**(8): 3430-3436.

Ragin, R. C., P. K. Donahoe, M. K. Kenneally, M. F. Ahmad and D. T. MacLaughlin (1992). "Human mullerian inhibiting substance: enhanced purification imparts biochemical stability and restores antiproliferative effects." Protein Expr Purif **3**(3): 236-245.

Rebar, R., H. L. Judd, S. S. Yen, J. Rakoff, G. Vandenberg and F. Naftolin (1976). "Characterization of the inappropriate gonadotropin secretion in polycystic ovary syndrome." J Clin Invest **57**(5): 1320-1329.

Roland, A. V. and S. M. Moenter (2014). "Reproductive neuroendocrine dysfunction in polycystic ovary syndrome: Insight from animal models." Front Neuroendocrinol.

Roland, A. V., C. S. Nunemaker, S. R. Keller and S. M. Moenter (2010). "Prenatal androgen exposure programs metabolic dysfunction in female mice." J Endocrinol **207**(2): 213-223.

Schaeffer, M., F. Langlet, C. Lafont, F. Molino, D. J. Hodson, T. Roux, L. Lamarque, P. Verdie, E. Bourrier, B. Dehouck, J. L. Baneres, J. Martinez, P. F. Mery, J. Marie, E. Trinquet, J. A. Fehrentz, V. Prevot and P. Mollard (2013). "Rapid sensing of circulating ghrelin by hypothalamic appetite-modifying neurons." Proc Natl Acad Sci U S A **110**(4): 1512-1517.

Simerly, R. B. (1989). "Hormonal control of the development and regulation of tyrosine hydroxylase expression within a sexually dimorphic population of dopaminergic cells in the hypothalamus." Brain Res Mol Brain Res **6**(4): 297-310.

Simerly, R. B. (2002). "Wired for reproduction: organization and development of sexually dimorphic circuits in the mammalian forebrain." Annu Rev Neurosci **25**: 507-536.

Sir-Petermann, T., M. Maliqueo, B. Angel, H. E. Lara, F. Perez-Bravo and S. E. Recabarren (2002). "Maternal serum androgens in pregnant women with polycystic ovarian syndrome: possible implications in prenatal androgenization." Hum Reprod **17**(10): 2573-2579.

Sir-Petermann, T., M. Maliqueo, E. Codner, B. Echiburu, N. Crisosto, V. Perez, F. Perez-Bravo and F. Cassorla (2007). "Early metabolic derangements in daughters of women with polycystic ovary syndrome." J Clin Endocrinol Metab **92**(12): 4637-4642.

Sullivan, S. D. and S. M. Moenter (2004). "Prenatal androgens alter GABAergic drive to gonadotropin-releasing hormone neurons: implications for a common fertility disorder." Proc Natl Acad Sci U S A **101**(18): 7129-7134.

Wild, R. A., E. Carmina, E. Diamanti-Kandarakis, A. Dokras, H. F. Escobar-Morreale, W. Futterweit, R. Lobo, R. J. Norman, E. Talbott and D. A. Dumesic (2010). "Assessment of cardiovascular risk and prevention of cardiovascular disease in women with the polycystic ovary syndrome: a consensus statement by the Androgen Excess and Polycystic Ovary Syndrome (AE-PCOS) Society." J Clin Endocrinol Metab **95**(5): 2038-2049.

Chapter 6:

Prenatal AMH exposure induces a transgenerational transmission of the PCOS-like phenotype across multiple generations

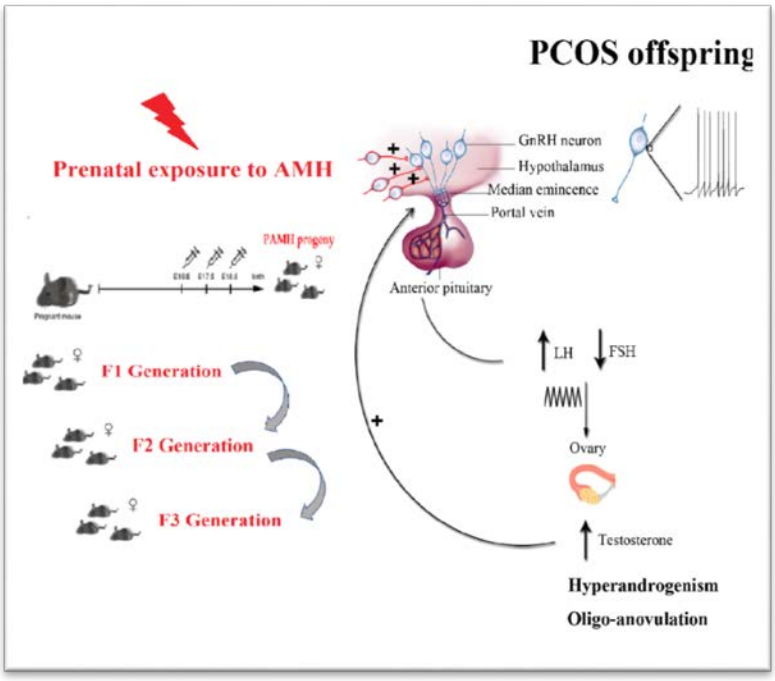

Chapter Six

Prenatal AMH exposure induces a transgenerational transmission of the PCOS-like phenotype across multiple generations

Nour El Houda Mimouni [1,2], Anne-Laure Barbotin [1,3], Isabel Paiva [4], Vincent Prevot [1,2], Anne-Laurence Boutiller[4] and Paolo Giacobini [1,2]

(Mimouni et al, *In preparation*)

1 Jean-Pierre Aubert Research Center (JPArC), Laboratory of Development and Plasticity of the Neuroendocrine Brain, Inserm, UMR-S 1172, Lille, France

2 University of Lille, FHU 1,000 Days for Health, School of Medicine, Lille, France

3 CHU Lille, Institut de Biologie de la Reproduction-Spermiologie-CECOS, Lille, France

4 Laboratory of Cognitive and Adaptive Neuroscience, National Centre for Scientific Research, Strasbourg.

Context

Described in 1935 by Stein and Leventhal, the definition of this syndrome is still at the core of the debate due to its complex clinical manifestations. According to various population studies in conducted in geographically distinct populations, the prevalence of the syndrome is estimated to reach 18% following the Rotterdam criteria (Azziz, Woods et al. 2004),(March, Moore et al. 2010), (Asuncion, Calvo et al. 2000).

Additionally, clinical observations indicate that the risk of developing PCOS rises to 20-40% in first-degree relatives of PCOS women (Kahsar-Miller, Nixon et al. 2001), (Legro, Driscoll et al. 1998, Franks, Webber et al. 2008). However, varying manifestations of reproductive and metabolic are observed in first-degree relatives of PCOS patients (Sir-Petermann, Maliqueo et al. 2002, Sir-Petermann, Ladron de Guevara et al. 2012). One portion of the daughters and sisters of women with PCOS have higher levels of adrenal ovarian androgens from adolescence into adulthood (Yildiz, Yarali et al. 2003, Azziz, Woods et al. 2004). And another portion of female first-degree relatives of PCOS women seem to have a considerable risk of insulin resistance, hyperinsulinemia, type2 diabetes, and/or impaired glucose tolerance (Sir-Petermann, Maliqueo et al. 2002, Kent, Gnatuk et al. 2008). However, less is known about the phenotype of sons of PCOS women, who are exposed during gestation but not systematically investigated in adulthood.

Using our PCOS-like mouse model, this chapter aims to:

- Further explore the role of AMH in the onset of PCOS-like traits in a transgenerational inheritance context.
- Investigate how early exposure to AMH excess would affect the neuroendocrine and reproductive features of the male offspring at birth, puberty and in adulthood.

Results

FIGURE 1

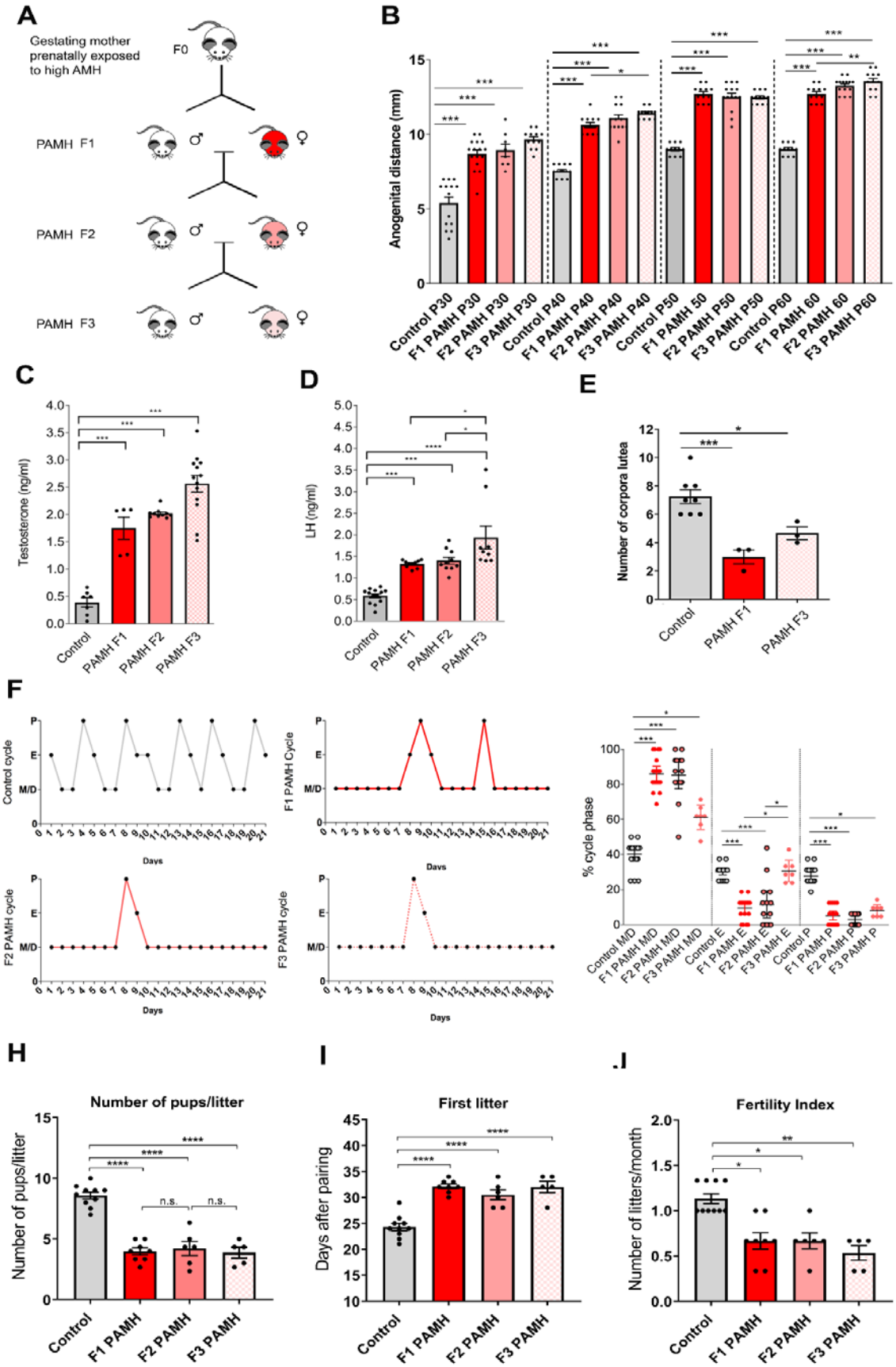

Prenatal AMH exposure induces a transgenerational transmission of the PCOS-like phenotype across multiple generations.

A) Schematic illustration of the mating strategy employed to generate the F1, F2, F3 PAMH progeny. Whereby Pregnant female mice (F0) were treated with PBS (Control) or with the bioactive form of AMH (PAMH:Prenatal AMH treatement), from embryonic day E16.5 to E18.5, to generate the first progeny of (F1) PAMH males and females which were then crossed to produce the second (F2) and third (F3) PAMH generations . F2 and F3 PAMH females were not subjected to further AMH exposures.

(B) Anogenital distance (AGD) was measured over post-natal days (P) 30, 40,50 and 60 in adult control females (n = 11-14), F1 PAMH (n = 12-16), F2 PAMH (n = 7-14), F3 PAMH (n =12). AGD was significantly longer in PAMH females as compared to the control group throughout post-natal development. Comparisons were performed using One-way ANOVA followed and Tukey's multiple comparison *post hoc* test : (**** P < 0.0001, **P30:** F (3, 46) = 36.00; **P40:** F (3, 47) = 112; **P50:** F (3, 45) = 92.88; **P60:** F (3, 45) = 171.8).

(C) Plasma testosterone concentration was measured by ELISA in adult females (P60) in diestrus: Control (n = 7), F1 PAMH (n = 5), F2 PAMH (n = 10) and F3 PAMH (n = 13).

(D) Plasma LH level was measured by sandwich ELISA in (P60-P90) diestrus female offspring: Control (n = 13), F1 PAMH females (n = 10), F2 PAMH females (n = 10), F3 PAMH females (n = 9). comparisons between groups were computed using one-way ANOVA and Tukey's multiple comparison *post hoc* test (**** P < 0.0001, **T:** F (3, 31) = 45.95, **** P < 0.0001, **LH:** F(3,33) = 30.52)

(**E**) Quantification of the number of corpora lutea (CL) in the ovaries of adult diestrus female mice: Control (n = 4), F1 PAMH (n = 4) and F3 PAMH (n=3). Data are represented as mean ± s.e.m. comparisons between groups were computed using one-way ANOVA and Tukey's multiple comparison *post hoc* test. Both groups of PAMH females from the first and third generation displayed a reduced number of CL as compared to control females (***p= 0.0007; F(2, 11)= 15.03).

(F) Representative estrous cyclicity of 8 mice/treatment group during 16 consecutive days. M/D: Metestrus/Diestrus phase, P: Proestrus, E: Estrus.

(G) Quantitative analysis of ovarian cyclicity in the adult female (P60-P90) offspring mice from control and PAMH mice. Scatter plot representing the percentage (%) of time spent in each estrous cycle respectively in control (*n* = 19), PAMH F1 females (*n* = 11), PAMH F2 females (*n* = 11), PAMH F3 females (*n* = 7), M/D: Metestrus/Diestrus phase, P: Proestrus, E: Estrus. Comparisons between treatment groups were performed using Kruskal-Wallis test followed by Dunn's multiple comparison post *hoc* test: **M/D:** *** $P < 0.0001$; **P:** *** $P < 0.0001$; **E:** *** $P < 0.0001$. The horizontal line in each scatter plot corresponds to the median value. The vertical line represents the 25^{th} – 75^{th} percentile range.

(G-H-I) Fertility tests of adult offspring mice (P90). Inexperienced males and primiparous females, selected from at least three different litters, were used for the 90 days mating protocol test. Control females were paired with control males (*n* = 10), F1 PAMH (1^{st} generation) females were paired with F1 PAMH males (*n* = 8), F2 PAMH (2^{nd} generation) females were paired with F2 PAMH males (*n* = 6), and finally F3 PAMH (3^{rd} generation) females were paired with F3 PAMH males (*n*=5). **(G)** Number of pups/litter **(H)** Time to first litter (number of days to first litter after pairing) **(I)** Fertility index (number of litters per females over 3 months) were quantified per generation and pairing.

PAMH adult female and male mice from all 3 generations showed a persistent impaired fertility as indicated by a significant delay in their first litter, fewer litters and fewer pups per litter produced over a 3-month period. Data are represented as mean ± s.e.m. Statistical analysis was performed using One-way ANOVA and Tukey's multiple comparison *post hoc* test: Time to first litter, $F(_{3,25})=27.97$, ***$P < 0.0001$; Number of pups/litter, $F(_{3,25})= 43.66$ *** $P < 0.0001$; Analysis of fertility index between groups was assessed using Kruskal Wallis followed by Dunn's multiple comparisons post hoc test: ***P= 0.0005.

Prenatal AMH exposure induces a transgenerational transmission of the PCOS-like phenotype towards multiple generations of female progeny

Polycystic ovary syndrome (PCOS) is a heterogeneous disorder characterized by multiple endocrine and metabolic disturbances. It is the leading cause of infertility, characterized by anovulation, cycle disorders, hyperandrogenism and severe hormonal imbalance (March, Moore et al. 2010) (Azziz, Woods et al. 2004, Norman, Dewailly et al. 2007) (Goodarzi, Dumesic et al. 2011) (Dumesic, Oberfield et al. 2015)

In the past decades, several large series of family-based and twin studies have highlighted a strong familiar component in PCOS (Cooper, Spellacy et al. 1968, Hague, Adams et al. 1988, Legro, Driscoll et al. 1998, Rodin, Bano et al. 1998). Thus, only a small portion of candidate genes has been identified by genome-wide association studies (GWAS) and linkage studies (Chen, Zhao et al. 2011) (Franks, Gharani et al. 2001, Dadachanji, Shaikh et al. 2018) suggesting that environmental factors such as high androgen levels during early embryonic life might play role in the onset of the syndrome in the unborn fetus. (Abbott, Barnett et al. 2005, Abbott and Bacha 2013).

Giving the strong heritable characteristics of PCOS, we next sought to investigate if putative long-term consequences of prenatal exposure to excessive AMH levels are transmitted across multiple generations in female mice and would in turn, mirror the transmission of the cardinal neuroendocrine features observed in first degree relatives of PCOS women. In order to further delineate if the elevation of AMH levels observed in women with PCOS during pregnancy could be one of the drivers of the condition and its transmission in the progeny or inversely a consequence of the neuroendocrine disturbances of the syndrome.

In order to test this hypothesis, we treated pregnant females with PBS (Control) or with the bioactive form of AMH (human recombinant AMHC, 0.12 mg/Kg/d; prenatal AMH-treated, PAMH) from embryonic day E16.5 to E18.5, to generate F1 PAMH males and females, that we ultimately crossed to produce the second (F2) and third (F3) PAMH generations. No further AMH exposure for any subsequent generations (F2 and F3 PAMH) was thus employed **(Figure 1A)**.

Hyperandrogenism is a hallmark of the syndrome, along with the disproportionately high LH secretion with relatively constant low FSH secretion observed in PCOS patients (Balen, Conway et al. 1995). This increase is explained by an increased pulse frequency of the hypothalamic gonadotropin-releasing hormone (GnRH) which may favor the production of the β-subunit of LH over the β-subunit

of FSH and/or by increased pituitary sensitivity to GnRH stimulation which results in an elevated LH/FSH ratio increased in more than 75% of PCOS patients (McCartney, Eagleson et al. 2002) (Taylor, McCourt et al. 1997) (Waldstreicher, Santoro et al. 1988).

Interestingly, growing clinical investigations in daughters and first-degree female relatives of PCOS women report clinical and biological signs of hyperandrogenism as well as an increase in LH levels in these patients.

Therefore, we sought to evaluate the androgenic impregnation across the 3 PAMH generations of female offspring by measuring the ano-genital distance (AGD) at postnatal day 30 (P30), (P40), (P50) and (P60) (**Figure 1B**). All of the three PAMH generations studied (F1, F2 and F3) displayed a significantly longer ano-genital distance as compared the control female offspring at the different time points of postnatal development analyzed, indicating a higher androgenic impregnation in these mice.

Subsequently, we uncovered a significant and persistent elevation in both circulating levels of testosterone and LH in the F1, F2 and F3 PAMH females in comparison with the control group. **(Figure 1C, 1D)**

Together, these results suggest that a single intrauterine exposure to elevated AMH levels during embryogenesis could be responsible for the transmission of pcos-like traits of hyperandrogenism and altered LH levels to the subsequent non-exposed generations of PAMH female offsprings.

Several studies have reported that the incidence of oligomenorrhea and PCO is amplified in first-degree relatives of PCOS patients as compared with the controls (Cooper, Spellacy et al. 1968), (Wilroy, Givens et al. 1975, Givens 1988). Another study conducted in a large group of hirsute women with or without oligomenorrhea and their family members, described a higher prevalence of hirsutism, oligomenorrhea and infertility in first degree relatives as compared to controls (Ferriman and Purdie 1979). (Lunde, Magnus et al. 1989).

To evaluate if prenatal AMH treatment would transgenerational alter reproductive phenotype of the PAMH females in a transgenerational manner, we have monitored the estrus cyclicity in the different groups during 16 days and the results confirm that the F1 PAMH females exhibit alterations in estrus cyclicity and ovarian function as previously described in the female PAMH mice (Tata, Mimouni et al. 2018). We thus report for the first time in this study that these alterations are transmitted to the F2 and F3 PAMH females, which also rarely entered the preovulatory stage of the estrous cycle and

displayed prolonged time in metestrus/diestrus as compared to the control female offspring **(Figure 1F)** and dysovulation **(Figure 1G)** as compared to the control littermates. These results are consistent with the analysis of the ovarian histology of the PAMH mice, which revealed a persistent decrease in the number of corpora lutea (CL) in the F1 PAMH and F3 PAMH offspring. **(Figure 1E).**

Finally, using a 90 days fertility test protocol, we meticulously examined the main reproductive characteristics of each group, in other terms: Fertility index (number of litters per month), First litter (days to first litter after pairing) and the number of pups per litter.

A significant fertility impairment was detected in all of the three PAMH generations studied, and was reflected by a longer interval between litters, a reduced number of pups per litter and a diminished fertility index as compared to the control groups **(Figure 1B).** Furthermore, in the F2 and F3 PAMH breedings, we observed a significantly higher impact on fertility parameters of first litter and litter size in comparison to the F1 PAMH breeding, suggesting that a unique exposition to AMH in the late stages of embryonic development induces long term reproductive damage maintained across generations and which could even result in a worsen phenotype than the one observed in the first generation directly exposed to AMH treatment during gestation.

Unexpectedly, the F1 and F3 PAMH males breedings with control females also provoke a likewise decrease in fertility as indicated by a significant delay in their first litter, smaller litters and fewer pups per litter produced over a 3-month period. Suggesting that the prenatal exposition to elevated AMH levels impacts the fertility of the male progeny and this defect is transmitted to the subsequent generations.

Altogether, our results provide compelling evidence that the effects of AMH-dependent developmental programming in early life environment is not only transmitted from parent to offspring but extends to generations beyond.

FIGURE 2

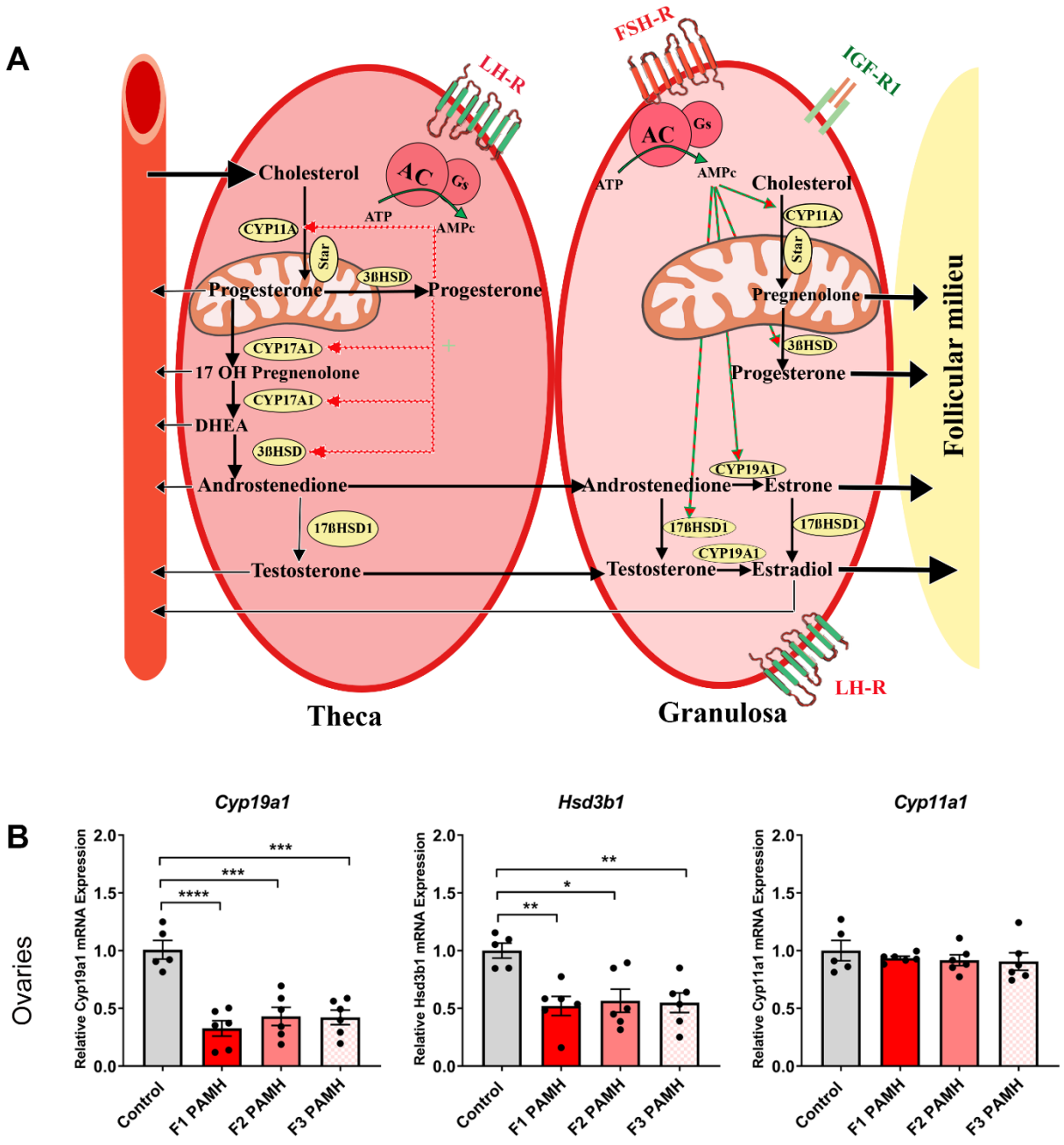
A
LH-R
FSH-R
IGF-R1
AC
Gs
ATP
AMPc
Cholesterol
CYP11A
Star
3ßHSD
Progesterone
CYP17A1
17 OH Pregnenolone
DHEA
Androstenedione
17ßHSD1
Testosterone
Pregnenolone
CYP19A1
Estrone
Estradiol
Follicular milieu
Theca
Granulosa
B
Ovaries
Cyp19a1
Hsd3b1
Cyp11a1
Relative Cyp19a1 mRNA Expression
Relative Hsd3b1 mRNA Expression
Relative Cyp11a1 mRNA Expression
Control
F1 PAMH
F2 PAMH
F3 PAMH

A severe decrease in mRNA expression levels of key genes involved in ovarian steroidogenesis is maintained across the subsequent generations of the PAMH PCOS-like mouse model

(A) Simplified schematic representation of the steroidogenesis in the theca and granulosa cells of the ovary. Steroidogenesis is a multi-step process in which, cholesterol, the main precursor of steroids is ultimately converted into androgens and estrogens. **(StAR)** steroidogenic acute regulatory protein, **(HSD3B1)** hydroxyl-Δ-5-steroid dehydrogenase, 3 β-and steroid Δ-isomerase 1, **(CYP17A1)** cytochrome P450, family 17, subfamily A polypeptide 1, **(CYP11A1)** cytochrome P450, family 11, subfamily A, polypeptide 1, **(CYP19A1)** cytochrome P450, family 19, subfamily A, polypeptide 1a, (**IGF1)** insulin-like growth factor 1**, (LHR)** Luteinizing hormone receptor**, (FSHR)** Follicule stimulating hormone receptor. **(DHEA)** Dehydroepiandrosterone.

(B) Real time PCR analysis of the most relevant steroidogenic markers in the ovaries of adult diestrus females. We extracted mRNA from control ovaries (*n*=5); F1 PAMH(*n*=6); F2 PAMH (*n*=6); F3 PAMH (*n*=6). Quantitative analysis of real time PCR shows that AMH prenatal treatment severely impacts the mRNA expression levels of *Cyp19a1, Hsd3b1* in the ovaries of F1, F2 and F3 PAMH females in comparison with the control ovaries. However, no differences were observed in the mRNA expression levels of *Cyp11a1* between the two groups. Data are represented as mean +/- sem. Differences between groups were assessed using One-way ANOVA and Tukey's multiple comparison *post hoc* test: ***Cyp19a1:*** ****$P < 0.0001$, F (3, 19) = 16.74***; Hsd3b1:*** **P=0.0035, F (3, 19) = 6.424 ***Cyp11a1:*** *P=0.7214, F(3, 19)= 0.4483.*

The most common biochemical abnormality in women with PCOS is excessive production of ovarian androgens. This feature well correlates with the observation that PCOS women exhibit higher ovarian steroidogenic activity than healthy patients (secretion of higher levels of testosterone, androstenedione, of progesterone)(Nelson, Legro et al. 1999, Nelson, Qin et al. 2001).

For this reason, we evaluated the relative expression of the same genes involved in the androgen biosynthetic pathway in the ovaries (Figure 2A) in control and F1, F2, F3 PAMH ovaries. Our results show that there are no changes in the relative expression levels of *Cyp11a1*. Conversely, there is drastic decrease in the relative expression of *Cyp19a1* which is responsible for the conversion of testosterone into Estradiol, and *Hsd3b1* which converts pregnenolone to progesterone. Overall, our findings strengthen the rationale about the role of AMH *in utero* as a trigger of PCOS-like disturbances observed in the adulthood, and most importantly that this could be transmitted to the generations beyond.

FIGURE 3

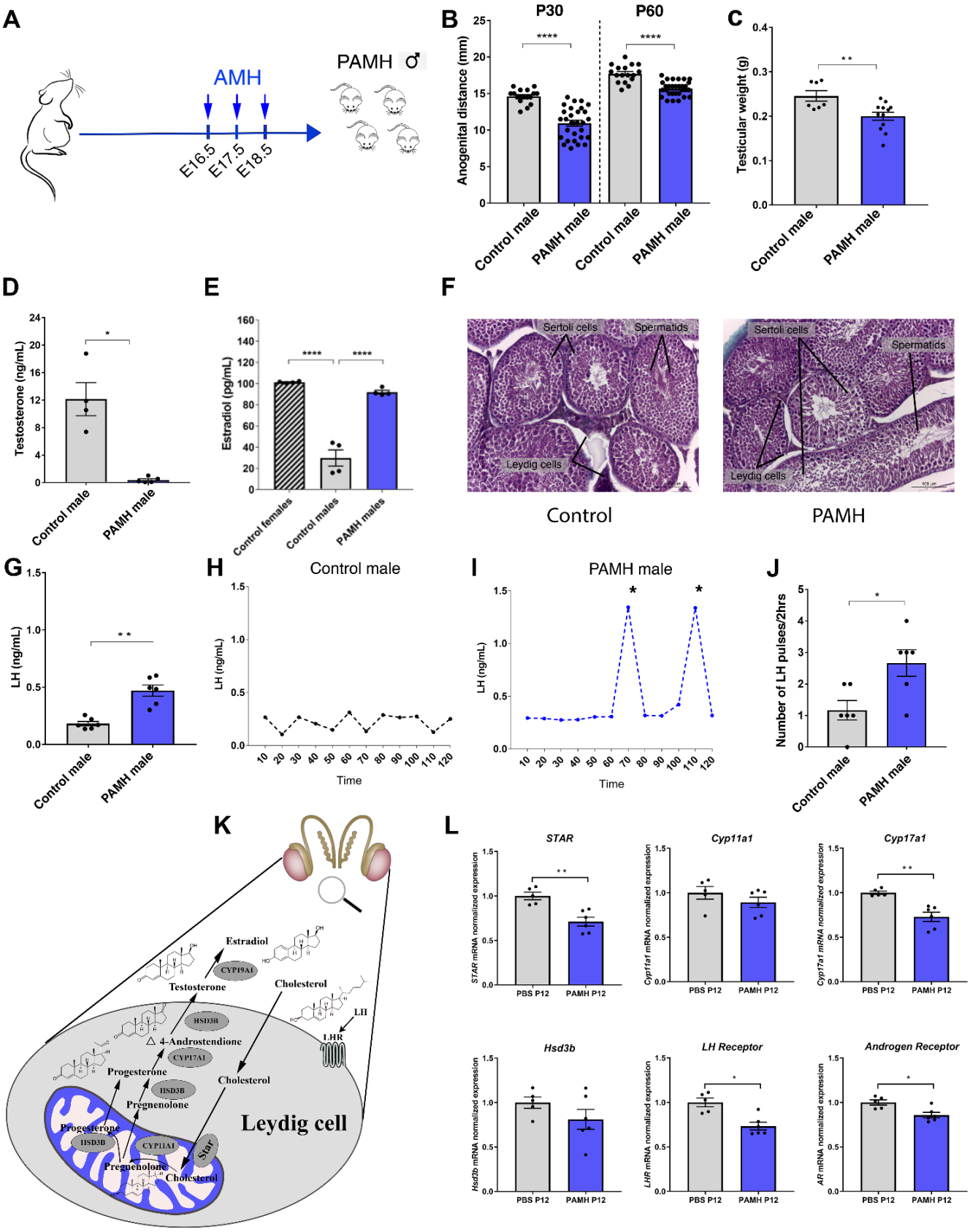
A
AMH
PAMH ♂
E16.5
E17.5
E18.5
B
P30
P60
Anogenital distance (mm)
Control male
PAMH male
C
Testicular weight (g)
D
Testosterone (ng/mL)
E
Estradiol (pg/mL)
Control females
Control males
PAMH males
F
Sertoli cells
Spermatids
Leydig cells
Control
PAMH
G
LH (ng/mL)
H
Control male
Time
I
PAMH male
J
Number of LH pulses/2hrs
K
Estradiol
Testosterone
Cholesterol
LH
LHR
4-Androstendione
Progesterone
Pregnenolone
Leydig cell
CYP19A1
HSD3B
CYP17A1
CYP11A1
Star
L
STAR
Cyp11a1
Cyp17a1
Hsd3b
LH Receptor
Androgen Receptor
PBS P12
PAMH P12

Figure 3: Prenatal exposition to AMH : description of a male phenotype

(A) Schematic of experimental design whereby pregnant dams were subjected to different treatments by intraperitoneal (i.p.) injections during the late gestational period (embryonic days E16.5 - E18.5) to generate the PAMH male progeny. **(B)** Anogenital distance (AGD) was measured over post-natal days (P) 30 and 60 in adult male controls (n = 17), PAMH (n = 30), AGD was significantly shorter in PAMH males (****P < 0.0001) as compared to the control group throughout post-natal development. Comparisons were performed using Mann-Whitney U test. **(C)** Testicular weight was assessed in control adult mice (n=7) and PAMH adult mice (n=12). Comparisons were performed using Mann-Whitney U test. PAMH male mice exhibited a significant decrease in testicular weight and size as compared to control littermates (** P= 0.0098). **(D)** Mean plasma testosterone levels were measured in adult males (P90). Results show that PAMH mice (n = 10) exhibited a drastic decrease (****P < 0.0001) in testosterone levels as compared to control males (n= 8). Comparisons were performed using Mann-Whitney U test.

(E) Mean circulating Estradiol (E2) levels were measured in the three following groups: control males (n=4), control females (n=4) and PAMH males (n=4). Comparisons between groups were assessed using One-way ANOVA and Tukey's multiple comparison *post hoc* test: (****P<0.0001) $F_{(2, 9)}$ = 74.10.

(F) Representative photomicrographs of testes from 4 months -old control and PAMH mice. Testis sections (5 μm thick) were stained with haematoxylin–eosin. In PAMH mice, the testes did not display any major alterations in the histological organization of Sertoli cells, Leydig cells, as compared to control littermates.

(G) Plasma LH level was measured in adult males (P90). Mean circulating LH levels were significantly higher in adult PAMH (n = 6) males as compared to control littermates (n = 6). Comparisons were performed using Mann-Whitney U test (** p=0.0022).

(H-I) Representative graphs for LH pulsatility over 2-hr in one adult control male versus one adult PAMH male. Asterisks indicate the number of LH pulses. **(J)** Number of LH pulses over 2 hours: Tail blood was collected every 10 min for 2 h and LH level measured from 10 a.m-12 p.m in adult male mice (P60) (Control, n = 6; PAMH, n = 6). PAMH male offsprings exhibit an increased LH pulsatility

as compared to the control offsprings. Comparisons were performed using Mann-Whitney *U* test (*p=0.0390).

(K) Simplified schematic representation of the steroidogenesis in the Leydig cells. Steroidogenisis is a multi-step process in which, Cholesterol, the main precursor of steroids is ultimately converted into androgens and estrogens. **(StAR)** steroidogenic acute regulatory protein, **(HSD3B1)** hydroxyl-Δ-5-steroid dehydrogenase, 3 β-and steroid Δ-isomerase 1, **(CYP17A1)** cytochrome P450, family 17, subfamily A polypeptide 1, **(CYP11A1)** cytochrome P450, family 11, subfamily A, polypeptide 1, **(CYP19A1)** cytochrome P450, family 19, subfamily A, polypeptide 1a, (**IGF1)** Luteinizing hormone receptor **(LHR).**

(L) To examine the mRNA expression of steroidogenic markers in male testes during development (*STAR, Cyp17a1, Cyp11a1,HSD3B1) as well as Androgen Receptor and LH receptor*). We extracted mRNA from control testes, *n*=6 and PAMH testes, *n*=6) at post-natal day 12 (P12). Quantitative analysis of relative mRNA expression shows that AMH prenatal treatment severely impacts the mRNA expression levels of *STAR, Cyp17a1, LHR* and *AR* in the testes of PAMH males in comparison with the control offspring. However, no differences were observed in the mRNA expression levels of *Cyp11a1* and *HSD3B1* between the two groups. Data are represented as mean +/- sem. Differences between groups were assessed using Mann Whitney test.

Figure3: Prenatal exposition to AMH : description of a male phenotype

In most PCOS studies, male family members are not systematically characterized, only few attempts were made to identify a male phenotype of boys or men born to PCOS mothers.

One of the few studies describing a male phenotype was conducted by Hague and al. Their work uncovered oligospermia and increased LH secretion in some of the male subjects of the study participants (Hague, Adams et al. 1988), further studies on first degree relatives of PCOS patients revealed an increase in premature baldness in man born to PCOS mothers and male relatives (Ferriman and Purdie 1979), (Lunde, Magnus et al. 1989). However their altered metabolic phenotype has been reported in many investigations (Yildiz, Yarali et al. 2003, Sam, Coviello et al. 2008).

In this novel study we aimed at characterizing the male equivalent of PCOS-like progeny exposed to prenatal AMH treatment.

For this purpose, we treated pregnant females with PBS (Control) or with the bioactive form of AMH (human recombinant AMHC, 0.12 mg/Kg/d; prenatal AMH-treated, PAMH) at the end of gestation and studied the neuroendocrine reproductive features of the male offspring at birth, puberty and in adulthood **(Figure 3A).** To exclude any morphogenetic effects that exogenous AMH could have, we treated the pregnant females during this specific temporal window because it lies beyond the developmental stages during which gonadal and genital tract differentiation takes place in mice (E12.5-E14.5).

We first evaluated the androgenic impregnation in these mice by measuring the ano-genital distance (AGD) from postnatal day 30 (P30) to (P60) (**Figure 3B**). The PAMH male offspring displayed a significantly shorter ano-genital distance as compared the control male offspring, implying that testosterone levels could be altered in our mice model.

We then assessed the histological and ponderal features of testes in adult mice **(Figures 3C, 3F)**. Histological analysis of testes did not uncover any major alterations in the histological organization of Sertoli and Leydig cells, between control and PAMH testes **(Figure 3F)**. further exploration of the size and distribution is currently conducted. However the evaluation of testicular weight, revealed a significant decrease in the testicular weight in PAMH mice in comparison with control males. **(Figure 3C)**. It has been reported in the literature, that significant positive associations between measures of testes size and T levels exist in different species (Uglem, Mayer et al. 2002, Garamszegi, Eens et al. 2005, Preston, Stevenson et al. 2012) and that prenatal androgenization alters the testicular development (Connolly, Rae et al. 2013)

To confirm this, we measured circulating testosterone levels in the control mice and PAMH mice which were exposed to maternal hyperandrogenism and uncovered a drastic decrease in the hormonal levels of testosterone as compared to their control littermates. **(Figure 2C).**

Moreover, pulsatile GnRH, released into hypophyseal portal blood, induces LH and FSH production which drive pulsatile T secretion by Leydig cells into the spermatic vein ((Santen 1975). Since circulating T levels appeared to be significantly low in PAMH mice, we next sought to investigate whether, the male progeny embryonically exposed to AMH, would exhibit an altered GnRH neuronal

secretion, we thus assessed LH secretion as an indirect measurement of GnRH secretion, **(Figure 3G**). Surprisingly, PAMH males exhibit significantly higher LH levels as compared to control males.

We thenceforth evaluated LH pulsatility by serial blood sampling in **(Figure 3H, 3I, 3J)** which revealed that PAMH animals had a significantly higher LH pulse frequency as compared to control males, which physiologically (in control animals) exhibit a diminish number of LH pulses.

T and Estradiol (E2) are known to act as feedback signals, E2 excerces a negative action at the central level by its inhibitory action on LH and FSH gonadotropin secretion. Therefore, Estradiol levels were also investigated in these mice and found to be higher in PAMH males as compared to control males, similar to the E2 levels displayed in control females. **(Figure 3E)**.

In males, both T and E2 are secreted in the Leydig cells of testes during steroidogenesis, which is a multi-step process in which cholesterol is converted to androgens and estrogens. The enzymes controlling this process are several specific cytochrome P450 enzymes (CYPs), hydroxysteroid dehydrogenases (HSDs). Cholesterol is transported to the mitochondria by an LH-dependent mechanism regulated by a transfer protein called steroidogenesis activator protein (StAR), whose essential role represents a limiting step of steroidogenesis (Miller 1988, Stocco 2001). Once cholesterol penetrates the mitochondria, it is converted to pregnenolone by the cytochrome P450 scc (side-chain cleavage), also called CYP11A1, when pregnenolone leaves the mitochondria it becomes the substrate for cytochrome P450c17 (Cyp17a1) which has two activities: converting the pregnenolone and progesterone to 17α-hydroxy pregnenolone and 17α - hydroxyprogesterone, respectively, and transforming 17α-hydroxypregnenolone to dehydroepiandrosterone (DHEA) or 17α -hydroxyprogesterone to androstenedione. The last step is accomplished by the aromatase CYP19a1 by converting testosterone into estradiol **(Figure 3K).**

In this study, we investigated the origin of the decline in testosterone levels observed in PAMH males, by analyzing mRNA expression levels in the testes of control and PAMH male at post-natal day 12 (P12) early life development. Hence, we report a considerable decrease in the mRNA expression of the main enzymes involved in steroidogenic (*Cyp19a1*, *StAR*, *Cyp17a1*) as well as *LH receptor* in the testes of PAMH mice in comparison with control. **(Figure 3L).** In contrast, no differences were perceived in the mRNA expression levels of *Cyp11a1* and *HSD3B1*. This reduced steroidogenic activity could explain the decrease in testosterone levels observed in adulthood in these mice.

FIGURE 4

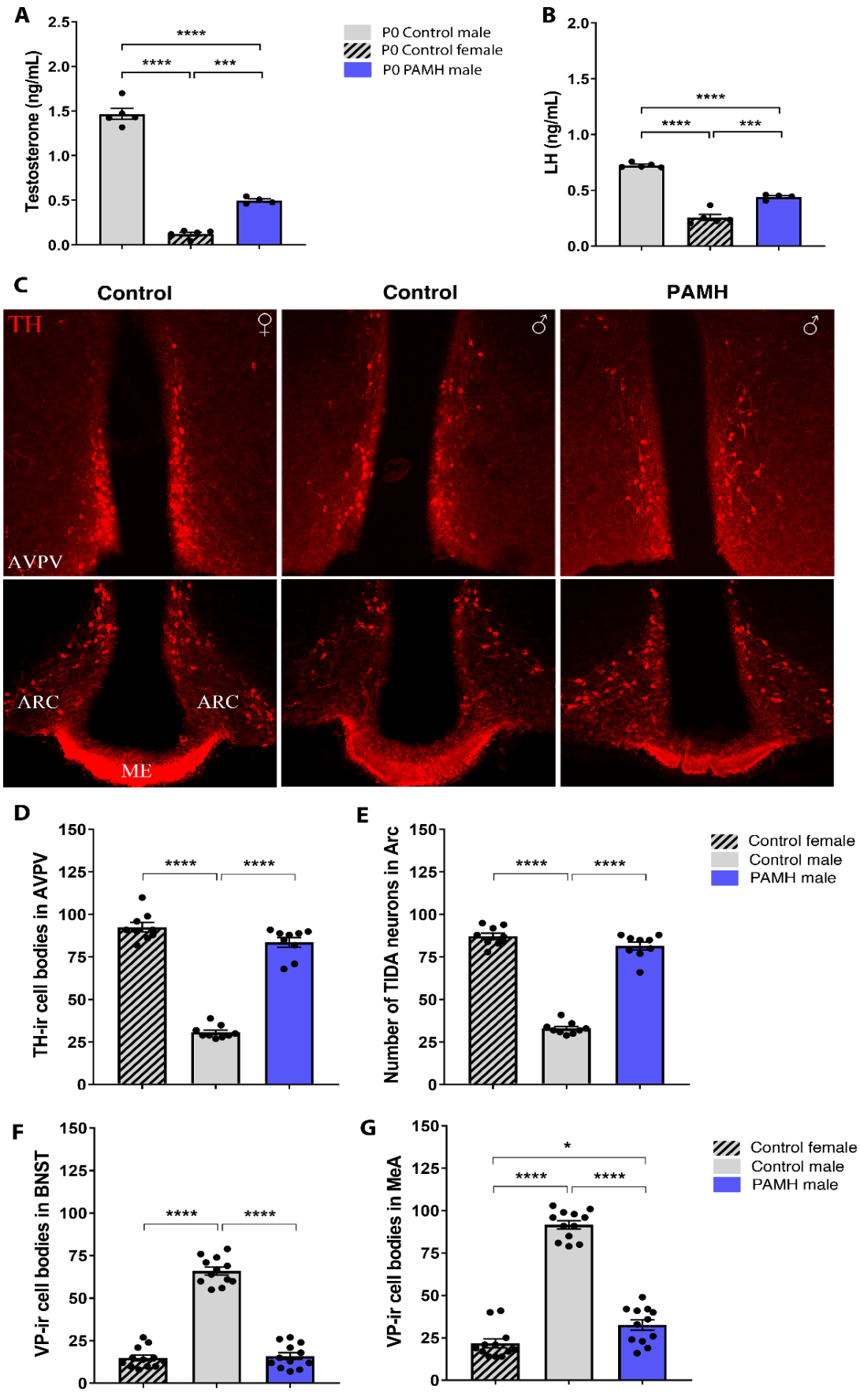
A
Testosterone (ng/mL)
2.5
2.0
1.5
1.0
0.5
0.0
****
****
***
P0 Control male
P0 Control female
P0 PAMH male
B
LH (ng/mL)
2.0
1.5
1.0
0.5
0.0
****
****
***
C
Control
Control
PAMH
TH
♀
♂
♂
AVPV
ARC
ARC
ME
D
TH-ir cell bodies in AVPV
150
125
100
75
50
25
0
****
****
E
Number of TIDA neurons in Arc
150
125
100
75
50
25
0
****
****
Control female
Control male
PAMH male
F
VP-ir cell bodies in BNST
150
125
100
75
50
25
0
****
****
G
VP-ir cell bodies in MeA
150
125
100
75
50
25
0
*
****
****
Control female
Control male
PAMH male

Figure 4: PAMH male offspring exhibit a feminization of the brain.

(**A-B**) Plasma T and LH levels were measured in pups 2 hours after birth (Control males, *n* = 4; control females, *n* = 5; PAMH males, *n* = 5). Statistics were computed with One-way ANOVA and Tukey's multiple comparison *post hoc* test: **Testosterone**: $F_{(2, 11)}$ =283.5, ***P < 0.0001; **LH:** $F_{(2, 11)}$ = 153.2, ***P < 0.0001. (**C**) Photomicrographs of TH-immunoreactive neurons in the anteroventral periventricular nucleus (AVPV) and arcuate nucleus (ARC) of a control male, control female and PAMH male at P60. ME: Median Eminence **(D)** TH immunoreactive (-ir) neurons in the AVPV were quantified in these animal groups (*n* = 9 per sex and treatment). The number of AVPV TH-ir neurons are represented as the mean ± s.e.m. One-way ANOVA and Tukey's multiple comparisons *post-hoc* test, $F_{(2,24)}$ = 193.1, ***P < 0.0001. **(E)** Quantification of the tuberoinfundibular dopaminergic (TIDA) immunoreactive neurons in the ARC; (*n* = 9 per sex and treatment). Data are represented as the mean ± s.e.m. One-way ANOVA and Tukey's multiple comparisons *post-hoc* test: $F_{(2,24)}$ = 252.5 ; ***P < 0.0001. (**F-G**) Quantification of the VP-immunoreactive neurons in the bed nucleus of the stria terminalis (BNST) and medial amygdala (MeA) of a male, control female and PAMH male at P60. (*n* = 12 per sex and treatment). Data are represented as the mean ± s.e.m. One-way ANOVA and Tukey's multiple comparisons *post-hoc* test: BNST, $F_{(2,33)}$ = 185.8 ; MeA, $F_{(2,33)}$ = 205.8,* P < 0.05, ***P < 0.0001.

PAMH male offspring exhibit a feminization of the brain.

Prenatal life, early childhood and adolescence are critical periods marked by the influence of environmental factors in mammals. During these phases of development, the brain undergoes significant growth and remodeling, and is particularly vulnerable to external signals. During this temporal window of embryonic development, under the action of the gonadal steroids, the brain irreversibly engages in a differentiation path of the male or female direction.

The neonatal testosterone surge is responsible for establishing brain sexual dimorphisms that underpin sexually dimorphic physiology and behavior (Clarkson and Herbison 2016) (Simerly 2002, McCarthy, Arnold et al. 2012). The masculinizing and defeminizing effects of testosterone are mainly mediated by its metabolite, estradiol, (McCarthy 2008), tthrough the aromatization of testosterone by the enzyme P450 aromatase (CYP19A1).

We thus, analyzed whether the late gestational, AMH-dependent maternal hyperandrogenism previously described (Tata, Mimouni et al. 2018) might interfere with the appropriate establishment of brain sexual dimorphism in the male offspring.

In most vertebrates, gonadal T secretion occurs in a sexually dimorphic pattern during the first hours following birth (0-4 hours at P0), being elevated in newborn males but not in females (Corbier, Edwards et al. 1992). We therefore measured T levels 2 hours post-partum in control males and females as well as in PAMH male pups. We report that PAMH adult male failed to engage the testosterone surge at birth observed in control newborns **(Figure 4A)**. Interestingly, as stated above **(Figure 3D)**, the levels of testosterone remain dramatically low in PAMH males as compared to the control group, when measured in adulthood.

Few hours after the testosterone surge, most studies indicate the existence of an LH surge shortly after T in males. Remarkably PAMH male mice display no evidence of a neonatal LH surge, and their LH levels mirror the levels observed in control females rather than the ones detected in control males **(Figure 4B).**

Furthermore, using immunohistochemistry we labeled some of the main sexually dimorphic neuronal populations in rodents' brains. **(Figure 4C)** The evaluation of sexually dimorphic areas of the brains of control males and females and PAMH males allowed us to uncover a feminization of the brains of PAMH mice, this has been confirmed by quantitative analysis of immunoreactive sexually dimorphic neurons (Vasopressin, Tyrosine Hydroxylase and TIDA neurons), these mentionned neuronal populations were quantified in every group and the results show that the number of Immunoreactive neurons is closer in numbers to the one observed in control female brains than in males. **(Figure 4D, 4E, 4F, 4J).** Suggesting that the exposition to elevated levels of AMH during embryogenesis has a feminizing effect on male offspring and conversely, this same prenatal exposition induces a masculinization of the fetal brain of female offspring.

FIGURE 5

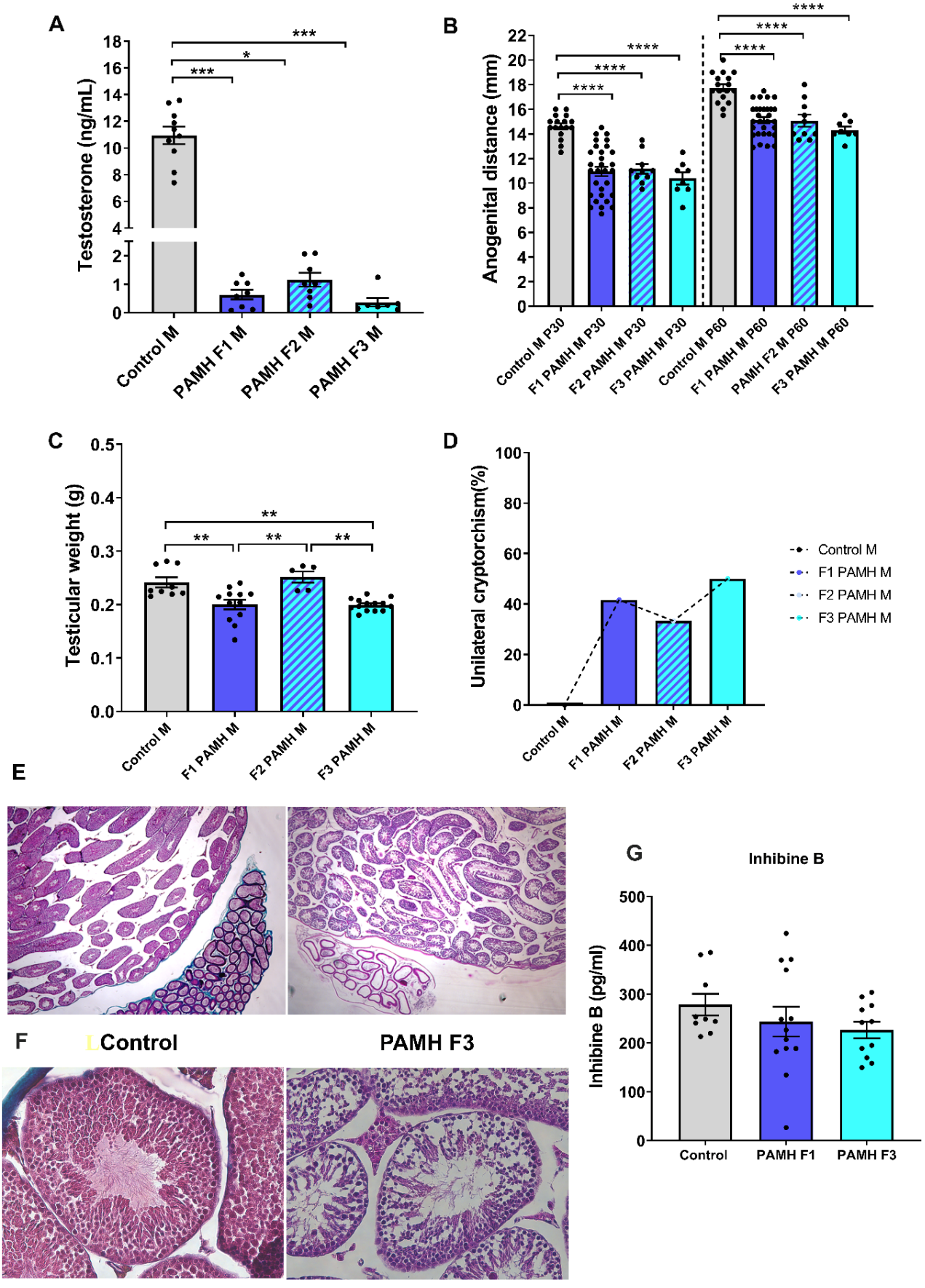
A
Testosterone (ng/mL)
Control M
PAMH F1 M
PAMH F2 M
PAMH F3 M
B
Anogenital distance (mm)
Control M P30
F1 PAMH M P30
F2 PAMH M P30
F3 PAMH M P30
Control M P60
F1 PAMH M P60
PAMH F2 M P60
F3 PAMH M P60
C
Testicular weight (g)
Control M
F1 PAMH M
F2 PAMH M
F3 PAMH M
D
Unilateral cryptorchism(%)
Control M
F1 PAMH M
F2 PAMH M
F3 PAMH M
E
F
Control
PAMH F3
G
Inhibine B
Inhibine B (pg/ml)
Control
PAMH F1
PAMH F3

Figure 5: PAMH males exhibit a drastic decrease in testosterone levels and testicular weight, an altered testicular histology, and high prevalence of cryptorchidism which are maintained across 3 generations.

(A) Mean testosterone levels in adult mice P90 over 3 generations. Here we assessed the reproductive phenotype in control male mice (*n*=10) and in 3 subsequent generations of PAMH mice (F1 *n*= 10; F2 *n*= 10; F3 *n*= 8). Data are represented as mean +/- sem. Our results show that the testosterone levels remain considerably low in adulthood (***$P < 0.0001$).

(B) Agnogenital distance (AGD) was measured in adult mice at P30 and P60 (Controls, *n*=17; PAMH F1, *n*= 30; PAMH F2 *n*= 10; PAMH F3 *n*= 8). We demonstrate that the AGD is significantly shorter in the PAMH male mice as compared to the controls. Data were analyzed using One-way ANOVA followed by Tukey's multiple post *hoc* tests. Results are represented as mean values. (P30: ***$P < 0.0001$; $F(3, 61) = 21.17$; P60: ***$P < 0.0001$; $F(3, 61) = 20.10$).

(C) Testicular weight was evaluated in control adult male mice (*n*= 9) as well as in the F1 (*n*= 12), F2 (*n*= 5), F3 (*n*= 15) PAMH male mice. Comparisons were computed using One-way ANOVA followed by Tukey's multiple post *hoc* test. ***$P < 0.0001$; $F(3, 36) = 10.80$.

(D) Percentage of cryptorchidism observed in each group. The cryptorchidism was recorded when one of the testes showed aberrant upper position in every animal. The percentage of cryptorchidism was calculated for each group using the following formula: Total number of analyzed mice / the number of mice who displayed cryptorchidism) X 100). PAMH male mice displayed strikingly high prevalence of cryptorchidism as compared to controls, suggestive of a defective testicular migration.

(E-F) Representative photomicrographs of testes from 4 month-old control and PAMH F3 mice. at 10X and 20X magnification, respectively. Testis sections (5 μm thick) were stained with haematoxylin–eosin. Testis from PAMH mice exhibit an altered histological distribution as indicated by the Sertoli and leydig cell distribution, along with a decrease number of spermatids in the seminiferous tubules.

(G) Circulating Inhibin B levels were measured in adult control male mice (*n*= 9), F1 PAMH mice (*n*= 13) and F3 PAMH mice (*n*= 11) and were thereafter analyzed using Kruskal-Wallis test followed by Dunn's multiple comparisons test, No differences were observed between the studied groups ($p=0.3084$)

Material and Methods

Animals

Timed-pregnant female wild-type C57BL/6J (B6) (Charles River, USA) were group-housed under specific pathogen-free conditions in a temperature-controlled room (21-22°C) with a 12-h light/dark cycle and *ad libitum* access to food and water. Standard diet (9.5mm Pelleted RM3, Special Diets Services, France) was given to all mice during breeding, lactation and growth of young stock. Nutritional profile of the standard diet RM3 is the following: Protein 22.45%, Fat 4.2%, Fiber 4.42%, Ash 8%, Moisture 10%, Nitrogen free extract 50.4%; Calories: 3.6 kcal/gr.

Mice were randomly assigned to groups at the time of purchase or weaning to minimize any potential bias. No data sets were excluded from analyses.

Animal studies were approved by the Institutional Ethics Committees of Care and Use of Experimental Animals of the University of Lille (France; Ethical protocol number: APAFIS#2617-2015110517317420 v5). All experiments were performed in accordance with the guidelines for animal use specified by the European Council Directive of 22 September 2010 (2010/63/EU). The sample size, sex and age of the animals used is specified in the text and/or figure legends.

Prenatal anti-Müllerian Hormone (PAMH) treatment

Timed-pregnant adult (3-4 months) C57BL6/J (B6) dams were injected daily intraperitoneally (i.p.) from embryonic day (E) 16.5 to 18.5 with 200 µL of a solution containing respectively: 1) 0.01 M phosphate buffered saline (PBS, pH 7.4, prenatal control-treated), 2) PBS with 0.12 $mgKg^{-1}$/d human anti-Müllerian hormone (AMH) (AMH_C, R&D Systems, rhMIS 1737-MS-10, prenatal AMH (PAMH)-treated).

Assessment of phenotype, estrous cycle and fertility

Control, F1 PAMH, F2 PAMH and F3 PAMH female offspring were weaned at post-natal day P21 and checked for vaginal opening (VO) and time of first estrus. Anogenital distance (AGD) was measured at different ages during post-natal development (P30, 35, 40, 50 and 60). At VO and in adulthood (P60), vaginal smears were performed daily for 16 consecutive days (4-cycles) for analysis of age of first estrus and estrous cyclicity. Vaginal cytology was analyzed under an inverted microscope to

identify the specific day of the estrous cycle. The reproductive competency of these animals was determined by pairing the following mice: Control females mated with untreated C57BL6J (B6) wild-type males, PAMH females mated with PAMH males, PAMH F2 females mated with F2 PAMH males, and F3 PAMH females mated with F3 PAMH males for a period of 3 months. Unexperienced males and primiparous females, selected from at least three different litters, were used for the 90-days mating protocol test.

Number of pups/litter (number of pups), fertility index (number of litters per females over 3 months), and time to first litter (number of days to first litter after pairing) were quantified per treatment and pairing.

Assessment of Testicular weight and cryptorchidism

The cryptorchidism was recorded when one of the testes showed aberrant upper position in every animal. The percentage of cryptorchidism was calculated for each group using the following formula: Total number of analyzed mice / the number of mice who displayed cryptorchidism) X 100). Ponderal characteristics of testis from control and PAMH males were routinely measured during each experiment.

Ovarian and Testicular histology

Ovaries were collected from 3-4-month-old diestrus mice, and testes from 4 months old male mice, immersion-fixed in 4% PFA solution and stored at 4°C. Paraffin-embedded ovaries and testes were sectioned at a thickness of 5 μm (histology facility, University of Lille 2, France) and stained with hematoxylin-eosin (Sigma Aldrich, Cat # GHS132, HT1103128). Sections were examined throughout the ovary and testis.

Total numbers of corpora lutea (CL) was classified and quantified as previously reported {Caldwell, 2017 #540}. To avoid repetitive counting, each follicle was only counted in the section where the oocyte's nucleolus was visible. Using an ocular scale, follicles were classified by diameter into preantral, large growing (200–400 μm) and cystic follicles (> 400 μm). To avoid repetitive counting, CL were counted every 100 μm by comparing the section with the preceding and following sections.

CL were characterized by a still present central cavity, filled with blood and follicular fluid remnants or by prominent polyhedral to round luteal cells.

Perfusions

Adult mice (P60-P90) were anesthetized with i.p. injections of 100 mg/kg of ketamine-HCl and 10 mg/kg xylazine-HCl and perfused transcardially with 20ml of saline, followed by 100 ml of 4% PFA in 0.1M phosphate buffer (PB) (4% PFA/0.1M PB; pH 7.6). Brains were collected, post-fixed in the same fixative for 2h at 4 °C, cryoprotected overnight in PB/Sucrose 30% at 4°C, embedded in OCT-embedding medium (Tissue-Tek), frozen and stored at -80°C until cryosectioning.

Immunohistochemistry

Tissues were cryosectioned coronally (Leica cryostat) at 35µm for free-floating immunohistochemistry (IHC). Sections were blocked in an incubation solution of Tris-buffered saline (TBS 0.05M, pH 7.6), 0.25% bovine serum albumin (BSA; Sigma, A9418), 0.3% Triton X-100 (TBS-T; Sigma, T8787) with 10% normal donkey serum (NDS; D9663; Sigma) for 2h at room temperature before incubation with the following different primary antisera (depending on experiment) for 72h at 4°C: Monoclonal mouse anti-Tyrosine Hydroxylase (TH) antibody (Millipore MAB318; 1:3000), guinea pig anti-(Arg^8)-Vasopressin (Peninsula Laboratories #T-5048; 1:2500), rabbit anti-cFos (Santa Cruz Biotechnology #sc-52; 1:5000), and a rabbit anti-kisspeptin (A. Caraty #566 1:10,000, Institut National de la Recherche Agronomique){Clarkson, 2014 #542}. After TBS rinses, immunoreactivity (i.r) was revealed using the corresponding secondary antibodies (Life Technologies, Molecular Probes, Invitrogen) all 1:400, [Alexa-Fluor 488-conjugated #A21206; Alexa-Fluor 647-conjugated #A31573, #A31571; Alexa-Fluor 568-conjugated #A10042, #A10037] for 90 min in incubation solution at RT. After TBS washes, sections were incubated with 0.02% Hoechst (H3569; Invitrogen) in TBS-T for 15-mins at RT and mounted on gelatin-coated slides and coverslipped with mowiol medium (Sigma #81381).

For confocal observation and analyses, an inverted laser scanning Axio observer microscope (LSM 710, Zeiss) with an EC Plan NeoFluor ×100/1.4 numerical aperture oil-immersion objective (Zeiss)

was used with an argon laser exciting at 488nm and helium laser exciting at 543nm (Imaging Core Facility of IFR114, of the University of Lille 2, France).

Immunohistochemical analysis

Analysis of sexually dimorphic brain nuclei

For single-labeled Tyrosine Hydroxylase (TH) IHC, the number of TH-i.r cell bodies located within anteroventral periventricular nuclei were counted. For single-labeled Vasopressin (VP) IHC, the number of VP-i.r cell bodies located within the bed nucleus stria terminalis (BNST) and Medial Amygdala (MeA) were counted. For both TH and VP single-labeled IHC, each section containing the AVPV or the BNST and MeA were analyzed in each sex, mouse and treatment (3-5 sections per mouse). For single-labeled kisspeptin IHC, the number of kisspeptin-i.r cell bodies were counted in the rostral periventricular area of the third ventricle (RP3V), which comprises the anteroventral periventricular nucleus (AVPV) and the preoptic periventricular nucleus. Two brain sections at each level of the RP3V were analyzed per mouse, and the number of kisspeptin positive cells counted and combined to produce the mean number of kisspeptin neurons per section for the RP3V of each mouse.

The mean number of TH-, VP- and Kiss-i.r neurons counted per section for the sexually dimorphic brain regions of each mouse and treatment were then grouped to provide the mean ± s.e.m. values for the experimental groups.

Pulsatile LH measurements

Males and diestrus female adult mice were habituated with daily handling for 3–weeks. Blood samples (5µl) were taken from the tail at 10-min intervals for 2h (between 10:00and 12:00) during diestrus, diluted in 45µl PBS-Tween (0.05%) and immediately frozen and kept at -80°C. LH levels were determined by the previously described sensitive LH sandwich ELISA. A 96-well high-affinity binding microplate (Corning) was coated with 50µl of capture antibody (monoclonal antibody, anti-bovine LHβ subunit, 518B7; L. Sibley; University of California, UC Davis) at a final dilution of 1:1000 (in Na_2CO_3/$NaHCO_3$, 0.1M, pH 9.6) and incubated overnight at 4°C. Wells were incubated with 200µl blocking buffer (5% (w/v) skim milk powder in 1 X PBS-T pH 7.4 [0.01M PBS, 0.05% Tween 20 (Sigma

#P9416)] for 2hr at RT. A standard curve was generated using a two-fold serial dilution of mouse LH (reference preparation, AFP-5306A; National Institute of Diabetes and Digestive and Kidney Diseases National Hormone and Pituitary Program (NIDDK-NHPP) in 0.25% (w/v) BSA (Sigma, A9418) in PBS-T. The LH standards and blood samples were incubated with 50µl of detection antibody (rabbit LH antiserum, AFP240580Rb; NIDDK-NHPP) at a final dilution of 1:10,000 for 1.5h at RT. Each well containing bound substrate was incubated with 50µl of horseradish peroxidase-conjugated antibody (goat anti-rabbit; Vector Laboratories, PI-1000) at a final dilution of 1:10,000. After a 1.5h incubation, 100µl 1-Step™ Ultra TMB-Elisa Substrate Solution (ThermoFisher Scientific, Cat #34028) was added to each well and left at RT for 10 min. The reaction was halted by the addition of 50µl of 3M HCL to each well, and absorbance read at 490nm.

Hormonal ELISA Assays

LH levels were determined by a sandwich ELISA, as described previously {Vidal, 2012 #550}, using the mouse LH–RP reference provided by A.F. Parlow (National Hormone and Pituitary Program, Torrance, CA). Plasma T , E2, Inhibin B levels were analyzed using commercial ELISA kits Testosterone: (Demeditec Diagnostics, GmnH, DEV9911) {Moore, 2015 #505}; E2: ; Inhibin B: (Anshlab #AL-163), according to the manufacturers' instructions.

Quantitative RT-PCR analyses

Brain, testes and ovaries tissues were harvest from female and male controls and PAMH were isolated for total RNA was using Trizol (ThermoFisher Scientific, Cat #15596026) and the RNeasy Lipid Tissue Mini Kit (Qiagen; Cat # 74804) using the manufacturer's instructions. For gene expression analyses, mRNAs obtained were reverse transcribed using SuperScript® IV Reverse Transcriptase (Life Technologies). Real-time PCR was carried out on Applied Biosystems 7900HT Fast Real-Time PCR system using exon-boundary-specific TaqMan® Gene Expression Assays (Applied Biosystems): *Cyp19a1* (Cyp19a1-*Mm00484049_m1); Cyp11a1* (Cyp11a1- *Mm00490735_m1*); *Cyp17a1* (Cyp17a1-*Mm00484040_m1); Hsd3b1* (Hsd3b1-*Mm01261921_mH*); *Lhr* (Lhcgr-*Mm00442931_m1*); *StAR* (StAR-*Mm00441556_m1)* and *AR* (AR-*Mm00442681_m1)* Control housekeeping genes*: ActB (*ActB-*Mm00607939_s1); Gapdh* (GAPDH-*Mm99999915_g1*).

Quantitative RT-PCR was performed using TaqMan® Low-Density Arrays (Applied Biosystems) on an Applied Biosystems thermocycler using the manufacturer's recommended cycling conditions. Gene expression data were analyzed using SDS 2.4.1 and Data Assist 3.01 software (Applied Biosystems), with *ActB* and *Gapdh* as control house-keeping mRNA following a standardized procedure. Values are expressed relative to control values, as appropriate, set at 1.

Statistical analyses

All analyses were performed using Prism 8 (Graphpad Software, San Diego, CA) and assessed for normality (Shapiro–Wilk test) and variance, when appropriate. Sample sizes were chosen according to standard practice in the field.

For animal studies, data were compared using an unpaired two-tailed Student's *t*-test or a one-way ANOVA for multiple comparisons followed by Tukey's multiple comparison *post-hoc* test. Data analyses for percentages were performed using either a Mann-Whitney *U* test (comparison between two experimental groups) or Kruskal-Wallis test (comparison between three or more experimental groups) followed by a Dunn's *post hoc* analysis. The number of biologically independent experiments, sample size, *P* values, age and sex of the animals are all indicated in the main text or figure legends. All experimental data are indicated as mean ± s.e.m or as the 25th–75th percentile, line at median. The significance level was set at $P < 0.05$. Symbols in figures correspond to the following significance levels: * $P < 0.05$, ** $P < 0.001$, *** $P < 0.0001$.

Discussion

Polycystic Ovary Syndrome (PCOS) is the most common cause of anovulatory infertility of women of reproductive age (Wood et al., 2007; Dumont et al., 2015).

Despite great efforts of clinicians, therapeutic management of PCOS patients is strictly symptomatic and progress towards a cure has been delayed by its poorly understood etiology.

PCOS has been a matter of scientific interest for many years, which was initially considered as a polygenic gonadal pathology. Familiar clustering and twin studies conducted in geographically distinct populations of PCOS patients and their relatives suggest a strong heritable component in PCOS. (McAllister, Legro et al. 2015). However, the candidate genes identified account for <10% of the estimated 70% heritability of PCOS, implying a considerable environmental contribution to the phenotypic expression of PCOS (Hayes, Urbanek et al. 2015) (Azziz, Carmina et al. 2016).

Contemporary understanding of PCOS suggest that it may originate during intrauterine development, which sheds to light the role of environmental factors such androgen excess during this critical developmental window.

Regarding the heritability of the syndrome, clinical observations indicate that the risk of developing PCOS rises to 20-40% in first-degree relatives of PCOS women (Kahsar-Miller, Nixon et al. 2001) (Legro, Driscoll et al. 1998, Franks, Webber et al. 2008). However, varying manifestations of reproductive and metabolic are observed in first-degree relatives of PCOS patients (Sir-Petermann, Maliqueo et al. 2002, Sir-Petermann, Ladron de Guevara et al. 2012). One portion of the daughters and sisters of women with PCOS have higher levels of adrenal ovarian androgens from adolescence into adulthood (Yildiz, Yarali et al. 2003, Azziz, Woods et al. 2004). And another portion of female first-degree relatives of PCOS women seem to have a considerable risk of insulin resistance, hyperinsulinemia, type2 diabetes, and/or impaired glucose tolerance (Sir-Petermann, Maliqueo et al. 2002, Kent, Gnatuk et al. 2008).

Recent studies have reported that PCOS women exhibit elevated AMH levels during pregnancy as compared to healthy women (Tata, Mimouni et al. 2018), (Valdimarsdottir, Valgeirsdottir et al. 2019). AMH is a member of transforming growth factor-beta (TGF-β) superfamily secreted by the granulosa cells of small antral and pre-antral follicles to regulate early follicular development (Sahmay, Aydin et al. 2014). Interestingly, our team previously showed that AMH has an extra-gonadal role by centrally stimulating GnRH neurons, which express AMHR2 in both humans and rodents (Cimino, Casoni et al. 2016).

Giving the strong heritable characteristics of PCOS, the present study aimed to further explore the role of AMH in the onset of PCOS-like traits in a transgenerational inheritance context. Therefore, we investigated the putative long-term consequences of prenatal exposure to excessive AMH levels across subsequent generations of F1, F2 and F3 females and we demonstrate that the fertility of these PAMH females in comparison with control littermates is adversely affected. The females of each of the three generations of exhibit a decrease in litter size and fertility index, pronounced delay in time of first litter, disrupted estrus cyclicity, and lower numbers of corpora lutea.
These findings indicate that the previously described dysfunctional ovulation and fertility in the F1 PAMH females are transmitted to the F2 and F3 PAMH female offspring. The findings obtained from our pre-clinical PCOS model correlate well with a large number of clinical surveys, reporting the amplified incidence of menstrual irregularities and subfertility/infertility among daughters and sisters of PCOS women as compared to healthy controls (Cooper, Spellacy et al. 1968), (Wilroy, Givens et al. 1975, Givens 1988) (Ferriman and Purdie 1979), (Lunde, Magnus et al. 1989).

Hyperandrogenemism is a predominant feature of PCOS and a major contributor to abnormalities such hirsutism and acne. These PCOS traits were also repeatedly described in first degree relatives PCOS women (Ferriman and Purdie 1979).
We have previously described that AMH-driven maternal hyperandrogenism could lead to an increase of testosterone levels in the first generation of PAMH females. Our novel findings show that the biological hyperandrogenism is transmitted to F2 and F3 progeny of PAMH females, as indicated by their longer ADG distance across post-natal development suggestive of an increased androgenic impregnation, along with a significant increase in testosterone levels as compared to control females.

Nevertheless, ovulatory dysfunction and hyperandrogenism were not the only PCOS-like features transferred across the PAMH generations studied. Here, we demonstrate that F2 and F3 PAMH females also exhibit persistent alterations at a central level as indicated by LH circulating levels, which were significantly elevated in F2 and F3 PAMH offspring, when compared with controls.

Altogether, these findings strengthen our hypothesis about PCOS originating *in utero* and appear to consolidate the role of AMH as a trigger of the pathogenesis. Our findings show that a short prenatal exposure to elevated AMH levels has a profound impact on the programing of fetal brain circuits inducing PCOS-like manifestations in adulthood. This appears to be inherited by subsequent

generations, which will as well manifest excessive androgen secretion, alterations in gonadotropin secretion, severely impaired fertility, and disrupted ovulation.

Since, excessive production of ovarian androgens is the most consistently expressed trait of the disorder and that steroidogenic activity is increased in PCOS patients compared to healthy patients. (Takayama, Fukaya et al. 1996) (Nelson, Legro et al. 1999, Nelson, Qin et al. 2001) We sought to dissect the mechanisms that may underpin the transgenerational transmission by checking the expression of the key genes implicated in the androgen biosynthetic pathway in the ovaries associated with PCOS: *Cyp11a1*, *Cyp19a1 Hsd3b1.*

Although, some studies suggest an implication of the gene *Cyp11a1* in PCOS (Wood, Ho et al. 2004) which catalyzes the first step of steroidogenesis, we report the absence of any changes in the relative mRNA expression of the *Cyp11a1* in our model. Conversely, we uncovered a drastic decrease in the relative mRNA expression of *Cyp19a1*, which is responsible for the conversion of testosterone into estradiol, and *Hsd3b1,* which converts pregnenolone to progesterone. This well correlates with the previous studies associating the down regulation of *CYP19A1* aromatase gene in luteinized granulosa cells from PCOS women (Yang, Ruan et al. 2015).

As we confirmed a clear decrease in the expression levels of aromatase in the progeny of PAMH mice, it seems crucial to delineate subsequently if this decrease could be related to an epigenetic process involving DNA methylation or histone modification to better understand the transgenerational inheritance mechanism. It is now largely documented that environmental influences during the period of developmental plasticity leads to an epigenetic change within the first-generation offspring's germline that is then transmitted to F2 offspring and beyond. (Perera and Herbstman 2011).

A first hint into resolving this enigma was provided by Yu, sun et al, when they analyzed ovaries of PCOS and control Chinese women and uncovered a hypermethylation of the promoter of *CYP19a1* gene which could explain the repression of its expression (Yu, Sun et al. 2013).

In most PCOS studies, phenotypes of daughters and sisters of PCOS women were investigated but less is known about boys born to PCOS mothers. Male family members are not systematically characterized, only few attempts were made to identify a male phenotype of first-degree male relatives of PCOS women.

One of the few studies describing a male reproductive phenotype was conducted by Cohen et al. Their work uncovered oligospermia and increased LH secretion in some of the male subjects of the study participants (Cohen, Givens et al. 1975) Some other investigations revealed higher AMH levels compared to sons born to healthy mothers (Recabarren, Sir-Petermann et al. 2008) . Additional studies have highlighted the altered metabolic profile observed in first-degree relatives of PCOS women (Yildiz, Yarali et al. 2003, Sam, Coviello et al. 2008) (Recabarren, Smith et al. 2008). Among those metabolic alterations, an increase in insulin resistance and glucose intolerance have been observed.

The second part of this study aimed at investigating how early exposure to AMH excess the neuroendocrine and reproductive features of the male offspring at birth, puberty and in adulthood. The PAMH male offspring displayed a significantly diminished testicular weight, shorter ano-genital distance and lower T levels as compared the control male offspring. It is consistent with previous investigations, reporting that prenatal androgenization alters the testicular development in several species (Rojas-Garcia, Recabarren et al. 2010), (Recabarren, Rojas-Garcia et al. 2008), (Connolly, Rae et al. 2013).

In most vertebrates, gonadal T secretion occurs in a sexually dimorphic pattern during the first hours following birth (0-4 hours at P0). It is reportedly elevated in newborn males but not in females (Corbier, Edwards et al. 1992). In this study, we report that PAMH adult male failed to engage the testosterone surge at birth observed in control newborns. Interestingly, as stated above the levels of testosterone remain dramatically low in PAMH males as compared to the control group, when measured in adulthood, suggesting an impact on the HPG axis and decreased steroidogenic activity at a testicular level.

Few hours after the testosterone surge, most studies indicate the existence of an LH surge shortly after T in males. Remarkably PAMH male mice display no evidence of a neonatal LH surge, and their LH levels at P0 mirror the levels observed in control females rather than the ones detected in control males.

Pulsatile GnRH, released into hypophyseal portal blood, stimulates LH and FSH production which drive pulsatile T secretion by Leydig cells into the spermatic vein (Santen 1975). In this context, we attempted to investigate whether, the male progeny embryonically exposed to AMH would have would exhibit an altered GnRH neuronal secretion, we thus assessed LH secretion as an indirect

measurement of GnRH secretion. Our data show that PAMH males exhibit significantly higher circulating LH levels and an increase in LH pulses number as compared to control males.

Considering that PAMH males exhibit low testosterone levels, no changes in inhibin B and high LH pulsatility, there might be an intrinsic defect in hypothalamic circuits controlling negative feedback in adulthood. Maternal AMH-driven hyperandrogenism could also be responsible of this central defect, by driving the secretion of GnRH and LH secretion through its receptor AMHR2 present on GnRH neurons (Cimino, Casoni et al. 2016) in the dams as previously described, leading to a programmation of the fetal brains resulting in an altered hypothalamic GnRH secretion.

Remarkably, the prenatal administration of GnRH antagonist rescues the testosterone levels, Anogenital distance and LH and levels in these mice (data not shown) suggesting that the defect is rather central which highlight the implication of the GnRH system in PCOS. Further electrophysiological studies are required to confirm the hypothesis.

Dogma holds that during a specific period of embryonic development, under the action of the gonadal steroids, the brain irreversibly engages in a differentiation path of the male or female path and that the neonatal testosterone surge is responsible for establishing brain sexual dimorphisms that underpin sexually dimorphic physiology and behavior, (Simerly 2002, McCarthy, Arnold et al. 2012),(Ciofi, Lapirot et al. 2007),(Clarkson and Herbison 2016). The masculinizing and defeminizing effects of testosterone are mainly mediated by its metabolite, estradiol, (McCarthy 2008), through the aromatization of testosterone by the CYP19A1 aromatase.

We thus, analyzed whether the late gestational, AMH-dependent maternal hyperandrogenism previously described (Tata, Mimouni et al. 2018) might interfere with the appropriate establishment of sexually dimorphic circuitries in the male offspring brains.

The evaluation of sexually dimorphic areas of the brains of control males, females and PAMH males allowed us to uncover a feminization of the brains of PAMH mice. This has been confirmed by quantitative analysis of immunoreactive sexually dimorphic neurons (Vasopressin, Tyrosine Hydroxylase and TIDA neurons) in each group. Our result show that the number of Immunoreactive neurons is comparable to the one observed in control female brains than in males. Suggesting that the exposition to elevated levels of AMH during embryogenesis has a feminizing effect on male offspring partly through a suppression of the essential T surge at birth.

Previous studies have shown that the genetically male individuals (XY) with complete androgen insensitivity syndrome (CAIS) due to a dysfunctional androgen receptor gene exhibit a feminine phenotype with heavy psychosexual outcomes (Money, Ehrhardt et al. 1968), (Wisniewski, Migeon et al. 2000), it is unclear if this feminine behavior could be due to the brain's inability to respond to fetal testosterone or to social rearing as females since early childhood.

Additionally, studies of amniotic testosterone in humans suggest that fetal testosterone is related to specific sexually dimorphic aspects of cognition and behavior (Auyeung, Baron-Cohen et al. 2009, Auyeung, Baron-Cohen et al. 2009) other investigation suggest that children born to PCOS mothers have a greater risk of autism (Cherskov, Pohl et al. 2018).

Further exploration of the behavior of the feminized PAMH males is therefore required to investigate putative cognitive deficiencies along with sexual behavior which are controlled by the sexually dimorphic regions of the brain.

Next, in the search of the mechanism behind the severe decline in testosterone levels observed in PAMH males, we assessed the expression levels of the main genes involved in the steroidogenesis at testicular level of control and PAMH males.

In males, steroidogenesis takes place in the Leydig cells of testes, where cholesterol is transported to the mitochondria by an LH-dependent mechanism regulated by a transfer protein called steroidogenesis activator protein (StAR), whose essential role represents a limiting step of steroidogenesis (Miller 1988, Stocco 2001), cholesterol is finally converted to androgens and estrogens in a multi-step process involving specific cytochrome P450 enzymes (CYPs), hydroxysteroid dehydrogenases (HSDs).

In this study, we report a considerable decrease in the mRNA expression of *Cyp19a1*, *StAR*, *Cyp17a1* as well as *LH receptor* and *Androgen receptor* (AR) in the testes of PAMH mice in comparison with control testis. In contrast, no differences were perceived in the mRNA expression levels of *Insl3, Cyp11a1* and *Hsd3b1*.

Finally, giving that AMH gestational exposure reprograms the fetal brain and induces a transmission of altered reproductive and neuroendocrine traits across generations in females, we conducted a similar transgenerational characterization in males.

Here we demonstrate that PAMH males from all three generations have a decrease in testosterone, reduced testicular weight consistent with severe morphological alterations in the testis and as well as a higher risk of developing cryptorchidism.

Cryptorchidism is the most common congenital abnormality of the male genitalia and affects about three in every ten male infants born prematurely, it is described as defect in testicular decent but the etiology of this abnormality is unclear. In both humans and rodents, the testicular descent occurs in two phases: Firstly, the transabdominal descent occurs in humans between week 10 and 15 of gestation and in mice between embryonic days (E) 14.5 and E16.5, this travel from the urogenital ridge to the inguinal region, which seems to be regulated by the insulin-like factor 3 (INSL3) secreted by the Leydig cells (Zimmermann, Steding et al. 1999), (Nef and Parada 1999). And secondly, the inguinoscrotal descent is finalized before birth in humans, and in mice, the testes and epididymides move inside the scrotum within the first 2 weeks of neonatal development, this process is androgen-dependent and relies on testosterone and androgen receptors to orchestrate descent of the testis from the inguinal canal to the scrotum. Using a Cre-loxP approach, a conditional inactivation of the androgen receptor (*Ar*) gene was established at the level of the gubernacular ligament connecting the epididymis to the caudal abdominal wall resulted in subfertility due to cryptorchidism in mice suggesting that a defect in androgen secretion or signaling could be involved in the testicular descent alteration (Kaftanovskaya, Huang et al. 2012). This might explain the link between the decrease of testosterone and the higher prevalence of cryptorchidism observed in the PAMH males studied.

Collectively, our findings suggest a novel mechanism whereby the intrauterine exposure to excess AMH profoundly impacts the HPG axis of the male progeny, by increasing GnRH hypothalamic secretion thus stimulating LH secretion from the pituitary in one hand. And by suppressing the testosterone surge in males at birth leading to a feminization of the sexually dimorphic circuitries of the fetal brain in the other hand. This decrease in testosterone is also observed in adulthood and could likely be explained by a disrupted testicular steroidogenic activity and AR receptor signaling at an early stage of the postnatal development leading to morphological defects in the testes. Thus, it of clinical interest to relate findings from this study to the reproductive phenotype of sons of PCOS women, who are exposed to higher levels of T during gestation but not systematically investigated

in adulthood. Furthermore, identifying a male phenotype may also improve the phenotyping of female family members by identifying familial traits that are gender independent.

Given that we have previously shown that AMH cannot pass the placental barrier, it is unlikely that the gene expression differences could be attributed to a direct effect of AMH on the fetal testes. It is more likely that these differences relate to an AMH-dependent maternal hyperandrogenism that impacts fetal testis development.

Among the most interesting and unexpected findings to emerge from our recent pre-clinical PCOS model is that the effects of *in utero* exposure to excess AMH expand from the generation gestating at the time of exposure (F1) to their offspring (F2), who arose from gametes that may have been exposed, to the subsequent generation (F3). Thus, suggesting a strong implication of AMH-driven programing of the fetal brain of females in the development of cardinal PCOS-like disturbances in adulthood. A better understanding of how developmental programming effects are transmitted is essential for the implementation of initiatives treatment strategies of PCOS patients and their first-degree relatives.

References

Abbott, D. H. and F. Bacha (2013). "Ontogeny of polycystic ovary syndrome and insulin resistance in utero and early childhood." Fertil Steril **100**(1): 2-11.

Abbott, D. H., D. K. Barnett, C. M. Bruns and D. A. Dumesic (2005). "Androgen excess fetal programming of female reproduction: a developmental aetiology for polycystic ovary syndrome?" Hum Reprod Update **11**(4): 357-374.

Asuncion, M., R. M. Calvo, J. L. San Millan, J. Sancho, S. Avila and H. F. Escobar-Morreale (2000). "A prospective study of the prevalence of the polycystic ovary syndrome in unselected Caucasian women from Spain." J Clin Endocrinol Metab **85**(7): 2434-2438.

Auyeung, B., S. Baron-Cohen, E. Ashwin, R. Knickmeyer, K. Taylor and G. Hackett (2009). "Fetal testosterone and autistic traits." Br J Psychol **100**(Pt 1): 1-22.

Auyeung, B., S. Baron-Cohen, E. Ashwin, R. Knickmeyer, K. Taylor, G. Hackett and M. Hines (2009). "Fetal testosterone predicts sexually differentiated childhood behavior in girls and in boys." Psychol Sci **20**(2): 144-148.

Azziz, R., E. Carmina, Z. Chen, A. Dunaif, J. S. E. Laven, R. S. Legro, D. Lizneva, B. Natterson-Horowtiz, H. J. Teede and B. O. Yildiz (2016). "Polycystic ovary syndrome." Nature Reviews Disease Primers **2**: 16057.

Azziz, R., K. S. Woods, R. Reyna, T. J. Key, E. S. Knochenhauer and B. O. Yildiz (2004). "The prevalence and features of the polycystic ovary syndrome in an unselected population." J Clin Endocrinol Metab **89**(6): 2745-2749.

Balen, A. H., G. S. Conway, G. Kaltsas, K. Techatrasak, P. J. Manning, C. West and H. S. Jacobs (1995). "Polycystic ovary syndrome: the spectrum of the disorder in 1741 patients." Hum Reprod **10**(8): 2107-2111.

Chen, Z. J., H. Zhao, L. He, Y. Shi, Y. Qin, Y. Shi, Z. Li, L. You, J. Zhao, J. Liu, X. Liang, X. Zhao, J. Zhao, Y. Sun, B. Zhang, H. Jiang, D. Zhao, Y. Bian, X. Gao, L. Geng, Y. Li, D. Zhu, X. Sun, J. E. Xu, C. Hao, C. E. Ren, Y. Zhang, S. Chen, W. Zhang, A. Yang, J. Yan, Y. Li, J. Ma and Y. Zhao (2011). "Genome-wide association study identifies susceptibility loci for polycystic ovary syndrome on chromosome 2p16.3, 2p21 and 9q33.3." Nat Genet **43**(1): 55-59.

Cherskov, A., A. Pohl, C. Allison, H. Zhang, R. A. Payne and S. Baron-Cohen (2018). "Polycystic ovary syndrome and autism: A test of the prenatal sex steroid theory." Translational Psychiatry **8**(1): 136.

Cimino, I., F. Casoni, X. Liu, A. Messina, J. Parkash, S. P. Jamin, S. Catteau-Jonard, F. Collier, M. Baroncini, D. Dewailly, P. Pigny, M. Prescott, R. Campbell, A. E. Herbison, V. Prevot and P. Giacobini (2016). "Novel role for anti-Mullerian hormone in the regulation of GnRH neuron excitability and hormone secretion." Nat Commun **7**: 10055.

Ciofi, P., O. C. Lapirot and G. Tramu (2007). "An androgen-dependent sexual dimorphism visible at puberty in the rat hypothalamus." Neuroscience **146**(2): 630-642.

Clarkson, J. and A. E. Herbison (2016). "Hypothalamic control of the male neonatal testosterone surge." Philos Trans R Soc Lond B Biol Sci **371**(1688): 20150115.

Cohen, P. N., J. R. Givens, W. L. Wiser, R. S. Wilroy, R. L. Summitt, S. A. Coleman and R. N. Andersen (1975). "Polycystic ovarian disease, maturation arrest of spermiogenesis, and Klinefelter's syndrome in siblings of a family with familial hirsutism." Fertil Steril **26**(12): 1228-1238.

Connolly, F., M. T. Rae, L. Bittner, K. Hogg, A. S. McNeilly and W. C. Duncan (2013). "Excess androgens in utero alters fetal testis development." Endocrinology **154**(5): 1921-1933.

Cooper, H. E., W. N. Spellacy, K. A. Prem and W. D. Cohen (1968). "Hereditary factors in the Stein-Leventhal syndrome." Am J Obstet Gynecol **100**(3): 371-387.

Corbier, P., D. A. Edwards and J. Roffi (1992). "The neonatal testosterone surge: a comparative study." Arch Int Physiol Biochim Biophys **100**(2): 127-131.

Dadachanji, R., N. Shaikh and S. Mukherjee (2018). "Genetic Variants Associated with Hyperandrogenemia in PCOS Pathophysiology." Genet Res Int **2018**: 7624932.

Dumesic, D. A., S. E. Oberfield, E. Stener-Victorin, J. C. Marshall, J. S. Laven and R. S. Legro (2015). "Scientific Statement on the Diagnostic Criteria, Epidemiology, Pathophysiology, and Molecular Genetics of Polycystic Ovary Syndrome." Endocr Rev **36**(5): 487-525.

Ferriman, D. and A. W. Purdie (1979). "The inheritance of polycystic ovarian disease and a possible relationship to premature balding." Clin Endocrinol (Oxf) **11**(3): 291-300.

Franks, S., N. Gharani and M. McCarthy (2001). "Candidate genes in polycystic ovary syndrome." Hum Reprod Update **7**(4): 405-410.

Franks, S., L. J. Webber, M. Goh, A. Valentine, D. M. White, G. S. Conway, S. Wiltshire and M. I. McCarthy (2008). "Ovarian morphology is a marker of heritable biochemical traits in sisters with polycystic ovaries." J Clin Endocrinol Metab **93**(9): 3396-3402.

Garamszegi, L. Z., M. Eens, S. Hurtrez-Bousses and A. P. Moller (2005). "Testosterone, testes size, and mating success in birds: a comparative study." Horm Behav **47**(4): 389-409.

Givens, J. R. (1988). "Familial polycystic ovarian disease." Endocrinol Metab Clin North Am **17**(4): 771-783.

Goodarzi, M. O., D. A. Dumesic, G. Chazenbalk and R. Azziz (2011). "Polycystic ovary syndrome: etiology, pathogenesis and diagnosis." Nat Rev Endocrinol **7**(4): 219-231.

Hague, W. M., J. Adams, S. T. Reeders, T. E. Peto and H. S. Jacobs (1988). "Familial polycystic ovaries: a genetic disease?" Clin Endocrinol (Oxf) **29**(6): 593-605.

Hayes, M. G., M. Urbanek, D. A. Ehrmann, L. L. Armstrong, J. Y. Lee, R. Sisk, T. Karaderi, T. M. Barber, M. I. McCarthy, S. Franks, C. M. Lindgren, C. K. Welt, E. Diamanti-Kandarakis, D. Panidis, M. O. Goodarzi, R. Azziz, Y. Zhang, R. G. James, M. Olivier, A. H. Kissebah, E. Stener-Victorin, R. S. Legro and A. Dunaif (2015). "Genome-wide association of polycystic ovary syndrome implicates alterations in gonadotropin secretion in European ancestry populations." Nat Commun **6**: 7502.

Kaftanovskaya, E. M., Z. Huang, A. M. Barbara, K. De Gendt, G. Verhoeven, I. P. Gorlov and A. I. Agoulnik (2012). "Cryptorchidism in mice with an androgen receptor ablation in gubernaculum testis." Mol Endocrinol **26**(4): 598-607.

Kahsar-Miller, M. D., C. Nixon, L. R. Boots, R. C. Go and R. Azziz (2001). "Prevalence of polycystic ovary syndrome (PCOS) in first-degree relatives of patients with PCOS." Fertil Steril **75**(1): 53-58.

Kent, S. C., C. L. Gnatuk, A. R. Kunselman, L. M. Demers, P. A. Lee and R. S. Legro (2008). "Hyperandrogenism and hyperinsulinism in children of women with polycystic ovary syndrome: a controlled study." J Clin Endocrinol Metab **93**(5): 1662-1669.

Legro, R. S., D. Driscoll, J. F. Strauss, 3rd, J. Fox and A. Dunaif (1998). "Evidence for a genetic basis for hyperandrogenemia in polycystic ovary syndrome." Proc Natl Acad Sci U S A **95**(25): 14956-14960.

Lunde, O., P. Magnus, L. Sandvik and S. Hoglo (1989). "Familial clustering in the polycystic ovarian syndrome." Gynecol Obstet Invest **28**(1): 23-30.

March, W. A., V. M. Moore, K. J. Willson, D. I. Phillips, R. J. Norman and M. J. Davies (2010). "The prevalence of polycystic ovary syndrome in a community sample assessed under contrasting diagnostic criteria." Hum Reprod **25**(2): 544-551.

McAllister, J. M., R. S. Legro, B. P. Modi and J. F. Strauss, 3rd (2015). "Functional genomics of PCOS: from GWAS to molecular mechanisms." Trends Endocrinol Metab **26**(3): 118-124.

McCarthy, M. M. (2008). "Estradiol and the developing brain." Physiol Rev **88**(1): 91-124.

McCarthy, M. M., A. P. Arnold, G. F. Ball, J. D. Blaustein and G. J. De Vries (2012). "Sex differences in the brain: the not so inconvenient truth." J Neurosci **32**(7): 2241-2247.

McCartney, C. R., C. A. Eagleson and J. C. Marshall (2002). "Regulation of gonadotropin secretion: implications for polycystic ovary syndrome." Semin Reprod Med **20**(4): 317-326.

Miller, W. L. (1988). "Molecular biology of steroid hormone synthesis." Endocr Rev **9**(3): 295-318.

Money, J., A. A. Ehrhardt and D. N. Masica (1968). "Fetal feminization induced by androgen insensitivity in the testicular feminizing syndrome: effect on marriage and maternalism." Johns Hopkins Med J **123**(3): 105-114.

Nef, S. and L. F. J. N. g. Parada (1999). "Cryptorchidism in mice mutant for Insl3." **22**(3): 295.

Nelson, V. L., R. S. Legro, J. F. Strauss, 3rd and J. M. McAllister (1999). "Augmented androgen production is a stable steroidogenic phenotype of propagated theca cells from polycystic ovaries." Mol Endocrinol **13**(6): 946-957.

Nelson, V. L., K. N. Qin, R. L. Rosenfield, J. R. Wood, T. M. Penning, R. S. Legro, J. F. Strauss, 3rd and J. M. McAllister (2001). "The biochemical basis for increased testosterone production in theca cells propagated from patients with polycystic ovary syndrome." J Clin Endocrinol Metab **86**(12): 5925-5933.

Norman, R. J., D. Dewailly, R. S. Legro and T. E. Hickey (2007). "Polycystic ovary syndrome." Lancet **370**(9588): 685-697.

Perera, F. and J. Herbstman (2011). "Prenatal environmental exposures, epigenetics, and disease." Reprod Toxicol **31**(3): 363-373.

Preston, B. T., I. R. Stevenson, G. A. Lincoln, S. L. Monfort, J. G. Pilkington and K. Wilson (2012). "Testes size, testosterone production and reproductive behaviour in a natural mammalian mating system." **81**(1): 296-305.

Recabarren, S. E., P. P. Rojas-Garcia, M. P. Recabarren, V. H. Alfaro, R. Smith, V. Padmanabhan and T. Sir-Petermann (2008). "Prenatal testosterone excess reduces sperm count and motility." Endocrinology **149**(12): 6444-6448.

Recabarren, S. E., T. Sir-Petermann, R. Rios, M. Maliqueo, B. Echiburu, R. Smith, P. Rojas-Garcia, M. Recabarren and R. A. Rey (2008). "Pituitary and testicular function in sons of women with polycystic ovary syndrome from infancy to adulthood." J Clin Endocrinol Metab **93**(9): 3318-3324.

Recabarren, S. E., R. Smith, R. Rios, M. Maliqueo, B. Echiburu, E. Codner, F. Cassorla, P. Rojas and T. Sir-Petermann (2008). "Metabolic profile in sons of women with polycystic ovary syndrome." J Clin Endocrinol Metab **93**(5): 1820-1826.

Rodin, D. A., G. Bano, J. M. Bland, K. Taylor and S. S. Nussey (1998). "Polycystic ovaries and associated metabolic abnormalities in Indian subcontinent Asian women." Clin Endocrinol (Oxf) **49**(1): 91-99.

Rojas-Garcia, P. P., M. P. Recabarren, L. Sarabia, J. Schon, C. Gabler, R. Einspanier, M. Maliqueo, T. Sir-Petermann, R. Rey and S. E. Recabarren (2010). "Prenatal testosterone excess alters Sertoli and germ cell number and testicular FSH receptor expression in rams." Am J Physiol Endocrinol Metab **299**(6): E998-e1005.

Sahmay, S., Y. Aydin, M. Oncul and L. M. Senturk (2014). "Diagnosis of Polycystic Ovary Syndrome: AMH in combination with clinical symptoms." J Assist Reprod Genet **31**(2): 213-220.

Sam, S., A. D. Coviello, Y. A. Sung, R. S. Legro and A. Dunaif (2008). "Metabolic phenotype in the brothers of women with polycystic ovary syndrome." Diabetes Care **31**(6): 1237-1241.

Santen, R. J. (1975). "Is aromatization of testosterone to estradiol required for inhibition of luteinizing hormone secretion in men?" J Clin Invest **56**(6): 1555-1563.

Simerly, R. B. (2002). "Wired for reproduction: organization and development of sexually dimorphic circuits in the mammalian forebrain." Annu Rev Neurosci **25**: 507-536.

Sir-Petermann, T., A. Ladron de Guevara, E. Codner, J. Preisler, N. Crisosto, B. Echiburu, M. Maliqueo, F. Sanchez, F. Perez-Bravo and F. Cassorla (2012). "Relationship between anti-Mullerian hormone (AMH) and insulin levels during different tanner stages in daughters of women with polycystic ovary syndrome." Reprod Sci **19**(4): 383-390.

Sir-Petermann, T., M. Maliqueo, B. Angel, H. E. Lara, F. Perez-Bravo and S. E. Recabarren (2002). "Maternal serum androgens in pregnant women with polycystic ovarian syndrome: possible implications in prenatal androgenization." Hum Reprod **17**(10): 2573-2579.

Stocco, D. M. (2001). "StAR Protein and the Regulation of Steroid Hormone Biosynthesis." **63**(1): 193-213.

Takayama, K., T. Fukaya, H. Sasano, Y. Funayama, T. Suzuki, R. Takaya, Y. Wada and A. Yajima (1996). "Immunohistochemical study of steroidogenesis and cell proliferation in polycystic ovarian syndrome." Hum Reprod **11**(7): 1387-1392.

Tata, B., N. E. H. Mimouni, A. L. Barbotin, S. A. Malone, A. Loyens, P. Pigny, D. Dewailly, S. Catteau-Jonard, I. Sundstrom-Poromaa, T. T. Piltonen, F. Dal Bello, C. Medana, V. Prevot, J. Clasadonte and P. Giacobini (2018). "Elevated prenatal anti-Mullerian hormone reprograms the fetus and induces polycystic ovary syndrome in adulthood." Nat Med **24**(6): 834-846.

Taylor, A. E., B. McCourt, K. A. Martin, E. J. Anderson, J. M. Adams, D. Schoenfeld and J. E. Hall (1997). "Determinants of abnormal gonadotropin secretion in clinically defined women with polycystic ovary syndrome." J Clin Endocrinol Metab **82**(7): 2248-2256.

Uglem, I., I. Mayer and G. Rosenqvist (2002). "Variation in plasma steroids and reproductive traits in dimorphic males of corkwing wrasse (Symphodus melops L.)." Horm Behav **41**(4): 396-404.

Valdimarsdottir, R., H. Valgeirsdottir, A. K. Wikstrom, T. K. Kallak, E. Elenis, O. Axelsson, K. Ubhayasekhera, J. Bergquist, T. T. Piltonen, P. Pigny, P. Giacobini and I. S. Poromaa (2019). "Pregnancy and neonatal complications in women with polycystic ovary syndrome in relation to second-trimester anti-Mullerian hormone levels." Reprod Biomed Online **39**(1): 141-148.

Waldstreicher, J., N. F. Santoro, J. E. Hall, M. Filicori and W. F. Crowley, Jr. (1988). "Hyperfunction of the hypothalamic-pituitary axis in women with polycystic ovarian disease: indirect evidence for partial gonadotroph desensitization." J Clin Endocrinol Metab **66**(1): 165-172.

Wilroy, R. S., Jr., J. R. Givens, W. L. Wiser, S. A. Coleman, R. N. Andersen and R. L. Summitt (1975). "Hyperthecosis: an inheritable form of polycystic ovarian disease." Birth Defects Orig Artic Ser **11**(4): 81-85.

Wisniewski, A. B., C. J. Migeon, H. F. Meyer-Bahlburg, J. P. Gearhart, G. D. Berkovitz, T. R. Brown and J. Money (2000). "Complete androgen insensitivity syndrome: long-term medical, surgical, and psychosexual outcome." J Clin Endocrinol Metab **85**(8): 2664-2669.

Wood, J. R., C. K. Ho, V. L. Nelson-Degrave, J. M. McAllister and J. F. Strauss, 3rd (2004). "The molecular signature of polycystic ovary syndrome (PCOS) theca cells defined by gene expression profiling." J Reprod Immunol **63**(1): 51-60.

Yang, F., Y. C. Ruan, Y. J. Yang, K. Wang, S. S. Liang, Y. B. Han, X. M. Teng and J. Z. Yang (2015). "Follicular hyperandrogenism downregulates aromatase in luteinized granulosa cells in polycystic ovary syndrome women." Reproduction **150**(4): 289-296.

Yildiz, B. l. O., H. Yarali, H. Oguz and M. Bayraktar (2003). "Glucose Intolerance, Insulin Resistance, and Hyperandrogenemia in First Degree Relatives of Women with Polycystic Ovary Syndrome." The Journal of Clinical Endocrinology & Metabolism **88**(5): 2031-2036.

Yildiz, B. O., H. Yarali, H. Oguz and M. Bayraktar (2003). "Glucose intolerance, insulin resistance, and hyperandrogenemia in first degree relatives of women with polycystic ovary syndrome." J Clin Endocrinol Metab **88**(5): 2031-2036.

Yu, Y. Y., C. X. Sun, Y. K. Liu, Y. Li, L. Wang and W. Zhang (2013). "Promoter methylation of CYP19A1 gene in Chinese polycystic ovary syndrome patients." Gynecol Obstet Invest **76**(4): 209-213.

Zimmermann, S., G. Steding, J. M. A. Emmen, A. O. Brinkmann, K. Nayernia, A. F. Holstein, W. Engel and I. M. Adham (1999). "Targeted Disruption of the Insl3 Gene Causes Bilateral Cryptorchidism." Molecular Endocrinology **13**(5): 681-691.

ANNEX

eLIFE elifesciences.org

RESEARCH ARTICLE

Defective AMH signaling disrupts GnRH neuron development and function and contributes to hypogonadotropic hypogonadism

Samuel Andrew Malone[1,2], Georgios E Papadakis[3], Andrea Messina[3], Nour El Houda Mimouni[1,2], Sara Trova[1,2], Monica Imbernon[1,2], Cecile Allet[1,2], Irene Cimino[1], James Acierno[3], Daniele Cassatella[3], Cheng Xu[3], Richard Quinton[4], Gabor Szinnai[5], Pascal Pigny[6], Lur Alonso-Cotchico[7], Laura Masgrau[7,8], Jean-Didier Maréchal[7], Vincent Prevot[1,2], Nelly Pitteloud[3]*, Paolo Giacobini[1,2]*

[1]Jean-Pierre Aubert Research Center (JPArc), Laboratory of Development and Plasticity of the Neuroendocrine Brain, Inserm, UMR-S 1172, Lille, France; [2]University of Lille, FHU 1, 000 Days for Health, Lille, France; [3]Faculty of Biology and Medicine, Service of Endocrinology, Diabetology and Metabolism, University Hospital, Lausanne, Switzerland; [4]Institute of Genetic Medicine and the Royal Victoria Infirmary, University of Newcastle-upon-Tyne, Newcastle-upon-Tyne, United Kingdom; [5]Pediatric Endocrinology and Diabetology, University of Basel Children's Hospital, Basel, Switzerland; [6]CHU Lille, Laboratoire de Biochimie et Hormonologie, Centre de Biologie Pathologie, Lille, France; [7]Departament de Química, Universitat Autònoma de Barcelona, Bellaterra, Spain; [8]Institut de Biotecnologia i de Biomedicina, Universitat Autònoma de Barcelona, Bellaterra, Spain

***For correspondence:** Nelly.Pitteloud@chuv.ch (NP); paolo.giacobini@inserm.fr (PG)

Competing interests: The authors declare that no competing interests exist.

Funding: See page 31

Received: 27 March 2019
Accepted: 28 June 2019

Reviewing editor: Joel K Elmquist, University of Texas Southwestern Medical Center, United States

© Copyright Malone et al. This article is distributed under the terms of the Creative Commons Attribution License, which permits unrestricted use and redistribution provided that the original author and source are credited.

Abstract Congenital hypogonadotropic hypogonadism (CHH) is a condition characterized by absent puberty and infertility due to gonadotropin releasing hormone (GnRH) deficiency, which is often associated with anosmia (Kallmann syndrome, KS). We identified loss-of-function heterozygous mutations in anti-Müllerian hormone (*AMH*) and its receptor, *AMHR2*, in 3% of CHH probands using whole-genome sequencing. We showed that during embryonic development, AMH is expressed in migratory GnRH neurons in both mouse and human fetuses and unconvered a novel function of AMH as a pro-motility factor for GnRH neurons. Pathohistological analysis of *Amhr2*-deficient mice showed abnormal development of the peripheral olfactory system and defective embryonic migration of the neuroendocrine GnRH cells to the basal forebrain, which results in reduced fertility in adults. Our findings highlight a novel role for AMH in the development and function of GnRH neurons and indicate that AMH signaling insufficiency contributes to the pathogenesis of CHH in humans.
DOI: https://doi.org/10.7554/eLife.47198.001

Introduction

Gonadotropin releasing hormone (GnRH) is essential for puberty onset and reproduction. GnRH is released into the pituitary portal blood vessels for delivery to the anterior pituitary. There, GnRH controls the production and release of the gonadotropins LH (luteinizing hormone) and FSH (follicle stimulating hormone), which in turn stimulate gametogenesis and sex steroid production in the gonads (***Christian and Moenter, 2010***). GnRH–secreting neurons are unusual neuroendocrine cells,

as they originate in the nasal placode outside the central nervous system during embryonic development, and migrate to the hypothalamus along the vomeronasal and terminal nerves (VNN, TN) (**Wray et al., 1989**; **Schwanzel-Fukuda and Pfaff, 1989**). This process is evolutionarily conserved and follows a similar spatio-temporal pattern in all mammals (**Wray et al., 1989**; **Schwanzel-Fukuda and Pfaff, 1989**), including humans (**Schwanzel-Fukuda et al., 1996**; **Casoni et al., 2016**). Disruption of GnRH neuronal migration and/or defective GnRH synthesis and secretion leads to congenital hypogonadotropic hypogonadisms (CHH), a rare endocrine disorder (prevalence: 1 in 4000) characterized by absent or incomplete puberty resulting in infertility (**Boehm et al., 2015**). CHH is clinically and genetically heterogeneous with several causal genes identified to date (**Boehm et al., 2015**), and follows various modes of transmission, including oligogenic inheritance (**Sykiotis et al., 2010**). However, the mutations identified so far only account for half of clinically reported cases, suggesting that other causal genes remain to be discovered. Unravelling new genetic pathways involved in the regulation of the development of the GnRH system is relevant for understanding the basis of pathogenesis leading to CHH in humans.

AMH is a TGF-β family member and it signals by binding to a specific type II receptor (AMHR2) (**di Clemente et al., 1994**; **Baarends et al., 1994**), which heterodimerizes with one of several type I TGF-β receptors (Acvr1 [Alk2], Bmpr1a [Alk3] and Bmpr1b [Alk6]), to recruit Smad proteins that subsequently undergo nuclear translocation to regulate target gene expression (**Josso and Clemente, 2003**). Although AMH signaling has been traditionally reported to play a crucial role during sex differentiation and gonadal functions (**Josso et al., 1998**; **Behringer et al., 1994**), accumulating evidence has started to shed light on unexpected functions of AMH in the central nervous system as well as in the pituitary (**Lebeurrier et al., 2008**; **Wang et al., 2009**; **Tata et al., 2018**; **Cimino et al., 2016**; **Garrel et al., 2016**). We have previously shown that GnRH neurons express AMHR2 from early fetal development to adulthood and that AMH stimulates GnRH neuronal activity and hormone secretion in mature GnRH cells (**Cimino et al., 2016**). Here, we expand this information by demonstrating that GnRH cells also express AMH during their migratory process, both in mice and human fetuses and we describe a novel role of AMH as a potent stimulator of GnRH cell motility. Finally, we show that pharmacological or genetic invalidation of Amhr2 signaling in vivo alters GnRH migration and the projections of VNN/TN to the basal forebrain, which results into a reduced size of this neuronal population in adult brains, altered ovulation and fertility. The involvement of the AMH signaling pathway in GnRH ontogeny and secretion led to the identification of four heterozygous loss-of-function mutations in *AMH* and *AMHR2* among 136 CHH patients. Collectively, this study identified a novel embryonic role of AMH in the development and function of GnRH neurons and provides genetic evidence that disturbance of AMH signaling can contribute to CHH phenotype in humans.

Results

Amh is expressed by GnRH migratory cells in mouse and human fetuses

We have recently shown that migratory GnRH neurons and developing vomeronasal/olfactory axons express Amhr2 in mammals (**Cimino et al., 2016**). In this study, we investigated whether migratory GnRH neurons expressed Amh in addition to Amhr2. In order to do so, we first isolated GnRH neurons through fluorescence activated cell sorting (FACS) from *Gnrh1 <GFP>* embryos (**Spergel et al., 1999**) at embryonic day 12.5 (E12.5), coincident with the beginning of the GnRH neuronal migratory process (**Wray et al., 1989**; **Schwanzel-Fukuda and Pfaff, 1989**), at postnatal day 12 (PN12) and at postnatal day 90 (PN90; **Figure 1a,b**). These experiments revealed expression of *Amh* already at E12.5 both in GnRH neurons and in total head extracts (**Figure 1a**). Moreover, real-time PCR experiments showed increasing expression of *Amh* in GnRH neurons from early embryonic development (E12.5) to adult life (PN90; **Figure 1a,b**).

Ex vivo cultures of embryonic nasal explants have been used to study factors regulating GnRH migration by both our group (**Giacobini et al., 2004**; **Giacobini et al., 2007**) and others (**Fueshko and Wray, 1994**). At 4 days in vitro, olfactory axons, which express βIII−tubulin (TUJ1), emerge from the nasal explant tissue mass and GnRH neurons begin migrating out from the explant, tightly associated to those fibers (**Figure 1c**). We generated nasal explants from *Gnrh1 <GFP>* embryos and we immunostained these primary cultures using an antibody directed against the biologically active form of Amh (C-terminal region; **Figure 1d–f**). These experiments revealed the

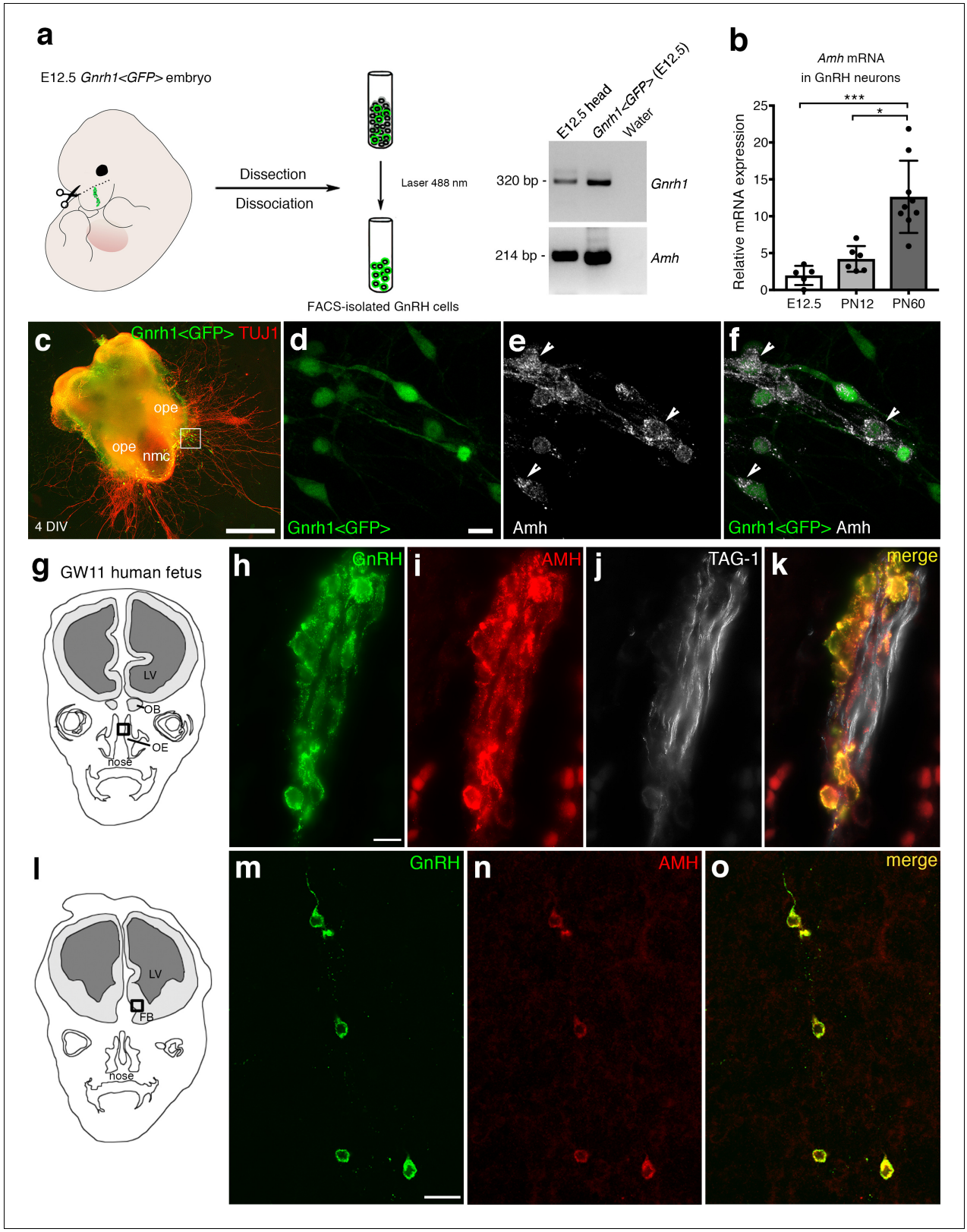

Figure 1. AMH is expressed in migratory GnRH neurons in mouse and human fetuses. (**a**) Schematic illustrates isolation of *Gnrh1 <GFP>* expressing cells in the nasal region of embryonic day 12.5 animals (E12.5) through fluorescent activated cell sorting (FACS). Gel on the right-hand side is a representative qualitative PCR depicting *GnRH* and *Amh* expression in migratory GnRH cells and in the head of E12.5 *Gnrh1 <GFP>* embryos. (**b**) Quantitative analysis of *Amh* mRNA expression in FACS-isolated GnRH neurons at E12.5 (n = 5), postnatal day 12 (PN12, n = 6) and postnatal day 60

Figure 1 continued on next page

Figure 1 continued

(PN60, *n* = 9). Data are represented as median values with the 25th-75th percentile range. Comparisons between groups were performed using a Kruskal-Wallis test followed by Dunn's post hoc analysis. *p=0.0398, ***p=0.0006. (**c**) Representative image of a nasal explant (out of *n* = 3) generated from a *Gnrh1 <GFP>* embryo and cultured for 4 days (DIV: days in vitro) before immunostaining for tubulin βIII (TUJ1, red). (**d–f**) Higher magnification picture of inset in **d**) showing migratory GFP-positive GnRH neurons (green) expressing Amh (white). (**g**) Schematic representation of a GW11 human fetus head (coronal view) illustrating the nasal area (box) used for immunofluorescence. (**h–k**) GnRH (green), AMH (red) and TAG-1 (white) expression in a coronal section of a GW11 fetus (out of *n* = 2 GW11 fetuses, females). AMH is expressed in GnRH neurons but not on vomeronasal/terminal fibers. (**l**) Schematic representation of a GW11 human fetus head (coronal view) illustrating the forebrain area (box) used for immunofluorescence. (**m–o**) AMH is expressed in GnRH neurons that are migrating in the forebrain. NMC: nasal midline cartilage; OPE: olfactory placode epithelium; VNO: vomeronasal organ; OE: olfactory epithelium; OB: olfactory bulb; FB: forebrain; LV: lateral ventricle. Scale bars: (**c**) 500 μm; (**d–f**) 10 μm; (**h–k**) 10 μm; (**m–o**) 20 μm.

DOI: https://doi.org/10.7554/eLife.47198.002

The following source data is available for figure 1:

Source data 1. This spreadsheet contains the normalized values used to generate the bar plots shown in ***Figure 1b***.

DOI: https://doi.org/10.7554/eLife.47198.003

presence of Amh-immunoreactivity in punctated structures resembling vesicles (arrowheads in ***Figure 1e,f***) in migratory neurons.

In order to determine whether this expression pattern was evolutionarily conserved, we next evaluated the expression of AMH in GnRH neurons and along their migratory route during human fetal development at 11th gestational week (GW11) (see schematics in ***Figure 1g,l***). Triple-immunofluorescence staining of coronal sections of GW11 fetuses (*n* = 2 females) revealed that AMH is expressed in GnRH neurons but not on the vomeronasal/terminal nerves (TAG-1-positive) that form the migratory scaffold for GnRH neurons (***Figure 1h–k***). We further evaluated whether AMH expression was retained by all GnRH neurons that entered the brain (***Figure 1m–o***). Interestingly, at this developmental stage the only neurons expressing AMH in the forebrain were the GnRH neuroendocrine cells (***Figure 1m–o***). These data show that GnRH neurons start expressing Amh during their migratory process and maintain this expression until adulthood.

Pharmacological and genetic invalidation of Amhr2 disrupts GnRH neuronal migration and the olfactory axonal scaffold

Given the expression pattern of Amh and Amhr2 along the GnRH migratory pathway (***Cimino et al., 2016***), we next investigated whether Amh could play a role on the development of the GnRH and olfactory/vomeronasal system. As the expression of Amhr2 is a prerequisite for tissues to be responsive to the actions of Amh, we investigated whether acute pharmacological blockade of the receptor with an Amhr2 neutralizing antibody (Amhr2-NA) affects the development of the olfactory, vomeronasal and terminal systems and the GnRH migration. This was achieved by in utero injection of Amhr2-NA delivered into the olfactory pit of E12.5 embryos at the beginning of the migratory process, and subsequent analysis of GnRH migration and its axonal scaffold 48 hr later (***Figure 2a***). Correct injection site in the olfactory pits was validated using the Fluorogold tracer (***Figure 2b***).

We analyzed the number and distribution of GnRH neurons in E14.5 embryos, when the GnRH population is equally distributed in the nose and in the forebrain (***Wray et al., 1989***; ***Schwanzel-Fukuda and Pfaff, 1989***). At this stage, in control embryos GnRH neurons were located in the nose at the levels of the nasal/forebrain junction (N/FB J) and in the ventral forebrain (vFB; ***Figure 2c,e***). Notably, while GnRH cells normally turn ventrally toward the basal forebrain in control embryos (***Figure 2c,e***), in Amhr2-NA embryos fewer neurons reached the vFB region (***Figure 2d,f***) and several GnRH cells were found scattered in ectopic cortical regions (***Figure 2d***, arrows). At E14.5, the total number of GnRH neurons was comparable between control and Amhr2-NA-treated embryos (***Figure 2g***), indicating that Amhr2 neutralization had no effect on GnRH neuron survival. However, a significant accumulation of GnRH cells in the nasal compartment, concomitant to decreased cell numbers within the vFB, is suggestive of a delayed GnRH cell migration in Amhr2-NA injected embryos (***Figure 2h***).

Immunolabeling with peripherin, a neuron-specific intermediate filament protein expressed by rodent sensory and autonomic axons (***Parysek and Goldman, 1988***), including the developing olfactory nerve (ON) and VNN (***Casoni et al., 2016***; ***Fueshko and Wray, 1994***), was used to assess the development of the ON and VNN at E14.5 (***Figure 2c–f***). ON/VNN development progressed as

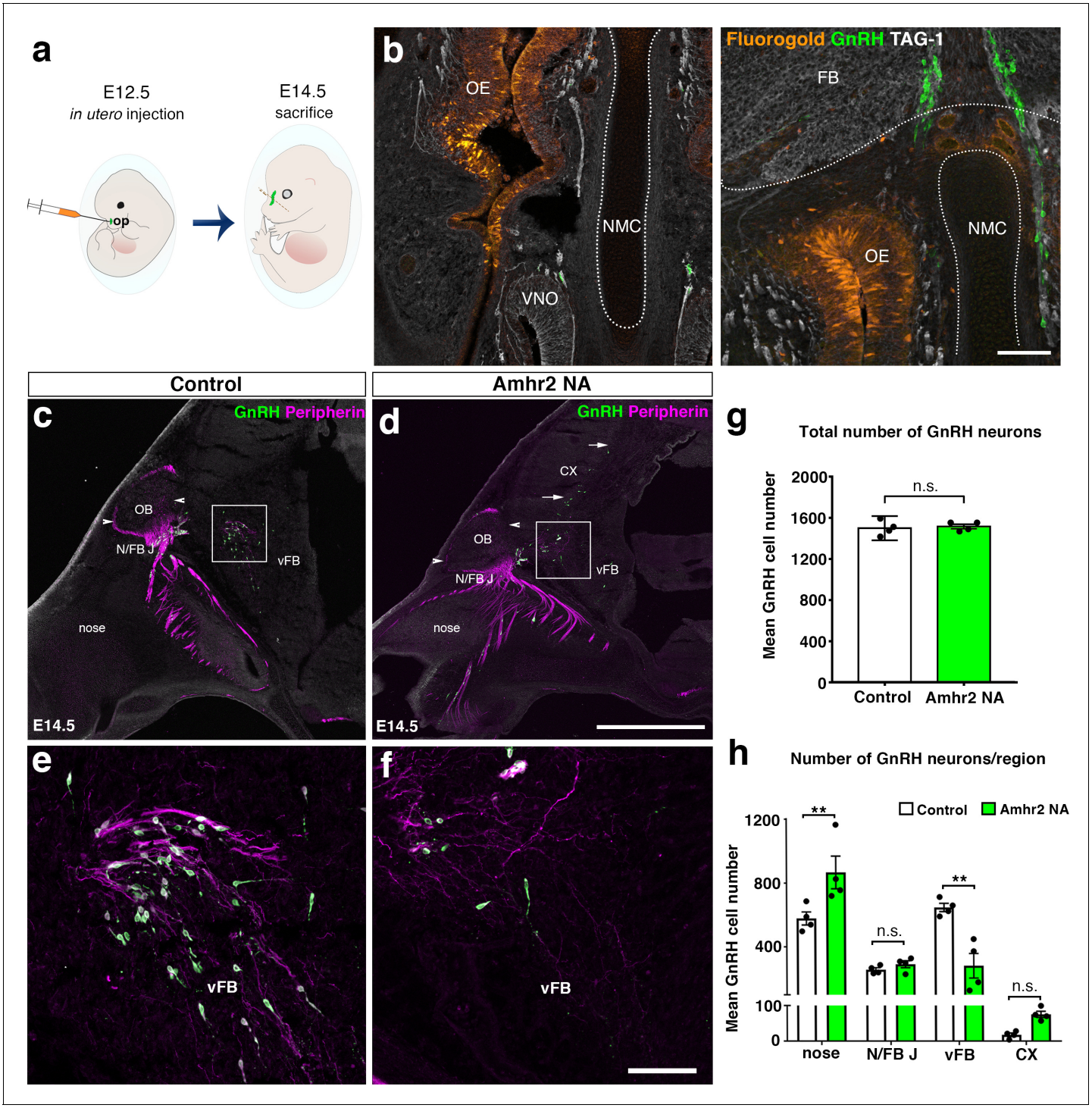

Figure 2. In utero pharmacological invalidation of Amhr2 disrupts GnRH neuronal migration and the olfactory/terminal nerve targeting. (**a**) Schematic of in utero injections targeting the olfactory pits. Injections were performed at E12.5 and embryos harvested 48 hr later. (**b**) Representative coronal section of an embryo head at E14.5 showing that olfactory pit Fluorogold delivery at E12.5 was successful. GnRH immunoreactive neurons are shown in green. (**c–f**) Representative photomicrographs of sagittal sections of mouse embryos injected at E12.5 with either saline or a neutralizing antibody for Amhr2 (Amhr2-NA) and immunostained for GnRH (green) and Peripherin (magenta) at E14.5. (**e, f**) Higher magnification confocal photomicrograph of boxed areas in **c** and **d**. (**g**) Quantification of the total number of GnRH immunoreactive neurons in saline-injected (control) and Amhr2-NA injected embryos (n = 4 for both groups, harvested from two independent dams). Data are represented as mean ± s.e.m (n = 4, unpaired two-tailed Student's t test: mean cell number, t_6 = 0.3796, p=0.7173). (**h**) Quantitative analysis of GnRH neuronal distribution throughout the migratory pathway in the two experimental groups. Data are represented as mean ± s.e.m (n = 4, two-way ANOVA, $F_{3,24}$ = 15.09, p<0.0001; followed by Holm-Šídák multiple

Figure 2 continued on next page

Figure 2 continued

comparison *post hoc* test, **p<0.005; n.s., not significant; N/FB J *Amhr2*$^{+/+}$ vs. N/FB J *Amhr2*$^{-/-}$p=0.99, CX *Amhr2*$^{+/+}$ vs. CX *Amhr2*$^{-/-}$p=0.88). Cx: cortex; FB: forebrain; N/FBJ: nasal/forebrain junction; oe: olfactory epithelium; NMC: nasal mesenchyme. Scale bars: (**b**) 100 µm; (**d**) 2.5 mm; (**f**) 50 µm.

DOI: https://doi.org/10.7554/eLife.47198.004

The following source data is available for figure 2:

Source data 1. This spreadsheet contains the values used to generate the bar plots shown in ***Figure 2g and h***.

DOI: https://doi.org/10.7554/eLife.47198.005

previously reported (***Yoshida et al., 1995***) in saline injected groups (Control); however, abnormal ON/VNN targeting occurred in embryos injected with Amhr2-NA. In these embryos, the axonal innervation of the olfactory bulb (OB) appeared incomplete as compared to controls (***Figure 2c,d***, arrowheads). This difference in axonal targeting was especially evident for the intracranial branch of the VNN projecting to the ventral forebrain (vFB; boxes in ***Figure 2c,d***). In control animals, normal targeting of peripherin-positive fibers was seen as they turn ventrally to target the hypothalamus (***Figure 2e***), whereas in Amhr2-NA injected embryos the fibers had a scattered appearance (***Figure 2f***) and failed to penetrate properly into the vFB.

In light of these results, we sought to determine whether genetic invalidation of *Amhr2* would lead to similar defects. We performed a detailed analysis of E13.5 wild type and *Amhr2*$^{-/-}$ embryos using whole mount immunostaining for GnRH and peripherin followed by iDISCO tissue-clearing (***Renier et al., 2014***) and light sheet microscopy (LSM) (***Figure 3a***; ***Figure 3—video 1***). In *Amhr2*$^{+/+}$ embryos, peripherin-positive fibers were seen to innervate almost completely the OB (***Figure 3b, f, h and j***, arrowheads), whereas in *Amhr2*$^{-/-}$ mice olfactory axons only partially innervated their target tissues (***Figure 3c, g, i and k***, arrowheads). Moreover, whereas in *Amhr2*$^{+/+}$ embryos GnRH neurons entered the brain along the TN projections and migrated to the ventral forebrain (vFB; ***Figure 3d and j***, arrows), in *Amhr2*$^{-/-}$ embryos GnRH neurons appeared more clustered in the nasal compartment, stuck in proximity to the VNO, and fewer GnRH cells reached the vFB at this embryonic stage (***Figure 3e and k***, arrows).

Altogether, these experiments revealed that pharmacological or genetic invalidation of Amhr2 leads to abnormal development of the olfactory system, aberrant intracranial projections of the vomeronasal nerve (terminal nerve) and defective GnRH migration to the basal forebrain.

Adult *Amhr2*-deficient mice show decreased GnRH cell number, LH secretion and fertility

To determine whether the delayed GnRH migratory process observed in *Amhr2* deficient embryos would result in a reduced number of GnRH neurons in adulthood, we immunostained for GnRH brains harvested from adult *Amhr2*$^{+/+}$ and *Amhr2*$^{-/-}$ animals. Knock-out mice had decreased GnRH immunoreactivity at the level of the organum vasculosum laminae terminalis (OVLT; ***Figure 4a–d***, arrows), where the majority of GnRH cell bodies are located, as well as in the median eminence (ME) of the hypothalamus (***Figure 4e–h***), which is the projection site of neuroendocrine GnRH cells. When we counted the total number of GnRH-positive cells in *Amhr2*$^{+/+}$, *Amhr2*$^{+/-}$ and *Amhr2*$^{-/-}$ female brains, we found no difference between wild type and heterozygous mice, while we observed a significant 40% reduction in GnRH cell number in *Amhr2*$^{-/-}$ mice as compared to the other genotypes (***Figure 4i***). Male and female homozygous animals showed a similar GnRH cell loss as compared to sex-matched wild-type littermates (***Figure 4—figure supplement 1***).

Since LH secretion is an indirect measurement of GnRH neuronal secretion, we measured LH in adult female mice. Circulating LH was found to be significantly lower in *Amhr2*$^{+/-}$ and *Amhr2*$^{-/-}$ animals as compared to wild-type littermates (***Figure 4j***), supporting an impairment of GnRH secretion in these animals. However, only *Amhr2*$^{-/-}$ mice exhibited reduced ovulation, as shown by the presence of fewer post-ovulation corpora lutea in the ovaries of *Amhr2*$^{-/-}$ mice as compared to *Amhr2*$^{+/-}$ and wild-type animals (***Figure 4k***).

We then evaluated LH pulsatility by serial blood sampling in female diestrous mice (***Figure 4l,m***) and found that both *Amhr2*$^{+/-}$ and *Amhr2*$^{-/-}$ animals had a significantly lower LH pulse frequency as compared to wild-type littermates. This is suggestive of an alteration in the hypothalamic network activity in *Amhr2* transgenic animals.

Figure 3. GnRH migration and olfactory innervation are perturbed in *Amhr2*$^{-/-}$ mice. (**a**) Schematic representation depicting whole-body iDISCO experiments in E13.5 *Amhr2*$^{+/+}$ and *Amhr2*$^{-/-}$ embryos. E13.5 embryos (n = 2 per genotype) were immunolabelled for Peripherin and GnRH, rendered optically transparent using iDISCO and imaged with a light-sheet microscope (LSM). (**b, c**) Frontal projection of the embryo heads, arrowheads indicate noticeable differences in Peripherin-positive fibers innervating the olfactory bulb (OB). Lateral projection views (**d, e**) showing defective GnRH migration and terminal nerve projections to the ventral forebrain (vFB, arrows). (**f, g**) Higher magnification photomicrographs depicting olfactory axon innervations of the right OB shown in **b** and **c**. Dotted circles define the anatomical border of the OB. (**h, i**) 3D rendering of figures in **f** and **g**. Arrowheads indicate observed differences in olfactory axon innervation between *Amhr2*$^{+/+}$ and *Amhr2*$^{-/-}$ embryos. (**j, k**) 3D rendering of peripherin and GnRH staining observed from a lateral projection in a representative *Amhr2*$^{+/+}$ and *Amhr2*$^{-/-}$ embryo. Cx: cortex; VNO: vomeronasal organ. Scale bars: (**b**) 400 µm; (**d**) 300 µm; (**f**) 130 µm.

DOI: https://doi.org/10.7554/eLife.47198.006

The following video is available for figure 3:

Figure 3—video 1. Light-sheet fluorescence microscopy video of solvent-cleared E13.5 *Amhr2*$^{+/+}$ and *Amhr2*$^{-/-}$ embryos immunostained *in toto* for GnRH (green) and peripherin (red).

DOI: https://doi.org/10.7554/eLife.47198.007

Finally, we tested fertility of *Amhr2* transgenic female and male mice by performing a constant breeding protocol over three months. We paired either *Amhr2*$^{+/+}$ sexually experienced males with females belonging to the three different genotypes and, inversely, we paired *Amhr2*$^{+/+}$ females with *Amhr2*$^{+/-}$ or *Amhr2*$^{-/-}$ males (***Figure 4n***). We found a significant impairement of fertility in both *Amhr2*$^{-/-}$ and *Amhr2*$^{+/-}$ females, as indicated by fewer litters per months, by fewer pups per litter and by a significant delay in the first litter after pairing as compared to *Amhr2*$^{+/+}$ females (***Figure 4n***). Heterozygous females displayed an intermediate phenotype between *Amhr2*$^{+/+}$ and *Amhr2*$^{-/-}$ mice, since all fertility measurements revealed statistically significant differences between *Amhr2*$^{+/-}$ and *Amhr2*$^{+/+}$ mice and between *Amhr2*$^{+/-}$ and *Amhr2*$^{-/-}$ mice (***Figure 4n***).

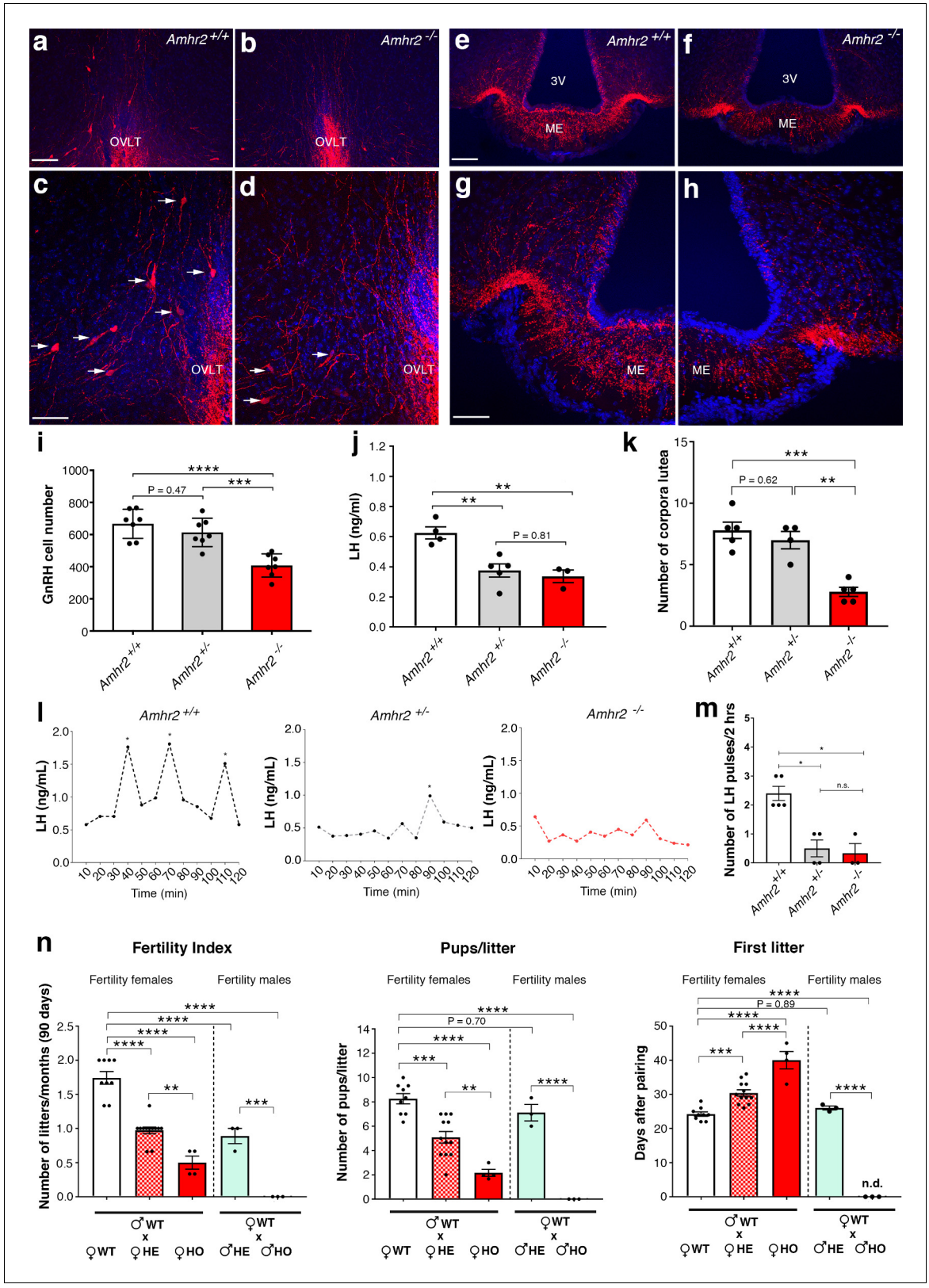

Figure 4. *Amhr2* mutant mice show reduced GnRH cell number and impaired LH secretion and fertility. (**a–h**) Immunolabelling of GnRH (red staining) in adult wild type and *Amhr2*$^{-/-}$ adult female mice (P90–P120). The majority of GnRH cell bodies are located at the level of the organum vasculosum laminae terminalis (OVLT) in both *Amhr2* $^{+/+}$ and *Amhr2* $^{-/-}$ mice, (arrows (**c, d**). (**e–h**) GnRH fiber projections at the level of the median eminence. (**i**) Total mean GnRH population in *Amhr2*$^{+/+}$, *Amhr2*$^{+/-}$ and *Amhr2*$^{-/-}$ adult female mice brains (3–4 months old). Comparisons between groups were

Figure 4 continued on next page

Figure 4 continued

performed using one-way ANOVA followed by Tukey's post hoc test (n = 7 for all groups, $F_{2,18}$ <0.0001; *Amhr2*$^{+/+}$ vs *Amhr2*$^{+/-}$ P = 0.4716; WT vs. *Amhr2*$^{-/-}$p<0.0001, *Amhr2*$^{+/-}$ vs *Amhr2*$^{-/-}$p=0.0007). (**j**) Plasma LH levels in adult mature (4–6 months old) diestrous females (*Amhr2*$^{+/+}$, n = 4; *Amhr2*$^{+/-}$, n = 5; *Amhr2*$^{-/-}$ n = 3). Statistical analysis was performed by one-way ANOVA ($F_{2,9}$ = 12.64, p=0.0024) followed by Tukey's multiple comparison post hoc test (*Amhr2*$^{+/+}$ vs. *Amhr2*$^{+/-}$ P = 0.005; *Amhr2*$^{+/+}$ vs. *Amhr2*$^{-/-}$p=0.046, *Amhr2*$^{+/-}$ vs. *Amhr2*$^{-/-}$p=0.8164). (**k**) Quantitative analyses of the mean number of corpora lutea (CL) in *Amhr2*$^{+/+}$ (n = 5), *Amhr2*$^{+/-}$ (n = 4) and *Amhr2*$^{-/-}$ (n = 5) adult ovaries (4–6 months old). Statistical significance between groups was assessed using one-way ANOVA ($F_{2,11}$ = 22.11, p=0.0001) followed by Tukey's multiple comparison *post hoc* test (*Amhr2*$^{+/+}$ vs. *Amhr2*$^{+/-}$ P = 0.6259; *Amhr2*$^{+/+}$ vs. *Amhr2*$^{-/-}$p=0.0002 and *Amhr2*$^{+/-}$ vs. *Amhr2*$^{-/-}$p=0.0012). (**l**) Representative graphs for LH pulsatility in female dioestrous adult mice of the corresponding genotype. Asterisks indicate the number of LH pulses per 2 hr interval. (**m**) Number of LH pulses in adult (P60) diestrous females (*Amhr2*$^{+/+}$, n = 5; *Amhr2*$^{+/-}$, n = 4; *Amhr2*$^{-/-}$ n = 3). Statistical analysis was performed by non-parametric Kruskal-Wallis test p=0.0028 (*Amhr2*$^{+/+}$ vs. *Amhr2*$^{+/-}$ P = 0.041; *Amhr2*$^{+/+}$ vs. *Amhr2*$^{-/-}$p=0.038 and *Amhr2*$^{+/-}$ vs. *Amhr2*$^{-/-}$p>0.999). (**n**) Bar graphs illustrating the results of the constant mating protocol performed over 90 days on the following groups: (♀*Amhr2*$^{+/+}$ x ♂*Amhr2*$^{+/+}$, n = 9; ♀*Amhr2*$^{+/-}$ x ♂*Amhr2*$^{+/+}$, n = 12; ♀*Amhr2*$^{-/-}$ x ♂*Amhr2*$^{+/+}$, n = 4; ♀*Amhr2*$^{+/+}$ x ♂*Amhr2*$^{+/-}$, n = 3; ♀*Amhr2*$^{+/+}$ x ♂*Amhr2*$^{+/-}$, n = 3. Female and male mice were 4–6 months-old). Comparisons between groups were performed using one-way ANOVA (fertility index, $F_{4,26}$ = 51.47, p<0.0001; first litter, $F_{4,26}$ = 88.82, p<0.0001; pups per litter, $F_{4,26}$ = 29.67 P<0.0001) followed by Tukey's multiple comparison post hoc test, *p<0.05; **p<0.005; ***p<0.0005; ****p<0.0001. Each cluster of data points represents a different mouse. Data were combined from three independent experiments. Throughout the figure, data are displayed as mean ± s.e.m. *p<0.05; **p<0.005; ***p<0.0005; ****p<0.0001. Scale bars: (**a, b, e, f**) 100 μm; (**c, d, g, h**) 50 μm.

DOI: https://doi.org/10.7554/eLife.47198.008

The following source data and figure supplements are available for figure 4:

Source data 1. This spreadsheet contains the values used to generate the bar plots shown in ***Figure 4i j, k, m, n***.

DOI: https://doi.org/10.7554/eLife.47198.011

Figure supplement 1. GnRH cell number in *Amhr2* wild-type and knock-out animals as a function of sex.

DOI: https://doi.org/10.7554/eLife.47198.009

Figure supplement 1—source data 1. This spreadsheet contains the values used to generate the bar plots shown in ***Figure 4—figure supplement 1***.

DOI: https://doi.org/10.7554/eLife.47198.010

In heterozygous males, only the number of litters/90 days was found to be significantly reduced as compared to *Amhr2*$^{+/+}$ males (***Figure 4n***). *Amhr2*$^{-/-}$ males are completely infertile (***Figure 4n***), in agreement with previous reports showing that inactivation of *Amhr2* or *Amh* in humans and mice leads to persistent Müllerian duct syndrome (***Imbeaud et al., 1995***; ***Mishina et al., 1996***).

Taken together, these data support the physiological relevance of Amh signaling both in the development and homeostasis of the hypothalamic-pituitary-gonadal axis.

AMH increases GN11 cell migration via the Amhr2/Bmpr1b signaling pathway

The manipulation of the GnRH migratory system and functional experimentation on these neurons have been challenging because of their limited number (800 in rodents) and anatomical dispersal along their migratory route. The generation of immortalized GnRH neurons (GN11 and GT1-7 cell lines [***Radovick et al., 1991***; ***Mellon et al., 1990***]) has permitted the study of immature migratory (GN11 cells), and mature post-migratory (GT1-7 cells) GnRH neurons, respectively.

To assess whether immortilized GnRH cell lines retain expression of *Amh* and *Amh* receptors, RT-PCR analysis was performed (***Figure 5a***). Our data show that both GN11 and GT1-7 cells express *Amh* and *Amhr2*, even though the transcript levels were significantly higher in GT1-7 cells as compared to GN11 cells (***Figure 5a***). These data are consistent with our current (***Figure 1c***) and previous findings (***Cimino et al., 2016***) obtained from GnRH sorted cells. As for the Amh-type one receptors, both cell lines express *Acvr1* and *Bmpr1a*, with GT1-7 cells displaying higher levels of expression compared to GN1 cells (***Figure 5a***). Interestingly, GN11 cells, but not GT1-7 cells, express *Bmpr1b* (***Figure 5a***), indicating that Amhr2/Bmpr1b signaling maybe a putative hallmark of migratory GnRH neurons. These results point to the GN11 cell line as an appropriate in vitro model to test the functional role of Amh on cell motility.

Activation of the MAPK pathway (phosphorylation of ERK1/2) has been previously associated with increased GN11 cell motility (***Messina et al., 2011***; ***Hanchate et al., 2012***). Here, we found that AMH, at concentrations previously reported to be functional in other cell lines (***Garrel et al., 2016***), significantly increased the phosphorylation of ERK1/2 in GN11 cells in a dose- and time-dependent manner (***Figure 5b,c***). The AMH-dependent activation of MAPK pathway was prevented by the pharmacological blockage of Amhr2 (AMHR2 neutralizing antibody; AMHR2-NA; ***Figure 5b***).

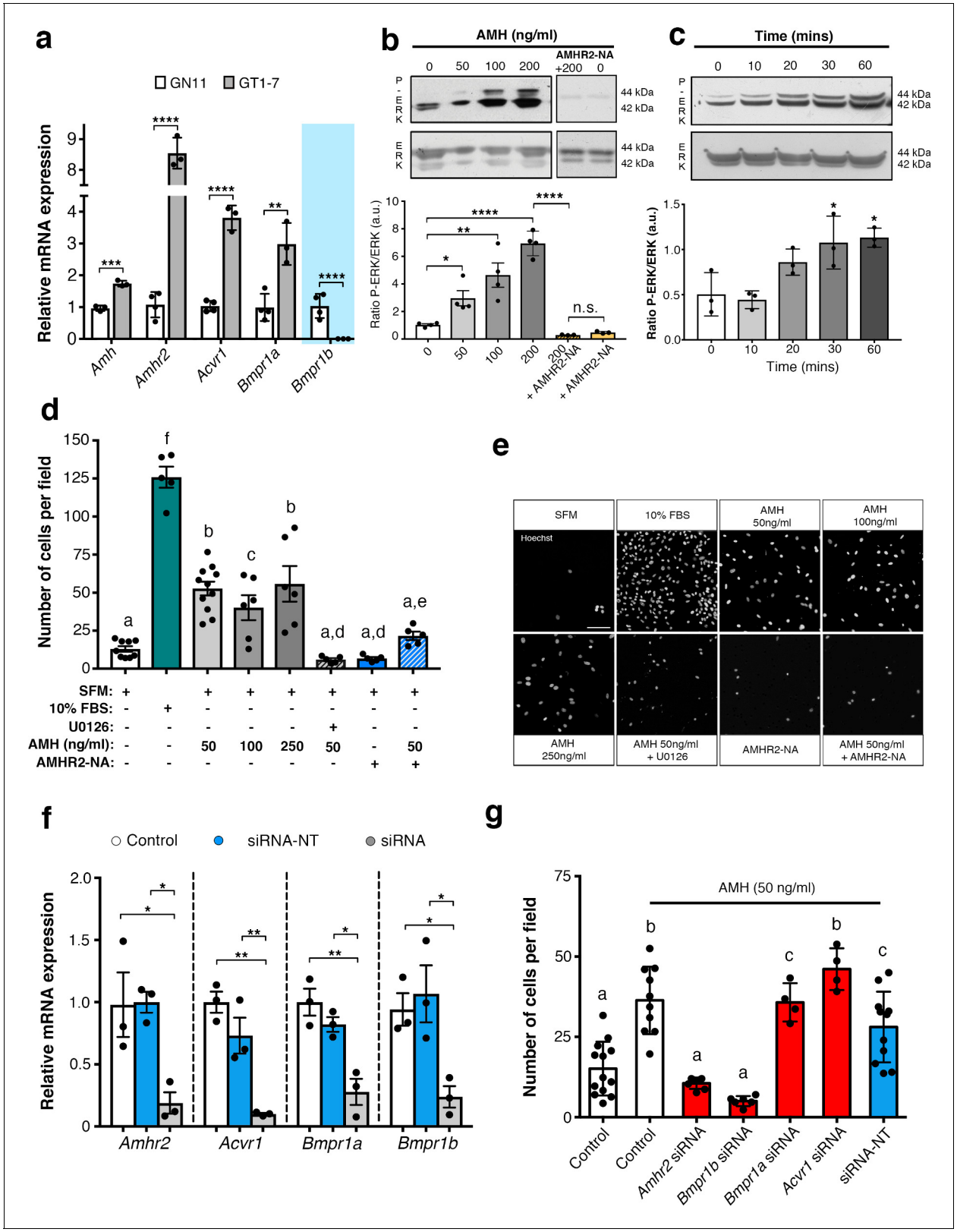

Figure 5. AMH promotes GnRH cell motility via Amhr2 and Bmpr1b signaling. (**a**) Quantitative RT-PCR analysis for *Amh*, *Amhr2*, *Acvr1* (Activin Receptor1; ALK2), *Bmpr1a* (Bone Morphogenetic Protein Receptor1a; ALK3) and *Bmpr1b* (Bone Morphogenetic Protein Receptor1b; ALK6) mRNA in GN11 (n = 4) and GT1-7 (n = 3) cells. Comparisons between treatment groups were performed using unpaired two-tailed Student's t test (*Amh* t_5 = 1.139, p=0.0004; *Amhr2* t_5 = 1.6, p<0.0001; *Acvr1* t_5 = 5.044, p<0.0001); *Bmpr1a* t_5 = 2.374, p<0.0044. (**b**) Representative western blot showing P-ERK1/2

Figure 5 continued on next page

Figure 5 continued

and total ERK1/2 in cell lysates of GN11 cells stimulated with indicated doses of AMH (n = 4). Right boxed figure is a representative blot showing P-ERK1/2 and total ERK1/2 in cell lysates of GN11 cells stimulated with anti-Amhr2 neutralizing antibody with or without 200 ng/ml of AMH (Amhr2-NA, n = 3 per condition). Bar graph illustrates the mean ratio P-ERK1/2 over total ERK1/2 (n = 4 for all except AMHR2-NA and AMHR2-NA + AMH 200 ng/ml, n = 3). Comparisons between treatment groups were performed using a two-way ANOVA ($F_{6,19}$ = 29.11, p<0.0001; followed by Holm-Šídák's multiple comparison post hoc test. Adjusted p values: 0 vs. 50 = 0.0461, 0 vs 100 = 0.0003, 0 vs 200 =<0.0001, 200 vs AMHR2-NA + 200 = <0.0001, 0 vs AMHR2-NA =>0.9999). (**c**) Representative western blot showing P-ERK1/2 and total ERK1/2 in cell lysates of GN11 cells stimulated with 50 ng/ml of AMH for the indicated times (minutes: min). Bar graph illustrates the mean ratio P-ERK1/2 over total ERK1/2 (n = 3 for all). Comparisons between treatment groups were performed using a one-way ANOVA ($F_{4,10}$ = 8.171, followed by Tukey's multiple comparison post hoc test. Adjusted p values: 0 vs. 10 = 0.9945, 0 vs. 20 = 0.2333, 0 vs. 30 = 0.0292, 0 vs. 60 = 0.0170). (**d**) Schematic representation on top of the graph bar illustrates the transwell assay used to assess cell motility in d, e, g, whereby AMH was placed on the top and lower chamber. Bar graph illustrates the mean number of migrated GN11 cells stimulated with serum free medium (SFM, basal conditions, n = 9), with 10% fetal bovine serum (FBS, strong inducer of cell motility, n = 5), or with the indicated doses of AMH with or without the MAPK Kinase inhibitor, U0126 (AMH 50 ng/ml n = 11, AMH 100 ng/ml n = 6, AMH 250 ng/ml n = 6, AMH 50 ng/ml + U0126 n=5), or with Amhr2-NA with or without AMH 50 ng/ml (n = 5). One-way ANOVA, $F_{7,44}$ = 38.48, followed by Tukey's multiple comparison post hoc test. (**a**): not significantly different from **a** groups (p>0.05); **b**: significantly different from **a**) groups (p<0.0001); **c**: SFM vs AMH 100 ng/ml, p<0.05; **d**: significantly different from **b** groups (p<0.001); **e**: AMH 50 ng/ml vs AMH 50 ng/ml + AMHR2 NA, p<0.05; **f**: significantly different from every other group (p<0.0001). (**e**) Representative photomicrographs showing Hoechst nuclear staining of the migrated GN11 cells after the different treatments, scale bar = 100 µm. (**f**) Real-time PCR analysis for *Amhr2, Acvr1, Bmpr1a* and *Bmpr1b* mRNA expression in untrasfected GN11 cells (Control) or in GN11 cells transfected with siRNAs targeting Amh receptors or with a non-targeting siRNA (siRNA-NT) (n = 3). Bar graph illustrates the mean ± s.e.m; one-way ANOVA followed by Tukey's post hoc comparison test (Amhr2 $F_{2,6}$ = 7.861, Control vs siRNA p=0.0339, Control vs siRNA-NT p=0.9958, siRNA vs siRNA-NT p=0.0305; Acvr1 $F_{2,6}$ = 22.73, Control vs siRNA p=0.0015, Control vs siRNA-NT p=0.2016, siRNA vs siRNA-NT p=0.0088; Bmpr1a $F_{2,6}$ = 16.16, Control vs siRNA p=0.0038, Control vs siRNA-NT p=0.4206, siRNA vs siRNA-NT p=0.0149; Bmpr1b F $_{2,6}$ P=7.777, Control vs siRNA p=0.0478, Control vs siRNA-NT p=0.8489, siRNA vs siRNA-NT p=0.0247). (**g**) Transwell assay was performed on GN11 cells transfected or not with indicated siRNAs and stimulated with or without AMH (50 ng/ml). Bar graph illustrates the mean number of migrated GN11 cells (Control, SFM n = 13, Control +AMH 50 ng/ml n = 10, *Amhr2* siRNA +AMH 50 ng/ml n = 7, *Acvr1* siRNA +AMH 50 ng/ml n = 4, *Bmpr1a* siRNA +AMH 50 ng/ml n = 4, *Bmpr1b* siRNA +AMH 50 ng/ml n = 6, siRNA-NT +AMH 50 ng/ml n = 11). Comparisons between treatment groups were performed using a one-way ANOVA followed by Tukey's post hoc comparison test ($F_{6,48}$ = 20.99, **a** not significantly different from other groups denoted **a**, p>0.05; **b** significantly different from groups denoted **a**, p<0.0001; **c** significantly different from groups denoted **a**), p<0.05. Throughout the figure, data were combined from three independent experiments and displayed as mean ± s.e.m. *p<0.05; **p<0.005; ***p<0.0005; ****p<0.0001.

DOI: https://doi.org/10.7554/eLife.47198.012

The following source data is available for figure 5:

Source data 1. This spreadsheet contains the values used to generate the bar plots shown in ***Figure 5a, b, c, d, f and g***.

DOI: https://doi.org/10.7554/eLife.47198.013

Using transwell assays, we showed that recombinant human AMH was able to significantly increase the motility of GN11 cells at all tested doses (50 ng/ml; 100 ng/ml; 250 ng/ml) compared to controls (serum-free medium, SFM; ***Figure 5d***). In agreement with our biochemical results (***Figure 5b,c***), the AMH-dependent induction of cell motility was prevented by the selective pharmacological antagonist of MAPK pathway (U0126 inhibits MEKK1, the upstream activator of ERK) and by AMHR2-NA (***Figure 5d,e***).

We next investigated which receptor complex was required to mediate the AMH-dependent cell migration in GN11 cells. This was achieved by targeted knockdown of Amh receptors through a small interfering RNA (siRNA) strategy. GN11 cells were transfected with a pool of siRNAs specific to mouse *Amhr2*, *Acvr1*, *Bmpr1a, Bmpr1b,* or with a pool of nontargeting siRNAs (siRNA-NT). Silencing efficiency was assessed analyzing gene expression levels in untransfected cells (Control) versus GN11 cells transfected with the *Amh* receptors targeted siRNAs and siRNA-NT (***Figure 5f***).

Knockdown of individual *Amh* receptors led to distinct motility responses of GN11 cells to AMH stimulation (***Figure 5g***). Transfection with the siRNA-*Acvr1*, siRNA-*Bmpr1a* or siRNA-NC RNA did not affect the GN11 response to AMH treatment (***Figure 5g***). In contrast, knockdown of *Amhr2* and *Bmpr1b* resulted in significantly reduced GN11 cell motility in response to AMH as compared to the control groups (mock and siRNA-NC transfected cells; ***Figure 5g***).

These data show that AMH promotes GN11 cell motility through the Amhr2/Bmpr1b receptor complex and activation of the MAPK intracellular pathway.

Table 1. Summary of heterozygous *AMH* or *AMHR2* mutations identified in patients with congenital hypogonadotropic hypogonadism.

cDNA and protein changes are based on reference cDNA sequence NM_000479.4 (AMH) and NM_020547.3 (AMHR2). Functional validation of the mutants has been performed in vitro evaluating AMH secretion in COS-7 cells, cell motility in GN11 cells, and measuring GnRH secretion in GT1-7 cells for nCHH-associated mutants. CHH, congenital hypogonadotropic hypogonadism; nCHH, normosmic CHH; KS, Kallmann syndrome; Sex: F: female; M: male; Inheritance: F: familial, S: sporadic; Puberty: A: absent puberty, P: partial puberty. MAF, minor allele frequency; ↓, decreased; NS, not significant; NA, not applicable.

												In vitro studies		
Gene	Family	Subject	Diagnosis	Sex	Inheritance	Puberty	Associated phenotypes	dbSNP number	Nucleotide change	Amino acid change	MAF (%) gnomAD MaxPop	Released AMH (COS-7 cells)	Cell motility (GN11 cells)	GnRH secretion (GT1-7 cells)
AMH	1	II-1	nCHH	M	F	P	High-arched palate Deviated nasal septum Hyperlaxity	rs200226465	c.295A > T	p.Thr99Ser	0.044	↓↓	↓↓	↓↓
	2	II-1	KS	M	S	A	Cryptochidism	rs370532523	c.451C > T	p.Pro151Ser	0.011	↓↓	↓↓	
	3	II-2	KS	F	F	P	Osteoporosis Scoliosis	rs752574731	c.714C > A	p.Asp238Glu	0.006	↓↓	↓↓	
AMHR2	4	II-1	nCHH	F	S	A	Osteoporosis	rs764761319	c.1330_1356del	p.Gly445_Leu453del	0.093		↓↓	↓↓

DOI: https://doi.org/10.7554/eLife.47198.015

CHH patients harbor heterozygous *AMH* and *AMHR2* mutations

In this study, we performed whole exome sequencing in 75 KS and 61 normosmic CHH (nCHH) probands who did not harbor pathogenic mutations in known CHH genes, and identified in three probands from European descent heterozygous missense mutations in *AMH* (**Table 1**, **Figure 6a,b**). These mutations (p.Thr99Ser, p.Pro151Ser, and p.Asp238Glu) lie in the N-terminal pro-protein domain (**Figure 6a**), and all affected amino acids were highly conserved across species (**Figure 6c**). Additionally, one female with normosmic CHH (nCHH) harbors a heterozygous in-frame 27-nucleotide deletion in *AMHR2*. This p.Gly445_Leu453del deletion lies within the catalytic intracellular serine/threonine domain of the receptor, which is highly conserved among mammals (**Figure 6d–6f**).

We observed variable degrees of spontaneous puberty (absent to partial) among the probands carrying an *AMH* or *AMHR2* mutations. Two probands had KS with no other major associated non-reproductive phenotypes (**Table 1** and human case summaries in Materials and methods). All three probands with mutations in *AMH* (Families 1, 2, and 3) have a positive family history for partial phenotypes (e.g. delayed puberty, anosmia), consistent with variable expressivity (**Figure 6b**). The female proband carrying the *AMHR2* deletion (Family 4) has nCHH. Her mother, who did not carry the deletion, exhibited cleft lip/palate with normal reproduction (**Figure 6e**).

AMH and *AMHR2* mutations in CHH are loss-of-function

In order to test the functionality of the *AMH* and *AMHR2* mutants identified in KS and nCHH probands, we first transiently transfected COS-7 cells with plasmids encoding the human *AMH* wild-type (*AMH* WT) or the *AMH* variants and investigated whether the AMH secretory capacity of transfected cells was affected. All three of mutations tested (p.Pro151Ser, p.Asp238Glu, and p.Thr99Ser *AMH* mutants) showed significantly reduced AMH protein secretion in vitro (**Figure 7a** and **Table 1**), as assessed by automated chemoluminescent immunoassay.

To test the impact of *AMH* mutants on immortalized GnRH neurons' cell motility and to determine whether AMH promotes such response through an autocrine mechanism, we performed transwell migration assay on GN11 cells either treated with lipofectamine (mock), or transfected with the *AMH* WT or the *AMH* variants identified in CHH patients (**Figure 7b**). AMH overexpression (*AMH* WT) in GN11 cells significantly increased cell migration by 50% when compared with mock cells (**Figure 7b**). The AMH-dependent induction of cell motility was prevented when the cells where transfected with the mutants identified in KS patients (p.Pro151Ser and p.Asp238Glu) as well as with the mutant found in a nCHH proband (p.Thr99Ser; **Figure 7b** and **Table 1**). Moreover, since the latter *AMH* mutation was found in a male nCHH proband (LH 2.7 U/l; **Table 1**), and because we previously showed that AMH stimulates GnRH and LH secretion in rodents (**Cimino et al., 2016**), we wondered whether this mutant could also negatively impact on GnRH secretion. In order to assess that we used GT1-7 cells that express Amh type-I and type-II receptors (**Figure 5a**) and that display significant GnRH secretory activity (**Mellon et al., 1990**). GT1-7 cells were transfected with either *AMH* WT or p.Thr99Ser *AMH* and conditioned medium was collected 48 hr later for GnRH ELISA measurement. The p.Thr99Ser *AMH* variant significantly reduced GnRH secretion as compared to GT1-7 cells expressing the *AMH* WT (**Figure 7c**).

To functionally test the impact of the *AMHR2* deletion (p.Gly445_Leu453del) and determine whether this variant leads to defective AMH-induced motility, we transfected GN11 cells with a plasmid encoding the h*AMHR2* WT or the *AMHR2* p.Gly445_Leu453del mutant and performed migration assays culturing the cells with SFM alone or supplemented with recombinant human AMH protein (**Figure 7d**). Consistent with the data shown in **Figure 5**, AMH treatment significantly increased cell migration of *AMHR2* WT-transfected cells as compared with SFM (**Figure 7d**). This effect was significantly impaired when GN11 cells were transfected with the *AMHR2* mutant plasmid (**Figure 7d**). Since the *AMHR2* p.Gly445_Leu453del mutant was found in a female nCHH proband (LH <2.0 U/l; **Table 1**; human case summaries in Materials and methods), we also assessed whether AMH treatment increased GnRH release in GT1-7 cells expressing either *AMHR2* WT or the p.Gly445_Leu453del mutant (**Figure 7e**). These experiments revealed that AMH (50 ng/ml) stimulates GnRH secretion into medium of GnRH cells expressing the *AMHR2* WT, whereas introduction of the *AMHR2* mutant variant into GT1-7 cells significantly reduced the AMH-dependent GnRH secretion as compared to control conditions (**Figure 7e**).

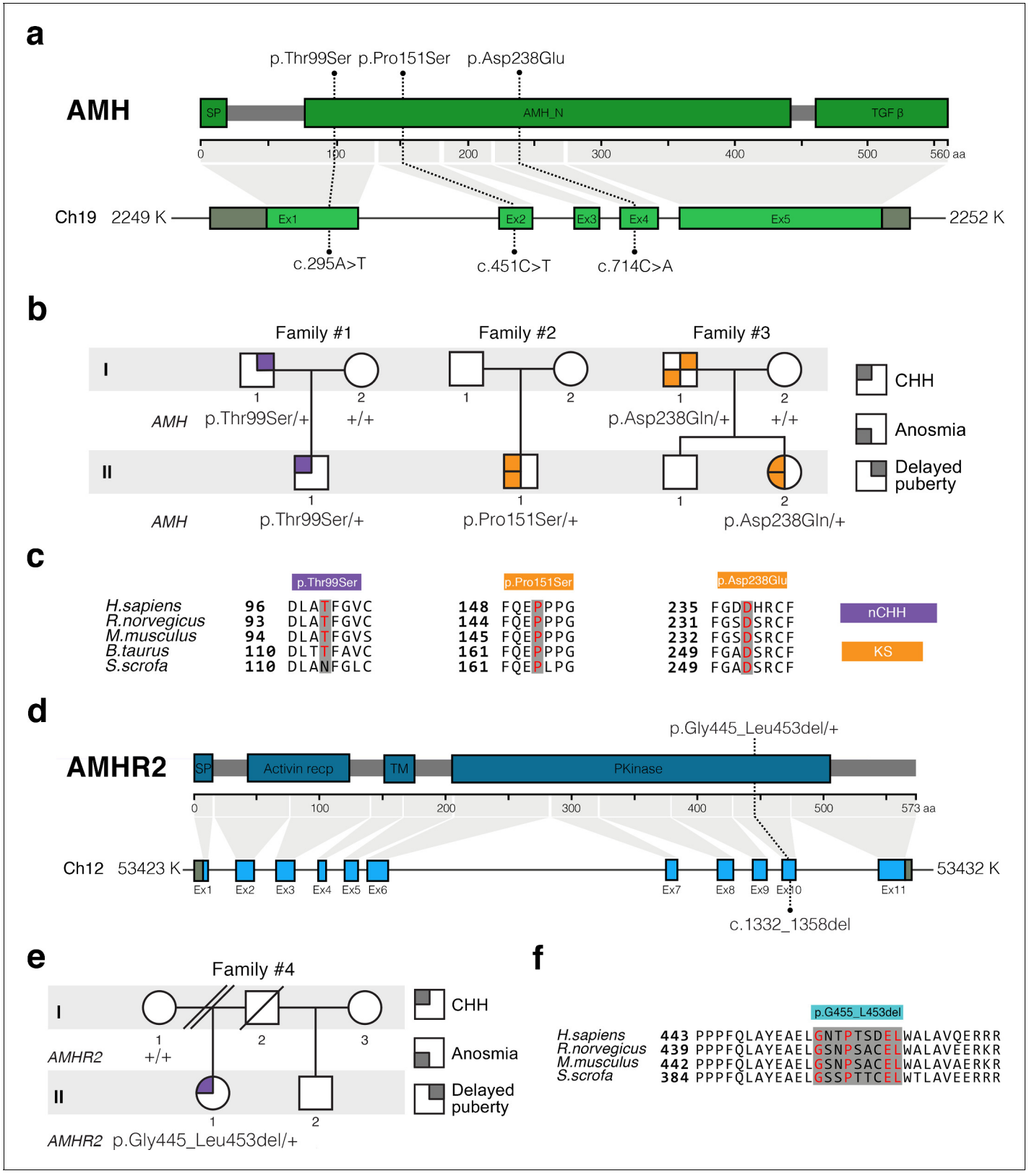

Figure 6. *AMH* and *AMHR2* heterozygous mutations in CHH probands. (**a**) Schematic illustration of *AMH* mutations in nCHH and KS probands. (**b**) Pedigrees of patients harboring *AMH* mutations. Circles denote females, squares denote males. The phenotype interpretation is explained in the square legend on the top of the figure. (**c**) The *AMH* mutations affect evolutionarily conserved amino acid residues. Alignment of partial protein sequences of *AMH* orthologs showing in red text the amino acid residues evolutionarily conserved. Purple highlights correspond to variants identified

Figure 6 continued on next page

Figure 6 continued

in nCHH probands and orange highlights correspond to variants identified in the KS cohort. (**d**) Schematic of the AMHR2 signal peptide (SP), activin receptor, transmembrane and kinase functional domains along with the p.Gly445_Leu453del variant identified in the cohort. This deletion lies within the catalytic intracellular serine/threonine kinase domain (PKinase) of the receptor. (**e**) Pedigree of the patient harboring the deletion in *AMHR2*. Circles denote females, squares denote males, double diagonal lines indicate divorce, single diagonal line indicates death. The phenotype interpretation is explained in the square legend on the top of the figure. (**f**) Alignment of partial protein sequences of mammalian AMHR2 orthologs flanking the deletion site.

DOI: https://doi.org/10.7554/eLife.47198.014

Finally, to evaluate the structural impact of the AMHR2 deletion (p.Gly445_Leu453del), a three-dimensional structural model of the corresponding mutated catalytic intracellular serine/threonine domain of the receptor was generated (DEL), as previously described (***Belville et al., 2009***). The model of the WT AMHR2 kinase domain presents a general fold of a two-domain kinase, with an N-lobe mainly composed of a five-stranded β-sheet and a mostly α-helical C-lobe. The deleted residues are located at the top of the C-lobe and are part of the αG helix and its preceding loop (***Figure 7f***). In both WT and DEL, the overall protein structure remains stable (***Figure 7—figure supplement 1***). Analysis of the interactions established in this zone reveals differences between the *AMHR2*-WT and the *AMHR2* p.Gly445_Leu453del mutant models. In the WT model, the structure is stabilized by hydrophobic interactions involving Leu444, Leu456 and Leu453, as well as by the hydrogen bonds Arg462-Glu443, Arg463-Tyr440 and Gln446-Glu441. For the *AMHR2* p.Gly445_Leu453del mutant model, the structure is stabilized mainly by hydrogen bonds: Arg462-Glu443, Arg462-Glu460 and Arg463-Tyr440 (***Figure 7—figure supplement 2***). The main structural fluctuations are observed in the loop regions of the proteins (***Figure 7g–i***). Comparison of *AMHR2* WT and *AMHR2* p.Gly445_Leu453del mutant simulations (***Figure 7g–i***) suggests there may be some differences in the dynamic behavior of some of these flexible regions, including the kinase activation loop. In summary, although *AMHR2* mutant tertiary structure is expected to be folded in a similar manner to that of the WT species, it is possible that the deletion results in some alterations in the intracellular signaling.

Taken together, these in vitro results confirm that the identified AMH and AMHR2 mutants are loss-of-function, supporting the role of AMH/AMHR2 signaling in GnRH neuronal migration and GnRH secretion and thus pointing toward a potential contribution of these variants to the pathogenesis of CHH.

Discussion

Originally identified in the mesenchyme of Müllerian ducts and in gonads (***Josso et al., 1998***), Amh and Amhr2 were subsequently documented in several other organs, including the brain (***Lebeurrier et al., 2008***; ***Wang et al., 2009***; ***Cimino et al., 2016***; ***Wang et al., 2005***) and the pituitary (***Garrel et al., 2016***), suggesting that Amh biological effects could be much broader than initially thought.

We recently reported Amhr2 expression in migratory GnRH neurons and along olfactory axons, both in mice and human fetuses (***Cimino et al., 2016***). In this study, we showed that GnRH neurons express Amh during fetal development and that this expression is retained both in rodents and humans. Our in vivo and in vitro analyses show that Amh signaling regulates migration of GnRH neurons toward the brain through an autocrine mechanism. This is strongly supported by our in vivo and in vitro data showing Amh expression in GnRH neurons and by the reduction in cell motility detected in GN11 cells when transfected with the h*AMH* CHH variants. Moreover, in this study, we showed that Amh acts as a promotility factor for GnRH neurons by signaling via Amhr2/Bmpr1b and activation of the MAPK pathway.

The animal experiments revealed that both acute neutralization of Amhr2 and genetic invalidation of this receptor lead to a strong accumulation of GnRH cells in the nasal region with defects in both the olfactory targeting to the OBs and alterations in the intracranial projections of the VNN/TN; defects that strongly resemble the phenotype previously described in histological analyses of KS human fetuses (***Schwanzel-Fukuda et al., 1996***; ***Teixeira et al., 2010***). Since Amh is only produced by GnRH neurons in the fetal brain and because the axonal scaffold of GnRH neurons express

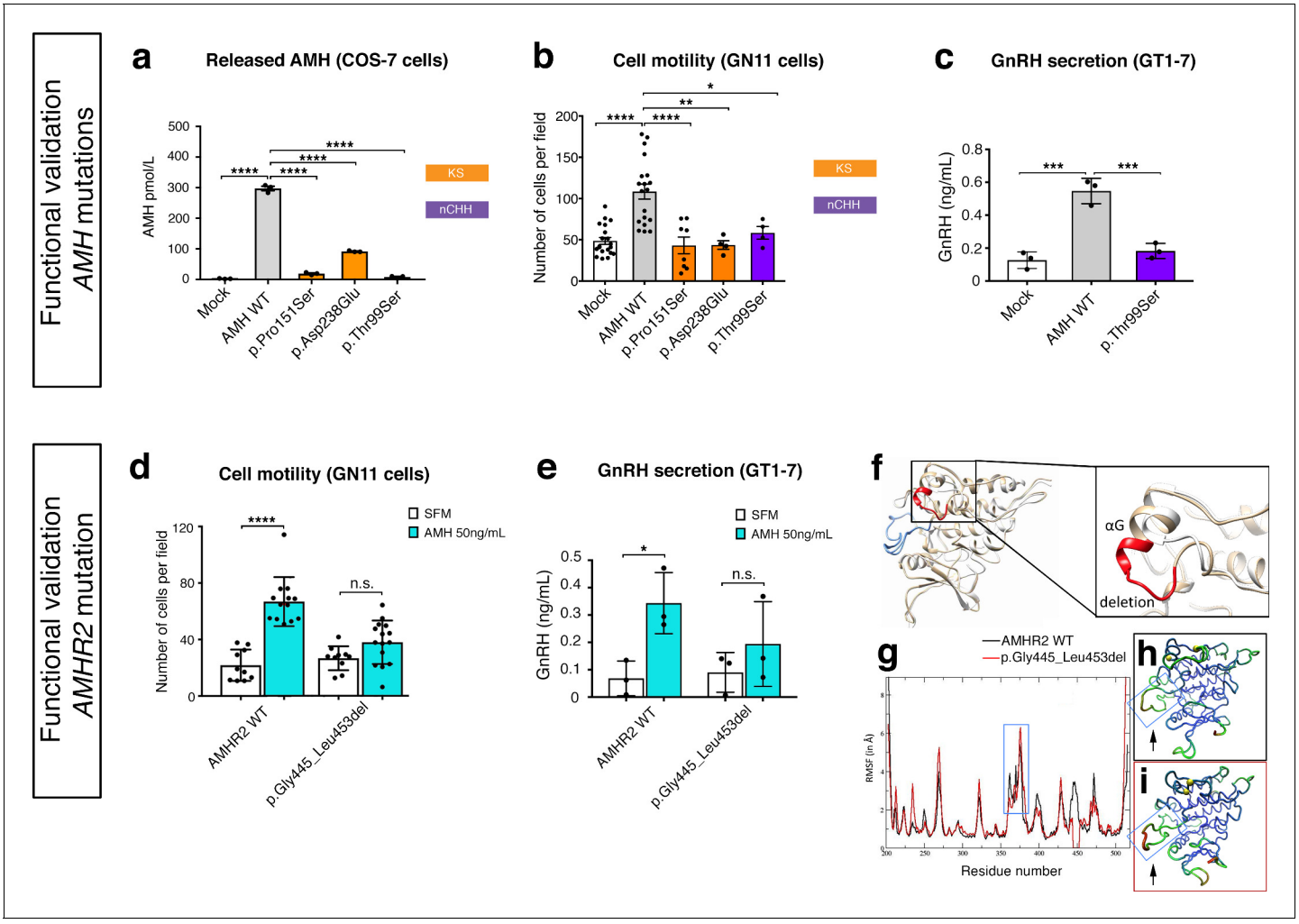

Figure 7. Functional validation of AMH variants. (**a**) AMH released in the medium of COS-7 cells transiently transfected either with lipofectamine alone (mock), or with a WT AMH or a variant AMH identified in CHH and KS probands. Bar graph illustrates the mean amount of AMH secreted in the conditioned medium of transfected COS-7 cells (n = 3 independent experiments per condition). Comparisons between treatment groups were performed using a one-way ANOVA followed by Tukey's post hoc comparison test ($F_{4,10}$ = 1193, Mock vs AMH WT p<0.0001, AMH WT vs p.Pro151Ser p<0.0001, AMH WT vs p.Asp238Glu p<0.0001, AMH WT vs p.Thr99Ser p<0.0001). No significant motility difference was detected between Mock, p.Thr99Ser and p.Pro151Ser mutated forms of AMH treatment, p>0.9 for all. (**b**) Transwell assay was performed on GN11 cells transiently transfected either with lipofectamine alone (mock), or with a WT AMH or a variant AMH identified in CHH and KS probands. Comparisons between treatment groups were performed using a one-way ANOVA followed by Tukey's post hoc comparison test ($F_{4,50}$ = 13.94, Mock vs AMH WT p<0.0001, AMH WT vs p.Pro151Ser p<0.0001, AMH WT vs p.Asp238Glu p<0.0014, AMH WT vs p.Thr99Ser p=0.0218. No significant motility difference was detected between Mock and mutated forms of AMH treatment, p>0.9 for all. (**c**) Quantification of GnRH secretion from GT1-7 cells transfected with lipofectamine alone (mock), or with a WT AMH or the p.Pro151Ser AMH variant identified in a nCHH proband. GnRH mean concentration measured in the medium (n = 3, one-way ANOVA: $F_{2,6}$ = 43.84, p=0.0003; followed by Tukey's multiple comparison post hoc test, mock vs. AMH WT p=0.0003, mock vs p.Thr99Ser p=0.5220, AMH WT vs p.Thr99Ser p=0.0007. (**d**) Transwell assay was performed on GN11 cells transiently transfected with the AMHR2 plasmid or with the AMHR2 variant and stimulated with either serum-free medium (SFM) or with recombinant AMH (50 ng/ml). Bar graph illustrates the mean number of migrated GN11 cells under different treatment conditions (SFM n = 10 for both WT and mutant AMHR2, AMH 50 ng/ml n = 12 for both WT and mutant AMHR2). Comparisons between treatment groups were performed using two-way ANOVA ($F_{1,43}$ = 16.5 P=0.0002; followed by Sidak's multiple comparison post hoc test, AMHR2 WT SFM vs AMHR2 WT + AMH 50 ng/ml p<0.0001, p.Gly445_Leu453del SFM vs p.Gly445_Leu453del + AMH 50 ng/ml P=0.1036). (**e**) Quantification of GnRH secretion from GT1-7 cells transfected with the same plasmids as in **d** (n = 3 independent experiments per condition). Experiments were replicated three times with comparable results. Two-way ANOVA, $F_{1,8}$ = 1.927, p<0.02025; followed by Holm-Šídák multiple comparison post hoc test, AMHR2 WT SFM vs AMHR2 WT + AMH 50 ng/ml P=0.0269, p.Gly445_Leu453del SFM vs p.Gly445_Leu453del + AMH 50 ng/ml P=0.4652. (**f**) Initial three-dimensional models of WT and p.Gly445_Leu453del catalytic intracellular serine/threonine domains of AMHR2. The backbone of the WT and deleted proteins are shown in tan or white cartoon representations, respectively, with the deleted 445–453 residues colored in red. The activation loop is depicted in blue. (**g–i**) Root-mean-square fluctuations (RMSF) of the C_α atoms along the simulations for the AMHR2 WT and the p.Gly445_Leu453del models. (**g**) RMSF (in Å) for the WT (black line) and the p.Gly445_Leu453del models (red

Figure 7 continued on next page

Figure 7 continued

line, being the average over the three 100 ns simulations) are given for each residue of the protein. For a better comparison, residue numbers were kept the same for both models. Molecular representation of the WT (**h**) and p.Gly445_Leu453del (**i**) models colored by RMSF: the blue-green-red scale corresponds to low-medium-high RMSF values. The yellow spheres indicate the first residues after the p.Gly445_Leu453del deletion. The activation loop region is highlighted inside a blue frame (arrows).

DOI: https://doi.org/10.7554/eLife.47198.016

The following source data and figure supplements are available for figure 7:

Source data 1. This spreadsheet contains the values used to generate the bar plots shown in ***Figure 7a–e***.

DOI: https://doi.org/10.7554/eLife.47198.019

Figure supplement 1. Root-mean-square deviations (RMSD) of the AMHR2 protein backbone along the simulations.

DOI: https://doi.org/10.7554/eLife.47198.017

Figure supplement 2. Molecular representation of main interactions stabilizing the zone around the AMHR2 deletion.

DOI: https://doi.org/10.7554/eLife.47198.018

Amhr2, we hypothesize that Amh signaling contributes to the correct development of the ventral branch of the vomeronasal/terminal nerves in the brain through a paracrine mechanism. Mono-allelic inactivation of *Amhr2* in mice is not sufficient to significantly alter GnRH neuronal migration, as indicated by the normal number of GnRH neurons observed in adult *Amhr2* heterozygous brains. On the other hand, the presence of only one *Amhr2*-null allele is sufficient to trigger significant impairments of LH secretion, LH pulsatlity and fertility in adult female mice. In heterozygous males, only the number of litters/90 days was found to be significantly reduced as compared to $Amhr2^{+/+}$ males, suggesting that sexual behavior but not fecundity is likely altered in $Amhr2^{+/-}$ males.

Bi-allelic inactivation of *Amhr2* in mice results instead into a significant reduction of the GnRH cell population in the brains of adult *Amhr2*-null mice of both sexes as compared to wild-type animals. Since male and female homozygous adult animals showed a comparable GnRH cell loss, it is likely that the GnRH migratory defect observed in *Amhr2*-deficient embryos is independent of the genetic sex of the animals.

We speculate that Amh/Amhr2 signaling can regulate, respectively, GnRH migration, during embryonic development, and GnRH/LH secretion postnatally. The latter point is also supported by our in vitro experiments showing AMH-induced GnRH secretion in GT1-7 cells.

Homozygous *Amhr2* female mice have a more pronounced phenotype than heterozygous animals, as they combine developmental defects in GnRH migration with severely impaired ovulation and fertility in adulthood. This strong phenotype could be the consequence of a lack of a broad spectrum of actions of Amh at different prenatal and postnatal stages, impacting the GnRH neuronal migration and the GnRH secretion, respectively, or gonadotrope function (***Garrel et al., 2016***; ***Garrel et al., 2019***). Moreover, since Amh is known to be expressed by granulosa cells in the ovaries (***Vigier et al., 1984***) and to regulate folliculogenesis (***Durlinger et al., 2001***; ***Durlinger et al., 1999***), it is likely that part of the reproductive phenotype of $Amhr2^{-/-}$ mice is also due in part to the lack of ovarian Amh. Dissecting the specific contribution of ovarian versus cerebral Amh in the control of fertility would only be possible using a neuronal specific knockout of *Amhr2,* which is not available yet. However, our previous (***Cimino et al., 2016***) and current findings, showing that Amh directly increases GnRH and LH secretion, support a role for Amh in the neuroendocrine regulation of fertility in physiological and pathological conditions.

Our study identified heterozygous mutations in CHH probands that affect highly conserved amino acids of AMH or its exclusive binding receptor, AMHR2. The AMH mutants display defects in AMH release. Since the described proAMH cleavage sites (***Mamsen et al., 2015***; ***Pankhurst and McLennan, 2013***) are not located in close proximity of these mutations, it is unlikely that they impinge on the cleavage of the proAMH. The decreased AMH secretion might rather result from altered protein trafficking leading to accumulation of the mutants AMH in the endoplasmic reticulum (ER) and defective release. The AMH mutants identified in KS probands also significantly reduced GN11 migration compared to the wild-type AMH. Interestingly, the p.Thr99Ser *AMH* mutation found in a nCHH proband compromises both GnRH cell motility in GN11 cells as well as GnRH secretion in GT1-7 cells. It is plausible that AMH mutants cause dominant negative effects by forming heterodimers with wild-type AMH, thus reducing AMHR2 activation and the downstream biological

response. Finally, the AMHR2 p.Gly445_Leu453del mutation identified in a female nCHH proband was also loss-of-function in in vitro migration and GnRH secretion assays.

The heterozygous mutations in *AMH* and *AMHR2* are found in 3% of CHH probands in our cohort (4 out of 136). This is consistent with the genetic landscape of CHH as the majority of known CHH genes have a low mutational prevalence (<5%) (**Boehm et al., 2015**). Variable expressivity was observed in family members carrying the same mutation, consistent with the fact that CHH represents the more severe end of a large spectrum of manifestations. This is a common theme in the genetics of CHH, and factors such as digenic/oligogenic inheritance (**Boehm et al., 2015**; **Sykiotis et al., 2010**; **Pitteloud et al., 2007**), epigenetic regulation or non-genetic contributions likely play important roles. As the current study is limited by the small number of probands harboring *AMH* and *AMHR2* mutations, confirmation in larger CHH cohorts will be necessary to establish the specific contributions of these two genes in the pathogenesis of CHH.

Notably, homozygous or compound heterozygous loss-of-function mutations in *AMH* (OMIM: 600957) or *AMHR2* (OMIM: 600956) cause PMDS in both mice and humans (**Imbeaud et al., 1995**; **Mishina et al., 1996**). PMDS is characterized by the retention of Müllerian duct derivatives (the uterus, fallopian tubes, and upper part of the vagina) in males (**Josso and Clemente, 2003**; **Behringer et al., 1994**; **Mishina et al., 1996**; **Belville et al., 1999**; **Belville et al., 2004**; **Orvis et al., 2008**). Interestingly, we identified two mutations (AMH p.Pro151Ser and AMHR2 p.Gly445_Leu453-del) (**Picard et al., 2017**) in our CHH cohort previously associated with autosomal recessive PMDS. MRI or pelvic ultrasounds were performed in the two male CHH patients harboring *AMH* mutations, including the patient carrying the p.Pro151Ser. No defects in the internal genitalia were identified, consistent with the fact that monoallelic defects in *AMH* or *AMHR2* do not cause PMDS (**Picard et al., 2017**). Notably, parents of PMDS probands carrying heterozygote *AMH* or *AMHR2* mutations are fertile (**Picard et al., 2017**; **Josso et al., 2005**); however, detailed reproductive and olfactory phenotyping in these parents have not been reported. Furthermore, there are few studies examining the hormonal profile of patients with PMDS although spontaneous puberty is reported based on clinical observation (**Josso et al., 2005**). To assess pubertal and reproductive defects in PMDS patients or family members, detailed reproductive phenotyping will be necessary.

Taken together, these data demonstrate the pleiotropic roles of *AMH* and *AMHR2* in shaping internal genitalia and GnRH neuron migration. Different mechanistic actions of the mutants (i.e. recessive vs. dominant negative vs. haploinsufficiency) in combination with tissue-specific signaling pathway might guide the final phenotype.

AMH and *AMHR2* mutations affecting GN11 cell motility were found in both KS and nCHH individuals. We thus speculate that GnRH migratory defects could also occur in some cases of nCHH. This hypothesis challenges the current dogma, whereby defects in GnRH cell migration lead to KS and not nCHH (**Boehm et al., 2015**). Yet, increasing genetic evidence indicates that CHH genes do not segregate into 2 (i.e. KS and nCHH) but rather three categories: 1) KS only, 2) nCHH only and 3) both KS and nCHH. The latter includes genes involved in GnRH neuron migration such as *FGFR1*, *SEMA7A*, *AXL* (**Boehm et al., 2015**). We recently showed that GnRH neurons in human fetuses migrate into the brain in tight associations with vomeronasal and terminal nerves and not olfactory nerves (**Casoni et al., 2016**). Another recent study demonstrated that correct development of the OBs and axonal connection to the forebrain are not required for GnRH neuronal migration (**Taroc et al., 2017**), thus implying a stronger contribution of the vomeronasal/terminal nerve as a scaffold for the GnRH migration. Taken together, this evidence indicates that the vomeronasal and the terminal nerve play important roles in the ontogenesis and migration of GnRH neurons in vertebrates, and raises the intriguing possibility that some genetic forms of nCHH might be due to defective central projections of the vomeronasal/terminal nerves leading to subsequent alterations of the GnRH migratory process.

In conclusion, this work highlights the role of AMH/AMHR2 signaling in GnRH neuronal migration, hormone secretion and regulation of fertility, and identifies heterozygous mutations in *AMH* and *AMHR2* in CHH patients.

Materials and methods

Key resources table

Reagent type (species) or resource	Designation	Source or reference	Identifiers	Additional information
Strain, strain background (*Mus musculus*)	C57BL/6J	Charles River		
Strain, strain background (*M. musculus*)	Amhr2-Cre Knock-in	***Jamin et al., 2002***		DOI: 10.1038/ng1003
Strain, strain background (*M. musculus*)	Gnrh1 < GFP>	***Spergel et al., 1999***		DOI: 10.1523/JNEUROSCI.19-06-02037.1999
Recombinant DNA reagent	AMH-His	GeneCust		Seq ref: NM_000479.3
Recombinant DNA reagent	AMHR2-His	GeneCust		Seq Ref: NM_000479.3
Recombinant DNA reagent	AMH-p.Thr99Ser-His	This Paper		
Recombinant DNA reagent	AMH-p.Pro151Ser-His	This Paper		
Recombinant DNA reagent	AMH-p.Asp238Glu-His	This Paper		
Recombinant DNA reagent	AMHR2-p.Gly445_Leu453del-His	This Paper		
Cell line	GN11	***Radovick et al., 1991***	Lab Stock	https://doi.org/10.1073/pnas.88.8.3402 GN11 cells were isolated from a male mouse
Cell line	GT1-7	***Mellon et al., 1990***	Lab Stock; RRID:CVCL_0281	https://doi.org/10.1016/0896-6273(90)90028-E GT1-7 cells were isolated from a mouse, unknown sex
Cell line	COS-7		Lab Stock; RRID:CVCL_0224	COS-7 cells were isolated from a monkey
Transfected construct	Amhr2 SMARTpool siRNA	Dharmacon	#M-053605-00-0005	
Transfected construct	Acvr1 SMARTpool siRNA	Dharmacon	#M-042047-01-0005	
Transfected construct	Bmpr1a SMARTpool siRNA	Dharmacon	# M-040598-01-0005	
Transfected construct	Bmpr1b SMARTpool siRNA	Dharmacon	# M-051071-00-0005	
Transfected construct	Non-targeting siRNA control pool	Dharmacon	# D-001206-13-05	
Antibody	Phospho-ERK1/2 (Thr202/Tyr204) (rabbit)	Cell Signaling	#9101L; RRID:AB_331646	1:1000
Antibody	ERK1/2 (Thr202/Tyr204) (rabbit)	Cell Signaling	#9102L; RRID:AB_330744	1:1000
Antibody	AMH (mouse)	Abcam	#Ab24542 ; RRID:AB_2801539	1:500
Antibody	AMH (rabbit)	Abcam	#Ab103233; RRID:AB_10711946	1:500
Antibody	AMHR2 (rabbit)	CASLO	Custom made #56G	1:2000
Antibody	GnRH (rabbit)	Prof. G Tramu, Univ. Bordeaux, France	Lab Stock	1:3000

Continued on next page

Continued

Reagent type (species) or resource	Designation	Source or reference	Identifiers	Additional information
Antibody	Peripherin (Contactin1) (rabbit)	Millipore	#AB1530; RRID:AB_90725	1:1000
Antibody	β-III tubulin (TUJ-1) (mouse)	Sigma Aldrich	#T8660; RRID:AB_477590	1:800
Antibody	AMHR2 Neutralizing Antibody	R and D systems	#AF1618 ; RRID: AB_2226485	1:200
Antibody	Actin (mouse)	Sigma Aldrich	#A5316; RRID:AB_476743	1:1000
Antibody	Donkey anti-rabbit IgG AlexaFluor 488 (H + L)	Molecular Probes	#A-21026; RRID:AB_141708	1:500
Antibody	Donkey anti-rabbit IgG AlexaFluor 555 (H + L)	Molecular Probes	#A-31572; RRID:AB_162543	1:500
Antibody	Donkey anti-mouse IgG AlexaFluor 488 (H + L)	Molecular Probes	#A-21202; RRID:AB_141607	1:500
Antibody	Donkey anti-mouse IgG AlexaFluor 555 (H + L)	Molecular Probes	#A-31570; RRID:AB_2536180	1:500
Antibody	Donkey anti-goat IgG AlexaFluor 488 (H + L)	Molecular Probes	#A-11055; RRID:AB_142672	1:500
Antibody	Donkey anti-goat IgG AlexaFluor 555 (H + L)	Molecular Probes	#A-21432; RRID:AB_141788	1:500
Antibody	Donkey anti-goat IgG AlexaFluor 647 (H + L)	Molecular Probes	#A-21447; RRID:AB_141844	1:500
Antibody	Donkey anti-guinea pig IgG AlexaFluor 488 (H + L)	Jackson ImmunoResearch	#706-545-148; RRID:AB_2340472	1:500
Antibody	Horse anti-mouse IgG peroxidase labelled	Vector	#PI-2000; RRID:AB_2336177	1:5000
Sequence-based reagent	Amh Taqman gene expression assay	Thermofisher Scientific	Mm00431795_g1	
Sequence-based reagent	GnRH Taqman gene expression assay	Thermofisher Scientific	Mm01315605	
Sequence-based reagent	Amhr2 Taqman gene expression assay	Thermofisher Scientific	Mm00513847_m1	
Sequence-based reagent	Acvr1 Taqman gene expression assay	Thermofisher Scientific	Mm01331069_m1	
Sequence-based reagent	Bmpr1a Taqman gene expression assay	Thermofisher Scientific	Mm00477650_m1	
Sequence-based reagent	Bmpr1b Taqman gene expression assay	Thermofisher Scientific	Mm03023971_m1	

Continued on next page

Continued

Reagent type (species) or resource	Designation	Source or reference	Identifiers	Additional information
Sequence-based reagent	Rn18s Taqman gene expression assay	Thermofisher Scientific	Hs99999901-s1	
Sequence-based reagent	Actb Taqman gene expression assay	Thermofisher Scientific	Mm00607939	
Peptide, recombinant protein	Recombinant Human AMH-C Fragment (goat)	R and D systems	#1737 MS; RRID:AB_2273957	
Commercial assay or kit	Papain Dissociation System	Worthington	#LK003150	
Commercial assay or kit	Lipofectamine 2000	ThermoFisher Scientific	#11668019	
Commercial assay or kit	AMH Access Dxi chemiluminescent immunoassay	Beckman Coulter	#B13127	
Commercial assay or kit	GnRH EIA kit	Phoenix Pharmaceuticals Inc	#EK-040-02CE	
Commercial assay or kit	Annexin V Apoptosis Detection Kit	Thermofisher Scientific	#88-8007-74	
Commercial assay or kit	SureSelect All Exon capture V2	Agilent Technologies	#5190–9493	
Commercial assay or kit	Gentra Puregene Blood Kit	Qiagen	#158389	
Chemical compound, drug	Flurogold Tracer	Sigma Aldrich	#39286	1:1500
Chemical compound, drug	MAPK Kinase inhibitor	Calbiochem	#U0126	10 µM
Software, algorithm	FACSDiva	BD Biosciences	8.1	http://www.bdbiosciences.com/sg/instruments/software/downloads/
Software, algorithm	SDS	Applied Biosystems	2.4.1	https://www.thermofisher.com/fr/fr/home/technical-resources/software-downloads/applied-biosystems-7900ht-fast-real-timespcr-system.html
Software, algorithm	Data Assist	Applied Biosystems	3.0.1	https://www.thermofisher.com/fr/fr/home/technical-resources/software-downloads/dataassist-software.html
Software, algorithm	ImageJ	NIH	3.0.1	https://imagej.net/Welcome
Software, algorithm	IMARIS	Bitplane	9.1	https://imaris.oxinst.com/
Software, algorithm	Photoshop	Adobe	4.0	https://www.adobe.com/la/products/photoshop.html
Software, algorithm	Illustrator	Adobe	4.0	https://www.adobe.com/products/illustrator.html
Software, algorithm	Prism 6	Graphpad Software	6.0	https://www.graphpad.com/scientific-software/prism/

Continued on next page

Continued

Reagent type (species) or resource	Designation	Source or reference	Identifiers	Additional information
Software, algorithm	Inspector Pro	La Vision Biotec	4.0	
Software, algorithm	Burrows-Wheeler Alignment Algorithm			http://bio-bwa.sourceforge.net/
Software, algorithm	SnpEff	Switch Laboratoty	4.0	http://snpeff.sourceforge.net/
Software, algorithm	dbNSFP	Liu et al., Human Mutation. 2011	2.9	http://varianttools.sourceforge.net/Annotation/dbNSFP
Software, algorithm	Modeller	Webb et al., Curr Protoc Bioinformatics. 2016	9.2	https://salilab.org/modeller/

Animals and cell lines

C57BL/6J mice (Charles River, USA) were housed under specific pathogen-free conditions in a temperature-controlled room (21–22˚C) with a 12 hr light/dark cycle and ad libitum access to food and water. *Amhr2*-Cre knock-in mice have been previously characterized (***Jamin et al., 2002***). *Gnrh1<GFP>* (***Spergel et al., 1999***) mice were a generous gift of Dr. Daniel J. Spergel (Section of Endocrinology, Department of Medicine, University of Chicago, IL). Mice were genotyped by PCR using primers listed in ***Supplementary file 1***.

Animal studies were approved by the Institutional Ethics Committees of Care and Use of Experimental Animals of the Universities of Lille 2 (France). All experiments were performed in accordance with the guidelines for animal use specified by the European Union Council Directive of September 22, 2010 (2010/63/EU) and the approved protocol (APAFIS#13387–2017122712209790 v9) by the Ethical Committee of the French Ministry of Education and Research.

All efforts were made to minimize animal suffering and animal care was supervised by veterinarians and animal technicians skilled in rodent healthcare and housing. Mice of the appropriate genotype were randomly allocated to experimental groups.

COS-7 cells (originally from the lab stock of Luca Tamagnone lab), GN11 and GT1-7 cells (***Radovick et al., 1991***; ***Mellon et al., 1990***) (originally from the lab stock of Pamela Mellon lab and from the lab stock of Sally *Radovick* lab) were grown in DMEM with 10% fetal bovine serum (Invitrogen). They were authenticated based on morphology, and DNA staining revealed no mycoplasma contamination.

Immunofluorescence

Embryos were harvested at embryonic day E14.5 from black C57BL/6 mice. Heads from the embryos were washed thoroughly in cold 0.01M PBS, fixed in fixative solution [4% paraformaldehyde (PFA), 0.01M PBS, pH 7.4] for 6–8 hr at 4˚C and cryoprotected in 30% sucrose overnight at 4˚C. The following day, heads were embedded in OCT embedding medium (Tissue-Tek, Torrence, CA), frozen on dry ice, and stored at −80˚C until sectioning. The embryo heads were coronally cryosectioned (Leica Microsystems, Wetzlar Germany) at 16 µm intervals directly onto slides and stored at −80˚C until use. Adult mice were anesthetized with 80 mg/kg of ketamine-HCl and 8 mg/kg xylazine-HCl and transcardially perfused with 40 ml of saline, followed by 100 ml of 4% PFA, pH 7.4. Brains were collected, postfixed in the same fixative for 2 hr at 4˚C and cryoprotected in 30% sucrose overnight. Embedded in OCT embedding medium, frozen on dry ice and stored at −80˚C until cryosectioning. Adult brains were sectioned at 35 µm using the cryostat and stored in anti-freeze medium at −20˚C until use. Immunolabelling for mouse and human samples was completed as follows: sections were thawed at RT before 3 × 5 min washes in 0.01M PBS. Sections were then incubated with primary antibodies (Key Resources Table) in a solution containing 10% normal donkey serum and 0.3% Triton X100 for 3 days at 4˚C. 3 × 5 min washes in 0.01M PBS were followed by incubation in appropriately conjugated secondary antibodies (Key Resources Table) for 1 hr before incubation with Hoechst

1:1000. After 3 × 5 min washes in 0.01M PBS sections were coverslipped using Mowiol as an anti-fade mounting medium.

Nasal explants

Embryos were obtained from timed-pregnant animals. Vaginal plug dates were designed as E0.5. Nasal pits of E11.5 WT C57BL/6J mice were isolated under aseptic conditions in Grey's Balanced Salt Solution (Invitrogen) enriched with glucose (Sigma-Aldrich) and maintained at 4˚C until plating. Explants were placed onto glass coverslips coated with 10 µl of chicken plasma (Cocalico Biologicals, Inc). Thrombin (10 µl; Sigma-Aldrich) was then added to adhere (thrombin/plasma clot) the explant to the coverslip. Explants were maintained in defined serum-free medium (SFM) (***Fueshko and Wray, 1994***) containing 2.5 mg/ml Fungizone (Sigma-Aldrich) at 37˚C with 5% CO (***Wray et al., 1989***) for up to 30 days in vitro (div). From culture days 3 to 6, fresh medium containing fluorodeoxyuridine (8×10^{-5} M; Sigma-Aldrich) was provided to inhibit the proliferation of dividing olfactory neurons and non-neuronal explant tissue. The medium was replaced with fresh SFM twice a week.

In utero injections

Vaginal plug dates were designed as E0.5. Timed-pregnant mice (n = 2) carrying E12.5 embryos were anesthetized with isoflurane, and the uterine horns were gently placed outside the abdominal cavity and constantly hydrated with 35˚C sterile saline. Using a Nanofil syringe and a 35 GA needle attachment (World Precision Instruments), 2 µl containing 0.4 µg of Amhr2 Neutralizing Antibody (Amhr2-NA, 1:200, R and D system, AF1618) and Fluorogold tracer 1:1500 (Sigma Aldrich, #39286) diluted in saline was injected intra-utero in the olfactory placode of each embryo of one uterine horn. In order to consistently obtain control and Amhr2-NA treated embryos from the same pregnant animals and limit biases associated with the staging of the embryonic development, the embryos of the contralateral horn were injected with saline and Fluorogold of both dams. The concentration of AMHR2-NA was determined based on the manufacturer's recommendations. The uteri were gently returned and the mothers sutured and monitored for few days. Embryos were collected at embryonic day 14.5 (E14.5), fixed, cryoprotected, frozen and cut as described above (Immunofluorescence). Fluorogold was used in order to verify the specificity of the injection sites and only embryos confirmed as optimal hits (fluorogold fluorescence within the olfactory epithelium) were used for the GnRH quantitative analysis (n = 4 per treatment group, from two independent dams).

GnRH cell counting

Serial sagittal sections (16 µm) from E14.5 WT embryos, (n = 4 per group) were prepared as described above. Quantitative analysis of GnRH neuronal number, as a function of location, was performed over four regions (the nasal compartment, the nasal/forebrain junction, ventral forebrain and cortex). Serial coronal sections (35 µm) of *Amhr2*$^{+/+}$, *Amhr2*$^{+/-}$ and *Amhr2*$^{-/-}$ mouse brains were used to count the total number of GnRH cells throughout the entire brain and combined to give group means ± SEM. Vaginal plug dates were designed as E0.5.

Fluorescence activated cell sorting (FACS)

Embryos were harvested at E12.5 from timed-pregnant *Gnrh1 <GFP>* mice, previously anesthetized with an intraperitoneal injection of 80 mg/kg of ketamine-HCl and 8 mg/kg xylazine-HCl and sacrificed by cervical dislocation. Juvenile (P12) and adult female mice (3 months old) were anesthetized with 80 mg/kg of ketamine-HCl and 8 mg/kg xylazine-HCl before being sacrificed by cervical dislocation. Microdissections from embryonic nasal region and post-natal/adult hypothalamic preoptic region were enzymatically dissociated using Papain Dissociation System (Worthington, Lakewood, NJ) to obtain single-cell suspensions as previously described (***Messina et al., 2016***). After dissociation, the cells were physically purified using a FACSAria III (Beckman Coulter) flow cytometer equipped with FACSDiva software (BD Biosciences). The sort decision was based on measurements of GFP fluorescence (excitation: 488 nm, 50 mW; detection: GFP bandpass 530/30 nm, autofluorescence bandpass 695/40 nm) by comparing cell suspensions from GnRH-GFP and wild-type animals. For each animal, 500 GFP-positive cells were sorted directly into 8 µl extraction buffer: 0.1% Triton X-100 (Sigma-Aldrich) and 0.4 U/µl RNaseOUT (Life Technologies). Captured cells were used to synthesize first-strand cDNA using the protocol detailed below.

Immortalized cell cultures

GN11, GT1-7 and COS-7 cells were grown in monolayers at 37˚C under 5% CO_2, in DMEM (ThermoFisher, Invitrogen) containing 1 mM pyruvate, 2 mM L-glutamine (ThermoFisher, Invitrogen), 100 µg/ml streptomycin, 100 U/ml penicillin and 9 mg/ml glucose (MP Biomedicals, Santa Ana, CA), supplemented with 10% fetal bovine serum (complete medium). Cells were maintained below full confluence by trypsination and seeding onto 10 cm^2 dishes. Cells used for experiments were between their third and eighth passage. Cells were treated with recombinant human AMH (1737-MS; R and D systems) at the concentrations ranging from 10 ng/ml to 250 ng/ml.

Quantitative RT-PCR

For gene expression analyses, cDNA obtained from RT-PCR were reverse transcribed using SuperScript III Reverse Transcriptase (ThermoFisher, Invitrogen). Real-time PCR was carried out on Applied Biosystems 7900HT Fast Real-Time PCR System using exon-span-specific TaqMan Gene Expression Assays (Applied Biosystems, Carlsbad CA). The list of primers used for these experiments is the following: *Amh* (Mm00431795_g1), *Gnrh1* (Mm01315605), *Amhr2* (Mm00513847_m1); *Acvr1* (Mm01331069_m1); *Bmpr1a* (Mm00477650_m1); *Bmpr1b* (Mm03023971_m1). Control housekeeping genes: *Rn18s* (Hs99999901-s1) and *Actb* (Mm00607939). Amperase activation was achieved by heating to 50˚C for 2 min, before denaturing at 95˚C for 20 s, followed by 40 cycles of 1 s 95˚C with a 20 s extension time at 60˚C. Gene expression data were analyzed using SDS 2.4.1 and Data Assist 3.0.1 software (Applied Biosystems, Carlsbad, CA), with *ActB* and *Rn18s* as control house-keeping mRNA following a standardized procedure (***Schmittgen and Livak, 2008***). Values are normalized relative to control values and expressed, as appropriate, to 1.

Western blot

Culture plates were frozen as described above quickly thawed and protein immediately extracted with 150 µl of freshly prepared lysis buffer [25 mM Tris pH 7.4, 50 mM β-glycerophosphate, 1% Triton x100, 1.5 mM EGTA, 0.5 mM EDTA, 1 mM sodium orthovanadate, 10 µg/ml Leupeptin and Pepstatin A, 10 µg/ml aprotinin, 100 µg/ml PMSF (reagents sourced from Sigma Aldrich, St. Louis, MO)]. Protein extracts were then homogenized using a 26 gauge needle before centrifuging at 12.000 g for 15 mins at 4˚C. The supernatant was recovered and protein quantified using the Bradford method (BioRad, Hercules, CA). 1x sample and 4x loading buffer (ThermoFisher, Invitrogen) were added to the samples, which were then boiled for 10 min before electrophoresis at 120V for 100 mins in 4–12% tris-acetate precast SDS-polyacrylamide gels according to the protocol supplied with the NuPAGE system (ThermoFisher, Invitrogen). After size fractionation, the proteins were transferred onto a PVDF membrane (0.2 µm pore size, LC2002; Invitrogen, Carlsbad, CA) in the blot module of the NuPAGE system (ThermoFisher, Invitrogen) maintained at 1A for 75 min at room temperature (RT). Blots were blocked for 1 hr in tris-buffered saline with 0.05% Tween 20 (TBST) and 5% non-fat milk at RT, incubated overnight at 4˚C with their respective primary antibody in TBST 5% bovine serum albumin (Sigma Aldrich, Cat A7906), and washed four times with TBST before being exposed to horseradish peroxidase-conjugated secondary antibodies diluted in 5% non-fat milk TBST for 1 hr at RT. The immunoreactions were detected with enhanced chemiluminescence (NEL101; PerkinElmer, Boston, MA).

Cell transfections for functional validations

Expression vectors encoding for human AMH and AMHR2 were obtained from Genescript. Briefly, a cDNA containing the entire coding region of the human *AMH* transcript (NM_000479.3) and *AMHR2* (NM_020547.3) were inserted into a modified pcDNA3.1+expression vector containing a his-tag at the 5'end (GeneCust). The plasmids encoding the variants (AMH: p.Thr99Ser, p.Pro151Ser, p.Asp238Glu, and AMHR2: p.Gly455_Leu453del) were generated by site directed mutagenesis using the QuickChange XLII Kit (Stratagene) and confirmed by Sanger sequencing. Primers flanking the mutations (see primers list in ***supplementary file 1***) were used for subsequent PCR amplifications.

COS-7, GN11 or GT1-7 cells were grown to 70% confluence in 10 cm^2 dish without the presence of antibiotics in preparation for transfection. For each plasmid, oligomer-Lipofectamine 2000 complexes were prepared as follows: vectors were diluted in 500 µl OptiMEM Reduced Serum Medium without serum and gently mixed, for a final concentration of 400 nM). Lipofectamine 2000

(ThermoFisher, Invitrogen) was mixed gently before use, then diluted 10 µl in 500 µl OptiMEM (ThermoFisher, Invitrogen). Tubes were gently mixed and incubated for 5 min at room temperature. After the 5-min incubation, the diluted vector was combined with the diluted Lipofectamine 2000 and incubated for 20 min at room temperature. During the incubation, cells were trypsinized and dissociated, then re-suspended in the lipofectamine containing vector mixture. Cells were then incubated at 37˚C in a 5% CO_2 incubator for 48 hr, changing the medium to OptiMEM supplemented with 5% fetal bovine serum after 6 hr. Conditioned media was collected for AMH or GnRH quantitation and transfected cells used for either western blotting or transwell migration assays.

AMH quantification

AMH levels in conditioned media were measured by an automatic chemoluminescent immunoassay on a Dxi system (Beckman Coulter, France) after a 1/10 dilution in the Sample Diluent A. This assay detects proAMH and the cleaved $AMH_{N,C}$ complex. The limit of quantification of the assay is 0.57 pmol/L with an intra- and inter-assay imprecision less than 5%.

Determination of GnRH secretion

GT1-7 cells were transiently transfected in OptiMem with either *AMH* WT or p.Thr99Ser h*AMH* variants. 48 hr later, the medium was collected and frozen until EIA measurement. In another set of experiments, GT1-7 cells were transiently transfected with either *AMHR2* WT or with the *AMHR2* CHH variants. 48 hr later, the cells were treated for 4 hr with either PBS or recombinant AMH (1737-MS; R and D systems, 50 ng/ml). Finally, the medium was frozen until EIA measurement. The collected media from these experiments were analyzed for GnRH content following a GnRH EIA protocol (EK-040-02CE, Phoenix Pharmaceuticals Inc, CA).

Transwell migration assay

Transwell chambers were used according to manufacturer's instructions (Falcon). In brief, GN11 cells grown in complete medium until sub-confluence were harvested and re-suspended at a density of 1 $\times$ 10^5 cells/µl in SFM. Cells were seeded on the upper side of 8 µm pore membranes and incubated for 12 hr with SFM, human recombinant AMH (1737-MS; R and D systems, 50–250 ng/ml) or with DMEM supplemented with 10% fetal bovine serum. Each factor (serum, AMH, inhibitors and antibodies) was placed on the upper and lower chamber of the transwell. GN11 cells were incubated in the presence of recombinant AMH (50 ng/ml) together with MAPK inhibitor (UO126; Calbiochem) at a concentration of 10 µM, as previously described (***Balland et al., 2014***). In another set of experiments, GN11 cells were treated for 12 hr with Amhr2-NA (R and D system, AF1618), at the same concentration (1:200) used for the *in utero* injections experiments (***Figure 2***), in the presence or absence of recombinant AMH (50 ng/ml). Cells on the upper side of the filters were mechanically removed and cells on the lower side fixed in 4% PFA for 30 min before nuclei labelling with DAPI. Four non-overlapping regions were imaged per membrane using a Zeiss 20x objective (N.A. 0.8) mounted on a Axio Imager Z2 light microscope (Zeiss), with nuclei counted using an ImageJ plugin (National Institute of Health, Bethseda) and averaged to produce an average per well. n for each experiment is detailed in the figure legends.

siRNA transfections

GN11 cells were grown to 70% confluence in 10 cm^2 dish without the presence of antibiotics in preparation for transfection. For siRNA experiments, GN11 cells were transiently transfected with 75 nM SMARTpool siRNA targeting mouse *Amhr2*, *Acvr1*, *Bmpr1a*, *Bmpr1b,* or 75 nM nontargeting SMARTpool siRNA (siRNA NT) as negative control (Dharmacon, Horizon Discovery LTD, Cambridge, UK). Gene knockdown was assessed by quantitative PCR.

Ovarian histology

Ovaries were collected from 6-month-old mice, immersion-fixed in 4% PFA solution and stored at 4˚C. Paraffin-embedded ovaries were sectioned at a thickness of 5 µm (histology facility, University of Lille 2, France) and stained with hematoxylin-eosin (Sigma Aldrich, Cat # GHS132, HT1103128). Sections were examined throughout the ovary. Corpora lutea (CL) were classified and quantified as previously reported (***Caldwell et al., 2017***). To avoid repetitive counting, CL were counted every 100

µm by comparing the section with the preceding and following sections. CL were characterized by a still present central cavity, filled with blood and follicular fluid remnants or by prominent polyhedral to round luteal cells.

Pulsatile LH measurement

Mice were habituated with daily handling for 3–4 weeks. Blood samples (5 µl) were taken from the tail in 10 min intervals for 2 hr (between 12h00 hours and 15h00 hours), diluted in PBS-Tween and immediately frozen. LH levels were determined by sandwich ELISA (***Steyn et al., 2013***). A 96-well high-affinity binding microplate (9018; Corning) was coated with 50 µl of capture antibody (monoclonal antibody, anti-bovine LH beta subunit, 518B7; University of California) at a final dilution of 1:1000 (in 1 x PBS, 1.09 g of Na2HPO4 (anhydrous), 0.32 g of NaH2PO4 (anhydrous) and 9 g of NaCl in 1000 ml of distilled water) and incubated overnight at 4˚ C. Wells were incubated with 200 ml of blocking buffer (5% (w/v) skim milk powder in 1 x PBS-T (1 x PBS with 0.05% Tween 20) for 2 hr at room temperature. A standard curve was generated using a twofold serial dilution of mLH (reference preparation, AFP-5306A; National Institute of Diabetes and Digestive and Kidney Diseases - National Hormone and Pituitary Program (NIDDK-NHPP)) in 0.2% (w/v) bovine serum albumin 1 x PBS-T. The LH standards and blood samples were incubated with 50 ml of detection antibody (polyclonal antibody, rabbit LH antiserum, AFP240580Rb; NIDDK-NHPP) at a final dilution of 1:10,000 for 1.5 hr (at RT). Each well containing bound substrate was incubated with 50 µl of horseradish peroxidase-conjugated antibody (polyclonal goat anti-rabbit; Vector) at a final dilution of 1:10,000. After a 1.5 hr incubation, 100 µl of o-phenylenediamine (002003; Invitrogen), substrate containing 0.1% H_2O_2 was added to each well and left at RT for 30 min. The reaction was stopped by the addition of 50 ml of 3M HCl to each well, and absorbance of each well was read at a wavelength of 490 nm. Pulses were confirmed using DynPeak (***Vidal et al., 2012***).

Fertility test

The reproductive competency of these animals was determined by pairing the following mice: *Amhr2*$^{+/+}$ males mated with *Amhr2*$^{+/+}$ females, *Amhr2*$^{+/-}$ females, or with *Amhr2*$^{-/-}$ females, or inversely, for a period of 3 months. One male and one female were housed in each cage during the constant breeding protocol. Each litter was sacrificed at birth to allow the dams to re-enter estrous cyclicity within a few days. Number of pups/litter, fertility index (number of litters per female per month, averaged during the 3 months), and time to first litter (number of days to first litter after pairing) were quantified per pairing.

iDISCO

Experiments were performed as previously described (***Renier et al., 2014***) and detailed below.

Sample pre-treatment with methanol

Samples were washed in PBS (twice for 1 hr), followed by 50% methanol in PBS (once for 1 hr), 80% methanol (once for 1 hr) and 100% methanol (twice for 1 hr). Next, samples were bleached in 5% H2O2 in 20% DMSO/methanol (2 ml 30% H_2O_2/2 ml DMSO/8 ml methanol, ice cold) at 4˚C overnight. Next, samples were washed in methanol (twice for 1 hr), in 20% DMSO/methanol (twice for 1 hr), 80% methanol (once for 1 hr), 50% methanol (once for 1 hr), PBS (twice for 1 hr), and finally, PBS/0.2% TritonX-100 (twice for 1 hr) before proceeding to the staining procedures.

Whole-mount immunostaining

Samples were incubated at 37˚C on an adjustable rotator in 10 ml of a blocking solution (PBSGNaT) of 1X PBS containing 0.2% gelatin (Sigma), 0.5% Triton X-100 (Sigma-Aldrich) and 0.01% NaAzide for three nights. Samples were transferred to 10 ml of PBSGNaT containing primary antibodies (Table S1) and placed at 37˚C in rotation for 7 days This was followed by six washes of 30 min in PBSGT at RT and a final wash in PBSGT overnight at 4˚C. Next, samples were incubated in secondary antibodies (1:400, Alexa 568, Alexa 647) diluted in 10 ml PBSGNaT for 2 days at 37˚C in a rotating tube. After six 30 min washes in PBS at room temperature, the samples were stored in PBS at 4˚C in the dark until clearing.

Tissue clearing

All incubation steps were performed at RT in a fume hood, on a tube rotator at 14 rpm covered with aluminium foil to avoid contact with light. Samples were dehydrated in a graded series (50%, 80%, and 100%) of tetrahydrofurane (THF; anhydrous, containing 250 ppm butylated hydroxytoluene inhibitor, Sigma-Aldrich) diluted in H_2O as follow: 1) 50% THF overnight at RT; 2) 80% THF 1 hr at RT; 3) 100% THF 1h30 at RT; 4) 100% THF 1h30 at RT. This was followed by a delipidation step of 30–40 min in 100% dichloromethane (DCM; Sigma-Aldrich). Samples were cleared in dibenzylether (DBE; Sigma-Aldrich) for 2 hr at RT on constant agitation and in the dark. Finally, samples were moved into fresh DBE and stored in glass tube in the dark and at RT until imaging. We could image samples, as described below, without any significant fluorescence loss for up to 6 months.

Imaging

3D imaging was performed as previously described (***Belle et al., 2014***). An ultramicroscope (LaVision BioTec) using ImspectorPro software (LaVision BioTec) was used to perform imaging. The light sheet was generated by a laser (wavelength 488 or 561 nm, Coherent Sapphire Laser, LaVision BioTec) and two cylindrical lenses. A binocular stereomicroscope (MXV10, Olympus) with a 2 × objective (MVPLAPO, Olympus) was used at different magnifications (1.6×, 4×, 5×, and 6.3×). Samples were placed in an imaging reservoir made of 100% quartz (LaVision BioTec) filled with DBE and illuminated from the side by the laser light. A PCO Edge SCMOS CCD camera (2560 × 2160 pixel size, LaVision BioTec) was used to acquire images. The step size between each image was fixed at 2 µm.

Image analysis

For confocal observations and analyses, an inverted laser scanning Axio observer microscope (LSM 710, Zeiss, Oberkochen, Germany) with EC Plan NeoFluor 10×/0.3 NA, 20×/0.5 NA and 40×/1.3 NA (Zeiss, Oberkochen, Germany) objectives were used (Imaging Core Facility of IFR114 of the University of Lille, France).

Images, 3D volume, and movies were generated using Imaris x64 software (version 7.6.1, Bitplane). Stack images were first converted to imaris file (.ims) using ImarisFileConverter and 3D reconstruction was performed using 'volume rendering'. Optical slices of samples were obtained using the 'orthoslicer' tools. The surface of the samples was created using the 'surface' tool by creating a mask around each volume. 3D pictures were generated using the 'snapshot' tool. ImageJ (National Institute of Health, Bethesda) and Photoshop CS6 (Adobe Systems, San Jose, CA) were used to process, adjust and merge the photomontages. Figures were prepared using Adobe Photoshop and Abode Illustrator CS6.

Human CHH subjects

The CHH cohort included 180 probands (105 KS and 75 nCHH). The majority of the patients were male (n = 127). The diagnosis of CHH was made on the basis of: i) absent or incomplete puberty by 17 years of age; ii) low/normal gonadotropin levels in the setting of low serum testosterone/estradiol levels; and iii) otherwise normal anterior pituitary function and normal imaging of the hypothalamic-pituitary area (***Pitteloud et al., 2002***). Olfaction was assessed by self-report and/or formal testing (***Lewkowitz-Shpuntoff et al., 2012***). When available, family members were included for genetic studies. This study was approved by the ethics committee of the University of Lausanne, and all participants provided written informed consent prior to study participation.

Human case summaries

Family # 1, Patient II-1

AMH p.Thr99Ser (heterozygous)

The caucasian male proband consulted our clinic at age 32 for symptomatic hypogonadism accompanied by mild anemia and oligospermia. He was previously diagnosed with delayed puberty at age 17 but was never offered testosterone replacement nor was he followed up to ensure pubertal completion. Physical examination revealed partial but incomplete puberty (testicular volume 12 ml bilaterally, pubic hair Tanner IV) as well as eunuchoid proportions (arm span 184 cm for height of 176 cm). Targeted clinical exam detected slight hyperlaxity, high-arched palate and pectum excavatum. Blood tests confirmed a hypogonadotropic hypogonadism (testosterone 7.5 nmol/l, LH 2.7 U/l, FSH

3.6 U/l) without dysfunction of other pituitary axes. Formal olfactory testing confirmed normal sense of smell. Pituitary MRI and GnRH-stimulation test were normal. Bone density scan typically detected osteopenia at the lumbar spine. Family history included delayed puberty and growth in his father while mother's puberty was normal (menarche at 11 years old). The proband harbors a heterozygous mutation in *AMH* inherited by his father who as stated above has a partial phenotype (delayed puberty). He also harbors a *GNRHR* variant, which was not considered as pathogenic or likely pathogenic by our filtering process, due to its presence only at heterozygous state for a gene with autosomal recessive transmission mode. Given his request for fertility, HCG treatment was introduced, allowing for increase of testosterone and stimulation of spermatogenesis.

Family # 2, Patient II-1

AMH p.Pro151Ser (heterozygous)

This anosmic male proband was diagnosed at 2 years old for unilateral cryptorchidism, treated by left orchidopexy. Subsequent follow up showed no signs of puberty at 17.5 years with prepubertal testes (volume 2 ml bilaterally). Serum testosterone was low while gonadotropines were undetectable (LH/FSH < 1.0 U/L). Formal smell testing confirmed anosmia (UPSIT: 11/40, <5th %ile) and he was diagnosed with Kallmann syndrome. Intramuscular injections of testosterone were initiated with good effect on virilization. A cranial MRI showed normal pituitary size and absent olfactory bulbs. Family history was negative for pubertal delay. Parents refused to participate in the genetic study and undergo smell testing. The patient harbors a rare mutation in *AMH* with no changes in known CHH genes. A pelvic MRI was performed in July 2017 and showed no argument in favor of PMDS.

Family # 3, Patient II-2

AMG p.Asp238Gln (heterozygous)

The female proband originated from Kazakhstan consulted us at age of 27.9 years for infertility. She presented with primary amenorrhea at age 17. She described onset of breast development at 13 years, which rapidly stalled (Tanner II-III). She was placed on estrogen-progesterone replacement (estradiol/dihydrogesterone) at age 18. She remained amenorrheic during multiple treatment pauses. When assessed in our clinic and several months after withdrawal of estrogen pills, hypogonadotropic hypogonadism was confirmed (estradiol 0.05 nmol/l, LH 0.5 U/l, FSH 1.4 U/l) with otherwise normal pituitary function and adequate response to GnRH stimulation (LH baseline 0.4 U/l, peak 6.3 U/l; FSH baseline 1.2 U/l, peak 6.4 U/l). A 10 hr frequent sampling did not detect any LH pulses. Olfactory assessment by 12-item Sniffin' Sticks revealed hyposmia (12/16). Her physical status was notable for eunuchoid proportions and moderate scoliosis without dysmorphic features. Cranial MRI showed a small pituitary gland, while bone density scan indicated osteoporosis. Polycystic ovaries syndrome was excluded as well as a non-classic congenital adrenal hyperplasia. We concluded to KS diagnosis with partial GnRH deficiency and resumed estrogen/dihydrogesterone treatment. Family history included delayed puberty in the father (first shaving at age 18, continued growing until age 24). The latter was also anosmic, while the mother exhibited normal puberty (menarche at 13 years old) and olfactive function. The patient harbors an *AMH* mutation, inherited by the partially affected father. No changes in known CHH genes were seen.

Family # 4, Patient II-1

AMHR2 p.Gly445_Leu453del (heterozygous)

The female Caucasian patient presented with primary amenorrhea and absent pubertal development at age 17. She remained amenorrheic until age 22, and then was offered oral contraceptives (estradiol, norgestrel). Endocrinology assessment in her native country (Serbia) led to diagnosis of hypogonadotropic hypogonadism at age 33 (estradiol <0.04 nmol/l, LH <2.0 U/l, FSH 0.1 U/l) with otherwise normal pituitary function, assessed by an insulin tolerance test. Similarly, LHRH stimulation test showed adequate pituitary response (LH baseline 2.0 U/l, peak 6.5 U/l; FSH baseline 1.8 U/l, peak 6.3 U/l). Pituitary MRI was normal as well as formal smell test (Sniffin' Sticks 14/16, > 25th %ile). The patient consulted us to discuss ovulation induction by pulsatile GnRH treatment. After withdrawal of estrogen pills, hypogonadotropic hypogonadism was confirmed (estradiol <0.04 nmol/l, LH 0.4 U/l, FSH 1.4 U/l). Physical exam did not show any associated phenotypes. Family history was unremarkable for pubertal timing but her mother exhibited history of cleft lip/palate, corrected

surgically at infancy. Detailed history of the father was impossible as he was deceased. A half paternal brother had normal puberty and fathered a child without difficulty. The patient harbored a heterozygous deletion in *AMHR2*. Sequencing of *AMHR2* in the patient's mother and half paternal brother showed no mutation.

Genetic studies

Genomic DNA was extracted from peripheral-blood samples using the Puregene Blood Kit (Qiagen), following the manufacturer's protocol. Exome capture was performed using the SureSelect All Exon capture v2 and v5 (Agilent Technologies, Santa Clara, CA) and sequenced on the HiSeq2500 (Illumina, San Diego, CA) at BGI (BGI, Shenzen, PRC). Raw sequences (fastq files) were analyzed using an in-house pipeline that utilizes the Burrows-Wheeler Alignment algorithm (BWA) (**Li and Durbin, 2009**) for mapping the reads to the human reference sequence (GRCh37), and the Genome Analysis Toolkit (GATK) (**DePristo et al., 2011**) for the detection of single nucleotide variants (SNVs) and insertion/deletions (Indels). The resulting variants were annotated using SnpEff version 4.0 (**Cingolani et al., 2012**) and dbNSFP version 2.9 (**Liu et al., 2013**) to calculate minor allele frequency (MAF).

We evaluated coding exons and intronic splice regions (≤6 bp from the exons) of the known CHH genes for pathogenic and likely pathogenic variants according to ACMG guidelines (**Richards et al., 2015**). The included CHH genes are: *ANOS1* (NM_000216.2), *SEMA3A* (NM_006080), *FGF8* (NM_033163.3), *FGF17* (NM_003867.2), *SOX10* (NM_006941), *IL17RD* (NM_017563.3), *AXL* (NM_021913), *FGFR1* (NM_023110.2), *HS6ST1* (NM_004807.2), *PCSK1* (NM_000439), *LEP* (NM_000230), *LEPR* (NM_002303), *FEZF1* (NM_001024613), *NSMF* (NM_001130969.1), *PROKR2* (NM_144773.2), *WDR11* (NM_018117), *PROK2* (NM_001126128.13), *GNRH1* (NM_000825.3), *GNRHR* (NM_000406.2), *KISS1* (NM_002256.3), *KISS1R* (NM_032551.4), *TAC3* (NM_013251.3), and *TACR3* (NM_001059.2).

Forty-four probands harbored pathogenic or likely pathogenic variants in the known CHH genes, and were excluded for subsequent analysis. The remaining 136 probands were then evaluated for mutations in *AMH* and *AMHR2*. Only variants with MAF <0.1% were used for subsequent analysis. *AMH* and *AMHR2* variants were confirmed by Sanger sequencing on both strands with duplicate PCR reactions and are described according to HGVS nomenclature (**den Dunnen and Antonarakis, 2000**).

Computational modelling of the p.Gly445_Leu453del *AMHR2* intracellular domain

For the WT AMHR2 kinase domain, a previous model (referred as WT) based on the crystallographic structure of the human activin type II B receptor (PDB code 2qlu), which shares ~35% sequence identity with AMHR2, was used (for more details see **Belville et al., 2009**). The 3D-model bearing the p.Gly445_Leu453del deletion (referred as DEL) was generated on the basis of the WT model, using the Modeler V9.2 package (**Sali and Blundell, 1993**) and evaluated by Errat (**Colovos and Yeates, 1993**). The three-dimensional models generated were submitted to a 100 ns molecular dynamics simulation. Both systems were set up following the same protocol and using the xleap program. The system was embedded in a cubic box with edges at 15 Å from the protein and sodium ions were added to neutralize the simulation cell (4 and 6 for WT and DEL models, respectively). The protein was described by the ff14sb forcefield (**Maier et al., 2015**) water molecules with the TIP3P (**Jorgensen et al., 1983**) one and the ions94.lib library was used for the sodium cations. Non-bonded interactions were calculated with a cutoff of 10 Å, whereas long range electrostatic interactions were calculated with the Ewald Particle Mesh method (**Essmann et al., 1995**). A time step of 1 fs was used to integrate the equation of motion with a Langevin integrator (**Schneider and Stoll, 1978**; **Brünger et al., 1984**). Constant temperature and pressure were achieved by coupling the systems to a Monte Carlo barostat at 1.01325 bar. Bonds involving hydrogen atoms were constrained using the SHAKE algorithm (**Ryckaert et al., 1977**). The simulations were performed with OpenMM 7.0 (**Eastman and Pande, 2015**) following a standard protocol included into OMMProtocol application (https://github.com/insilichem/ommprotocol): model systems were initially energy minimized (3000 steps); then, thermalization of water molecules and side chains was achieved by increasing the temperature from 100 K up to 300 K; finally, 100 ns of production simulations were performed. For

the model containing the deletion, simulations were performed in triplicate. Molecular graphics were produced with the UCSF Chimera package (**Pettersen et al., 2004**), except for the RMSF one that was done with VMD (**Humphrey et al., 1996**).

Collection and processing of human fetuses

Tissues were made available in accordance with French bylaws (Good practice concerning the conservation, transformation and transportation of human tissue to be used therapeutically, published on December 29, 1998). The studies on human fetal tissue were approved by the French agency for biomedical research (Agence de la Biomédecine, Saint-Denis la Plaine, France, protocol n°: PFS16–002). Non-pathological human fetuses (11 weeks post-amenorrhea, n = 2, females) were obtained from voluntarily terminated pregnancies after obtaining written informed consent from the parents (Gynaecology Department, Jeanne de Flandre Hospital, Lille, France). Fetuses were fixed by immersion in 4% paraformaldehyde (PFA) at 4˚C for 7 days. The tissues were then cryoprotected in 30% sucrose/PBS at 4˚C overnight, embedded in Tissue-Tek OCT compound (Sakura Finetek, USA), frozen in dry ice and stored at −80˚C until sectioning. Frozen samples were cut serially at 20 µm using a Leica CM 3050S cryostat (Leica Biosystems Nussloch GmbH, Germany) and immunolabeled as described above and as previously described (**Casoni et al., 2016**).

Sex determination of human fetuses

Sex determination of two human fetuses (Gestational weeks 11: GW11) was obtained by isolating DNA from extracted tissues using the NucleoSpin Tissue Kit (Macherey-Nagel), according to manufacturer instructions, and the extracted DNA was stored at −20˚C until use. The DNA concentration (absorbance at 260 nm) and purity (A260/A280 ratio) were assessed using the NanoDrop 1000 Spectrophotometer (ThermoScientific). A PCR was performed in a PTC-200 thermocycler (MJ Research) using the following steps: 94˚C for 3 min and 35 cycles of 94˚C for 1 min; 56˚C for 30 s; 72˚C for 30 s and 72˚C for 5 min. For genotyping the following primers were used: *SRY* sense 5'-AGCGATGATTACAGTCCAGC-3' and antisense 5'-CCTACAGCTTTGTCCAGTGG-3'; *FGF16* sense 5'-CGGGAGGGATACAGGACTAAAC-3' and antisense 5'-CTGTAGGTAGCATCTGTGGC-3'. The presence of DNA extracted from the two sexual chromosome X (*FGF16*: 495 bp) and Y (*SRY*: 538 bp) was assessed by electrophoresis on a 2% agarose gel.

The DNA was visualized thank to SybrGreen staining under an UV transilluminator (Biorad Gel Doc XR + with Image Lab Solfware) and compared against a known molecular weight marker (DNA Step Ladder 50 bp, Promega).

Statistical analysis

Sample sizes for physiological and neuroanatomical studies and gene expression analyses were estimated based on prior experience and those represented in the extant literature. Typically, mice taken from at least two different litters for each group were used. No stringent randomization method was used to assign subjects in the experimental groups or to process data.

Quantitative RT-PCR gene expression data were analyzed using SDS 2.4.1 and Data Assist 3.0.1 software (Applied Biosystems, Carlsbad, CA). All other analyses were performed using Prism 5 (GraphPad Software). Data sets were assessed for normality (Shapiro-Wilk test) and variance. Where appropriate a one-way or two-way ANOVA followed by post hoc testing (specified in the figure legends) was performed and for non-Gaussian distributions, a Kruskal-Wallis test followed by Dunn's multiple comparison test was used – indicated in figure legends. Exact P/adjusted p values are given in figure legends where possible. α was set at 0.05 for all experiments excluding WES data.

Ethics

Animal experimentation: the study was performed in strict accordance with the Guidelines specified by the European Union Council Directive of September 22, 2010 (2010/63/EU). The protocols were approved by the Ethical Committee of the French Ministry of Education and Research (APAFIS#13387–2017122712209790 v9).

Human fetal material: the study was approved by the French agency for biomedical research (Agence de la Biomédecine, Saint-Denis la Plaine, France, protocol n°: PFS16–002). Non-pathological human fetuses were obtained from voluntarily terminated pregnancies after obtaining written

informed consent from the parents (Gynaecology Department, Jeanne de Flandre Hospital, Lille, France).

Human subjects: this study was approved by the ethics committee of the University of Lausanne, and all participants provided written informed consent prior to study participation.

Acknowledgements

We thank M Tardivel and A Bongiovanni (microscopy core facility), M-H Gevaert (histology core facility), D Taillieu and J Devassine (animal core facility) and the BICeL core facility of the Lille University School of Medicine for expert technical assistance. This work was supported by: the Institut National de la Santé et de la Recherche Médicale (INSERM), France [grant number U1172]; Agence Nationale de la Recherche (ANR), France [ANR-14-CE12-0015-01 RoSes and GnRH to P.G.]; the Centre Hospitalier Régional Universitaire, CHU de Lille, France (Bonus H to P.G. and Ph.D. fellowship to NEHM); the European Research Council (ERC) under the European Union's Horizon 2020 research and innovation program (ERC-2016-CoG to P.G. grant n° 725149/REPRODAMH); Horizon 2020 Marie Sklodowska-Curie actions – European Research Fellowship (H2020-MSCA-IF-2017) to MI; the Spanish Ministerio de Ciencia e Innovación (grants CTQ2017-87889-P and CTQ2017-83745-P to LM, LAC and J-DM); the Generalitat de Catalunya (grant 2017SGR1323 to LAC and J-DM). Support of COST Action CM1306 is kindly acknowledged. LAC thanks Generalitat de Catalunya for her Ph.D. grant. LM thanks the 'Talent 2017' program from the Universitat Autònoma de Barcelona.

Additional information

Funding

Funder	Grant reference number	Author
Agence Nationale de la Recherche	ANR-14-CE12-0015-01	Paolo Giacobini
Horizon 2020 Framework Programme	ERC-2016-CoG 725149	Paolo Giacobini
Spanish Ministerio de Ciencia e Innovación	CTQ2017-87889-P	Lur Alonso-Cotchico Laura Masgrau Jean-Didier Maréchal
Spanish Ministerio de Ciencia e Innovación	CTQ2017-83745-P	Lur Alonso-Cotchico Laura Masgrau Jean-Didier Maréchal
Horizon 2020 Framework Programme	H2020-MSCA-IF-2017	Monica Imbernon
Generalitat de Catalunya	2017SGR1323	Lur Alonso-Cotchico Jean-Didier Maréchal

The funders had no role in study design, data collection and interpretation, or the decision to submit the work for publication.

Author contributions

Samuel Andrew Malone, Andrea Messina, Formal analysis, Investigation, Writing—original draft; Georgios E Papadakis, Resources, Data curation, Writing—original draft, Writing—review and editing; Nour El Houda Mimouni, Data curation, Investigation, Visualization; Sara Trova, Investigation, Visualization; Monica Imbernon, Pascal Pigny, Data curation, Investigation; Cecile Allet, Methodology; Irene Cimino, Lur Alonso-Cotchico, Data curation, Formal analysis, Investigation; James Acierno, Data curation, Software, Formal analysis, Writing—original draft; Daniele Cassatella, Software, Formal analysis, Validation; Cheng Xu, Investigation; Richard Quinton, Gabor Szinnai, Resources; Laura Masgrau, Formal analysis, Validation, Investigation; Jean-Didier Maréchal, Data curation, Formal analysis, Supervision; Vincent Prevot, Conceptualization, Data curation; Nelly Pitteloud, Conceptualization, Data curation, Funding acquisition, Writing—original draft, Writing—review and editing; Paolo Giacobini, Conceptualization, Formal analysis, Supervision,

Funding acquisition, Validation, Writing—original draft, Project administration, Writing—review and editing

Author ORCIDs

Vincent Prevot http://orcid.org/0000-0001-7185-3615
Paolo Giacobini https://orcid.org/0000-0002-3075-1441

Ethics

Human subjects: Human fetal material: the study was approved by the French agency for biomedical research (Agence de la Biomédecine, Saint-Denis la Plaine, France, protocol n°: PFS16-002). Non-pathological human fetuses were obtained from voluntarily terminated pregnancies after obtaining written informed consent from the parents (Gynaecology Department, Jeanne de Flandre Hospital, Lille, France). Human subjects: this study was approved by the ethics committee of the University of Lausanne, and all participants provided written informed consent prior to study participation.
Animal experimentation: Animal experimentation: the study was performed in strict accordance with the Guidelines specified by the European Union Council Directive of September 22, 2010 (2010/63/EU). The protocols were approved by the Ethical Committee of the French Ministry of Education and Research (APAFIS#13387-2017122712209790 v9).

Decision letter and Author response

Decision letter https://doi.org/10.7554/eLife.47198.023
Author response https://doi.org/10.7554/eLife.47198.024

Additional files

Supplementary files

- Supplementary file 1. List of primers used for genotyping and for mutagenesis experiments.
DOI: https://doi.org/10.7554/eLife.47198.020
- Transparent reporting form
DOI: https://doi.org/10.7554/eLife.47198.021

Data availability

All data generated or analysed during this study are included in the manuscript and supporting files. Raw data files have been provided for Figures 1, 2, 4, 5, 7, Figure 4-figure supplement 1. The human sequencing data from the patients and their family members in this study cannot be made available to prevent traceability of the patients and because not all participants gave their consent for releasing their data publicly. However, the source sequencing human data can be made available on request to the corresponding author (Dr. Nelly Pitteloud).

References

Baarends WM, van Helmond MJ, Post M, van der Schoot PJ, Hoogerbrugge JW, de Winter JP, Uilenbroek JT, Karels B, Wilming LG, Meijers JH. 1994. A novel member of the transmembrane serine/threonine kinase receptor family is specifically expressed in the gonads and in mesenchymal cells adjacent to the müllerian duct. *Development* **120**:189–197. PMID: 8119126

Balland E, Dam J, Langlet F, Caron E, Steculorum S, Messina A, Rasika S, Falluel-Morel A, Anouar Y, Dehouck B, Trinquet E, Jockers R, Bouret SG, Prévot V. 2014. Hypothalamic tanycytes are an ERK-gated conduit for leptin into the brain. *Cell Metabolism* **19**:293–301. DOI: https://doi.org/10.1016/j.cmet.2013.12.015, PMID: 24506870

Behringer RR, Finegold MJ, Cate RL. 1994. Müllerian-inhibiting substance function during mammalian sexual development. *Cell* **79**:415–425. DOI: https://doi.org/10.1016/0092-8674(94)90251-8, PMID: 7954809

Belle M, Godefroy D, Dominici C, Heitz-Marchaland C, Zelina P, Hellal F, Bradke F, Chédotal A. 2014. A simple method for 3D analysis of immunolabeled axonal tracts in a transparent nervous system. *Cell Reports* **9**:1191–1201. DOI: https://doi.org/10.1016/j.celrep.2014.10.037, PMID: 25456121

Belville C, Josso N, Picard JY. 1999. Persistence of müllerian derivatives in males. *American Journal of Medical Genetics* **89**:218–223. DOI: https://doi.org/10.1002/(SICI)1096-8628(19991229)89:4<218::AID-AJMG6>3.0.CO;2-E, PMID: 10727997

Belville C, Van Vlijmen H, Ehrenfels C, Pepinsky B, Rezaie AR, Picard JY, Josso N, di Clemente N, Cate RL. 2004. Mutations of the anti-mullerian hormone gene in patients with persistent mullerian duct syndrome: biosynthesis, secretion, and processing of the abnormal proteins and analysis using a three-dimensional model. *Molecular Endocrinology* **18**:708–721. DOI: https://doi.org/10.1210/me.2003-0358, PMID: 14673134

Belville C, Maréchal JD, Pennetier S, Carmillo P, Masgrau L, Messika-Zeitoun L, Galey J, Machado G, Treton D, Gonzalès J, Picard JY, Josso N, Cate RL, di Clemente N. 2009. Natural mutations of the anti-Mullerian hormone type II receptor found in persistent mullerian duct syndrome affect ligand binding, signal transduction and cellular transport. *Human Molecular Genetics* **18**:3002–3013. DOI: https://doi.org/10.1093/hmg/ddp238, PMID: 19457927

Boehm U, Bouloux PM, Dattani MT, de Roux N, Dodé C, Dunkel L, Dwyer AA, Giacobini P, Hardelin JP, Juul A, Maghnie M, Pitteloud N, Prevot V, Raivio T, Tena-Sempere M, Quinton R, Young J. 2015. Expert consensus document: european consensus statement on congenital hypogonadotropic hypogonadism–pathogenesis, diagnosis and treatment. *Nature Reviews Endocrinology* **11**:547–564. DOI: https://doi.org/10.1038/nrendo.2015.112, PMID: 26194704

Brünger A, Brooks CL, Karplus M. 1984. Stochastic boundary conditions for molecular dynamics simulations of ST2 water. *Chemical Physics Letters* **105**:495–500. DOI: https://doi.org/10.1016/0009-2614(84)80098-6

Caldwell ASL, Edwards MC, Desai R, Jimenez M, Gilchrist RB, Handelsman DJ, Walters KA. 2017. Neuroendocrine androgen action is a key extraovarian mediator in the development of polycystic ovary syndrome. *PNAS* **114**:E3334–E3343. DOI: https://doi.org/10.1073/pnas.1616467114, PMID: 28320971

Casoni F, Malone SA, Belle M, Luzzati F, Collier F, Allet C, Hrabovszky E, Rasika S, Prevot V, Chédotal A, Giacobini P. 2016. Development of the neurons controlling fertility in humans: new insights from 3D imaging and transparent fetal brains. *Development* **143**:3969–3981. DOI: https://doi.org/10.1242/dev.139444, PMID: 27803058

Christian CA, Moenter SM. 2010. The neurobiology of preovulatory and estradiol-induced gonadotropin-releasing hormone surges. *Endocrine Reviews* **31**:544–577. DOI: https://doi.org/10.1210/er.2009-0023, PMID: 20237240

Cimino I, Casoni F, Liu X, Messina A, Parkash J, Jamin SP, Catteau-Jonard S, Collier F, Baroncini M, Dewailly D, Pigny P, Prescott M, Campbell R, Herbison AE, Prevot V, Giacobini P. 2016. Novel role for anti-Müllerian hormone in the regulation of GnRH neuron excitability and hormone secretion. *Nature Communications* **7**:10055. DOI: https://doi.org/10.1038/ncomms10055, PMID: 26753790

Cingolani P, Platts A, Wang leL, Coon M, Nguyen T, Wang L, Land SJ, Lu X, Ruden DM. 2012. A program for annotating and predicting the effects of single Nucleotide Polymorphisms, SnpEff: snps in the genome of *Drosophila Melanogaster* strain w1118; iso-2; iso-3. *Fly* **6**:80–92. DOI: https://doi.org/10.4161/fly.19695, PMID: 22728672

Colovos C, Yeates TO. 1993. Verification of protein structures: patterns of nonbonded atomic interactions. *Protein Science* **2**:1511–1519. DOI: https://doi.org/10.1002/pro.5560020916, PMID: 8401235

den Dunnen JT, Antonarakis SE. 2000. Mutation nomenclature extensions and suggestions to describe complex mutations: a discussion. *Human Mutation* **15**:7–12. DOI: https://doi.org/10.1002/(SICI)1098-1004(200001)15:1<7::AID-HUMU4>3.0.CO;2-N, PMID: 10612815

DePristo MA, Banks E, Poplin R, Garimella KV, Maguire JR, Hartl C, Philippakis AA, del Angel G, Rivas MA, Hanna M, McKenna A, Fennell TJ, Kernytsky AM, Sivachenko AY, Cibulskis K, Gabriel SB, Altshuler D, Daly MJ. 2011. A framework for variation discovery and genotyping using next-generation DNA sequencing data. *Nature Genetics* **43**:491–498. DOI: https://doi.org/10.1038/ng.806, PMID: 21478889

di Clemente N, Wilson C, Faure E, Boussin L, Carmillo P, Tizard R, Picard JY, Vigier B, Josso N, Cate R. 1994. Cloning, expression, and alternative splicing of the receptor for anti-Müllerian hormone. *Molecular Endocrinology* **8**:1006–1020. DOI: https://doi.org/10.1210/mend.8.8.7997230, PMID: 7997230

Durlinger AL, Kramer P, Karels B, de Jong FH, Uilenbroek JT, Grootegoed JA, Themmen AP. 1999. Control of primordial follicle recruitment by anti-Müllerian hormone in the mouse ovary. *Endocrinology* **140**:5789–5796. DOI: https://doi.org/10.1210/endo.140.12.7204, PMID: 10579345

Durlinger AL, Gruijters MJ, Kramer P, Karels B, Kumar TR, Matzuk MM, Rose UM, de Jong FH, Uilenbroek JT, Grootegoed JA, Themmen AP. 2001. Anti-Müllerian hormone attenuates the effects of FSH on follicle development in the mouse ovary. *Endocrinology* **142**:4891–4899. DOI: https://doi.org/10.1210/endo.142.11.8486, PMID: 11606457

Eastman P, Pande VS. 2015. OpenMM: a hardware independent framework for molecular simulations. *Computing in Science & Engineering* **12**:34–39. DOI: https://doi.org/10.1109/MCSE.2010.27, PMID: 26146490

Essmann U, Perera L, Berkowitz ML, Darden T, Lee H, Pedersen LG. 1995. A smooth particle mesh ewald method. *The Journal of Chemical Physics* **103**:8577–8593. DOI: https://doi.org/10.1063/1.470117

Fueshko S, Wray S. 1994. LHRH cells migrate on peripherin fibers in embryonic olfactory explant cultures: an in vitro model for neurophilic neuronal migration. *Developmental Biology* **166**:331–348. DOI: https://doi.org/10.1006/dbio.1994.1319, PMID: 7958456

Garrel G, Racine C, L'Hôte D, Denoyelle C, Guigon CJ, di Clemente N, Cohen-Tannoudji J. 2016. Anti-Müllerian hormone: a new actor of sexual dimorphism in pituitary gonadotrope activity before puberty. *Scientific Reports* **6**:23790. DOI: https://doi.org/10.1038/srep23790, PMID: 27030385

Garrel G, Denoyelle C, L'Hôte D, Picard JY, Teixeira J, Kaiser UB, Laverrière JN, Cohen-Tannoudji J. 2019. GnRH transactivates human AMH receptor gene via Egr1 and FOXO1 in gonadotrope cells. *Neuroendocrinology* **108**:65–83. DOI: https://doi.org/10.1159/000494890, PMID: 30368511

Giacobini P, Kopin AS, Beart PM, Mercer LD, Fasolo A, Wray S. 2004. Cholecystokinin modulates migration of gonadotropin-releasing hormone-1 neurons. *Journal of Neuroscience* **24**:4737–4748. DOI: https://doi.org/10.1523/JNEUROSCI.0649-04.2004, PMID: 15152034

Giacobini P, Messina A, Wray S, Giampietro C, Crepaldi T, Carmeliet P, Fasolo A. 2007. Hepatocyte growth factor acts as a motogen and guidance signal for gonadotropin hormone-releasing hormone-1 neuronal migration. *Journal of Neuroscience* **27**:431–445. DOI: https://doi.org/10.1523/JNEUROSCI.4979-06.2007, PMID: 17215404

Hanchate NK, Giacobini P, Lhuillier P, Parkash J, Espy C, Fouveaut C, Leroy C, Baron S, Campagne C, Vanacker C, Collier F, Cruaud C, Meyer V, García-Piñero A, Dewailly D, Cortet-Rudelli C, Gersak K, Metz C, Chabrier G, Pugeat M, et al. 2012. SEMA3A, a gene involved in Axonal Pathfinding, is mutated in patients with Kallmann syndrome. *PLoS Genetics* **8**:e1002896. DOI: https://doi.org/10.1371/journal.pgen.1002896, PMID: 22927827

Humphrey W, Dalke A, Schulten K. 1996. VMD: visual molecular dynamics. *Journal of Molecular Graphics* **14**:33–38. DOI: https://doi.org/10.1016/0263-7855(96)00018-5, PMID: 8744570

Imbeaud S, Faure E, Lamarre I, Mattéi MG, di Clemente N, Tizard R, Carré-Eusèbe D, Belville C, Tragethon L, Tonkin C, Nelson J, McAuliffe M, Bidart JM, Lababidi A, Josso N, Cate RL, Picard JY. 1995. Insensitivity to anti-müllerian hormone due to a mutation in the human anti-müllerian hormone receptor. *Nature Genetics* **11**:382–388. DOI: https://doi.org/10.1038/ng1295-382, PMID: 7493017

Jamin SP, Arango NA, Mishina Y, Hanks MC, Behringer RR. 2002. Requirement of Bmpr1a for müllerian duct regression during male sexual development. *Nature Genetics* **32**:408–410. DOI: https://doi.org/10.1038/ng1003, PMID: 12368913

Jorgensen WL, Chandrasekhar J, Madura JD, Impey RW, Klein ML. 1983. Comparison of simple potential functions for simulating liquid water. *The Journal of Chemical Physics* **79**:926–935. DOI: https://doi.org/10.1063/1.445869

Josso N, Racine C, di Clemente N, Rey R, Xavier F. 1998. The role of anti-Müllerian hormone in gonadal development. *Molecular and Cellular Endocrinology* **145**:3–7. DOI: https://doi.org/10.1016/S0303-7207(98)00186-5, PMID: 9922092

Josso N, Belville C, di Clemente N, Picard JY. 2005. AMH and AMH receptor defects in persistent müllerian duct syndrome. *Human Reproduction Update* **11**:351–356. DOI: https://doi.org/10.1093/humupd/dmi014, PMID: 15878900

Josso N, Clemente N. 2003. Transduction pathway of anti-Müllerian hormone, a sex-specific member of the TGF-beta family. *Trends in Endocrinology & Metabolism* **14**:91–97. DOI: https://doi.org/10.1016/S1043-2760(03)00005-5, PMID: 12591180

Lebeurrier N, Launay S, Macrez R, Maubert E, Legros H, Leclerc A, Jamin SP, Picard JY, Marret S, Laudenbach V, Berger P, Sonderegger P, Ali C, di Clemente N, Vivien D. 2008. Anti-Mullerian-hormone-dependent regulation of the brain serine-protease inhibitor neuroserpin. *Journal of Cell Science* **121**:3357–3365. DOI: https://doi.org/10.1242/jcs.031872, PMID: 18796535

Lewkowitz-Shpuntoff HM, Hughes VA, Plummer L, Au MG, Doty RL, Seminara SB, Chan YM, Pitteloud N, Crowley WF, Balasubramanian R. 2012. Olfactory phenotypic spectrum in idiopathic hypogonadotropic hypogonadism: pathophysiological and genetic implications. *The Journal of Clinical Endocrinology & Metabolism* **97**:E136–E144. DOI: https://doi.org/10.1210/jc.2011-2041, PMID: 22072740

Li H, Durbin R. 2009. Fast and accurate short read alignment with Burrows-Wheeler transform. *Bioinformatics* **25**:1754–1760. DOI: https://doi.org/10.1093/bioinformatics/btp324, PMID: 19451168

Liu X, Jian X, Boerwinkle E. 2013. dbNSFP v2.0: a database of human non-synonymous SNVs and their functional predictions and annotations. *Human Mutation* **34**:E2393–E2402. DOI: https://doi.org/10.1002/humu.22376, PMID: 23843252

Maier JA, Martinez C, Kasavajhala K, Wickstrom L, Hauser KE, Simmerling C. 2015. ff14SB: improving the accuracy of protein side chain and backbone parameters from ff99SB. *Journal of Chemical Theory and Computation* **11**:3696–3713. DOI: https://doi.org/10.1021/acs.jctc.5b00255, PMID: 26574453

Mamsen LS, Petersen TS, Jeppesen JV, Møllgård K, Grøndahl ML, Larsen A, Ernst E, Oxvig C, Kumar A, Kalra B, Andersen CY. 2015. Proteolytic processing of anti-Müllerian hormone differs between human fetal testes and adult ovaries. *Molecular Human Reproduction* **21**:571–582. DOI: https://doi.org/10.1093/molehr/gav024, PMID: 25920489

Mellon PL, Windle JJ, Goldsmith PC, Padula CA, Roberts JL, Weiner RI. 1990. Immortalization of hypothalamic GnRH neurons by genetically targeted tumorigenesis. *Neuron* **5**:1–10. DOI: https://doi.org/10.1016/0896-6273(90)90028-E, PMID: 2196069

Messina A, Ferraris N, Wray S, Cagnoni G, Donohue DE, Casoni F, Kramer PR, Derijck AA, Adolfs Y, Fasolo A, Pasterkamp RJ, Giacobini P. 2011. Dysregulation of Semaphorin7A/β1-integrin signaling leads to defective GnRH-1 cell migration, abnormal gonadal development and altered fertility. *Human Molecular Genetics* **20**:4759–4774. DOI: https://doi.org/10.1093/hmg/ddr403, PMID: 21903667

Messina A, Langlet F, Chachlaki K, Roa J, Rasika S, Jouy N, Gallet S, Gaytan F, Parkash J, Tena-Sempere M, Giacobini P, Prevot V. 2016. A microRNA switch regulates the rise in hypothalamic GnRH production before puberty. *Nature Neuroscience* **19**:835–844. DOI: https://doi.org/10.1038/nn.4298, PMID: 27135215

Mishina Y, Rey R, Finegold MJ, Matzuk MM, Josso N, Cate RL, Behringer RR. 1996. Genetic analysis of the Müllerian-inhibiting substance signal transduction pathway in mammalian sexual differentiation. *Genes & Development* **10**:2577–2587. DOI: https://doi.org/10.1101/gad.10.20.2577, PMID: 8895659

Orvis GD, Jamin SP, Kwan KM, Mishina Y, Kaartinen VM, Huang S, Roberts AB, Umans L, Huylebroeck D, Zwijsen A, Wang D, Martin JF, Behringer RR. 2008. Functional redundancy of TGF-beta family type I receptors and

receptor-Smads in mediating anti-Mullerian hormone-induced mullerian duct regression in the mouse. *Biology of Reproduction* **78**:994–1001. DOI: https://doi.org/10.1095/biolreprod.107.066605, PMID: 18322278

Pankhurst MW, McLennan IS. 2013. Human blood contains both the uncleaved precursor of anti-Mullerian hormone and a complex of the NH2- and COOH-terminal peptides. *American Journal of Physiology-Endocrinology and Metabolism* **305**:E1241–E1247. DOI: https://doi.org/10.1152/ajpendo.00395.2013, PMID: 24045871

Parysek LM, Goldman RD. 1988. Distribution of a novel 57 kDa intermediate filament (IF) protein in the nervous system. *The Journal of Neuroscience* **8**:555–563. DOI: https://doi.org/10.1523/JNEUROSCI.08-02-00555.1988, PMID: 3276833

Pettersen EF, Goddard TD, Huang CC, Couch GS, Greenblatt DM, Meng EC, Ferrin TE. 2004. UCSF chimera–a visualization system for exploratory research and analysis. *Journal of Computational Chemistry* **25**:1605–1612. DOI: https://doi.org/10.1002/jcc.20084, PMID: 15264254

Picard JY, Cate RL, Racine C, Josso N. 2017. The persistent müllerian duct syndrome: an update based upon a personal experience of 157 cases. *Sexual Development* **11**:109–125. DOI: https://doi.org/10.1159/000475516, PMID: 28528332

Pitteloud N, Hayes FJ, Dwyer A, Boepple PA, Lee H, Crowley WF. 2002. Predictors of outcome of long-term GnRH therapy in men with idiopathic hypogonadotropic hypogonadism. *The Journal of Clinical Endocrinology & Metabolism* **87**:4128–4136. DOI: https://doi.org/10.1210/jc.2002-020518, PMID: 12213860

Pitteloud N, Quinton R, Pearce S, Raivio T, Acierno J, Dwyer A, Plummer L, Hughes V, Seminara S, Cheng YZ, Li WP, Maccoll G, Eliseenkova AV, Olsen SK, Ibrahimi OA, Hayes FJ, Boepple P, Hall JE, Bouloux P, Mohammadi M, et al. 2007. Digenic mutations account for variable phenotypes in idiopathic hypogonadotropic hypogonadism. *Journal of Clinical Investigation* **117**:457–463. DOI: https://doi.org/10.1172/JCI29884, PMID: 17235395

Radovick S, Wray S, Lee E, Nicols DK, Nakayama Y, Weintraub BD, Westphal H, Cutler GB, Wondisford FE. 1991. Migratory arrest of gonadotropin-releasing hormone neurons in transgenic mice. *PNAS* **88**:3402–3406. DOI: https://doi.org/10.1073/pnas.88.8.3402, PMID: 2014260

Renier N, Wu Z, Simon DJ, Yang J, Ariel P, Tessier-Lavigne M. 2014. iDISCO: a simple, rapid method to immunolabel large tissue samples for volume imaging. *Cell* **159**:896–910. DOI: https://doi.org/10.1016/j.cell.2014.10.010, PMID: 25417164

Richards S, Aziz N, Bale S, Bick D, Das S, Gastier-Foster J, Grody WW, Hegde M, Lyon E, Spector E, Voelkerding K, Rehm HL, ACMG Laboratory Quality Assurance Committee. 2015. Standards and guidelines for the interpretation of sequence variants: a joint consensus recommendation of the american college of medical genetics and genomics and the association for molecular pathology. *Genetics in Medicine* **17**:405–423. DOI: https://doi.org/10.1038/gim.2015.30, PMID: 25741868

Ryckaert J-P, Ciccotti G, Berendsen HJC. 1977. Numerical integration of the cartesian equations of motion of a system with constraints: molecular dynamics of n-alkanes. *Journal of Computational Physics* **23**:327–341. DOI: https://doi.org/10.1016/0021-9991(77)90098-5

Sali A, Blundell TL. 1993. Comparative protein modelling by satisfaction of spatial restraints. *Journal of Molecular Biology* **234**:779–815. DOI: https://doi.org/10.1006/jmbi.1993.1626, PMID: 8254673

Schmittgen TD, Livak KJ. 2008. Analyzing real-time PCR data by the comparative C(T) method. *Nature Protocols* **3**:1101–1108. DOI: https://doi.org/10.1038/nprot.2008.73, PMID: 18546601

Schneider T, Stoll E. 1978. Molecular-dynamics study of a three-dimensional one-component model for distortive phase transitions. *Physical Review B* **17**:1302–1322. DOI: https://doi.org/10.1103/PhysRevB.17.1302

Schwanzel-Fukuda M, Crossin KL, Pfaff DW, Bouloux PM, Hardelin JP, Petit C. 1996. Migration of luteinizing hormone-releasing hormone (LHRH) neurons in early human embryos. *The Journal of Comparative Neurology* **366**:547–557. DOI: https://doi.org/10.1002/(SICI)1096-9861(19960311)366:3<547::AID-CNE12>3.0.CO;2-M, PMID: 8907364

Schwanzel-Fukuda M, Pfaff DW. 1989. Origin of luteinizing hormone-releasing hormone neurons. *Nature* **338**:161–164. DOI: https://doi.org/10.1038/338161a0, PMID: 2645530

Spergel DJ, Krüth U, Hanley DF, Sprengel R, Seeburg PH. 1999. GABA- and glutamate-activated channels in green fluorescent protein-tagged gonadotropin-releasing hormone neurons in transgenic mice. *The Journal of Neuroscience* **19**:2037–2050. DOI: https://doi.org/10.1523/JNEUROSCI.19-06-02037.1999, PMID: 10066257

Steyn FJ, Wan Y, Clarkson J, Veldhuis JD, Herbison AE, Chen C. 2013. Development of a methodology for and assessment of pulsatile luteinizing hormone secretion in juvenile and adult male mice. *Endocrinology* **154**:4939–4945. DOI: https://doi.org/10.1210/en.2013-1502, PMID: 24092638

Sykiotis GP, Plummer L, Hughes VA, Au M, Durrani S, Nayak-Young S, Dwyer AA, Quinton R, Hall JE, Gusella JF, Seminara SB, Crowley WF, Pitteloud N. 2010. Oligogenic basis of isolated gonadotropin-releasing hormone deficiency. *PNAS* **107**:15140–15144. DOI: https://doi.org/10.1073/pnas.1009622107, PMID: 20696889

Taroc EZM, Prasad A, Lin JM, Forni PE. 2017. The terminal nerve plays a prominent role in GnRH-1 neuronal migration independent from proper olfactory and vomeronasal connections to the olfactory bulbs. *Biology Open* **6**:1552–1568. DOI: https://doi.org/10.1242/bio.029074, PMID: 28970231

Tata B, Mimouni NEH, Barbotin AL, Malone SA, Loyens A, Pigny P, Dewailly D, Catteau-Jonard S, Sundström-Poromaa I, Piltonen TT, Dal Bello F, Medana C, Prevot V, Clasadonte J, Giacobini P. 2018. Elevated prenatal anti-Müllerian hormone reprograms the fetus and induces polycystic ovary syndrome in adulthood. *Nature Medicine* **24**:834–846. DOI: https://doi.org/10.1038/s41591-018-0035-5, PMID: 29760445

Teixeira L, Guimiot F, Dodé C, Fallet-Bianco C, Millar RP, Delezoide AL, Hardelin JP. 2010. Defective migration of neuroendocrine GnRH cells in human arrhinencephalic conditions. *Journal of Clinical Investigation* **120**:3668–3672. DOI: https://doi.org/10.1172/JCI43699, PMID: 20940512

Vidal A, Zhang Q, Médigue C, Fabre S, Clément F. 2012. DynPeak: an algorithm for pulse detection and frequency analysis in hormonal time series. *PLOS ONE* **7**:e39001. DOI: https://doi.org/10.1371/journal.pone.0039001, PMID: 22802933

Vigier B, Picard JY, Tran D, Legeai L, Josso N. 1984. Production of anti-Müllerian hormone: another homology between sertoli and granulosa cells. *Endocrinology* **114**:1315–1320. DOI: https://doi.org/10.1210/endo-114-4-1315, PMID: 6546716

Wang PY, Koishi K, McGeachie AB, Kimber M, Maclaughlin DT, Donahoe PK, McLennan IS. 2005. Mullerian inhibiting substance acts as a motor neuron survival factor in vitro. *PNAS* **102**:16421–16425. DOI: https://doi.org/10.1073/pnas.0508304102, PMID: 16260730

Wang PY, Protheroe A, Clarkson AN, Imhoff F, Koishi K, McLennan IS. 2009. Müllerian inhibiting substance contributes to sex-linked biases in the brain and behavior. *PNAS* **106**:7203–7208. DOI: https://doi.org/10.1073/pnas.0902253106, PMID: 19359476

Wray S, Grant P, Gainer H. 1989. Evidence that cells expressing luteinizing hormone-releasing hormone mRNA in the mouse are derived from progenitor cells in the olfactory placode. *PNAS* **86**:8132–8136. DOI: https://doi.org/10.1073/pnas.86.20.8132, PMID: 2682637

Yoshida K, Tobet SA, Crandall JE, Jimenez TP, Schwarting GA. 1995. The migration of luteinizing hormone-releasing hormone neurons in the developing rat is associated with a transient, caudal projection of the vomeronasal nerve. *The Journal of Neuroscience* **15**:7769–7777. DOI: https://doi.org/10.1523/JNEUROSCI.15-12-07769.1995, PMID: 8613718